

**DYNAMIC BOUNDARY ELEMENT ANALYSIS
OF MACHINE FOUNDATIONS**

SUHOL BU

B. Sc., M. Eng.

**A thesis submitted to
the University of Glasgow
for the Degree of Doctor of Philosophy
in the Faculty of Engineering**

The Department of Civil Engineering

The University of Glasgow

March 1994

© Suhol Bu, 1994.

ProQuest Number: 13818755

All rights reserved

INFORMATION TO ALL USERS

The quality of this reproduction is dependent upon the quality of the copy submitted.

In the unlikely event that the author did not send a complete manuscript and there are missing pages, these will be noted. Also, if material had to be removed, a note will indicate the deletion.



ProQuest 13818755

Published by ProQuest LLC (2018). Copyright of the Dissertation is held by the Author.

All rights reserved.

This work is protected against unauthorized copying under Title 17, United States Code
Microform Edition © ProQuest LLC.

ProQuest LLC.
789 East Eisenhower Parkway
P.O. Box 1346
Ann Arbor, MI 48106 – 1346

Thesis
9785
copy 1



To
my family

ACKNOWLEDGEMENTS

The work described in this thesis was carried out in the department of Civil Engineering, Glasgow University. I would like to thank Professors D.R. Green and D. Muir Wood and Dr. J.G. Herbertson for providing excellent environment and facilities in the department to carry out this research.

I have good reason to be grateful to a large number of people, and would take this opportunity of expressing my sincere gratitude to all my friends and colleagues in the Department, especially to Mrs E. Davies and Ms B. Grant, for their kind assistance during my study in Glasgow University.

I would like to express my sincere thanks to my supervisor Dr T.G. Davies for his strong support, help, and encouragement throughout my whole study in Glasgow University. Without his invaluable guidance and patience towards my work, this research could not have been completed. Over the years he has taught me a great deal, and not only about boundary elements. I am proud to count him not only a supervisor, but as a friend.

Finally, and most importantly, I owe most affectionate thanks to my parents, sister, and my wife for their continuous spiritual and financial support.

ABSTRACT

The central theme of this thesis is the further development of boundary element methods for the analysis of three-dimensional machine foundations, pertaining to various (translational and rotational) modes of vibration and, in particular, to high frequency response. Surface and embedded rectangular foundations are considered. The soil is assumed to behave approximately as a linear elastic material for small amplitudes of strain. The problem is formulated and solved in the frequency domain. This work includes rigorous theoretical studies, effective numerical techniques for the solution of the boundary integral equations, and efficient computer implementation of the algorithm.

The derivation of the boundary integral formulation is reviewed and the dynamic fundamental solutions are examined in detail. The particular fundamental solutions for incompressible media has been derived in order to deal more effectively with these materials. Advanced integration schemes for non-singular and singular integrals have been developed in order to improve the computational accuracy and efficiency of the boundary element analysis. A novel infinite boundary element for dynamic analyses has been developed, which provides an efficient means for including far-field effects, without the necessity of explicit discrete representation outside the near field. The implementation and vectorization of the computer program using the IBM 3090-150 Vector Facility is described. Various numerical results for rectangular foundations are presented in order to illustrate the potential of the infinite boundary element formulation. Included among these are new results pertaining to the high frequency response of machine foundations.

CONTENTS

DEDICATION	
ACKNOWLEDGEMENTS	I
ABSTRACT	II
CONTENTS	III
NOTATION	VII
LIST OF TABLES	X
LIST OF FIGURES	XI

CHAPTER 1 INTRODUCTION

1.1 INTRODUCTION	1
1.2 ANALYTICAL METHODS	2
1.3 NUMERICAL METHODS	4
1.4 DESIGN METHODS	7
1.5 DISCUSSION	11
1.6 OUTLINE OF THESIS CONTENTS	12

CHAPTER 2 BOUNDARY ELEMENT FORMULATIONS FOR ELASTODYNAMICS

2.1 INTRODUCTION	16
2.2 INTEGRAL EQUATION FORMULATION	17
2.2.1 Introduction	17
2.2.2 Theory of Elastodynamics	18
2.2.3 Fundamental Solutions	20
2.2.4 The Dynamic Reciprocal Identity	21
2.2.5 Integral Equation Formulation	23
2.3 REDUCED ELASTODYNAMIC PROBLEMS	24
2.4 FUNDAMENTAL SOLUTION CHARACTERISTICS	27
2.4.1 Order of Singularity	27
2.4.2 Symmetry, Anti-symmetry and Simplification	28
2.4.3 Frequency Response	29
2.4.4 Fundamental Solutions For Incompressible Medium	31
2.5 DIRECT BOUNDARY ELEMENT FORMULATION	34
2.5.1 Boundary Constraint Equation	34
2.5.2 Numerical Implementation	36
2.5.3 Discussion	41
2.6 SUMMARY AND CONCLUSIONS	43

CHAPTER 3 INTEGRATION SCHEMES (I): NON-SINGULAR INTEGRALS

3.1	INTRODUCTION	49
3.2	NUMERICAL INTEGRATION	51
3.2.1	Introduction	51
3.2.2	Gauss-Legendre Formula	51
3.2.3	Integration Over General Regions	52
3.3	NUMERICAL EXPERIMENTS ON ERROR BOUNDS	53
3.3.1	Introduction	53
3.3.2	Error Bounds Of Gauss Integration	54
3.3.3	Empirical Method	55
3.3.4	Criteria For Selecting The Order Of Gauss Integration	58
3.4	ADAPTIVE INTEGRATION STRATEGIES	61
3.5	INTEGRALS WITH OSCILLATORY INTEGRANDS	62
3.5.1	Introduction	62
3.5.2	Gauss Integration Over Square Region	63
3.5.3	Adaptive Integration Strategy	65
3.6	CONCLUSIONS	66

CHAPTER 4 INTEGRATION SCHEMES (II): SINGULAR INTEGRALS

4.1	INTRODUCTION	95
4.2	WEAKLY SINGULAR INTEGRALS	96
4.2.1	Introduction	96
4.2.2	Sub-element Mapping	98
4.2.3	Weakly Singular Functions	99
4.2.4	Numerical Study	102
4.2.5	Effects Of Singular Vertex Angle	104
4.2.6	Integrals With Oscillatory Integrands	105
4.3	STRONGLY SINGULAR INTEGRALS	107
4.3.1	Introduction	107
4.3.2	Evaluation Of The Diagonal Block For Static Problems	107
4.3.3	Evaluation Of The Diagonal Block For Dynamic Problems	109
4.3.4	Halfspace Problems	110
4.4	CONCLUSIONS	111
APPENDIX 4.1 : ANALYTICAL INTEGRATION OF		

$$\int \frac{N_1}{r_1} dA$$

OVER A 2x2 SQUARE

APPENDIX 4.2 : ANALYTICAL INTEGRATION OF

$$\int \frac{N_{\alpha} e^{ikr}}{r} dA$$

OVER A TRIANGULAR REGION IN THE RADIAL DIRECTION

116

APPENDIX 4.3 : ANALYTICAL INTEGRATION OF THE AZIMUTHAL INTEGRAL
OVER AN INFINITE HEMISPHERE

118

CHAPTER 5 INFINITE BOUNDARY ELEMENTS

5.1	INTRODUCTION	159
5.2	ASYMPTOTIC BEHAVIOUR OF THE FAR FIELD	161
5.2.1	Introduction	161
5.2.2	Static Displacement Behaviour	162
5.2.3	Dynamic Displacement Behaviour	164
5.3	DISCRETIZATION AND MAPPING THEORY	166
5.3.1	Discretization Of The Far Field	166
5.3.2	Interpolation Of Displacements	167
5.3.3	Geometric Representation	168
5.3.4	Boundary Element Formulation For Halfspace Problems	172
5.4	INTEGRATION OVER INFINITE BOUNDARY ELEMENTS	174
5.4.1	Non-singular Static Integrals	174
5.4.2	Non-singular Oscillatory Integrals	175
5.4.3	Singular Integrals	177
5.5	ILLUSTRATIVE NUMERICAL EXAMPLES	179
5.5.1	Displacements Due To Uniformly Distributed Load	179
5.5.2	Vertical Static Stiffnesses Of Square Foundations	180
5.5.3	Vertical Dynamic Stiffnesses Of Square Foundations	182
5.6	CONCLUSIONS	183
APPENDIX 5.0	: DERIVATION OF THE DISCRETIZED BOUNDARY ELEMENT FORMULATION	185
APPENDIX 5.1	: SEMI-ANALYTICAL INTEGRATION OF	

$$\int \frac{D_s}{R^2} dS$$

188

OVER INFINITE ELEMENTS

APPENDIX 5.2 : INTEGRATION OF

$$\int T_{ij}^{st} dS$$

OVER S_B

191

CHAPTER 6 NUMERICAL IMPLEMENTATION

6.1	INTRODUCTION	214
6.2	STRUCTURE OF THE PROGRAM	215
6.3	PRE-PROCESSING	217
6.4	BOUNDARY CONDITIONS	219
6.4.1	Contact Condition At Soil-Foundation Interfaces	219
6.4.2	Difficulties In Modelling The Traction Discontinuity	222
6.4.3	The Elimination Method	223
6.4.4	Treatment Of Corners And Edges	227
6.5	MATRIX ASSEMBLY	230
6.5.1	Numerical Integration Modules	230
6.5.2	Assembly Of System Matrices	230
6.5.3	Symmetry	231
6.6	SOLUTION OF SYSTEM MATRIX	233
6.7	CALCULATION OF FOUNDATION STIFFNESSES	234
6.8	VECTORIZATION OF PROGRAM	234
6.8.1	Introduction	234
6.8.2	Vectorization Technique	235
6.8.3	Results	236
6.9	SUMMARY	237
APPENDIX 6.1	: INPUT SPECIFICATION	238
APPENDIX 6.2	: DATA GENERATED BY SUBROUTINE DATGEN	241

CHAPTER 7 DYNAMIC RESPONSE OF MACHINE FOUNDATIONS

7.1	INTRODUCTION	255
7.2	DYNAMIC STIFFNESSES AT VERY HIGH FREQUENCIES	257
7.3	EFFECTS OF FOUNDATION SHAPE	259
7.4	EFFECTS OF EMBEDMENT	261
7.5	INCOMPRESSIBLE MEDIA	264
7.5.1	Surface Foundations On Incompressible Halfspace	264
7.5.2	Embedded Foundations In Incompressible Halfspace	267
7.6	CONCLUSIONS	268

CHAPTER 8 CONCLUSIONS

8.1	SUMMARY AND CONCLUSIONS	291
8.2	RECOMMENDATIONS FOR FUTURE WORK	293

REFERENCES		295
------------	--	-----

Notation

[A]	the system matrix
A_0	the area of the foundation
A, A'	two distinct elastodynamic states
$A_1 \dots A_n$	are n "weights" of Gauss-Legendre integration
B	the radius of the circular foundation or one half the width of rectangular foundations
{B}	constant array
C	the imaginary part of the impedance function
C_e	the equivalent dashpot
\hat{C}_{ij}	is a 3x3 matrix arising from the treatment of the improper surface integral involving T_{ij}
C_{ij}	$= (\delta_{ij} - \hat{C}_{ij})$
C_1	the propagation velocity of dilatational waves
C_2	the propagation velocity of shear waves
C_R	the propagation velocity of Rayleigh waves
D	the maximum distance between the element being integrated and the error contour
D_d	dynamic decay function
D_{min}	the minimum distance between the boundary element being integrated and the source point
D_s	static decay function
E	modulus of elasticity
E_n	truncation errors incurred in Gauss-Legendre quadrature
F_{ijk}	the third order tensor
G	the shear modulus of elasticity
G_{ij}, T_{ij}	dynamic fundamental solutions
G_{ij}^{st}, T_{ij}^{st}	Static fundamental solutions
G_{ij}, T_{ij}	Stokes's solutions
I_a	the analytical integral value of an element
I_{ar}, I_{ai}	real part and imaginary part of an integral value, respectively
I_{bx}, I_{by}	the second moments of area about the X and Y axes of the base mat
I_j	the absolute integral value of jth patch
I_{nr}, I_{ni}	real part and imaginary part of an oscillatory integral, respectively
J	the jacobian
J_1	the jacobian for infinite elements
J_l	the jacobian relating the transformation from (ξ, η) system to (p, q) system
J_m	the jacobian relating the transformation from (s, t) system to (ξ, η) system
J_n	the jacobian relating the transformation from (x, y) system to (s, t) system
K	the real part of the impedance function
K_e	the stiffness of the equivalent spring
K_α^{st}	the static stiffness of the foundation
K_α	the impedance of the foundation
L	the length of the interface between finite and infinite boundary elements
L_e	the dimension of the element being integrated
M	the number of boundary elements
M_r	the mesh-foundation ratio
M_α	quadratic shape function
N	the aspect ratio
N_A	the dimension of matrix [A]
N_f	the number of elements for the discretization of soil-foundation interface
N_{max}	specified maximum allowable integration order
N_{min}	specified minimum allowable integration order
N_{req}	the required integration order
N_α	the shape functions

P_n the Legendre polynomial
 $Q(t)$ the time-dependent exciting force
 $[Q]$ the contribution of infinite region S_B
 $S=S_1+S_2$ the surface of the problem domain
 S_c soil-foundation interface
 S_F the core region
 S_H the hemispherical surface with radius approaching infinity
 S_I the far-field
 S_A the circular area which can be drawn around the source point such that it contains the core region
 S_B the surface of the halfspace with S_A deleted
 $[S^T]$ the transformation matrix
 $U_k(x, t)$ the displacement vector at a point x and time t
 U_{i0} initial displacement
 $U_{i\alpha}, T_{i\alpha}$ nodal values
 U_i, T_i the prescribed boundary quantities
 $[U], [T]$ coefficient matrices containing the contributions of integrals of G_{ij} and T_{ij} , respectively.
 $[U^F]$ displacement array at the foundation centre
 V_{La} Lysmer's analog velocity
 V_{i0} initial velocity
 V the problem domain
 V_{ce} the compression-extension wave velocity
 $X_{i\alpha}$ the nodal coordinates
 $\{X\}$ unknown nodal quantities
 $\{Y\}$ known nodal quantities
 $Z(t)$ the vertical displacement.

a, b integral interval
 $a_1 \dots a_n$ are n abscissae of Gauss-Legendre integration
 a_0 the dimensionless frequency
 $\{b\}$ sub-matrix of constant array $\{B\}$
 c_α the damping coefficient
 f_i the body force vector
 f^{2n} the $(2n)$ th derivative of f
 $g(\)$ the Dirac delta function
 i the unit imaginary number
 k_α the stiffness coefficient
 m total foundation mass
 m_e the equivalent mass
 m_f fictitious mass
 n the outward normal vector on a differential element of the surface
 n_j the outward pointing unit normal vector
 n_{r1}, n_{r2} integration order used in x_1 and x_2 directions, respectively.
 p an arbitrary point on a boundary element
 p_v uniformly distributed vertical load
 q_v the amplitude of time-dependent exciting force.
 q the number of nodes of an element
 r distance between the source point and field point
 r_e equivalent radius
 r_c the radius of the circular foundation
 r_0 the distance between the decay centre and the reference point
 t time
 $\{t\}, \{u\}$ nodal traction and displacement vectors
 u_z the far-field vertical displacement
 u_{0z} the vertical displacement at the reference point
 $u_{i\alpha}$ the far-field displacement
 $u_{i\alpha 0}$ the displacements at the reference point
 $\{u^p\}$ displacement at point p
 $w(x)$ weight function
 w_z vertical displacement
 x_i, y_i the global nodal coordinates
 y a point on the surface of the domain
 z the amplitude of the vertical displacement

α_s the singular vertex angle
 δ the radius of finite region S_A
 δ_{ij} the Kronecker delta
 ϵ relative error
 ϵ_a allowable error
 κ the wave number
 ρ the mass density.
 λ_R the Rayleigh wavelength
 ν Poisson's ratio.
 ν_i $=1/[\pi(1-\nu)]$
 ξ an interior point
 ω the frequency of the exciting force.
 τ_{ij} the stress tensor
 Δ_i i-th translational components of the foundation
 θ_i (small) rotational components with respect to the i-axis
 η, ξ the intrinsic coordinate system of the element
 $\dot{\quad}$ denotes differentiation with respect to time
 $*$ the Riemann convolution product

the subscripts

ijk Cartesian coordinate system
 α the vibration mode of the foundation.
 comma denotes differentiation with respect to a space variable

the superscripts

prime non-singular quantities
 asterisk singular quantities

LIST OF TABLES

TABLE 3.1	Values of D/L_e for the specified accuracy, $\int 1/r dS$
TABLE 3.2	Values of D/L_e for the specified accuracy, $\int 1/r^2 dS$
TABLE 3.3	Values of D/L_e for the specified accuracy, $\int e^{ikr}/r dS$
TABLE 3.4	Values of D/L_e for the specified accuracy, $\int e^{ikr}/r^2 dS$
TABLE 4.1	Numerical evaluation of singular integrals, $\int N/r dS$
TABLE 4.2	Numerical evaluation of singular integrals, $\int N/r^2 dS$
TABLE 4.3	Effect of the singular vertex angle
TABLE 4.4	Numerical evaluation of singular integrals, $\int Ne^{ikr}/r dS$
TABLE 4.5	Numerical evaluation of singular integrals, $\int Ne^{ikr}/r^2 dS$
TABLE 5.1	Asymptotic static far-field behaviour at the surface of a homogeneous halfspace
TABLE 5.2	Euler integration of oscillatory function $\int T_{13} D_d dS$
TABLE 5.3	Values of dimensionless displacement
TABLE 6.1	Subroutine functions
TABLE 6.2	CPU-time for vectorized and scalar programs

LIST OF FIGURES

- FIGURE 1.1 Allowable vertical vibration amplitude for a particular frequency of vibration
- FIGURE 1.2 Six modes of vibration for a rigid foundation
- FIGURE 1.3 Steady-state spectra predicted by Lysmer's analog
- FIGURE 1.4 Approximation of data points
-
- FIGURE 2.1a Symmetrical Behaviour of G_{ij}
- FIGURE 2.1b Symmetrical Behaviour of T_{ij}
- FIGURE 2.2a Convergence behaviour of G_{ij}
- FIGURE 2.2b Convergence behaviour of T_{ij}
- FIGURE 2.3 Various boundary elements
-
- FIGURE 3.1 Error contour of numerical integration over $1/r$
- FIGURE 3.2 Error contour of numerical integration over $1/r^2$
- FIGURE 3.3 Analytical contours and approximate contours in the first quadrant
- FIGURE 3.4 Equi-distant envelope of error contour
- FIGURE 3.5 Choice of required integration order, $1/r$
- FIGURE 3.6 Choice of required integration order, $1/r^2$
- FIGURE 3.7 Numerical example
- FIGURE 3.8 Adaptive integration scheme, $1/r$
- FIGURE 3.9 Adaptive integration scheme, $1/r^2$
- FIGURE 3.10 Error contour of numerical integration, e^{ikr}/r
- FIGURE 3.11 Error contour of numerical integration, e^{ikr}/r^2
- FIGURE 3.12 Comparisons between static and dynamic integrals, e^{ikr}/r
- FIGURE 3.13 Comparisons between static and dynamic integrals, e^{ikr}/r^2
-
- FIGURE 4A-1 The transformation from X-Y system to s-t system
- FIGURE 4A-2 The transformation of triangular sub-elements
- FIGURE 4A-3 Spherical coordinate system
- FIGURE 4A-4 Integration over the unbounded hemisphere
- FIGURE 4.1 Eight-noded rectangular element
- FIGURE 4.2 The sub-division and transformation method
- FIGURE 4.3 The distribution of integration points
- FIGURE 4.4 The behaviour of integrand N_i/r
- FIGURE 4.5 The behaviour of integrand N_i/r^2
- FIGURE 4.6 Study of singular vertex angle
- FIGURE 4.7 Maximum possible vertex angles
- FIGURE 4.8 Halfspace model
- FIGURE 4.9 Enclosing elements
-
- FIGURE A5.1-1 Semi-analytical integration over infinite element
- FIGURE A5.2-1 The polar coordinate system
- FIGURE 5.1 Load/displacement types
- FIGURE 5.2a The static decay function
- FIGURE 5.2b The far-field displacement behaviour
- FIGURE 5.3 The boundary of the halfspace model
- FIGURE 5.4 Fictitious decay centre
- FIGURE 5.5 The infinite boundary elements
- FIGURE 5.6 The interpolation of displacement over an infinite element
- FIGURE 5.7 The transformation of infinite element into an unit square
- FIGURE 5.8 Distribution of Gauss points over infinite element
- FIGURE 5.9 The sub-division of infinite elements
- FIGURE 5.10 Regula Falsi method
- FIGURE 5.11 Error contour of numerical integration over infinite elements
- FIGURE 5.12 Zeros of integrands $T_{13}D_d$ and $T_{23}D_d$
- FIGURE 5.13 The upper and lower bounds of numerical integration
- FIGURE 5.14 Zoning of the far-field

FIGURE 5.15	Effects of the size of mesh
FIGURE 5.16	Effects of discretization of foundation
FIGURE 5.17	Static stiffness of square foundation
FIGURE 5.18	The variation of k_v with respect to a_0
FIGURE 5.19	The variation of c_v with respect to a_0
FIGURE 5.20	Vertical displacement fields
FIGURE 6.1	Organization of the program
FIGURE 6.2	Boundary element mesh (quadrantal symmetry)
FIGURE 6.3	Contact conditions at soil-foundation interface
FIGURE 6.4	Traction discontinuities of embedded foundations
FIGURE 6.5	Double nodes at a corner
FIGURE 6.6	Traction boundary condition changes at the interface between two elements
FIGURE 6.7	2-D embedded foundation
FIGURE 6.8	The effect of embedment on static vertical foundation stiffness
FIGURE 6.9	Organization of integration module
FIGURE 6.10	Percentage of CPU time spent in subroutines
FIGURE 6.11	The performance of the scalar and vector programs
FIGURE 7.1	The rectangular foundation
FIGURE 7.2	Vertical impedance at high frequencies
FIGURE 7.3	Horizontal impedance at high frequencies
FIGURE 7.4	Rocking impedance at high frequencies
FIGURE 7.5	Cross-coupling impedance at high frequencies
FIGURE 7.6	Effect of aspect ratio on vertical impedance
FIGURE 7.7	Effect of aspect ratio on horizontal impedance (longitudinal direction)
FIGURE 7.8	Effect of aspect ratio on horizontal impedance (lateral direction)
FIGURE 7.9	Effect of aspect ratio on rocking impedance (about lateral axis)
FIGURE 7.10	Effect of aspect ratio on rocking impedance (about longitudinal axis)
FIGURE 7.11	Asymptotic damping behaviour in rocking vibration
FIGURE 7.12	The embedded foundation
FIGURE 7.13	Vertical impedances of embedded square foundations
FIGURE 7.14	Horizontal impedances of embedded square foundations
FIGURE 7.15	Rocking impedances of embedded square foundations
FIGURE 7.16	Cross-coupling impedances of embedded square foundations
FIGURE 7.17	Vertical impedances of square foundations on an incompressible halfspace
FIGURE 7.18	The "participating mass" model
FIGURE 7.19	Vertical impedances of square foundations embedded in incompressible soils
FIGURE 7.20	Horizontal impedances of square foundations embedded in incompressible soils
FIGURE 7.21	Rocking impedances of square foundations embedded in incompressible soils
FIGURE 7.22	Cross-coupling impedances of square foundations embedded in incompressible soils

CHAPTER 1

INTRODUCTION

1.1 Introduction

The need for effective and economical designs for foundations subjected to dynamic loads has become more important in recent years. This has been stimulated by the trend towards more sophisticated machines and the higher standard of in-service performance expected of such installations. General considerations and practical procedures for the design of machine foundations have been summarized by several authors, Richart et al(1970); Gazetas(1983); Davies(1991). However, the pioneering work of Richart et al(1970), which supersedes the simplified methods of Barkan(1962) and that school, is becoming increasingly outdated in view of the research work of the last two decades. For most machine foundations, the serviceability criterion is expressed in terms of the limiting amplitude of vibration at a particular frequency or a limiting value of peak velocity or peak acceleration. Serviceability is usually related to human sensitivity to vibration and/or the operational requirements of the installation itself(Figure 1.1). Often, the former condition is critical.

An important part of successful machine foundation design is the engineering analysis of the foundation response to the dynamic loads from the anticipated operation of the machine. Of particular interest is the evaluation of the steady-state response due to a harmonic excitation. Since the magnitudes

of vibration satisfying the design criteria usually involve displacement amplitudes of a few tens of micrometres, soils may be considered to behave approximately as linear elastic materials for small amplitudes of strain. In addition, analyses of experimental results (Dobry et al, 1986) suggest that in reasonably homogeneous soil deposits, a representative "equivalent" value of the shear modulus of the soil can be used to predict small-amplitude response of machine foundations. Consequently, in many cases, the soil properties can be defined by the mass density, ρ , Poisson's ratio, ν , and the shear modulus of elasticity, G . The effect of material damping in the soil can be incorporated by using the correspondence principle of viscoelasticity (Lysmer, 1980).

Practical analyses usually assume that massive machine foundations are rigid (Gazetas, 1983). Vertical and horizontal translations and rotations about horizontal and vertical axes are then sufficient to describe the motion of the foundation (Figure 1.2). It should be noted that vertical and torsional vibration can occur independently of any other motion, while horizontal translation and rocking are usually coupled. Theoretical studies (Achenbach, 1976; and Eringen and Suhubi, 1975) of wave propagation through an elastic halfspace form the mathematical basis of most numerical methods used to perform the analyses of these problems. A brief review of methods used for the analysis and design of machine foundations is presented below. More detailed reviews can be found in the relevant chapters. This chapter concludes with an outline of the scope and objectives of this study.

1.2 Analytical Methods

Reissner's pioneering work in 1936 (Sung, 1953) indicated that, based on the assumption of uniform contact pressure distribution, the vertical response of a disc resting on an

elastic halfspace can be evaluated by integrating Lamb's solution(1904) over the contact area. However, more accurate solutions necessitate knowledge of the distribution of the dynamic contact stresses beneath foundations. Several researchers(Sung, 1953; Thomson and Kobori, 1963; Arnold, et al, 1955; among others) extended Reissner's idea to obtain approximate solutions in the low frequency range by assuming various stress distributions in the elastic medium immediately underneath the footing. While these assumed stress distributions significantly simplify the analysis, it should be noted that this approach fails to satisfy the rigid body displacement condition, in general. To circumvent this difficulty, Sung(1953) and Thomson and Kobori(1963) computed the compliance of the foundation by assuming that the settlement was equal to the magnitude of the displacement at the centre of the footing. Arnold et al(1955) obtained close agreement with experimental results by taking a weighted average displacement; at any radius the weighting factor was taken to be proportional to the assumed static stress at that radius.

In order to carry out a rigorous analysis, it is necessary to model the vibrating soil-foundation system as a mixed boundary-value problem, in which the displacements are prescribed at the contact area between the soil and the foundation while the rest of the surface of the halfspace is traction-free. Approximate solutions to the mixed boundary-value problem has been obtained by a number of authors(Luco and Westmann, 1971; Karasudhi et al, 1968; Veletsos and Wei, 1971; and Pak and Gobert, 1991; among others) by assuming relaxed boundary conditions. These approximations entail the assumption that for vertical and rocking vibrations, the contact is assumed to be smooth while for torsional and horizontal vibrations, the normal contact traction is zero. Essentially, the problem may be formulated in terms of a set of dual integral equations; one equation specifies the displacements given by the foundation and the

second represents the traction-free condition exterior to the contact region(See Awojobi and Grootenhuis, 1965, for more details). The dual integral equations can be transformed into Fredholm integral equations of the second kind which may be solved numerically(Delves and Walsh, 1974).

Most analytical solutions for the dynamic response of foundations have been restricted to strip or circular foundations resting on elastic halfspaces, except for the results of rectangular foundations given by Thomson and Kobori (1963). Analytical methods necessarily involve many assumptions and simplifications that must be recognized, but they can often provide valuable insights less easily discerned from numerical analyses.

1.3 Numerical Methods

Fundamental to current methods of analysis of machine foundations is the evaluation of the dynamic stiffnesses ("impedances") of rigid massless foundations(the geometry of the massless foundation is taken equal to those of the real massive foundation). As shown by Gazetas(1983), the dynamic impedance is simply a generalisation of the spring and dashpot constants in Lysmer's analog(Lysmer and Richart, 1966). For each mode of excitation with harmonic frequency ω , the impedance may be cast in the complex (arithmetic) form:

$$K_{\alpha} = K + i\omega C \quad (1.1)$$

where K and C are the real and imaginary parts of the impedance, respectively; the subscript α is used in a generalized sense to denote the vibration mode of the foundation, and i is the unit imaginary number.

The determination of the impedances of machine foundations has

received considerable attention in recent years; extensive reviews were presented by Gazetas(1983) and Novak(1987). Because machine foundations can take complicated geometrical forms and may be buried beneath the ground surface, it is usually necessary to resort to numerical methods to calculate their impedances.

The Boundary Element Method

During the past two decades the boundary element method has emerged as a strong candidate for the analysis of dynamic problems(Banerjee and Butterfield, 1981; Beskos, 1987; Manolis and Beskos, 1988; and Manolis and Davies, 1993). Because the boundary element method takes into account the radiation conditions to infinity, it requires no special transmitting boundaries, unlike the finite element method. Furthermore, for linear problems only the surface of the problem domain needs to be discretized; i.e., the use of the boundary element method can reduce the spatial dimensions of the problem by one. Consequently, boundary element methods are ideally suited for analyses of three-dimensional machine foundations since almost all of their advantages are exploited.

Dominguez and Roesset(1978) were the first to use the boundary element method to compute the impedance function of rectangular foundations at the surface, or embedded in an elastic halfspace. Since then, many researchers have obtained solutions to foundation vibration problems using the boundary element method for low and moderate frequency of excitation (in general, $a_0 \leq 2$). They include: Ahmad and Bharadwaj(1991) and Antes and von Estorff(1989) for strip foundations; Alarcon et al(1989); Wang and Banerjee(1990); and Emperador and Dominguez (1989) for circular foundations; Tohdo et al(1986); Israil and Banerjee(1990); and Gazetas and Tassoulas(1987a and 1987b) for rectangular foundations; among many others. Clearly, the

exploitation of boundary element methods in the recent past represents one of the most important advances in the development of efficient procedures for the analysis of machine foundations. For the purposes of this thesis, this method of analysis has been employed to obtain numerical results for machine foundations subjected to high frequency loading. However, for completeness, a very brief review of the attributes of one possible alternative method (namely, the finite element method) follows.

The Finite Element Method

The finite element method is easily the most popular numerical technique for the solution of engineering problems (Zienkiewicz and Taylor, 1989). But the use of finite element methods for analyzing dynamic halfspace problems inevitably involves the truncation of the semi-infinite domain to a mesh of finite size; the difficulty then arises that outwardly propagating waves must be transmitted through (or absorbed) by the boundaries without reflection.

Special transmitting boundaries (Lysmer and Kuhlemeyer, 1969; Lysmer and Waas, 1972; and Kausel and Roesset, 1975; among many others) have been developed to prevent such spurious wave reflections. Two dimensional and axisymmetric transmitting boundaries can be accommodated without too much difficulty but truly three dimensional and fully general transmitting boundaries are very difficult to construct. Impedance functions for strip and circular foundations, obtained by finite element methods incorporating transmitting boundaries, have been presented by Kausel and Roesset (1975); Tassoulas and Kausel (1983); and Valliappan et al (1977). Because no satisfactory methods have been developed for allowing elastic waves to pass through the lower boundary of finite element models, it is necessary to assume that (rigid) rock occurs at

relative shallow depth. The high cost of three-dimensional analyses and these unresolved problems associated with the transmitting boundaries limit the use of the finite element method to analyze machine foundation problems.

Dynamic infinite elements have also been developed to represent the unbounded domain, see Bettess and Bettess (1991) and Bettess (1992) for more details. But, because there are three distinct waves in an elastic halfspace, the infinite element formulation for elastodynamics becomes extremely complicated.

Hybrid methods coupling the finite element method and the boundary element method have been shown in recently years to be an efficient means of eliminating the difficulty of artificial boundaries in the finite element mesh (Spyrakos et al, 1989; von Estorff and Prabucki, 1988; and Touhei and Yoshida, 1988). The basic idea is a combination of the boundary element method, which is used to deal with the unbounded exterior domain, and the finite element method, by which the core region is analyzed. By enforcing compatibility and equilibrium conditions at the common interface, Luco and Wong (1987) and Mita and Luco (1989a and 1989b) obtain impedance functions of three-dimensional embedded foundations.

1.4 Design Methods

Lysmer's Analog

Motivated by the similarity of response curves between the single-degree-of-freedom (SDOF) system and elastodynamic halfspace solutions, numerous attempts have been made to describe the response of foundations on the halfspace in terms of equivalent mass-spring-dashpot systems (Richart, 1960; Hsieh, 1962; Whitman, 1966; and Wolf, 1991). The procedure involves adjusting the frequency-dependent parameters of the equivalent

system such that the resulting response matches that predicted by the halfspace theory. In some cases, in addition to the mass of the foundation and the machine, a frequency-dependent "participating mass" of soil has to be invoked to obtain satisfactory results (Crockett and Hammond, 1948; Barkan, 1962; and Awojobi, 1971).

Lysmer and Richart (1966) developed a simplified analog for determining the vertical displacement $Z(t)$ of a rigid disc (radius r_c , mass m_e) resting on the elastic halfspace and subjected to a vertical load $Q(t)$, where t is time. The equation of motion for this analog is

$$m_e \frac{d^2 Z(t)}{dt^2} + C_e \frac{dZ(t)}{dt} + K_e Z(t) = Q(t) \quad (1.2)$$

where the static stiffness $K_e = 4Gr_c / (1-\nu)$, the high-frequency asymptotic damping value $C_e = \rho A_0 V_{ce}$, in which A_0 is the contact area (πr_c^2) and V_{ce} is the compression-extension wave velocity. Note that Equation (1.2) has a form similar to that of a SDOF system. A notable feature of the analog is that the lumped parameters, the equivalent mass m_e , dashpot C_e and spring K_e are independent of the frequency of the exciting force. It can be shown that (without invoking a participating soil mass) the analog yields response curves that only slightly differ from the 'exact' solution at low to moderate excitation frequencies (Figure 1.3). The success of Lysmer's analog in establishing the bridge between the halfspace-theory and the lumped parameter system has had a significant influence on the analysis of machine foundations.

The lumped-parameter approximations described by Whitman and Richart (1967) and Richart et al (1970) are extensions of Lysmer's analog to all vibration modes and to non-circular foundations. The usual practice for non-circular foundations is to take an equivalent circle of the same area (translational

modes) or equal moment of inertia (rotational modes). Lumped-parameter models with more than three components have been proposed by Wolf and Somaini (1986); de Barros and Luco (1990); Jean et al (1990); and Wolf (1991).

Impedance Methods

In recent years there has been a considerable increase in the number of simple engineering formulas and charts developed for the calculation of the foundation impedances. It continues the practice of approximating numerical or analytical results by algebraic expressions (Hsieh, 1962; Ratay, 1971; and Beredugo and Novak, 1972). The validity of this approach has been explored by Dobry et al (1986) and Gazetas and Stokoe (1991).

These engineering approximations are derived from results obtained from various researchers using different soil-foundation contact conditions; using a variety of analytical or numerical approaches; and using calculations performed with various degrees of precision. Usually, analytical and numerical results are plotted as raw data points in dimensionless charts, and approximations are developed to fit curves to these data points (Figure 1.4). A large number of simple algebraic formulas and dimensionless parametric charts have been developed in the literature (Dobry and Gazetas, 1985 and 1986; Pais and Kausel, 1988; Gazetas, 1991; Davies, 1991; among others). However, the approximations advanced for rectangular foundations (for example, Dobry and Gazetas, 1986; and Pais and Kausel, 1988) are based on scant data, especially for incompressible soils and particularly for high operating frequencies. These engineering approximations are generally limited to dimensionless frequencies (a_0) of less than two and Poisson's ratios between 0.25 to 0.4. The dimensionless frequency a_0 is given by the equation:

$$a_0 = \frac{\omega B}{C_2} \quad (1.3)$$

in which B is the radius of circular foundations or one-half the width of rectangular foundations and

$$C_2 = \sqrt{\frac{G}{\rho}} \quad (1.4)$$

is the propagation velocity of shear waves in the halfspace.

The use of simple engineering methods may involve some loss of precision. Nevertheless, well-conceived, simple equations, with adequate explanations of their basis and limitations, are extremely useful to practising engineers. They can provide practical design solutions and, more importantly, a simple guide to understand the role and significance of the main parameters controlling machine foundation dynamics. In practice, engineering approximations can be used for preliminary estimates, to understand behavioural aspects or when more rigorous analyses are not warranted.

Superstructure Response

Several substructure methods for the dynamic analysis of foundations have been presented in the literature (Kausel and Roesset, 1974; Kausel et al, 1978; and Roesset, 1980a). The basic approach in all these methods is to partition the complete soil-foundation system into two parts, the structure and the soil. The semi-infinite soil domain is analyzed first and the impedance, at the soil-foundation interface, is established. In the second step, these foundation stiffness are incorporated with the equations of motion of the structural system, and the overall response is computed. This approach offers considerable flexibility in the way each step is

handled.

Practical procedures for the evaluation of the steady-state response of rigid machine foundations have been described by Gazetas(1983). For example, the amplitude of the vertical displacement at the centre of gravity is given by equation:

$$z = \frac{q_v}{K_v(\omega) - m\omega^2} \quad (1.5)$$

in which, the subscript v is used to identify the (vertical) vibration mode, m is total foundation mass and q_v is the amplitude of the exciting force. Clearly, the evaluation of impedance functions for massless foundations plays a key role in the analysis of machine foundations. Once this has been done, the dynamic response of the actual system can be estimated by a straightforward operation.

1.5 Discussion

The analysis of machine foundations is concerned with attempts to develop rational methods to predict the response of foundations subjected to dynamic loads. Its history embraces that of developments in the mathematical and physical principles necessary to simulate this complicated problem, and of the advent of fast digital computers. Naturally, there has been continuous progress since the pioneering work of Reissner in 1936. Some of these works have of course been superseded because they are based on inadequate assumptions (for example, uniform contact stress distribution) or involve considerable simplifications of the physical model (eg, relaxed boundary conditions).

Because analytical methods can be used in very few highly idealized situations, there has been a great emphasis placed

on the development of numerical techniques. In particular, the boundary element method has been successfully used in recent years for the analysis of machine foundations. However, rigorous boundary element analyses of high frequency foundation response has remained unsolved because of the difficulties of representing and integrating the highly oscillatory spatial functions. In addition, solutions for the special case of incompressible media, since the effect of Poisson's ratio on the impedance function is particularly significant (Awojobi, 1971; and Veletsos and Wei, 1971), has not been rigorously studied by boundary element methods. These difficulties are overcome in the present study and a number of new results which should prove useful in practice are obtained.

1.6 Outline Of Thesis Contents

The object of the present study is the further extension and refinement of boundary element techniques for the analyses of machine foundations. Chapter II presents the derivation of the boundary integral formulation and a close study of the characteristics of the dynamic kernel functions. With respect to the improvement of computational accuracy and efficiency of the boundary element analysis, advanced integration schemes for non-singular and singular elements are developed in chapter III and chapter IV, respectively. A novel infinite boundary element for dynamic analyses is developed in chapter V, which provides an efficient means for including far-field effects, without the necessity of explicit discrete representation outside the near field. The implementation and vectorization of the boundary element method program are described in chapter VI. Chapter VII presents various results for rectangular foundations to illustrate the potential of the infinite boundary element formulation. In Chapter VIII, the conclusions of the study are drawn together and some suggestions made for further work in this area.

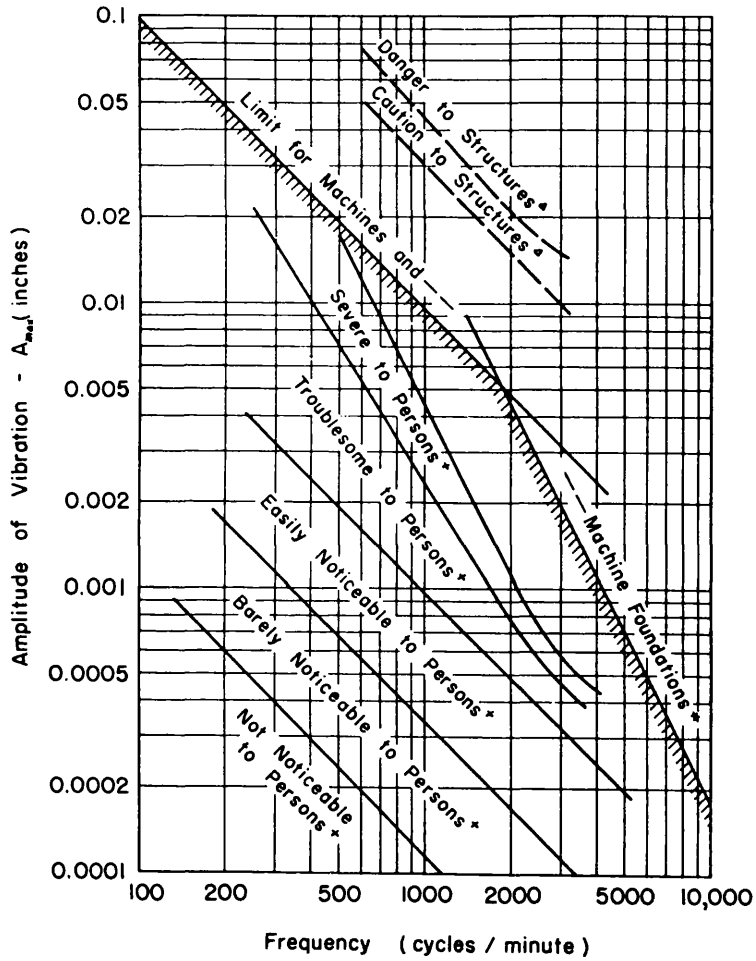


Figure 1.1 Allowable Vertical Vibration Amplitude For A Particular Frequency Of Vibration (from Richart, 1960)

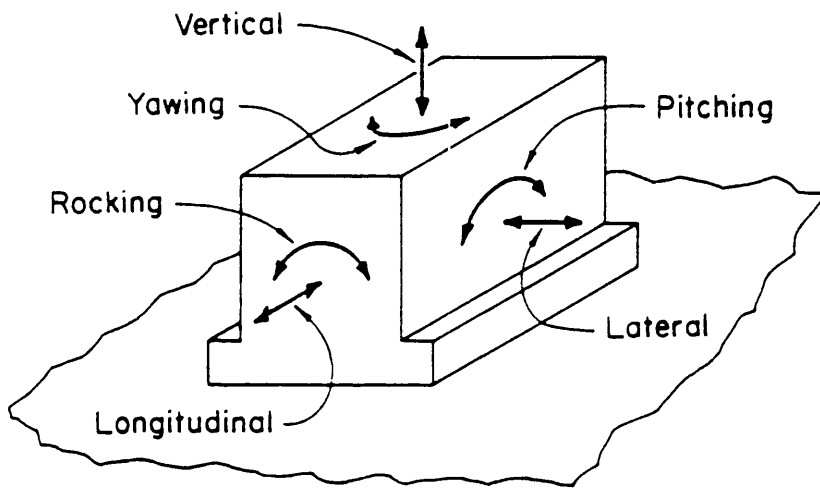


Figure 1.2 Six Modes of Vibration For A Rigid Foundation ((from Richart, 1960)

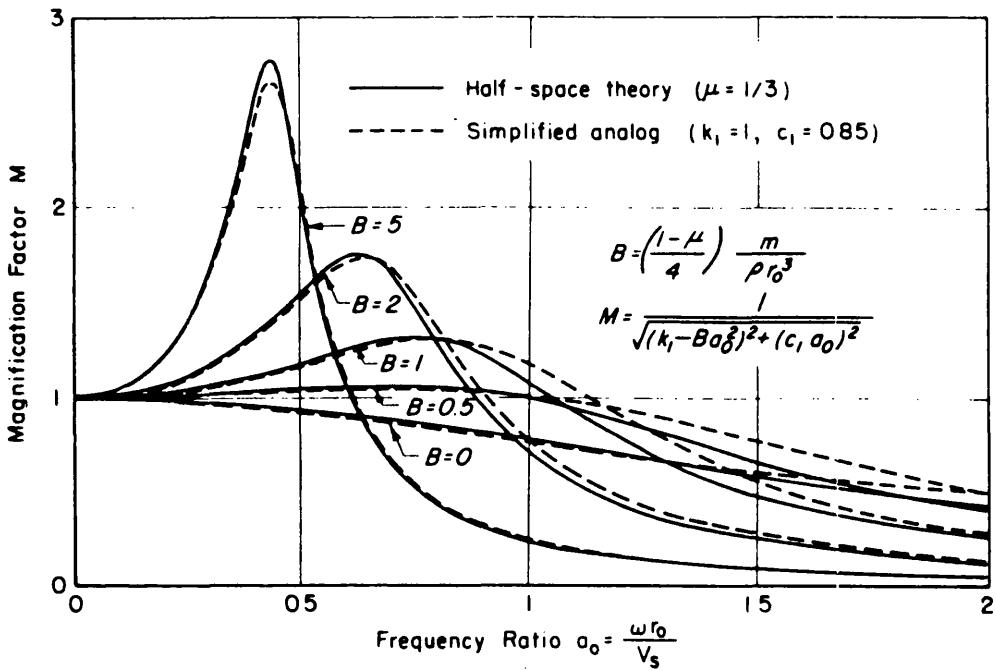
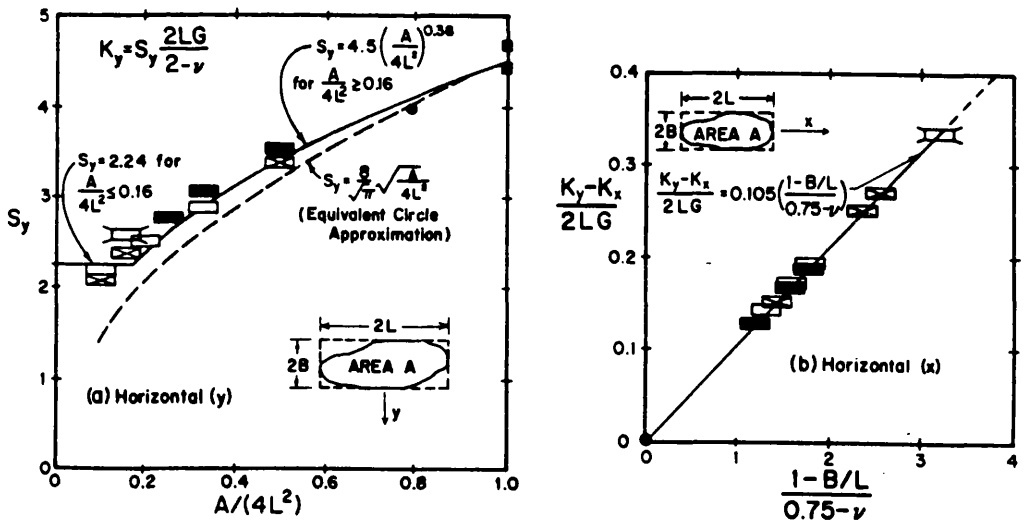


Figure 1.3: Steady-State Spectra Predicted By Lysmer's Analog (from Lysmer and Richart, 1966)



Horizontal Static Stiffnesses K_y and K_x versus Base Shape

Figure 1.4: Approximation Of Data Points (from Dobry and Gazetas, 1986)

CHAPTER 2

BOUNDARY ELEMENT FORMULATIONS FOR ELASTODYNAMICS

2.1 Introduction

During recent years, the boundary element method has found considerable applications in the solution of engineering problems, such as elastoplasticity, elastodynamics, diffusion problems and fracture mechanics. The periodical *Boundary Elements Abstracts and Newsletter*, besides the many scientific and technical journal articles and the proceedings of a number of international conferences, summarizes current research activities.

Cruse and Rizzo(1968) and Cruse(1968) were the first to use the boundary element method to solve general transient problems. In their studies, the direct boundary integral equations are derived to represent a system of constraint equations between the displacements and tractions on the boundary of the problem domain. Given the prescribed boundary conditions, numerical solutions of the boundary unknowns were obtained by employing a systematic discretization scheme. The interior displacement and traction fields can then be calculated without special difficulty. Since then, many researchers(reviewed by Beskos, 1987; and Manolis et al, 1993) have obtained solutions to elastodynamic problems using the boundary element method.

This chapter reviews the theoretical development of boundary

integral equations for linear elastodynamics and describes the implementation of the boundary element method; in particular for the solution of three-dimensional problems. The next section presents the derivation of the integral equations, which may be considered as a general formulation for the solution of elastodynamic problems. Section three presents the reduced elastodynamic equations and the corresponding full-space fundamental solutions, which are appropriate for steady-state problems. Following that, characteristics of the fundamental solutions and special formulae for incompressible medium are given in section four, with a view to preparing the ground for the implementation of the boundary element formulation. The derivation of direct boundary integral formulations for steady-state elastodynamics and the corresponding numerical solution procedures are described briefly in section five.

2.2 Integral Equation Formulation

2.2.1 Introduction

Many continuum problems in physics and the applied sciences are described by partial differential equations, allied with appropriate initial and boundary conditions. It is not surprising that the solution of such partial differential equations has been a major concern of analysts for over two centuries. Of course, solutions of specific initial-boundary value problems can be obtained in any one of many ways (Muskhelishvili, 1953; and Gladwell and Wait, 1979), but in this thesis, we concentrate on integral equation methods, dating from Fredholm (in 1905) and his contemporaries (see, for example, the historical review in Banerjee and Butterfield, 1981). With the aid of Green's functions (Roach, 1982), this analytical method recasts initial-boundary value problems from differential forms to integral forms. It should be noted that

the latter are often much more amenable to numerical solutions than the former. In addition, for certain classes of problems, only the boundary of the domain being investigated needs to be considered. As a consequence, integral equation methods afford a powerful means of attacking a wide range of physical and engineering problems, especially for problems characterized by infinite or semi-infinite domains (Mikhlin, 1965; and Jaswon and Symm, 1977).

In linear elastodynamics, the "direct" integral equation method starts with the dynamic reciprocal identity (Love, 1944, section 121) and, invoking the fundamental solutions of the governing equations, arrives at a formulation in terms of displacements and tractions on the boundary of the domain under consideration. This section briefly describes the derivation of integral equations for linear elastodynamics, which has been presented in considerable detail elsewhere. For more details, reference is made to Love (1944); Wheeler and Sternberg (1968); Eringen and Suhubi (1975); Achenbach (1976); and Hudson (1980).

2.2.2 Theory Of Elastodynamics

With the usual assumptions of small displacement theory and homogeneous, isotropic linear elastic material behaviour, the governing differential equation of dynamic equilibrium for a solid can be expressed as

$$(C_1^2 - C_2^2) U_{j,j_i} + C_2^2 U_{i,jj} + f_i = \ddot{U}_i \quad (2.1)$$

where the dilatational and shear wave velocities are given, respectively, as

$$C_1 = \sqrt{\frac{(2-2\nu)}{(1-2\nu)}} \cdot C_2 \quad (2.2)$$

$$c_2 = \sqrt{\frac{G}{\rho}} \quad (1.4, \text{ repeated})$$

In the above equations, $U_k = U_k(x, t)$ is the displacement vector at a point x and time t ; the comma and dot denote differentiation with respect to a space variable and time, respectively; f_i is the body force vector; summation over repeated indices is implied and rectangular cartesian coordinates is employed.

To complete the problem statement, the displacements and stresses must satisfy the initial conditions in the problem domain V :

$$\begin{aligned} U_i(x, 0) &= U_{i0}(x) \\ \dot{U}_i(x, 0) &= V_{i0}(x) \end{aligned} \quad (2.3)$$

and boundary conditions on the surface $S, =S_1+S_2$, of V :

$$\begin{aligned} U_i(x, t) &= U_i^*(x, t) && \text{on } S_1 \\ T_i(x, t) &= \tau_{ij}n_j = T_i^*(x, t) && \text{on } S_2 \end{aligned} \quad (2.4)$$

where U_{i0} and V_{i0} are given initial displacements and velocities; T_i and n_j are the traction components and the outward pointing unit normal vector, respectively, τ_{ij} is the stress tensor; U_i^* and T_i^* are the prescribed boundary quantities. In addition, the Sommerfeld radiation condition(see, for example, Eringen and Suhubi, 1975) must be satisfied if V is of infinite extent.

One of the requirements for a well-posed problem is that the governing equation has a unique solution. Proofs of the existence and uniqueness of the solution of the properly formulated boundary-initial value problem in elastodynamics

were given by Neumann (Love, 1944, section 124), which have been extended to unbounded domains by Wheeler and Sternberg (1968). In general, properly prescribed boundary conditions over the whole surface S of domain V will lead to a unique solution.

2.2.3 Fundamental Solutions

The fundamental solutions of the governing equation are of basic importance in the formulation of integral equations for elastodynamics. In an infinite medium, the wave field generated by a concentrated force of arbitrary time function is called Stokes' solution (See Love, 1944, section 212). The displacement component in the i -direction at point $x(x_1, x_2, x_3)$, due to a concentrated force acting at $\xi(\xi_1, \xi_2, \xi_3)$ in the j -direction is given by:

$$G_{ij}^*(x, t; \xi) = \frac{1}{4\pi\rho} \left\{ \left(\frac{3r_i r_j}{r^3} - \frac{\delta_{ij}}{r} \right) \int_{\frac{1}{c_1}}^{\frac{1}{c_2}} \lambda \cdot g(t - \lambda r) d\lambda \right. \\ \left. + \frac{r_i r_j}{r^3} \left[\frac{1}{c_1^2} \cdot g\left(t - \frac{r}{c_1}\right) - \frac{1}{c_2^2} \cdot g\left(t - \frac{r}{c_2}\right) \right] + \frac{\delta_{ij}}{r c_2^2} \cdot g\left(t - \frac{r}{c_2}\right) \right\} \quad (2.5)$$

in which δ_{ij} denotes the Kronecker's delta, $g(\cdot)$ is the Dirac delta function, and

$$r = \sqrt{(x_i - \xi_i) \cdot (x_i - \xi_i)} \quad (2.6)$$

The corresponding stress tensor can be obtained by substituting $G_{ij}^*(x, t; \xi)$ into Hooke's law. Explicit expressions can be found in Eringen and Suhubi (1975):

$$\begin{aligned}
 T_{ij}^*(\mathbf{x}, t; \xi) &= \rho [(C_1^2 - 2C_2^2) G_{mk,m}^* \delta_{ij} + C_2^2 (G_{ik,j}^* + G_{jk,i}^*)] \cdot n_j \\
 &= F_{ijk}(\mathbf{x}, t, \xi) \cdot n_j
 \end{aligned} \tag{2.7}$$

where the third order tensor F_{ijk} is

$$\begin{aligned}
 F_{ijk}(\mathbf{x}, t, \xi) &= \frac{1}{4\pi} \left\{ -6C_2^2 \left[\frac{5r_i r_j r_k}{r^5} - \frac{\delta_{ij} r_k + \delta_{ik} r_j + \delta_{jk} r_i}{r^3} \right] \int_{\frac{1}{c_1}}^{\frac{1}{c_2}} \lambda \cdot g(t - \lambda r) d\lambda \right. \\
 &+ 2 \cdot \left[\frac{6r_i r_j r_k}{r^5} - \frac{\delta_{ij} r_k + \delta_{ik} r_j + \delta_{jk} r_i}{r^3} \right] \left[g\left(t - \frac{r}{C_2}\right) - \frac{C_2^2}{C_1^2} \cdot g\left(t - \frac{r}{C_1}\right) \right] \\
 &\quad + \frac{2r_i r_j r_k}{r^4 C_2} \left[\dot{g}\left(t - \frac{r}{C_2}\right) - \frac{C_2^3}{C_1^3} \cdot \dot{g}\left(t - \frac{r}{C_1}\right) \right] \\
 &\quad - \frac{\delta_{ij} r_k}{r^3} \left(1 - \frac{2C_2^2}{C_1^2} \right) \left[g\left(t - \frac{r}{C_1}\right) + \frac{r}{C_1} \cdot \dot{g}\left(t - \frac{r}{C_1}\right) \right] \\
 &\quad \left. - \frac{\delta_{ik} r_j + \delta_{jk} r_i}{r^3} \left[g\left(t - \frac{r}{C_2}\right) + \frac{r}{C_2} \cdot \dot{g}\left(t - \frac{r}{C_2}\right) \right] \right\}
 \end{aligned} \tag{2.8}$$

2.2.4 The Dynamic Reciprocal Identity

The dynamic reciprocal identity (Love, 1944, section 121), which is an extension of Betti's reciprocal theorem to dynamic conditions, relates two distinct elastodynamic states of the same body. The identity presents a relation between two sets of displacements and stresses both satisfying the equation of dynamic equilibrium and Hooke's Law for homogeneous, isotropic, linearly elastic bodies, but with different distributions of

body forces, different initial conditions and different boundary conditions. Wheeler and Sternberg(1968) have extended this identity to unbounded bodies. The dynamic reciprocal identity is fundamental to the derivation of the integral representation for elastodynamics.

Let V be a regular region with boundary S and consider two distinct elastodynamic states

$$A = [U_i, T_i, f_i]$$

and

$$A' = [U'_i, T'_i, f'_i] \quad (2.9)$$

defined in that region and with initial conditions

$$U_i(x, 0) = U_{i0}(x)$$

$$\dot{U}_i(x, 0) = V_{i0}(x)$$

$$U'_i(x, 0) = U'_{i0}(x) \quad (2.10)$$

$$\dot{U}'_i(x, 0) = V'_{i0}(x)$$

Then, for $t \geq 0$

$$\begin{aligned} & \int_S T_i * U'_i dS + \int_V \rho [f_i * U'_i + V_{i0} U'_i + U_{i0} \dot{U}'_i] dV \\ & = \int_S T'_i * U_i dS + \int_V \rho [f'_i * U_i + V'_{i0} U_i + U'_{i0} \dot{U}_i] dV \end{aligned} \quad (2.11)$$

in which, the asterisk represents the Riemann convolution

product, i.e.,

$$\begin{aligned}
 f(x, t) * h(x, t) &= \int_0^t f(x, t-\tau) h(x, \tau) d\tau \\
 &= \int_0^t f(x, \tau) h(x, t-\tau) d\tau
 \end{aligned}
 \tag{2.12}$$

where f and h are functions of $x \in V$ and $t \geq 0$.

2.2.5 Integral Equation Formulation

By utilizing the dynamic reciprocal identity, where one of the two elastodynamics states is $[G_{ij}^*, T_{ij}^*]$, and the other one is the actual state, the direct integral formulation of elastodynamics for an interior point ξ is given by

$$\begin{aligned}
 U_i(\xi, t) &= \int_s [G_{ij}^* T_j(x, t) - T_{ij}^* U_j(x, t)] dS(x) + \rho \int_V G_{ij}^* F_j(x, t) dV(x) \\
 &\quad + \rho \int_V [G_{ij}^* V_{i0}(x) + \dot{G}_{ij}^* U_{i0}(x)] dV(x)
 \end{aligned}
 \tag{2.13}$$

The integral equations provide a complete representation of the solution to transient elastodynamic problems. In particular it should be noted that the first integral involves both the surface displacements and the surface tractions on the boundary of the problem domain. The last two integrals are related to the body forces. Since in certain problems body forces are absent (Achenbach et al, 1982), the integral identity is useful in the solution of many elastodynamic problems (for example, time-harmonic wave motions) in an unbounded medium.

The application of the integral equations to linear elastodynamic problems can be accomplished in the real time

domain directly through a time marching scheme (Ahmad and Banerjee, 1988b; and Dominguez and Gallego, 1992) or in the transformed domain with the aid of the Laplace transformation with respect to time (Cruse and Rizzo, 1968; and Doyle, 1966). Numerical inverse transformations are required in the latter approach to bring the Laplace transformed solution back to the original time domain. The integral equations for steady-state solutions can be obtained either from the equations of reduced elastodynamics or through the Fourier transformation with respect to time (the frequency domain formulations; see, for example, Kobayashi, 1987). Comparisons between these three different approaches (Manolis, 1983) indicated that the computational cost of the time domain analyses is greater than Laplace and Fourier transformed domain analyses.

2.3 Reduced Elastodynamic Problems

The importance of dynamic effects depends on the relative magnitudes of two characteristic times: the time characterizing the external application of the disturbance and the characteristic time of transmission of disturbances across the body. If the external disturbances vary in a simple harmonic manner with time and the motion is observed long after the initiation of the source, the physical components of the problem are also harmonic in time and are called steady-state. For practical purposes, it is usually assumed that the initial values for displacements and velocities are transient in nature and will disappear after a sufficient lapse of time. In this special case, consequently, the elastodynamic problem is simplified to a great extent since the time dependency is eliminated and the initial-boundary value problem is then reduced to a boundary value problem only.

Substituting the steady-state displacement vector and stress tensor

$$U(x, t) = u(x, \omega) e^{-i\omega t} \quad (2.14)$$

$$T(x, t) = t(x, \omega) e^{-i\omega t}$$

into equation(2.1), the governing equation of steady-state elastodynamics is:

$$(C_1^2 - C_2^2) u_{j,j i} + C_2^2 u_{i,j j} + f_i + \omega^2 u_i = 0 \quad (2.15)$$

As is evident, the exponential term $e^{-i\omega t}$ has been omitted for reasons of simplicity. This time-independent equation is called the reduced field equation of elastodynamics (Eringen and Suhubi, 1975), which is the same as that derived from the Fourier transformation. It should be noted that the originally hyperbolic governing equation has become elliptic in the frequency domain where it can be solved as a static-like problem with respect to frequency.

The integral equation formulation for the reduced elastodynamics becomes much simpler and can be written as

$$u_i(\xi, \omega) = \int_S [G_{ij}(x, \xi, \omega) t_j(x, \omega) - T_{ij}(x, \xi, \omega) u_j(x, \omega)] dS(x) + \rho \int_V G_{ij}(x, \xi, \omega) f_j(x, \omega) dV(x) \quad (2.16)$$

The corresponding fundamental solutions (Eringen and Suhubi, 1975) are given by

$$G_{ij}(x, \xi, \omega) = \frac{1}{4\pi G} [\Psi \delta_{ij} - \Gamma r_{,i} r_{,j}] \quad (2.17)$$

and

$$\begin{aligned}
 T_{ij}(x, \xi, \omega) = & \frac{1}{4\pi} \left\{ \left[\frac{d\Psi}{dr} - \frac{\Gamma}{r} \right] (\delta_{ij} \frac{\partial r}{\partial n} + r_{,j} n_i) - \frac{2\Gamma}{r} (r_{,i} n_j - 2r_{,i} r_{,j} \frac{\partial r}{\partial n}) \right. \\
 & \left. - 2 \frac{d\Gamma}{dr} r_{,i} r_{,j} \frac{\partial r}{\partial n} + \left[\left(\frac{C_1}{C_2} \right)^2 - 2 \right] \left(\frac{d\Psi}{dr} - \frac{d\Gamma}{dr} - \frac{2\Gamma}{r} \right) r_{,i} n_j \right\} \quad (2.18)
 \end{aligned}$$

where

$$r_{,i} = \frac{(x_i - \xi_i)}{r} \quad (2.19)$$

$$\begin{aligned}
 \Psi = & \frac{1}{r} \left[\left(-\frac{C_2^2}{\omega^2 r^2} + \frac{iC_2}{\omega r} + 1 \right) e^{\frac{i\omega r}{C_2}} \right. \\
 & \left. - \left(\frac{C_2}{C_1} \right)^2 \left(-\frac{C_1^2}{\omega^2 r^2} + \frac{iC_1}{\omega r} \right) e^{\frac{i\omega r}{C_1}} \right] \quad (2.20)
 \end{aligned}$$

$$\begin{aligned}
 \Gamma = & \frac{1}{r} \left[\left(-\frac{3C_2^2}{\omega^2 r^2} + \frac{3iC_2}{\omega r} + 1 \right) e^{\frac{i\omega r}{C_2}} \right. \\
 & \left. - \left(\frac{C_2}{C_1} \right)^2 \left(-\frac{3C_1^2}{\omega^2 r^2} + \frac{3iC_1}{\omega r} + 1 \right) e^{\frac{i\omega r}{C_1}} \right] \quad (2.21)
 \end{aligned}$$

and

$$\frac{\partial r}{\partial n} = r_{,i} n_i \quad (2.22)$$

in which n is the outward normal vector on a differential element of the surface S . These fundamental solutions are also called the full-space Green's functions. Their simple forms in the frequency domain have made them very popular among researchers in the field.

The static problem is a special case of the dynamic problem, for which $\omega=0$. For reasons of completeness, the static fundamental solutions G_{ij}^{st} and T_{ij}^{st} are given, respectively, as

$$G_{ij}^{st}(x, \xi) = \frac{1}{16\pi Gr(1-\nu)} [(3-4\nu)\delta_{ij} + r_{,i}r_{,j}] \quad (2.23)$$

$$T_{ij}^{st}(x, \xi) = \frac{-1}{8\pi(1-\nu)r^2} \{ [(1-2\nu)\delta_{ij} + 3r_{,i}r_{,j}] \frac{\partial r}{\partial n} + (1-2\nu)(r_{,j}n_i - r_{,i}n_j) \} \quad (2.24)$$

2.4 Fundamental Solution Characteristics

The mathematical properties and physical significance of fundamental solutions are of considerable importance in the solution of integral equations. For example, the singularities of fundamental solutions have a significant influence on the procedures used for both theoretical and numerical analysis. This section attempts to highlight some of the major features of the fundamental solutions, which will be cited whenever necessary.

2.4.1 Order Of Singularity

The singularities existing in the fundamental solutions are significant features of the boundary integral equations. By inspecting the fundamental solutions, it is evident that all these solutions have a singularity when r approaches to zero. As will be shown later, when $\omega \rightarrow 0$ ($r\omega/C_2 \leq 10^{-3}$) the dynamic fundamental solution converges to the static fundamental solution. Consequently, the asymptotic singular behaviour of

dynamic fundamental solutions, for any frequency, is identical to the static fundamental solutions. The order of singularities of both dynamic and static fundamental solutions are proportional to the following singular functions:

$$G_{ij}(x, \xi, \omega) \sim \frac{1}{r(x, \xi)}$$

$$T_{ij}(x, \xi, \omega) \sim \frac{1}{r^2(x, \xi)} \quad (2.25)$$

2.4.2 Symmetry, Anti-symmetry and Simplification

The symmetry of the displacement fundamental solution, which is well known in the literature, implies that $G_{ij}(x, \xi, \omega) = G_{ji}(x, \xi, \omega) = G_{ij}(\xi, x, \omega)$. On the other hand, the static traction fundamental solution are anti-symmetric, namely, $T_{ij}^{st}(x, \xi) = -T_{ji}^{st}(x, \xi) = -T_{ij}^{st}(\xi, x)$. As shown in Figure 2.1a and 2.1b, respectively, $G_{ij}(x, \xi) = G_{ij}(x', \xi)$ and $T_{ij}(x, \xi) = -T_{ij}(x', \xi)$, where x' is the symmetric point (with respect to ξ) of x . In these figures ω equals 300 rad/s, $\nu=0.25$, and ξ is at $(0,0,0)$ while x is located at $(d^*\cos(\theta), d^*\sin(\theta), 0)$, in which $\theta=30^\circ$ and d^* is the distance between x and ξ .

It is noted that if point x and point ξ are on the same plane (for example, the surface of the halfspace where $y_3=0$) then $r_{,3}=n_1=n_2=0$. Thus, the nine terms in G_{ij} reduce to five because $G_{13}=G_{23}=G_{31}=G_{32}=0$. In addition, because in this special case $\partial r/\partial n=0$, it is easy to show that only the off-diagonal terms of T_{ij} , namely, T_{13} , T_{23} , T_{31} and T_{32} , are different from zero. The forms of T_{ij} and G_{ij} for this particular case suggest a weak coupling between the horizontal and vertical motions. Notable simplifications in the boundary element analysis have been made

by neglecting the relatively small influence of the off-diagonal terms of the traction fundamental solution, eg, Karabalis and Beskos (1986) and Mohammadi and Karabalis (1990).

2.4.3 Frequency Response

It is of interest to examine the convergent behaviour of the dynamic fundamental solution to the static one as the frequency tends to zero. Attention is primarily focused here to small arguments. Expanding the exponential terms by the Taylor's series

$$e^x = \sum_{n=0}^{\infty} \frac{x^n}{n!} \quad (2.26)$$

with $n=3$, after some manipulations, Ψ and Γ can be approximated to

$$\Psi = \frac{1}{2r} \left[\left(1 - \left(\frac{\omega r}{C_2} \right)^2 + i \frac{\omega r}{C_2} \right) + \left(\frac{C_2}{C_1} \right)^2 \left(1 + i \frac{\omega r}{C_1} \right) \right] \quad (2.27)$$

$$\Gamma = \frac{1}{2r} \left[\left(-1 - \left(\frac{\omega r}{C_2} \right)^2 - i \frac{\omega r}{C_2} \right) + \left(\frac{C_2}{C_1} \right)^2 \left(1 + \left(\frac{\omega r}{C_1} \right)^2 + i \frac{\omega r}{C_1} \right) \right] \quad (2.28)$$

Furthermore, it is easy to show that

$$\frac{d\Psi}{dr} = \frac{1}{2r^2} \left[\left(-1 - \left(\frac{\omega r}{C_2} \right)^2 \right) - \left(\frac{C_2}{C_1} \right)^2 \right] \quad (2.29)$$

$$\frac{d\Gamma}{dr} = \frac{1}{2r^2} \left[\left(1 - \left(\frac{\omega r}{C_2} \right)^2 \right) + \left(\frac{C_2}{C_1} \right)^2 \left(-1 + \left(\frac{\omega r}{C_1} \right)^2 \right) \right] \quad (2.30)$$

Substitution of Equations (2.27)~(2.30) into Equations (2.17) and (2.18) leads, after lengthy manipulations, to

$$G_{ij} = \frac{1}{8\pi G r} \left\{ \left[\left(1 - \left(\frac{\omega r}{C_2} \right)^2 + i \frac{\omega r}{C_2} \right) + \left(\frac{C_2}{C_1} \right)^2 \left(1 + i \frac{\omega r}{C_1} \right) \right] \delta_{ij} \right. \\ \left. - \left[\left(-1 - \left(\frac{\omega r}{C_2} \right)^2 - i \frac{\omega r}{C_2} \right) + \left(\frac{C_2}{C_1} \right)^2 \left(1 + \left(\frac{\omega r}{C_1} \right)^2 + i \frac{\omega r}{C_1} \right) \right] r_{,i} r_{,j} \right\} \quad (2.31)$$

and

$$T_{ij} = \frac{1}{8\pi r^2} \left\{ \left[i \frac{\omega r}{C_2} + \left(\frac{C_2}{C_1} \right)^2 \left(-2 - \left(\frac{\omega r}{C_1} \right)^2 - i \frac{\omega r}{C_1} \right) \right] \left(\delta_{ij} \frac{\partial r}{\partial n} + r_{,j} n_i \right) \right. \\ \left. + \left[\left(-6 - 2 \left(\frac{\omega r}{C_2} \right)^2 - 4 i \frac{\omega r}{C_2} \right) + \left(\frac{C_2}{C_1} \right)^2 \left(6 + 2 \left(\frac{\omega r}{C_1} \right)^2 + 4 i \frac{\omega r}{C_1} \right) \right] r_{,i} r_{,j} \frac{\partial r}{\partial n} \right. \\ \left. + \left(-2 \left(\frac{\omega r}{C_2} \right)^2 - 3 \left(\frac{\omega r}{C_1} \right)^2 - 2 i \frac{\omega r}{C_2} - 2 i \frac{\omega r}{C_1} \right) \right. \quad (2.32) \\ \left. + \frac{C_1^2}{C_2^2} \left[\left(2 \left(\frac{\omega r}{C_2} \right)^2 + 2 i \frac{\omega r}{C_2} \right) + \left(2 + 4 \left(\frac{\omega r}{C_1} \right)^2 + 2 i \frac{\omega r}{C_1} \right) \right] r_{,i} n_j \right\}$$

Cancelling terms in the limit as the frequency tends to zero, it is easy to show that G_{ij} and T_{ij} (Equations 2.31 and 2.32) become identically equal to G_{ij}^{st} and T_{ij}^{st} , respectively.

Clearly, the convergent behaviour of these approximations depend on the magnitudes of $\omega r/C_1$ and $\omega r/C_2$. The latter is crucial because C_1 is greater than C_2 . Considering only relatively low values of $\omega r/C_2$, a series of numerical experiments were performed to study the discrepancy between the static fundamental solutions and the dynamic fundamental solutions. As shown in Figure 2.2, numerical results reveal

that for $\omega r/C_2 \leq 10^{-3}$, the imaginary parts of the dynamic fundamental solutions approach zero and, essentially, are negligible. It is also observed that for $\omega r/C_2 \leq 10^{-2}$, the real parts of the dynamic fundamental solutions and the static fundamental solutions are practically identical. However, the computation of dynamic fundamental solutions becomes unreliable (using single precision arithmetic) when $\omega r/C_2 \leq 10^{-6} \sim 10^{-7}$. As a consequence, in this work the static fundamental solution is used in the dynamic analysis when $\omega r/C_2 \leq 10^{-3}$.

2.4.4 Fundamental Solutions For Incompressible Medium

An important difficulty arises in numerical solutions to elastodynamic problems when Poisson's ratio equals 0.5, for which the dilatational wave velocity C_1 is infinity. This is an important problem in geotechnical engineering since it relates to saturated clays under undrained loading. A simple way of avoiding this difficulty is to use values of Poisson's ratio close to 0.5 but not equal to it. On the other hand, several researchers (for example, Gazetas and Dobry, 1984; Pais and Kausel, 1988; and Meek and Wolf, 1993) have attempted to use the Lysmer's analog wave velocity

$$V_{La} = \frac{3.4}{\pi(1-\nu)} C_2 \quad (2.33)$$

or an approximate velocity

$$V_a = \left(\frac{2}{1-\nu}\right)^{1/2} C_2 \quad (2.34)$$

to replace C_1 as Poisson's ratio approaches 0.5.

It should be noted that infinite wave velocities are not observed in the laboratory (Gazetas, 1983; and Nii, 1987), and

some analytical solutions for $\nu=0.5$ have been presented in the published literature (Veletsos and Wei, 1971; Awojobi, 1971; and Karasudhi et al, 1968). It is therefore necessary to investigate whether the solution of integral equations for incompressible media depends on the velocity of dilatational wave. It follows from equations (2.20) and (2.21) that Ψ and Γ can be written as

$$\Psi = \frac{1}{r} \left[\left(-\frac{C_2^2}{\omega^2 r^2} + \frac{iC_2}{\omega r} + 1 \right) e^{\frac{i\omega r}{c_2}} + \left(\frac{C_2^2}{\omega^2 r^2} - \frac{iC_2^2}{C_1 \omega r} \right) e^{\frac{i\omega r}{c_1}} \right] \quad (2.35)$$

and

$$\begin{aligned} \Gamma = \frac{1}{r} \left[\left(-\frac{3C_2^2}{\omega^2 r^2} + \frac{3iC_2}{\omega r} + 1 \right) e^{\frac{i\omega r}{c_2}} \right. \\ \left. + \left(\frac{3C_2^2}{\omega^2 r^2} - \frac{3iC_2^2}{C_1 \omega r} - \left(\frac{C_2}{C_1} \right)^2 \right) e^{\frac{i\omega r}{c_1}} \right] \end{aligned} \quad (2.36)$$

Noticing that, as ν approaching 0.5, $1/C_1 \rightarrow 0$ and $\exp(i\omega r/C_1) = 1$, it is clear that Ψ and Γ are independent of C_1 , namely,

$$\lim_{\nu=0.5} \Psi = \frac{1}{r} \left[\left(-\frac{C_2^2}{\omega^2 r^2} + \frac{iC_2}{\omega r} + 1 \right) e^{\frac{i\omega r}{c_2}} + \frac{C_2^2}{\omega^2 r^2} \right] \quad (2.37)$$

$$\lim_{\nu=0.5} \Gamma = \frac{1}{r} \left[\left(-\frac{3C_2^2}{\omega^2 r^2} + \frac{3iC_2}{\omega r} + 1 \right) e^{\frac{i\omega r}{c_2}} + \frac{3C_2^2}{\omega^2 r^2} \right] \quad (2.38)$$

Consequently, the displacement fundamental solution for $\nu=1/2$ is

$$G_{ij} = \frac{1}{4\pi Gr} \left\{ \left[\left(-\frac{C_2^2}{\omega^2 r^2} + \frac{iC_2}{\omega r} + 1 \right) e^{\frac{i\omega r}{C_2}} + \frac{C_2^2}{\omega^2 r^2} \right] \delta_{ij} - \left[\left(-\frac{3C_2^2}{\omega^2 r^2} + \frac{3iC_2}{\omega r} + 1 \right) e^{\frac{i\omega r}{C_2}} + \frac{3C_2^2}{\omega^2 r^2} \right] r_{,i} r_{,j} \right\} \quad (2.39)$$

Similarly, the traction fundamental solution T_{ij} for incompressible medium becomes

$$T_{ij} = \frac{1}{4\pi r^2} \left\{ \left[\left(6 \left(\frac{C_2}{\omega r} \right)^2 - 6 \frac{iC_2}{\omega r} + \frac{i\omega r}{C_2} - 3 \right) e^{\frac{i\omega r}{C_2}} - 6 \left(\frac{C_2}{\omega r} \right)^2 \right] (\delta_{ij} \frac{\partial r}{\partial n} + r_{,j} n_i) + \left[\left(-30 \left(\frac{C_2}{\omega r} \right)^2 + 30 \frac{iC_2}{\omega r} - 2 \frac{i\omega r}{C_2} + 12 \right) e^{\frac{i\omega r}{C_2}} + 30 \left(\frac{C_2}{\omega r} \right)^2 \right] r_{,i} r_{,j} \frac{\partial r}{\partial n} + \left[\left(6 \left(\frac{C_2}{\omega r} \right)^2 - 6 \frac{iC_2}{\omega r} - 2 \right) e^{\frac{i\omega r}{C_2}} - 6 \left(\frac{C_2}{\omega r} \right)^2 - 1 \right] r_{,i} n_j \right\} \quad (2.40)$$

Using the same procedure described in the previous sub-section, after mathematical manipulations, it is easy to demonstrate that, as $\omega \rightarrow 0$, these results converge to the static fundamental solutions for incompressible material, i.e.,

$$G_{ij}^{st} = \frac{1}{8\pi Gr} [\delta_{ij} + r_{,i} r_{,j}] \quad (2.41)$$

and

$$T_{ij}^{st} = -\frac{1}{4\pi r^2} [3r_{,i} r_{,j} \frac{\partial r}{\partial n}] \quad (2.42)$$

This approach provides important insights into the influence

of C_1 on the fundamental solutions. It has been demonstrated that, when Poisson's ratio equals $1/2$, the fundamental solutions are independent of the dilatational wave velocity. Consequently, the special fundamental solutions developed in this section are capable of dealing rigorously with incompressible soils. The potential of these fundamental solutions will be illustrated in Chapter 7.

2.5 Direct Boundary Element Formulation

2.5.1 Boundary Constraint Equation

The strategy of the boundary integral equations is to move the interior point ξ in equation(2.16) to the boundary and, consequently, the resulting boundary constraint equations relate all boundary displacements to all boundary tractions. Let y be a point on the surface of the domain, the following results have been given by Cruse and Rizzo(1968):

$$\lim_{\xi \rightarrow y} u_i(\xi, \omega) = u_i(y, \omega) \quad (2.43)$$

$$\begin{aligned} & \lim_{\xi \rightarrow y} \int_S t_i(x, \omega) G_{ij}(x, \xi, \omega) dS \\ &= \int_S t_i(x, \omega) G_{ij}(x, y, \omega) dS(x) \end{aligned} \quad (2.44)$$

and

$$\begin{aligned} & \lim_{\xi \rightarrow y} \int_S u_i(x, \omega) T_{ij}(x, \xi, \omega) dS \\ &= -\hat{C}_{ij}(y) u_i(y, \omega) + \int_S u_i(x, \omega) T_{ij}(x, y, \omega) dS(x) \end{aligned} \quad (2.45)$$

where $\hat{C}_{ij}(\gamma)$ is a 3x3 matrix arising from the treatment of the improper surface integral involving T_{ij} . It should be noted that $\hat{C}_{ij}(\gamma)$ are independent of the frequency. Hartmann(1981 and 1982) showed that $\hat{C}_{ij}(\gamma)$ is a function of the boundary geometry in the vicinity of γ and the Poisson's ratio:

γ on a smooth boundary

$$\hat{C}_{ij}(\gamma) = \frac{1}{2} \begin{vmatrix} 1 & 0 & 0 \\ 0 & 1 & 0 \\ 0 & 0 & 1 \end{vmatrix} \quad (2.46)$$

γ at an edge

$$\hat{C}_{ij}(\gamma) = \frac{1}{4} \begin{vmatrix} 1 & 0 & 0 \\ 0 & 1 & \nu_1 \\ 0 & \nu_1 & 1 \end{vmatrix} \quad (2.47)$$

in which

$$\nu_1 = \frac{1}{\pi(1-\nu)} \quad (2.48)$$

γ at a corner

$$\hat{C}_{ij}(\gamma) = \frac{1}{8} \begin{vmatrix} 1 & \nu_1 & \nu_1 \\ \nu_1 & 1 & \nu_1 \\ \nu_1 & \nu_1 & 1 \end{vmatrix} \quad (2.49)$$

Introducing equations (2.43)~(2.45) into equation(2.16) yields, on the assumption of zero body forces(Muskhelishvili, 1951, section 28; and Lamb, 1904), the well known boundary integral equations(for example, Banerjee et al, 1985; Manolis, 1983; Ahmad and Banerjee, 1988a):

$$\begin{aligned}
 (\delta_{ij} - \hat{C}_{ij})(y) u_i(y, \omega) = & \int_S [G_{ij}(x, y, \omega) t_i(x, \omega) \\
 & - T_{ij}(x, y, \omega) u_i(x, \omega)] dS(x)
 \end{aligned} \tag{2.50}$$

or

$$\begin{aligned}
 C_{ij}(y) u_i(y, \omega) = & \int_S [G_{ij}(x, y, \omega) t_i(x, \omega) \\
 & - T_{ij}(x, y, \omega) u_i(x, \omega)] dS(x)
 \end{aligned} \tag{2.51}$$

It is significant to note that all steps leading to the boundary integral equations are entirely analytical and classical. However, the analytical solution of the boundary integral equations is only possible for relative simple problems and it is therefore necessary to implement these equations using a numerical method; this is usually referred to as the boundary element method.

2.5.2 Numerical Implementation

The advancement of computers has made it possible to implement discretization processes arithmetically; as a result, numerical solutions of tolerable accuracy can be achieved. Some implementation aspects of the boundary integral equations have been presented by Banerjee and Butterfield(1981); Manolis and Beskos(1988); Becker(1992); and Davies(1993). This sub-section describes briefly the basic numerical techniques employed in the boundary element method. Detailed study of the computational procedure will be presented in subsequent chapters.

Discretization And Parametric Representations

Usually, the boundary under consideration can be discretized into constant, linear, or higher-order boundary elements, as shown in Figure 2.3. In the past, constant boundary elements have been popular because of their simplicity (Cruse, 1968; Dominguez and Roesset, 1978; Fukuzawa et al, 1985; Karabalis and Beskos, 1987a and 1987b; among others). However, the quality of the numerical results depends strongly on the closeness of the approximation used for describing field variables. The use of large size elements (in comparison with the wavelength) is not recommended because the accuracy of the representation of field variables over an element is significantly less than the accuracy of the numerical technique. In practice, as indicated by Davies and Bu (1993), quadratic elements with dimensions smaller than 1/4 Rayleigh wavelengths are essential for modelling wave fields accurately. Isoparametric shape functions, borrowed from finite element methods, are used in the present study to approximate the geometry and the field variables over rectangular boundary elements in terms of their nodal values.

The Cartesian coordinates of an arbitrary point p on a boundary element for three-dimensional problems are given in terms of the nodal coordinates $X_{i\alpha}$ as

$$x_i(p) = \sum_{\alpha=1}^q N_{\alpha}(\eta, \xi) X_{i\alpha} \tag{2.52}$$

where $i = 1, 2, 3$ and $\alpha = 1, \dots, q$, with q the number of nodal points necessary to describe the element. On the other hand, displacements and tractions at an arbitrary point p on a boundary element can be described in terms of nodal values $U_{i\alpha}$ and $T_{i\alpha}$ using the equations:

$$u_i(p) = \sum_{\alpha=1}^q N_{\alpha}(\eta, \xi) U_{i\alpha}$$

$$t_i(p) = \sum_{\alpha=1}^q N_{\alpha}(\eta, \xi) T_{i\alpha} \quad (2.53)$$

The shape functions N_{α} (Zienkiewicz and Taylor, 1989) are defined in the intrinsic coordinate system η and ξ , which vary from -1 to +1.

The jacobian operator relating the transformation from the Cartesian coordinate system to the element's intrinsic coordinate system (η, ξ) is

$$|J| = \begin{vmatrix} \frac{\partial x}{\partial \eta} & \frac{\partial y}{\partial \eta} \\ \frac{\partial x}{\partial \xi} & \frac{\partial y}{\partial \xi} \end{vmatrix} \neq 0 \quad (2.54)$$

Discretized Boundary Element Formulation

If the boundary is discretized into M elements, which are transformed onto the intrinsic coordinate system, the boundary integral equations for a given node y can be written as

$$C_{ij}(y) u_i(y, \omega) = \sum_{m=1}^M \int_{-1}^{+1} \int_{-1}^{+1} G_{ij}(x, y, \omega) t_i(x, \omega) |J| d\eta d\xi$$

$$- \sum_{m=1}^M \int_{-1}^{+1} \int_{-1}^{+1} T_{ij}(x, y, \omega) u_i(x, \omega) |J| d\eta d\xi \quad (2.55)$$

Substituting equation(2.53) into equation(2.55), the integrals over a boundary element can be written as, for example,

$$\begin{aligned}
 & \int_{-1}^{+1} \int_{-1}^{+1} T_{ij}(\mathbf{x}, y, \omega) u_i(\mathbf{x}, \omega) |J| d\eta d\xi \\
 &= \int_{-1}^{+1} \int_{-1}^{+1} T_{ij}(\mathbf{x}, y, \omega) \left[\sum_{\alpha=1}^q N_{\alpha} U_{i\alpha} \right] |J| d\eta d\xi \\
 &= \sum_{\alpha=1}^q U_{i\alpha} \int_{-1}^{+1} \int_{-1}^{+1} T_{ij}(\mathbf{x}, y, \omega) N_{\alpha} |J| d\eta d\xi \tag{2.56}
 \end{aligned}$$

Consequently, the discretized form of the boundary integral equations for a given node y is

$$\begin{aligned}
 C_{ij}(y) u_i(y, \omega) &= \sum_{m=1}^M \sum_{\alpha=1}^q T_{i\alpha} \int_{-1}^{+1} \int_{-1}^{+1} G_{ij}(\mathbf{x}, y, \omega) N_{\alpha} |J| d\eta d\xi \\
 &- \sum_{m=1}^M \sum_{\alpha=1}^q U_{i\alpha} \int_{-1}^{+1} \int_{-1}^{+1} T_{ij}(\mathbf{x}, y, \omega) N_{\alpha} |J| d\eta d\xi \tag{2.57}
 \end{aligned}$$

Numerical Integration

An essential aspect of the implementation of the boundary element method is the accurate evaluation of surface integrals appearing in the discretized boundary element formulation. This is the most time-consuming aspect of the boundary element analysis. The integral is singular if the source point y lies on the boundary element being integrated; otherwise, the integral is non-singular. Special attention is required in the

integration of integrals, due to their inherent singularities and oscillatory behaviour.

Methods for the evaluation of integrals in the boundary element method are reviewed by Hall(1988) and Guiggiani(1991). It becomes apparent that only integrals over constant element are amenable to analytical solutions. In general, all integrals are calculated numerically by means of Gauss quadrature.

System Matrix Equations

The boundary integral equations may be approximated by a system of simultaneous equations in terms of displacements and tractions at nodes of boundary elements by using nodal collocation(Delves and Walsh, 1974). By allowing the source point to coincide sequentially with all nodal points on the boundary, the matrix form of the global system of boundary integral equations can be expressed as

$$[U] \{t\} = [T] \{u\} \quad (2.58)$$

where $\{t\}$ and $\{u\}$ are the traction and displacement vectors for all the nodes, respectively, and $[U]$ and $[T]$ are coefficient matrices containing the appropriate contributions of the surface integrals of G_{ij} and T_{ij} . It should be noted that the C_{ij} matrix has been absorbed in the matrix $[T]$.

After introducing the boundary conditions, the final system of equations is obtained by interchanging columns in the matrices $[U]$ and $[T]$ to accumulate all unknowns into the vector $\{X\}$ on the left hand side as follows,

$$[A] \{X\} = \{B\} \quad (2.59)$$

For elastodynamic problems, the matrix [A] contains complex numbers and is non-symmetric and fully populated. Solutions of the matrix equation and corresponding error bounds have been presented by Fox(1964) and Delves and Walsh(1974), and others. In practice, the system matrix equations can be easily solved by using presently available computer software, for example, NAG subroutines(1983).

Solution Of Boundary Value Problems

Once the boundary values are unknown, they can be subsequently used to compute the displacements and tractions at any interior point of the domain with the aid of the integral equations formulation, i.e., equation(2.16). However, for the analyses of machine foundations, the displacements and the tractions at the soil-foundation interface are of interest only. The dynamic stiffness of the foundation is generally evaluated by integrating the traction over the contact area.

2.5.3 Discussion

In boundary element analyses, especially for three-dimensional problems, the computation of the integrals over boundary elements is an important aspect since it governs the accuracy of the numerical results and also because it usually requires the major part of the numerical effort. A number of methods have been developed to evaluate surface integrals involving "static" integrands(Lachat and Watson, 1976; Jun et al, 1985; Mustoe, 1984; and Hayami and Brebbia, 1988; among others). However, methods for evaluating surface integrals with oscillatory integrands are seldom discussed. Consequently, additional work is needed to develop accurate and effective methods for the evaluation of integrals arising in dynamic boundary element analyses. This will be presented in the next

two chapters.

The analysis of machine foundations involves the free surface of the halfspace; this boundary condition must be incorporated in the analysis. However, the limitation of computer capacity and computational cost have caused practical difficulties in incorporating the semi-infinite boundary into the numerical procedure. Traditional remedies to these difficulties are either to use the complicated halfspace Green's functions or large (but truncated) boundary element meshes.

Halfspace Green's Functions

A variety of special Green's functions corresponding to the homogeneous halfspace have been developed by Johnson(1974); Kobayashi and Nishimura(1980); Rizzo et al(1985); and Banerjee and Mamoon(1990). Because the use of these Green's functions leads to automatic satisfaction of the free boundary conditions, evaluations of integrals over the free surface of the halfspace are not necessary. However, the use of halfspace Green's functions in the frequency domain to solve halfspace problems may lead to fictitious eigenfrequency difficulties (Dominguez and Meise, 1991; Rizzo et al, 1985). The evaluation of these halfspace Green's functions is computationally expensive and the alternative full space fundamental solutions are preferred in most applications. However, Mita and Luco(1989a and 1989b) use halfspace Green's functions in their hybrid FE-BE analysis to compute impedance functions of embedded square foundations.

Truncated Mesh

Although the radiation condition is automatically satisfied by the full-space fundamental solutions used in the elastodynamic

boundary integral formulation, to obtain results of acceptable accuracy the boundary element analysis of machine foundations requires the discretization of the semi-infinite surface of the halfspace. The semi-infinite region is usually truncated at some "reasonable" distance (Alarcon et al, 1989; Israil and Banerjee, 1990; and many others). Because fundamental solutions contain exponential terms, they become increasingly oscillatory with increasing frequency. As a result, a finer discretization is required for analyses of high frequencies. On the other hand, unlike static analyses, the usual practice of extending the truncated mesh by using coarser elements at distant locations may mask the true physical behaviour, since these elongated elements are not capable of modelling the wavy nature of the field variables in the radial direction. Clearly, this method of analysis requires considerable computational resources, especially for three-dimensional problems.

Recently, the treatment of the semi-infinite halfspace by using elastodynamic infinite boundary elements has been proposed by Davies and Bu (1993). The infinite element methodology used in this approach is discussed in Chapter 5.

2.6 Summary and Conclusions

The derivation of the direct boundary integral formulation for steady state elastodynamics was presented in this chapter. It is evident that the derivation is entirely analytical and no approximations are introduced at this stage.

If series expansions of the fundamental solutions are developed, it can be shown that the static fundamental solutions are recovered as the frequency ω diminishes to a negligibly small value. Numerical results reveal that values of $\omega r/C_2 \approx 10^{-3}$ can be classed as the borderline between the

dynamic and static fundamental solutions, where the discrepancy between the two solutions is negligible.

The limiting forms of the fundamental solutions have been developed for $\nu=0.5$. These have applications for the analysis of dynamic problems of undrained saturated clays by the boundary element method. It is recognized that dynamic problems of this kind can not be solved otherwise by the boundary element method since the dilatational wave velocity(C_1) is theoretically infinite when Poisson's ratio equals to 0.5. With the limit forms derived here, problems involving incompressible material now present no particular difficulties.

Because analytical solutions are difficult to obtain, boundary integral formulations become of practical interest only when numerical techniques are employed for their solution. A brief description of the basic numerical procedures used in the boundary element method is given. It is noted that use of quadratic boundary elements with dimensions smaller than $1/4$ Rayleigh wavelength is essential for the boundary element method. The accuracy and efficiency of the boundary element analysis of machine foundations depend mainly on the integration scheme adopted for the evaluation of surface integrals and the sophistication of the modelling of the semi-infinite boundary of the halfspace. The former will be discussed in the next two chapters, while the latter will be presented in Chapter 5.

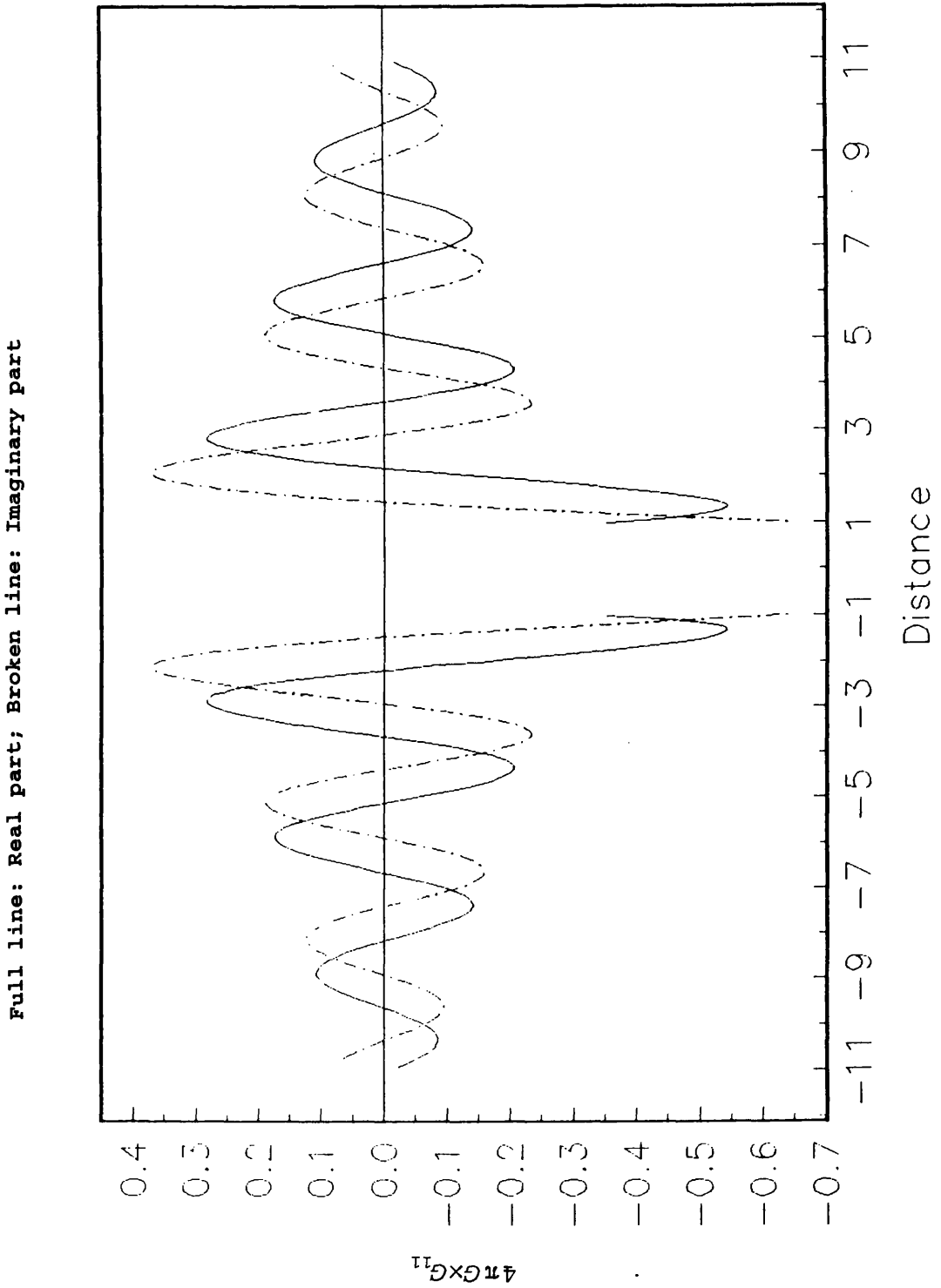


FIGURE 2.1a: Symmetrical Behaviour of G_{ij}

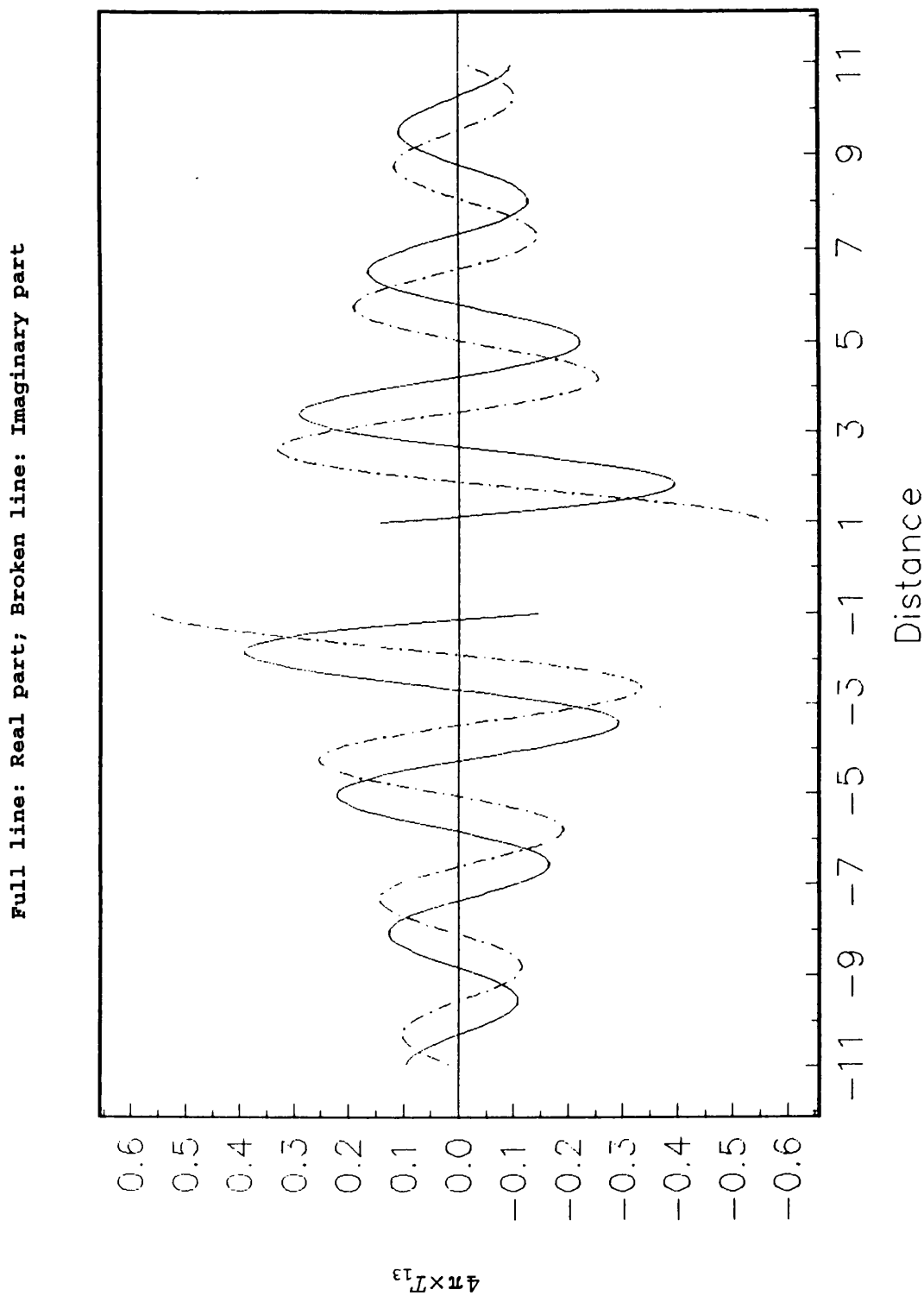


FIGURE 2.1b: Symmetrical Behaviour of T_{ij}

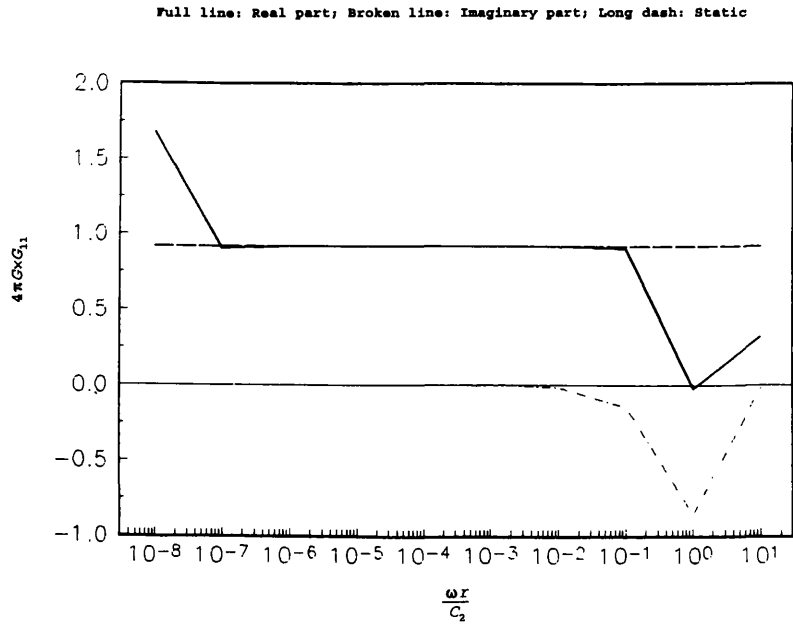


FIGURE 2.2a: Convergence Behaviour of G_{ij}

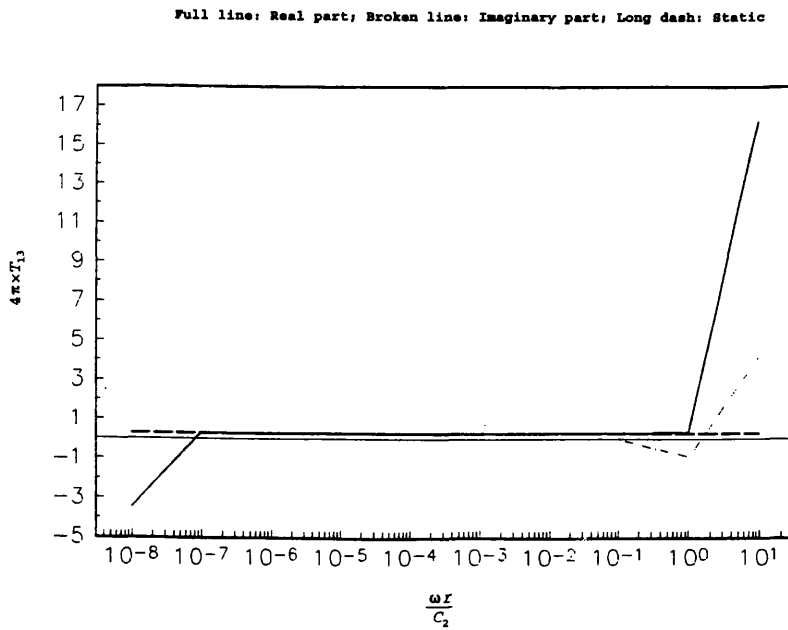
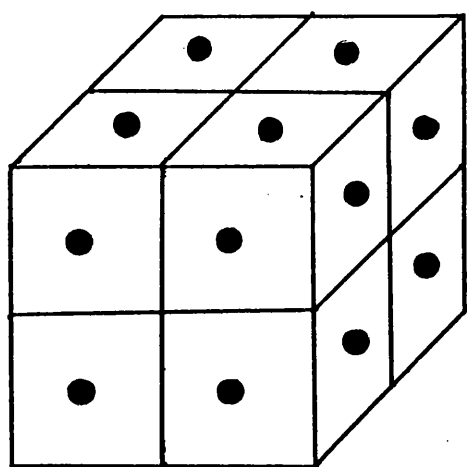
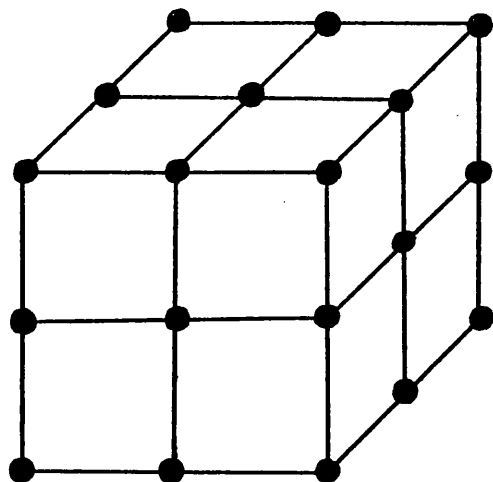


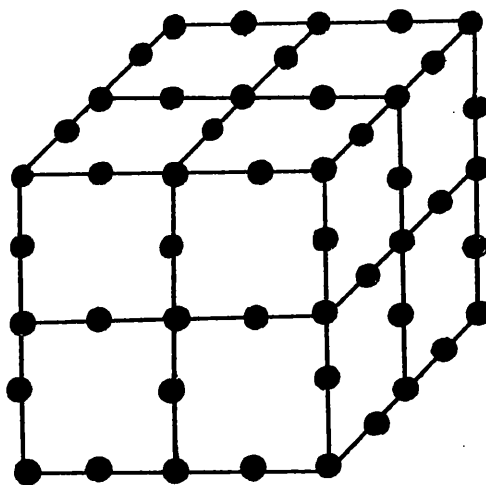
FIGURE 2.2b: Convergence Behaviour of T_{ij}



(a)



(b)



(c)

Figure 2.3 Three-Dimensional Body Discretized into
(a) Constant Boundary Elements,
(b) Linear Boundary Elements, and
(c) Quadratic Boundary Elements

CHAPTER 3

INTEGRATION SCHEMES (I) NON-SINGULAR INTEGRALS

3.1 Introduction

The evaluation of non-singular integrals is the most time consuming part of the boundary element analysis. In the 1960's and the early 1970's, most non-singular integrals over constant elements and linear elements were computed numerically using the Simpson's rule, e.g., Rizzo(1967) and Symm(1963). Lachat and Watson(1976) were the first to use Gauss integration for the three-dimensional boundary element analysis. In that landmark paper, they demonstrated that results of sufficient accuracy could be systematically obtained by judicious use of Gauss-Legendre quadrature and isoparametric representation of geometrical and field quantities. This important work initiated major improvements in the computational versatility and efficiency of the boundary element analysis. Since then, advanced numerical integration schemes have been implemented by many authors.

The adaptive integration schemes used by Lachat and Watson (1976) have been used widely in the application of Gauss-Legendre quadrature to the boundary element method. Based on the approximate error bounds of Gauss-Legendre quadrature, simple formulae were developed to determine the required number

CHAPTER 3 NUMERICAL INTEGRATION (I) : NON-SINGULAR INTEGRALS

of Gauss points for each element in order to assure approximately uniform precision of integration. They suggested that the order of integration should be chosen depending on the allowable error, the strength of the singularity, and the ratio of the minimum distance between the boundary element and the source point to a characteristic dimension of the element. Accordingly, Lachat and Watson(1976) increased the number of integration points as the minimum distance decreased and subdivided the element into sub-elements if the number of the required Gauss points was greater than the prescribed maximum integration rule. This adaptive scheme is typical of methods for improving the efficiency and accuracy of numerical integration. Because the use of invariant integration order in the boundary element analysis would result in either a significant amount of unnecessary computational effort or a noticeable loss of accuracy, Lachat and Watson's method has been subsequently adopted by Luchi and Rizzuti(1987) in fracture mechanics, Manolis et al(1986) in elastodynamics, and Mustoe(1984) in non-linear analysis, among many others.

The effectiveness of the adaptive integration scheme is clearly dependent on the use of efficient and accurate error estimates for the quadrature formulae. However, theoretical methods for estimating errors(See Davis and Rabinowitz, 1984, and Engels, 1980, for more details) are often too cumbersome for use in practical applications. Consequently, a critical part of the development of effective integration scheme is to establish an accurate estimate of the integration error. A series of numerical tests has been performed in this chapter to gain more insight into the error bounds of Gauss-Legendre quadrature. Based on these test results, reliable and efficient criteria are proposed for adaptive integration routines in the boundary element method.

3.2 Numerical Integration

3.2.1 Introduction

In recent years, there has been enormous productivity in the field of numerical integration (Davis and Rabinowitz, 1984; Engels, 1980; and Mori and Piessens, 1987). Methods which offer advantage in accuracy but were not popular in the past, because of irrational (maths) coefficients and/or lengthy, tedious calculations, present no special difficulty to computers and have come back into favour. Nowadays, most boundary element programs employ Gauss-Legendre quadrature, which gives excellent precision in comparison with other types of quadrature formulae used in the so-called first generation of BEM programs, for example, Jaswon and Symm (1977); Jaswon and Ponter (1963); Rizzo (1967); and Symm (1963).

3.2.2 Gauss-Legendre Formula

In the derivation of most quadrature formulae (Krylov, 1962; Davis and Rabinowitz, 1984), an integral is approximated by a linear combination of the values of the integrand at a set of discrete points:

$$\int_a^b w(x) f(x) dx \approx \sum_{i=1}^n \bar{A}_i f(\bar{a}_i) \quad (3.1)$$

$$-\infty < a < b < +\infty$$

in which, $w(x)$ is called a weight function, $\bar{a}_1, \bar{a}_2, \dots, \bar{a}_n$ are n abscissae usually chosen so as to lie in the interval of integration, and the numbers $\bar{A}_1, \bar{A}_2, \dots, \bar{A}_n$ are n "weights" accompanying these abscissae. Equidistant abscissae are assumed in the Newton-Cotes family of integration formulae; for

example, the trapezoidal rule and Simpson's rule.

Gauss (Goldstine, 1977) showed that if the weight function $w(x) = 1$ and the abscissae are taken as the n roots of the Legendre polynomial P_n on the interval $[-1, +1]$ then the integration rule

$$\int_{-1}^{+1} w(x) f(x) dx \approx \sum_{i=1}^n A_i f(a_i) \quad (3.2)$$

is exact for polynomials of order less than $2n$. It is worthy of note that the Newton-Cotes integration rules are exact for all polynomials of order less than n . Krylov (1962) has tabulated values of the weights A_i and the abscissae a_i to 20 decimal places for $n = 2$ to 48.

It should be noted that the weights and abscissae of the Gauss-Legendre quadrature are generally irrational numbers. In this study, in order to avoid rounding errors and typographical errors it was decided to develop a subroutine (GAUSS) to generate the abscissae and weights of Gauss-Legendre formula to any order. This subroutine is a refinement of the program GRULE given by Davis and Rabinowitz (1984).

3.2.3 Integration Over General Regions

Based on the "product rule", Gauss-Legendre formula can be extended to deal with multiple integrals. The integration formula in two dimensions can be obtained by repeated use of equation (3.2), namely,

$$\int_{-1}^{+1} \int_{-1}^{+1} f(x_1, x_2) dx_1 dx_2 \approx \sum_{i=1}^{n_{r1}} \sum_{j=1}^{n_{r2}} A_i A_j f(a_i, a_j) \quad (3.3)$$

Different integration orders, n_{r1} and n_{r2} , can be used in the x_1 and x_2 directions, respectively. This is desirable if, in a certain direction, the integrand varies strongly or the integration interval is large.

The product technique is the most obvious procedure of evaluating multiple integrals if not the most efficient, especially for irregularly-shaped integration domains. In general, results of sufficient accuracy for two-dimensional integrals can be obtained with reasonable efficiency by this means. Consequently, it has been widely used in practical applications (Zienkiewicz and Taylor; 1989, Banerjee and Butterfield, 1981; and Becker, 1992).

3.3 Numerical Experiments On Error Bounds

3.3.1 Introduction

An appreciation of how errors are engendered during numerical integration is an essential preliminary to confidence in the computed values. There are two sorts of error in Gauss-Legendre quadrature: round-off error and truncation error. In theory, Gauss-Legendre quadrature enables us to calculate an integral as accurately as we wish. However, practical computations can deal with only a finite number of terms of the infinite series. The truncation error is the residue of the truncated part of the infinite sum in equation(3.2). The round-off error arises from the fact that arithmetic calculations are limited in precision by the bit length of the particular computer used to perform the calculations. Davis and Rabinowitz(1984) have shown that the effect of round-off error is usually negligible, except for cases of numerical integration involving integration rules of very high order or, weights of mixed sign. For this reason, attention in this section is primarily focused on the truncation error of Gauss-

Legendre quadrature.

3.3.2 Error Bounds Of Gauss Integration

The truncation errors incurred in Gauss-Legendre quadrature are expressed theoretically in terms of the $(2n)$ th derivative of the integrand evaluated at some points ξ in the integration interval $[-1,+1]$, namely,

$$\begin{aligned}
 E_n(f) &= \left| \int_{-1}^{+1} w(x) f(x) dx - \sum_{i=1}^n A_i f(x_i) \right| \\
 &\leq \left| \frac{2^{2n+1} (n!)^4}{(2n+1) [(2n)!]^3} f^{2n}(\xi) \right| \qquad (3.4)
 \end{aligned}$$

Error estimates for product rules have been given by Stroud and Secrest(1966). These have been obtained by expressing the error as the sum of the errors predicted by equation(3.4). The error bound for two dimensional Gauss-Legendre quadrature can be written as

$$E_n(f) \leq 2 \cdot [|e_{r_1} \cdot f^{2n_{r_1}}(\xi)| + |e_{r_2} \cdot f^{2n_{r_2}}(\xi)|] \qquad (3.5)$$

where

$$e_{r_i} \approx \frac{4}{2^{2n_{r_i}} \cdot (2n_{r_i})!} \qquad (3.6)$$

The apparent disadvantage of these error estimates is that it is not always possible to differentiate the integrand to obtain an estimate for the error.

CHAPTER 3 NUMERICAL INTEGRATION (I) : NON-SINGULAR INTEGRALS

Several upper error bounds, which do not involve partial derivatives of the integrands, have been presented by McNamee(1964), Lether(1981), and Smith(1979). Error bound estimates for the product Gauss rule have been given by Stenger(1966), Barnhill(1968a and 1968b), and Lether(1970a, 1970b, and 1971). However, these error estimates usually exaggerate the true error by several orders of magnitude(Davis and Rabinowitz, 1984). In addition, most methods tend to have an obvious mathematical bias, and even the simplest method is tedious. Consequently, it is most desirable that the errors of numerical integration in boundary element analyses can be effectively estimated without recourse to complicated mathematical operations.

Based on certain simplifying assumptions, Lachat and Watson (1976) give approximate upper bounds for numerical integration of integrals over a segment and a rectangular region. Similar formulae have been presented by Watson(1979), Mustoe(1984), and Jun et al(1985). However, these estimates have been shown to be inaccurate(Hsiao and Kleinman, 1992). The present study uses numerical tests to investigate the error bounds of surface integrals.

3.3.3 Empirical Method

Test Procedure

Integrals in the boundary element method can be characterized by the strength of singularity, the size of the element being integrated, and the proximity of the source point. The last factor is normally defined by the minimum distance, D_{\min} , between the source point and the element and, in particular, as a ratio of some characteristic element dimension. Without loss of generality, in the present study the following analogous integrals:

$$\int_s \frac{1}{r^n} dS \quad (3.7)$$

are integrated over a 2x2 square. The superscript n takes the values 1 or 2, corresponding to the singularity of the displacement fundamental solutions and traction fundamental solutions, respectively.

The centre of the square is located at the origin of the X-Y coordinate system. Because of the symmetry conditions, we need consider only the first quadrant. The source point is assumed to lie within a region twice the size of the square, and the region is discretized into a 200x200 square grid. At each node of the grid the integrals have been computed by both Gauss-Legendre quadrature and analytical integration (where possible) using polar coordinates. For the numerical integration, a sequence of Gauss-Legendre formula with order n (n=2~11) is used. Utilization of high integration orders is not recommended, because the accuracy of the results may deteriorate due to round-off; numerical evidence has been given by Davis and Rabinowitz (1984). The analytical solutions are then used to compute the (absolute) relative error of the numerical results predicted by Gauss-Legendre quadrature. It should be noted that integrals of the integrand $(1/r^2)$ cannot be evaluated easily by analytical means over two-dimensional regions, in general. In these cases, the computation of relative error is based on the value obtained by subdividing the square into four equal parts and using the 11x11 integration rule for each sub-element.

Test Results

Once the relative errors have been evaluated for the whole region of interest, the contours of relative error for various Gauss-Legendre rules can be obtained (using the GHOST-80

CHAPTER 3 NUMERICAL INTEGRATION (I) : NON-SINGULAR INTEGRALS

graphical output system), as depicted in Figures 3.1 and 3.2. These contours reflect quite well the essential features of the error bounds of Gauss-Legendre integration.

It is significant to note that the error contours are not smooth. However, for the same integration order, contours of different accuracy have almost the same shape. Each contour has, for $n \times n$ integration rule, $(2n-2)$ lobes in the quadrant. The reason for this phenomenon will be discussed at greater length later.

These figures clearly show that, for a constant minimum distance from the square, the accuracy of Gauss-Legendre integration depends on the position of source point. In general, the greatest error occurs when the source point is close to the middles of the sides of the square; while the least error occurs when the source point is close to the corners. From these data, the error for any arbitrary source point can be predicted. It should be noted that Jun et al (1985) investigated the error bounds for Gauss-Legendre quadrature by considering only source points being on the extension of the diagonal of the square. Clearly, their results would underestimate the error of numerical integration in most practical cases.

Comparisons of the contours obtained by the same integration order for the integral $1/r$ and integral $1/r^2$ indicate that the strength of the singularity can significantly affect the accuracy of Gauss-Legendre quadrature. Stronger singularities usually require larger "minimum distances" from the integration region to achieve equivalent accuracy. The conclusion is drawn that, for a specified precision, the minimum order of integration rule depends on minimum distance, the strength of singularity, and the relative position of the source point to the element being integrated. These observations provide significant insights into the problem of how integrals in the

boundary element analysis may be computed expeditiously.

Discussion

As noted above the error contours are by no means smooth; the reasons for this are discussed below. Without loss of generality, we consider the integral:

$$I_s = \int_{-1}^{+1} \frac{1}{r} dx \tag{3.8}$$

over a segment (x=-1~+1, y=0). In the present study this integral is computed by both Gauss-Legendre quadrature and analytical integration.

For the purpose of clarity, typical contours of the integral value are depicted in Figure 3.3, in the first quadrant. It is of interest to note that the analytical contours are simple smooth curves while the approximate contours are wavy. By inspection, it can be seen that the number of intersections in each quadrant corresponds to the order of integration. Clearly, these intersections represent the points where Gauss-Legendre quadrature yields exact results. Migeot(1985) connected these intersection points, as exemplified by the normal curves to the contours in Figure 3.3, to trace the line of null errors. Evidently, as shown in Figure 3.3, the higher integration rules deviate less from the exact solution (contour).

3.3.4 Criteria For Selecting The Order Of Gauss Integration

Based on the extensive numerical tests described above, criteria for selecting the order of Gauss-Legendre integration

CHAPTER 3 NUMERICAL INTEGRATION (I) : NON-SINGULAR INTEGRALS

for non-singular integrals in the boundary element method have been developed in this thesis. As depicted in Figure 3.4, for each type (order) of singularity and allowable error, we can define a "maximum distance", D , between the element being integrated and the error contour measured.

Further numerical studies reveal that the characteristic ratio D/L_e for elements of different size are identical, where L_e is the dimension of the element. Values of D/L_e for specified tolerance levels have been tabulated in Tables 3.1 and 3.2. Comparisons of the required integration order for specific accuracies with the corresponding predictions by other authors are given in Figures 3.5 and 3.6. It is evident that the required integration order becomes very sensitive to the variation of D as the source point approaches the element (especially for $D/L_e < 0.15$). Considerable computational resources are needed to achieve sufficient accuracy for these "nearly singular" integrals. However, Lachat and Watson's method is not applicable to the evaluation of "nearly singular" integrals. Figures 3.5 and 3.6 also emphasize that the error estimate used by Lachat and Watson(1976) is grossly conservative. For example, for cases of the integrand= $1/r$, $D/L_e=0.5$, and allowable error=0.1%, the required integration order is four by the present study and eight by Lachat and Watson's method. This observation leads immediately to questions of the efficiency of their integration scheme. Several numerical examples will be presented in the subsequent sub-section to illustrate the deficiency of Lachat and Watson's method.

Based on the computed values of D/L_e , effective and reliable criteria for selecting the order of Gauss-Legendre integration are proposed as follows:

(I) integrand = 1/r

$$N_{req} = \underset{\epsilon_a = 10^{-3}}{\text{integer}} \left[\left(\frac{4L_e}{3D} \right)^{\frac{4}{5}} \right] + 1 \quad (3.9)$$

$$N_{req} = \underset{\epsilon_a = 10^{-4}}{\text{integer}} \left[\left(\frac{8L_e}{3D} \right)^{\frac{3}{4}} \right] + 1 \quad (3.10)$$

(II) integrand = 1/r²

$$N_{req} = \underset{\epsilon_a = 10^{-3}}{\text{integer}} \left[\left(\frac{2L_e}{D} \right)^{\frac{5}{6}} \right] + 1 \quad (3.11)$$

$$N_{req} = \underset{\epsilon_a = 10^{-4}}{\text{integer}} \left[\left(\frac{4L_e}{D} \right)^{\frac{3}{4}} \right] + 1 \quad (3.12)$$

In practical application, parameter D in these equations should be replaced by D_{min}, the minimum distance between the source point and the integration region.

Example: As depicted in Figure 3.7, the integral

$$\int \frac{1}{r} dA$$

over a 2x2 square is computed, with source point at (3,1). The allowable error is 0.1%. The minimum distance between the

source point and the integration region is 1. Based on Equation(3.9), the required integration order is three. The analytical solution of this integral is 2.07609 9164, while numerical integration gives 2.07661 6864. The computed error is 0.025%.

3.4 Adaptive Integration Strategies

Based on equations(3.9-3.12), two fundamentally different adaptive strategies can be developed for the application of Gauss-Legendre quadrature to three-dimensional boundary element analyses. The "order adaptive" method involves choosing the number of Gauss points needed in each direction over a boundary element. On the other hand, the sub-division adaptive method involves subdivision of boundary elements into subelements. In this study, integrations are performed by combining these two strategies as follows:

- (1) Calculate how many Gauss points, N_{req} , are needed to perform the integration with the required precision.
- (2) If N_{req} is less than some specified maximum allowable order of Gauss integration, N_{max} , compute the integral. Otherwise,
- (3) subdivide the region into sufficient subelements, and
- (4) determine the number of Gauss points required to integrate each sub-element and then compute the integral over each sub-element.

To illustrate the merits of the proposed integration scheme, several test integrals have been evaluated. The maximum and

the minimum allowable order of integration are 5 and 2, respectively. The allowable relative error is 10^{-3} . A graded element sub-division is employed to improve efficiency while still retaining accuracy. Subdivision schemes and numerical results are shown in Figures 3.8 and 3.9. Clearly, the adaptive strategy benefits from the fact that it increases the concentration of integration points near to the minimum distance location over the element. Results predicted by the method of Lachat and Watson(1976) are also given. For the same integration accuracy, the present study requires considerably less(perhaps a 60% reduction) computational effort than Lachat and Watson's method. It is evident that the proposed method is more efficient than that of Lachat and Watson(1976).

3.5 Integrals With Oscillatory Integrands

3.5.1 Introduction

The numerical evaluation of integrals with oscillatory integrands, for example, in the Fourier form:

$$\int_a^b f(x) \sin(mx) dx \quad (3.13)$$

$$\int_a^b f(x) \cos(mx) dx \quad (3.14)$$

and, in complex form,

$$\int_a^b f(x) e^{i\omega x} dx \quad (3.15)$$

has wide applications in applied mathematics, physics, and

engineering. Often, the use of conventional numerical integration, for example, Gauss-Legendre quadrature, to compute oscillatory integrals will result in the calculation of many positive and negative values which are nearly equal in absolute magnitude. The cancellation of the positive values and the negative values can result in slow convergence and numerical instability.

Approaches for evaluating rapidly oscillatory integrals (more than ten local maxima and minima over the range of integration) have been summarized by Davis and Rabinowitz (1984). However, these studies are restricted to one-dimensional integrals, and extension of these methods to higher dimensional integrals is not straightforward. This section develops the "order adaptive" scheme for the application of Gauss-Legendre quadrature to oscillatory integrals in three-dimensional boundary element analyses.

3.5.2 Gauss Integration Over Square Region

In a manner similar to the procedure described in section 3.3, an extensive series of numerical tests has been performed to investigate the error relating to the numerical integration of the following oscillatory integrals

$$\int_s \frac{e^{ikr}}{r} dS \tag{3.16}$$

and

$$\int_s \frac{e^{ikr}}{r^2} dS \tag{3.17}$$

over a square. In the above equations,

$$\kappa = \frac{\omega}{C_2} \quad (3.18)$$

is the wave number, where C_2 is the shear wave velocity.

For small wave numbers, numerical integration can be used for computing these integrals without considering their wavy nature. However, for larger wave numbers (i.e., high frequency) cases, the integrands oscillate rapidly, with respect to spatial distance from the source point. When the wavelength is less than the dimension of the element being integrated, numerical integration requires an increasingly large number of integration points to achieve the required accuracy. Perhaps more importantly, it becomes necessary to specify a large number of nodal points in order to capture the spatial variation in the field variables. Otherwise, high frequency waves are lost and the boundary element acts as a low-pass filter. As a consequence, the boundary elements must be limited in size in proportion to the lowest wavelength. In the present study, the maximum dimension of the largest element employed in the discretization scheme is limited to 1/4 Rayleigh wavelengths. Preliminary numerical studies for a wide range of frequencies reveal that this rule also eliminates the need to modify the integration rule (Gauss order) for different frequencies.

Analytical solutions of integrals (3.16) and (3.17) are extremely difficult. The evaluation of errors is based on numerically computed values of the integrals, I_a , obtained by subdividing the element into four parts and using 11x11 integration rule for each sub-element. Because the integrals are complex numbers, the relative error is determined as follows:

$$e = \max \left[\left| \frac{I_{ar} - I_{nr}}{I_{ar}} \right|, \left| \frac{I_{ai} - I_{ni}}{I_{ai}} \right| \right] \quad (3.19)$$

in which, I_{ar} and I_{ai} are the real parts and imaginary parts of I_a , respectively; and I_{nr} and I_{ni} are the real parts and imaginary parts of the corresponding numerical solution. However, if the absolute value of the real(imaginary) part is less than 1% of the imaginary(real) part, then the error is assumed to be equal to the error of the imaginary(real) part.

Typical plots of the relative error contours from the numerical integration for various values of frequency are given in Figures 3.10 and 3.11. In a manner similar to the static integrals, for a specified precision, the order of integration needed depends on the minimum distance, the strength of singularity of the non-oscillatory part and the relative position of the source point to the element being integrated. However, it is significant that allowable errors $\epsilon_a < 10^{-4}$ are difficult to obtain. The integration orders required to attain specified accuracies are given in Table 3.3 and 3.4.

Comparisons may be made with the results for (static) non-oscillatory integrals(Figures 3.12 and 3.13). It is observed that the differences between these two approaches are small. This observation confirms that the limitation on element size largely eliminates the need to consider the frequency parameter in numerical integration.

3.5.3 Adaptive Integration Strategy

Using the same procedures and definitions described in the previous section, practical criteria for selecting the order of integration, for $\epsilon_a = 10^{-3}$, can be derived as follows:

(I) integrand = e^{ikr}/r

$$N_{req} = \text{integer} \left(\frac{3L_e}{2D} \right)^{0.85+1} \quad (3.20)$$

(II) integrand = e^{ikr}/r^2

$$N_{req} = \text{integer} \left(\frac{3L_e}{D} \right)^{0.75+1} \quad (3.21)$$

3.6 Conclusions

Numerical integration is a crucial element in the implementation of boundary element methods. Because the evaluation of non-singular integrals consumes a significant amount of the computational time, sophisticated integration schemes to achieve results of high accuracy with the minimum cost have been developed in this study.

The estimation of quadrature error bounds has received considerable attention in the literature because of its importance in relation to adaptive integration schemes. However, these theoretical results are not readily applicable to the Green's functions employed here. By using numerical tests, an investigation into Gauss-Legendre quadrature errors for non-singular integrals has been carried out. In addition, exploitation of dimensionless quantities largely eliminates the influence of frequency. Systematic computation of integrals in both static and dynamic boundary element analyses can now be performed without special difficulty.

CHAPTER 3 NUMERICAL INTEGRATION (I) : NON-SINGULAR INTEGRALS

Numerical results reveal that the error bounds depend on the order of integration, the strength of singularity, and the relative position of the source point to the element being integrated. Based on the results of numerical tests, effective and simple criteria have been developed to determine how many Gauss points are required to yield specified integration accuracy. By combining these criteria with strategies for order and subdivision adaptations, effective integration schemes have been achieved. Test integrals have been presented to demonstrate the efficiency and accuracy of the proposed integration scheme. These criteria and methods could be implemented within other boundary element method codes without much difficulty.

TABLE 3.1 VALUES OF D/L_e FOR THE SPECIFIED ACCURACY

$$\int_s \frac{1}{r} ds$$

Gauss order	$\epsilon=10^{-2}$	$\epsilon=10^{-3}$	$\epsilon=10^{-4}$	$\epsilon=10^{-5}$
2x2	0.44	1.16	2.45	4.75
3x3	0.16	0.39	0.71	1.16
4x4	0.12	0.27	0.46	0.70
5x5	0.09	0.20	0.33	0.47
6x6	0.07	0.16	0.26	0.37
7x7	0.06	0.13	0.21	0.30
8x8	0.05	0.11	0.18	0.26
9x9	0.04	0.10	0.16	0.22
10x10	0.03	0.09	0.14	0.20
11x11	0.03	0.08	0.12	0.18

TABLE 3.2 VALUES OF D/L_e FOR THE SPECIFIED ACCURACY

$$\int_s \frac{1}{r^2} dS$$

Gauss order	$\epsilon=10^{-2}$	$\epsilon=10^{-3}$	$\epsilon=10^{-4}$	$\epsilon=10^{-5}$
2x2	0.84	1.89	3.76	7.08
3x3	0.33	0.65	1.10	1.86
4x4	0.23	0.41	0.65	0.98
5x5	0.17	0.29	0.43	0.61
6x6	0.14	0.24	0.35	0.48
7x7	0.12	0.20	0.29	0.38
8x8	0.10	0.17	0.25	0.33
9x9	0.09	0.15	0.22	0.29
10x10	0.08	0.13	0.19	0.25
11x11	0.08	0.12	0.17	0.23

TABLE 3.3 VALUES OF D/L_e FOR THE SPECIFIED ACCURACY

$$\int_s \frac{e^{ikr}}{r} ds$$

Gauss order	$\epsilon=10^{-3}$	$\epsilon=10^{-4}$
2x2	-	-
3x3	-	-
4x4	0.41	0.67
5x5	0.26	0.57
6x6	0.20	0.33
7x7	0.15	0.26
8x8	0.13	0.21
9x9	0.12	0.19
10x10	0.11	0.16
11x11	0.10	0.15

TABLE 3.4 VALUES OF D/L_ε FOR THE SPECIFIED ACCURACY

$$\int_s \frac{e^{ikr}}{r^2} dS$$

Gauss order	ε=10 ⁻³	ε=10 ⁻⁴
2x2	-	-
3x3	-	-
4x4	0.69	0.82
5x5	0.36	0.66
6x6	0.29	0.43
7x7	0.23	0.33
8x8	0.20	0.29
9x9	0.18	0.26
10x10	0.15	0.21
11x11	0.15	0.20

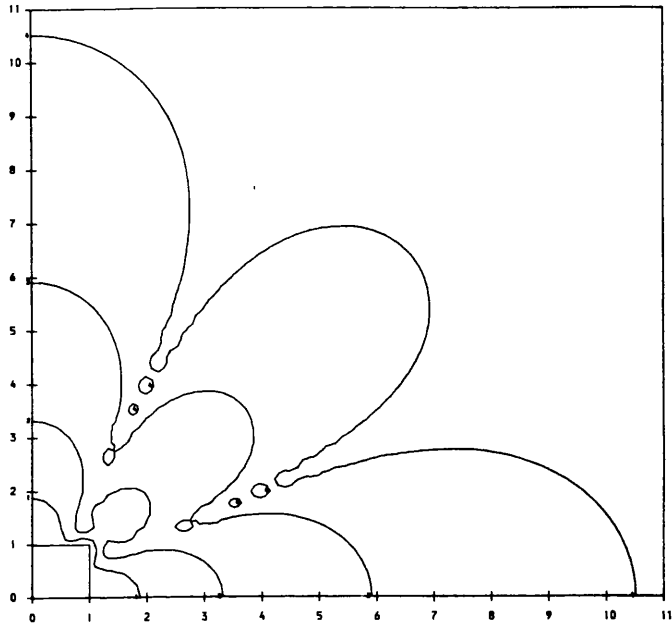


Figure 3.1a Error Contour Of Numerical Integration
Integrand = $1/r$, Integration Order = 2

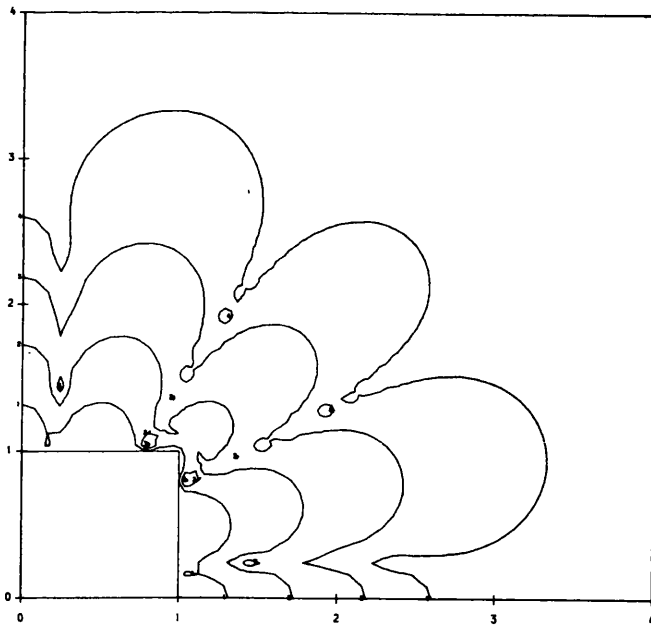


Figure 3.1b Error Contour Of Numerical Integration
Integrand = $1/r$, Integration Order = 3
Contour 1 : $\epsilon=10^{-2}$
Contour 2 : $\epsilon=10^{-3}$
Contour 3 : $\epsilon=10^{-4}$
Contour 4 : $\epsilon=10^{-5}$

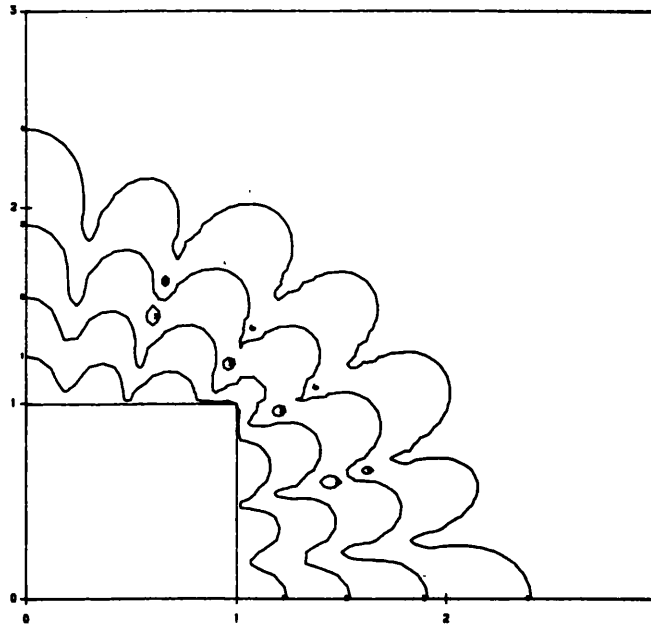


Figure 3.1c Error Contour Of Numerical Integration
Integrand = $1/r$, Integration Order = 4

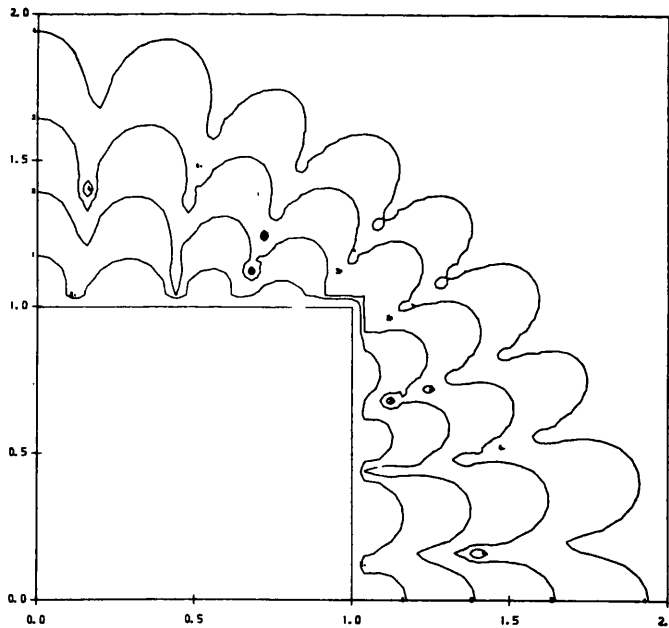


Figure 3.1d Error Contour Of Numerical Integration
Integrand = $1/r$, Integration Order = 5
Contour 1 : $\epsilon=10^{-2}$
Contour 2 : $\epsilon=10^{-3}$
Contour 3 : $\epsilon=10^{-4}$
Contour 4 : $\epsilon=10^{-5}$

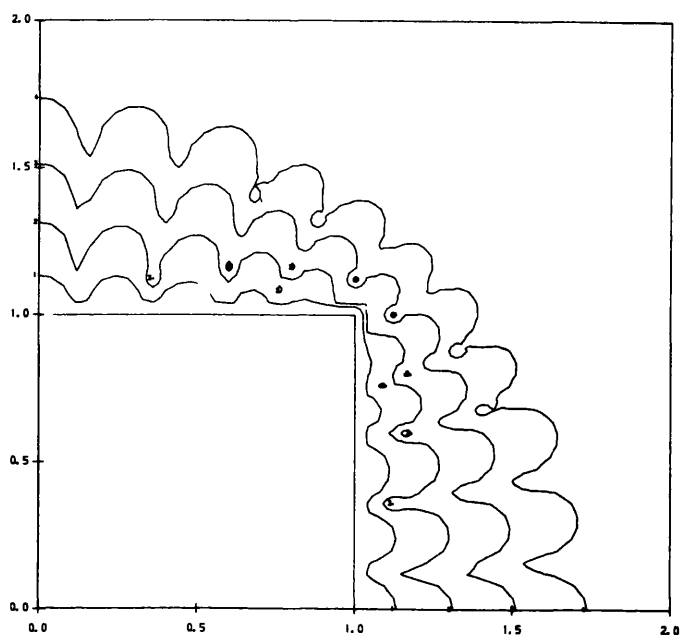


Figure 3.1e Error Contour Of Numerical Integration
Integrand = $1/r$, Integration Order = 6

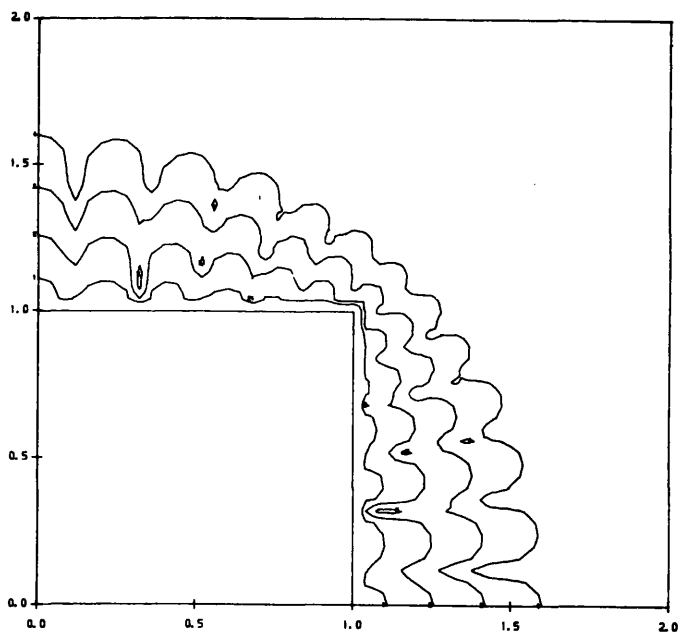


Figure 3.1f Error Contour Of Numerical Integration
Integrand = $1/r$, Integration Order = 7
Contour 1 : $\epsilon=10^{-2}$
Contour 2 : $\epsilon=10^{-3}$
Contour 3 : $\epsilon=10^{-4}$
Contour 4 : $\epsilon=10^{-5}$

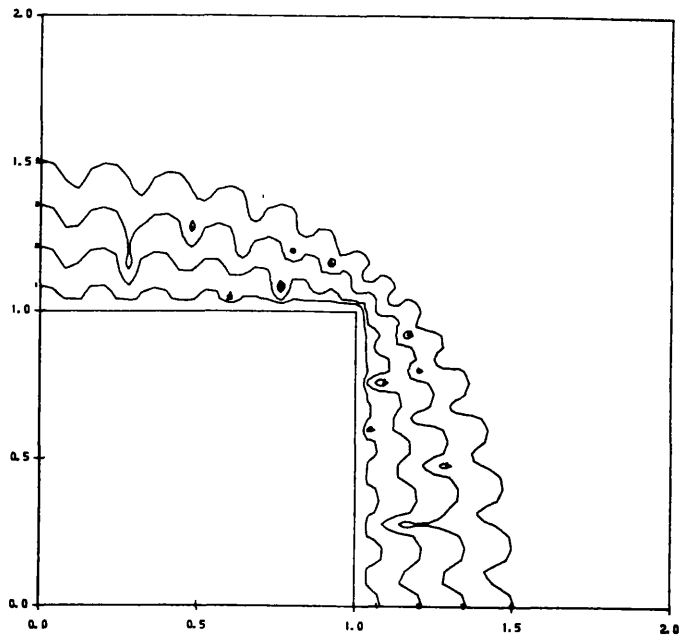


Figure 3.1g Error Contour Of Numerical Integration
Integrand = $1/r$, Integration Order = 8

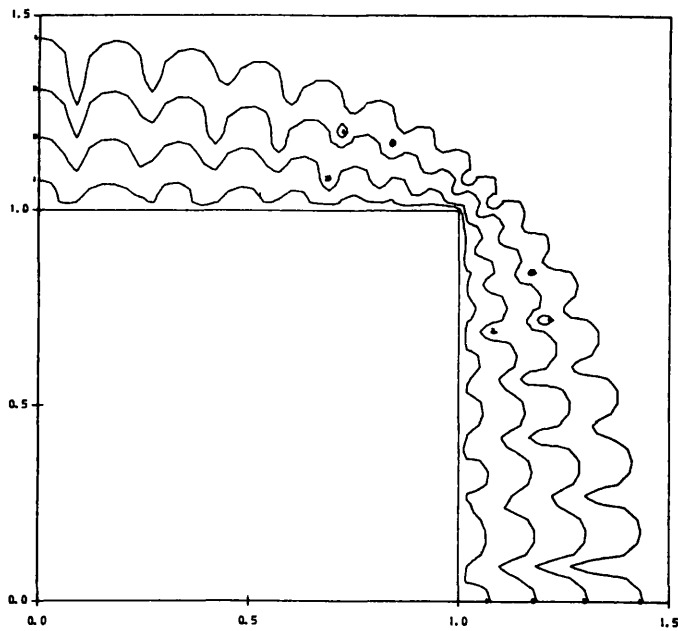


Figure 3.1h Error Contour Of Numerical Integration
Integrand = $1/r$, Integration Order = 9
Contour 1 : $\epsilon=10^{-2}$
Contour 2 : $\epsilon=10^{-3}$
Contour 3 : $\epsilon=10^{-4}$
Contour 4 : $\epsilon=10^{-5}$

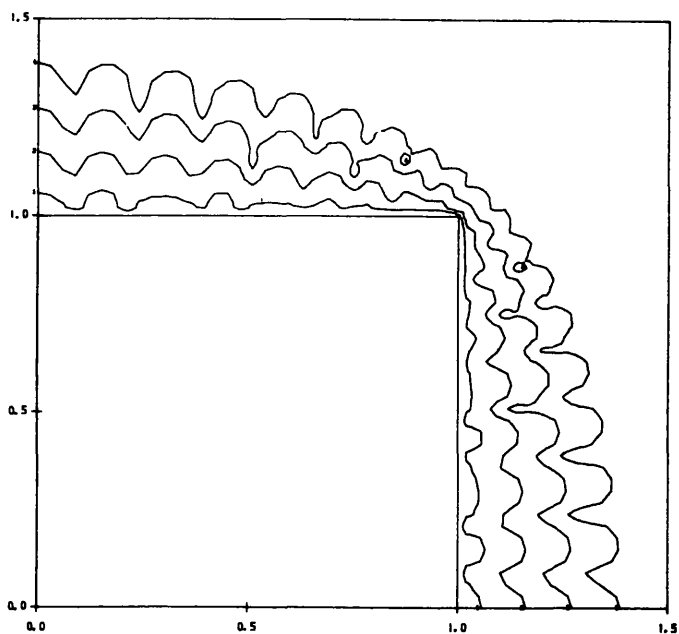


Figure 3.1i Error Contour Of Numerical Integration
Integrand = $1/r$, Integration Order = 10

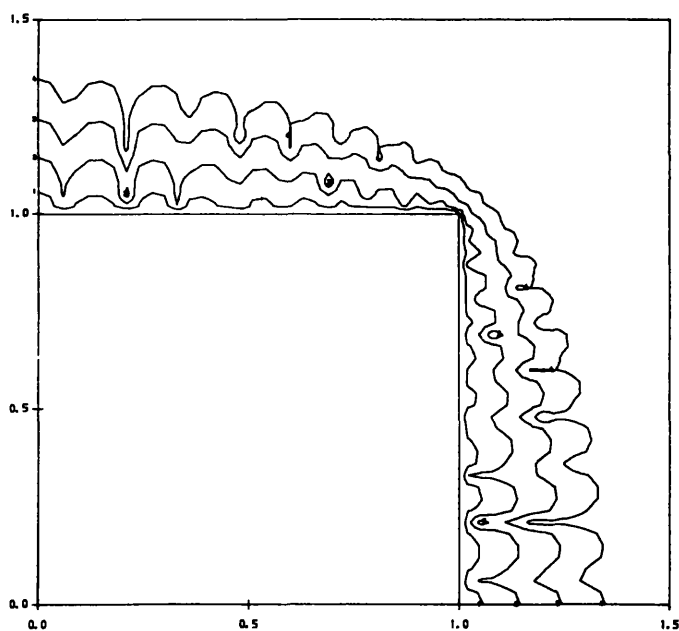


Figure 3.1j Error Contour Of Numerical Integration
Integrand = $1/r$, Integration Order = 11
Contour 1 : $\epsilon=10^{-2}$
Contour 2 : $\epsilon=10^{-3}$
Contour 3 : $\epsilon=10^{-4}$
Contour 4 : $\epsilon=10^{-5}$

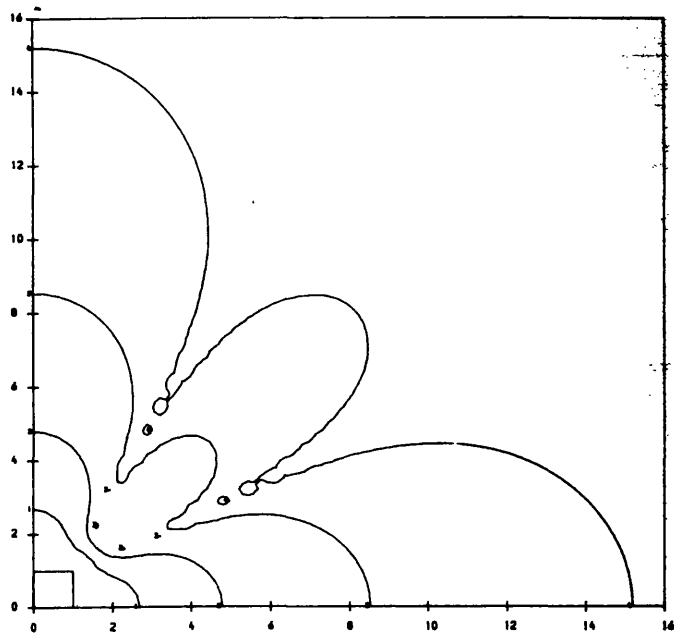


Figure 3.2a Error Contour Of Numerical Integration
Integrand = $1/r^2$, Integration Order = 2

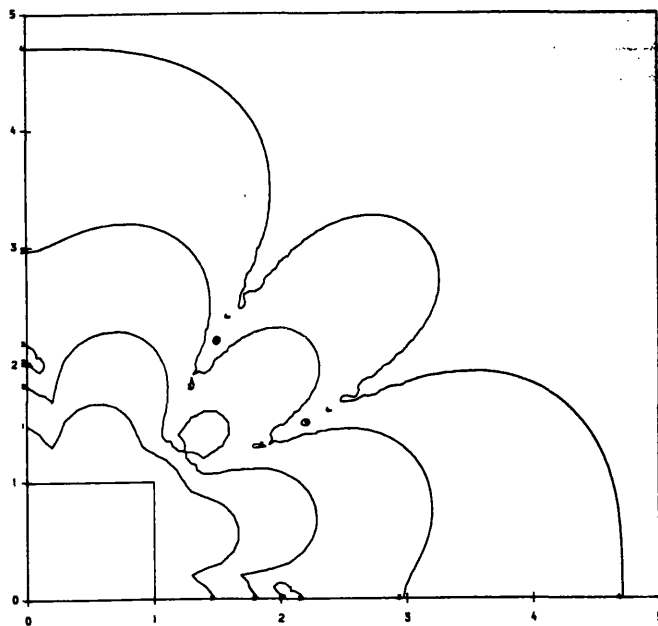


Figure 3.2b Error Contour Of Numerical Integration
Integrand = $1/r^2$, Integration Order = 3
Contour 1 : $\epsilon=10^{-2}$
Contour 2 : $\epsilon=10^{-3}$
Contour 3 : $\epsilon=10^{-4}$
Contour 4 : $\epsilon=10^{-5}$

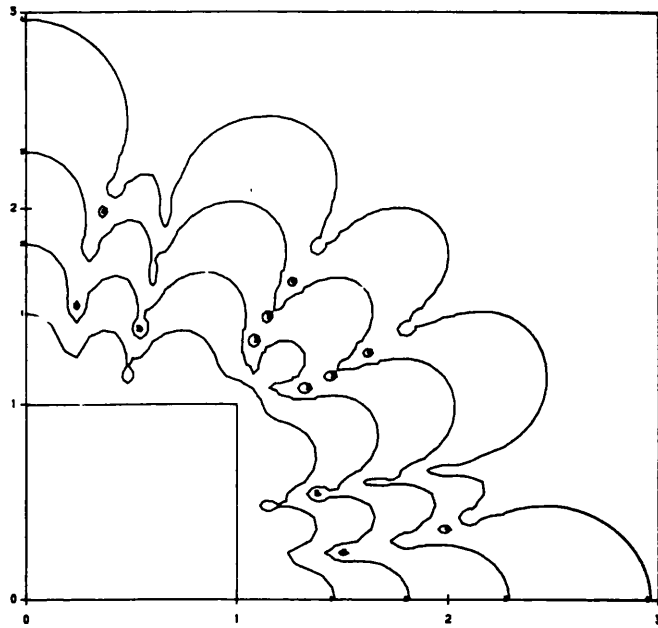


Figure 3.2c Error Contour Of Numerical Integration
Integrand = $1/r^2$, Integration Order = 4

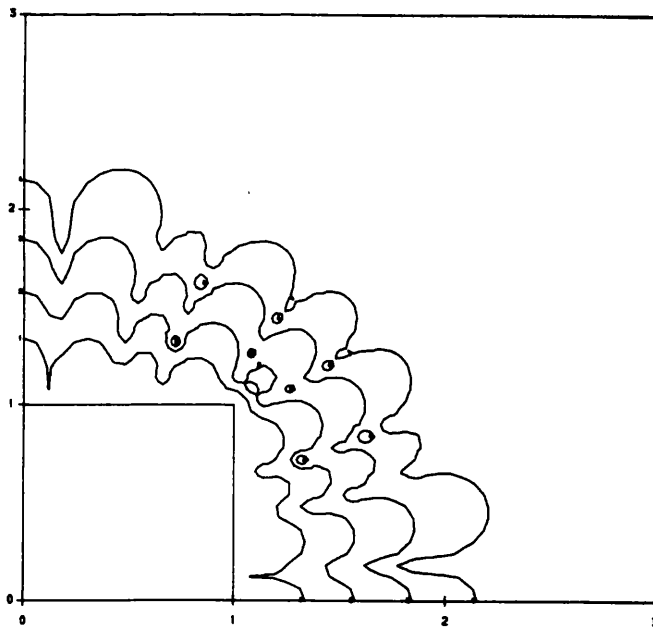


Figure 3.2d Error Contour Of Numerical Integration
Integrand = $1/r^2$, Integration Order = 5
Contour 1 : $\epsilon=10^{-2}$
Contour 2 : $\epsilon=10^{-3}$
Contour 3 : $\epsilon=10^{-4}$
Contour 4 : $\epsilon=10^{-5}$

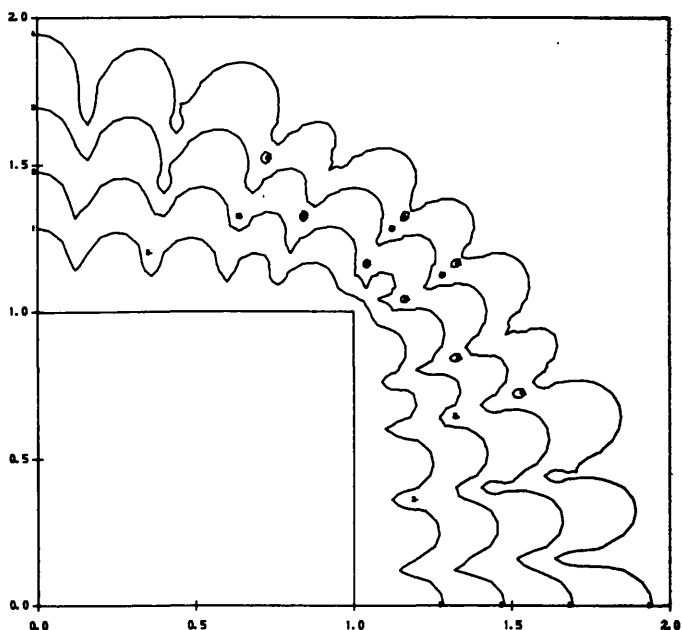


Figure 3.2e Error Contour Of Numerical Integration
Integrand = $1/r^2$, Integration Order = 6

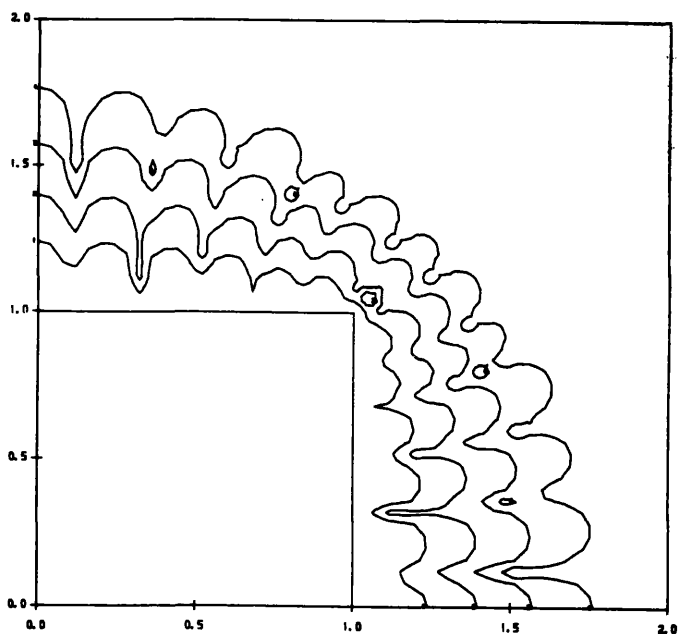


Figure 3.2f Error Contour Of Numerical Integration
Integrand = $1/r^2$, Integration Order = 7
Contour 1 : $\epsilon=10^{-2}$
Contour 2 : $\epsilon=10^{-3}$
Contour 3 : $\epsilon=10^{-4}$
Contour 4 : $\epsilon=10^{-5}$

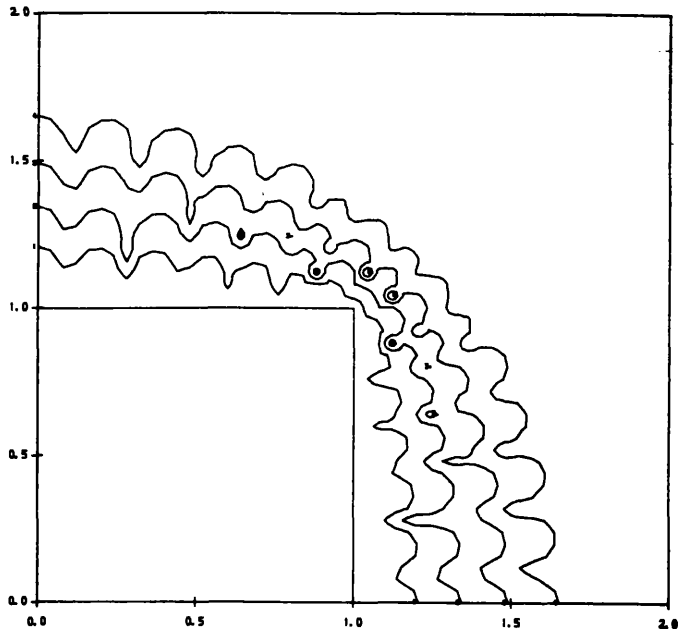


Figure 3.2g Error Contour Of Numerical Integration
Integrand = $1/r^2$, Integration Order = 8

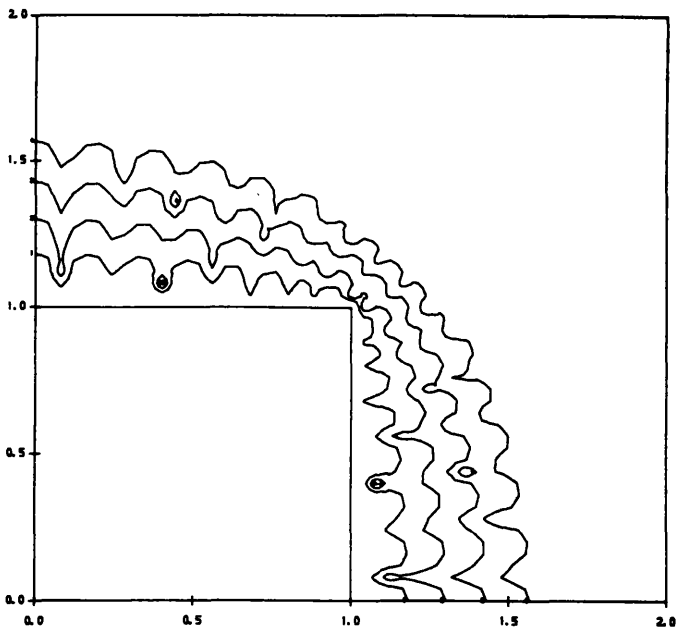


Figure 3.2h Error Contour Of Numerical Integration
Integrand = $1/r^2$, Integration Order = 9
Contour 1 : $\epsilon=10^{-2}$
Contour 2 : $\epsilon=10^{-3}$
Contour 3 : $\epsilon=10^{-4}$
Contour 4 : $\epsilon=10^{-5}$

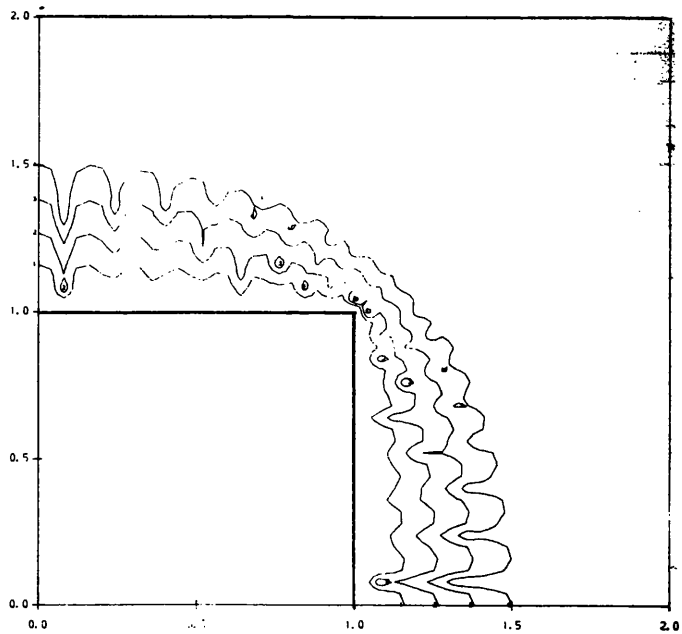


Figure 3.2i Error Contour Of Numerical Integration
Integrand = $1/r^2$, Integration Order = 10

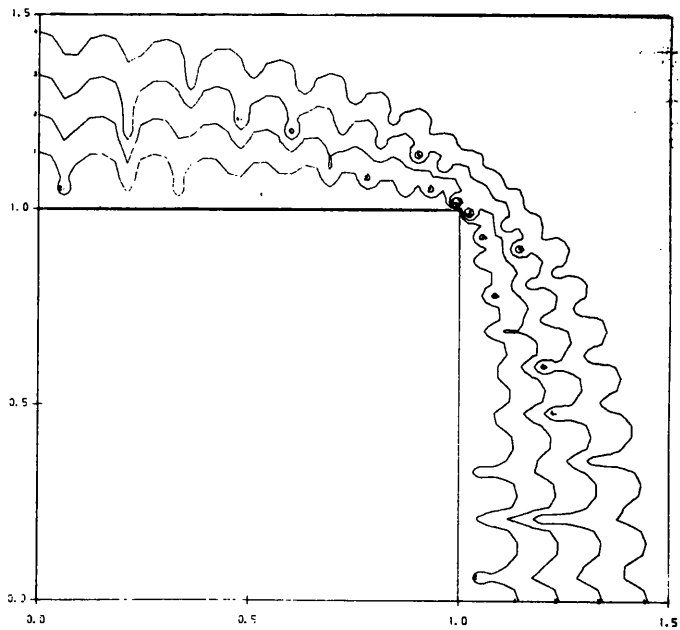


Figure 3.2j Error Contour Of Numerical Integration
Integrand = $1/r^2$, Integration Order = 11
Contour 1 : $\epsilon=10^{-2}$
Contour 2 : $\epsilon=10^{-3}$
Contour 3 : $\epsilon=10^{-4}$
Contour 4 : $\epsilon=10^{-5}$

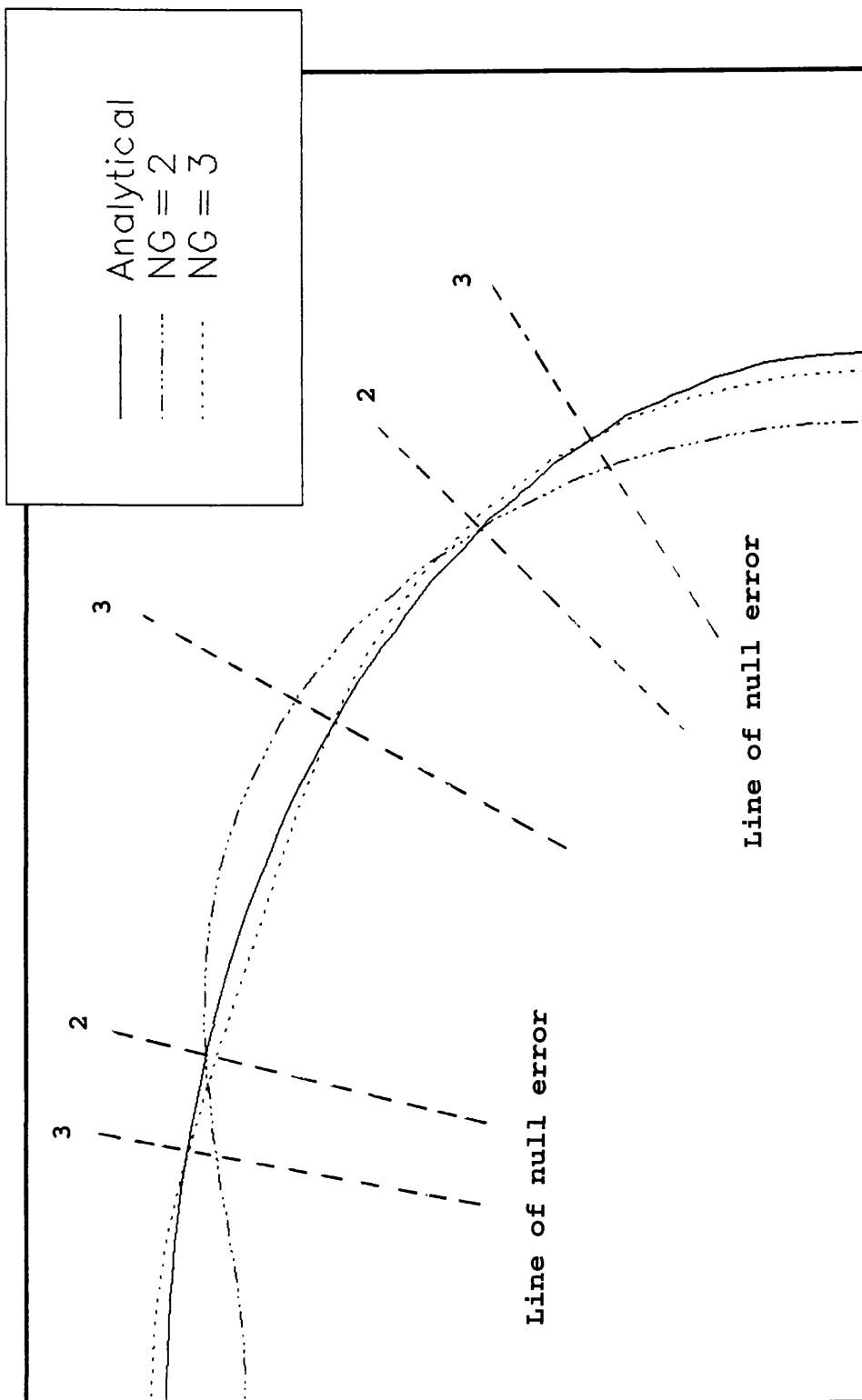


Figure 3.3 Analytical Contours and Approximate Contours In The First Quadrant, value of integral (3.8)=2.5.

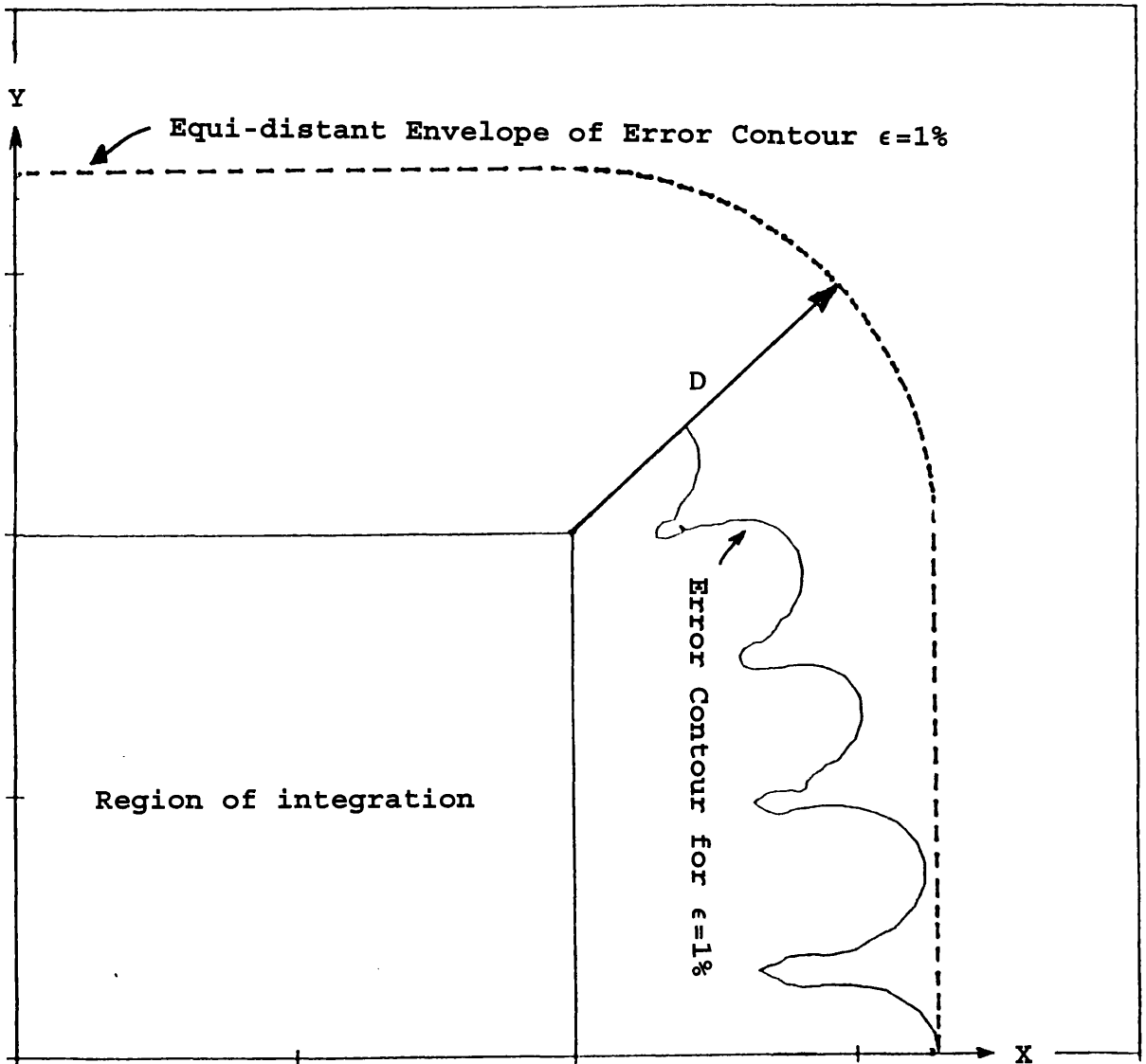


Figure 3.4: Equi-distant Envelope Of Error Contour
Note: D is the minimum distance between source point and integration region for which the maximum error is always less than the error contour value.

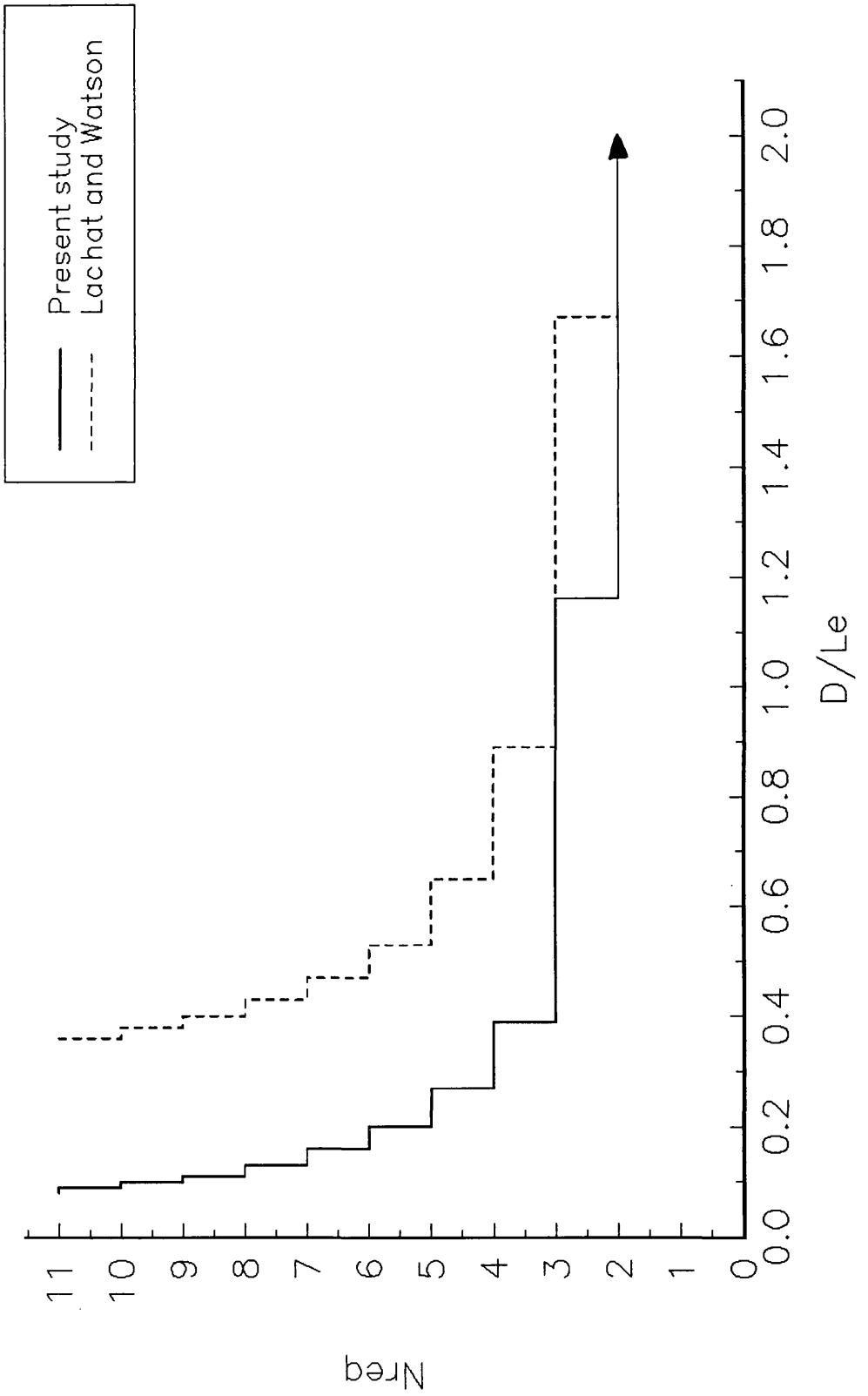


Figure 3.5: Choice of Required Integration Order
Integrand= $1/r$, Allowable error=0.1%.

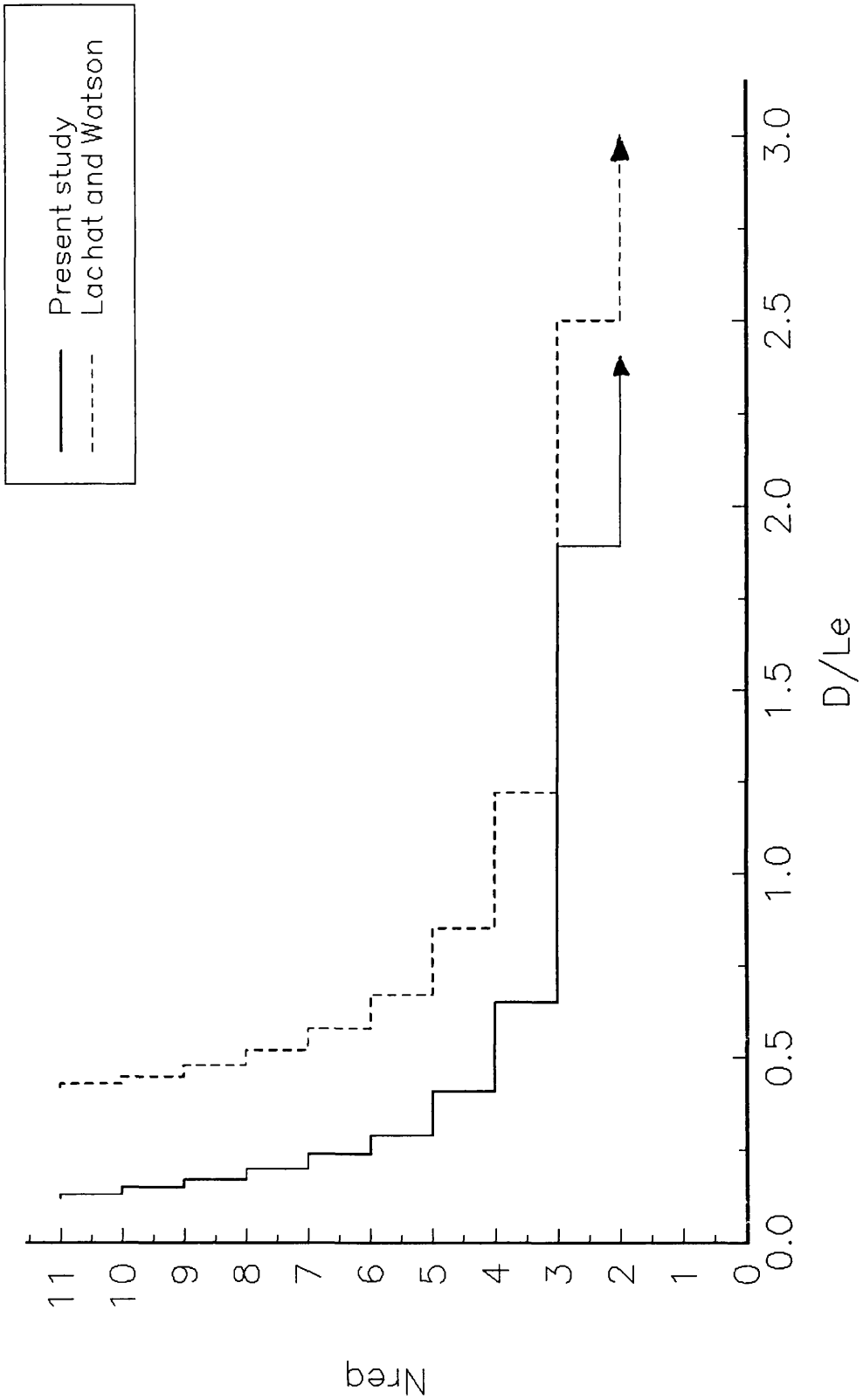


Figure 3.6: Choice of Required Integration Order
Integrand= $1/r^2$, Allowable error=0.1%.

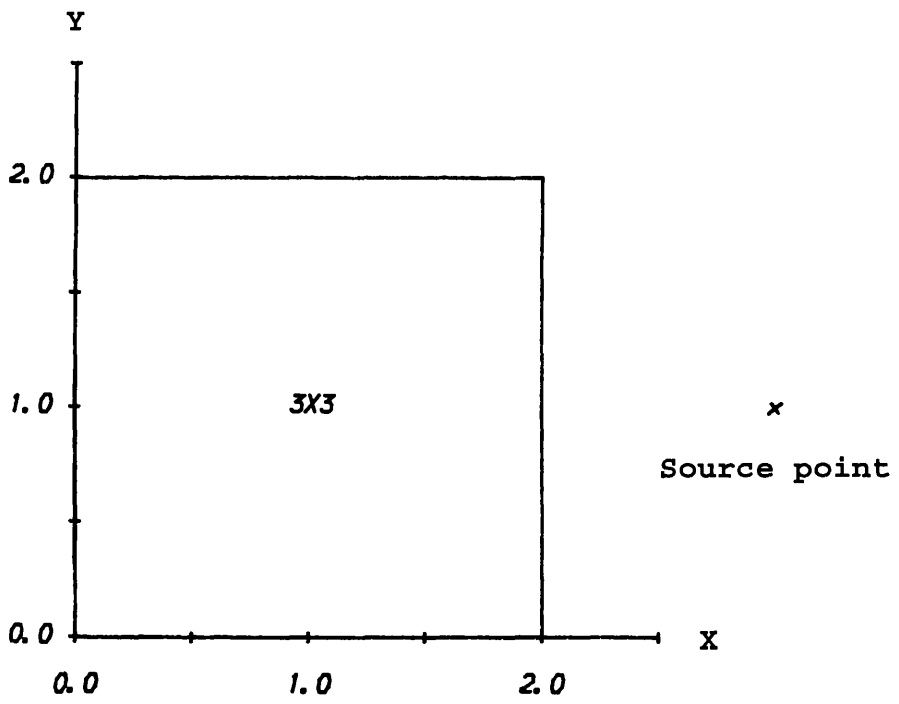
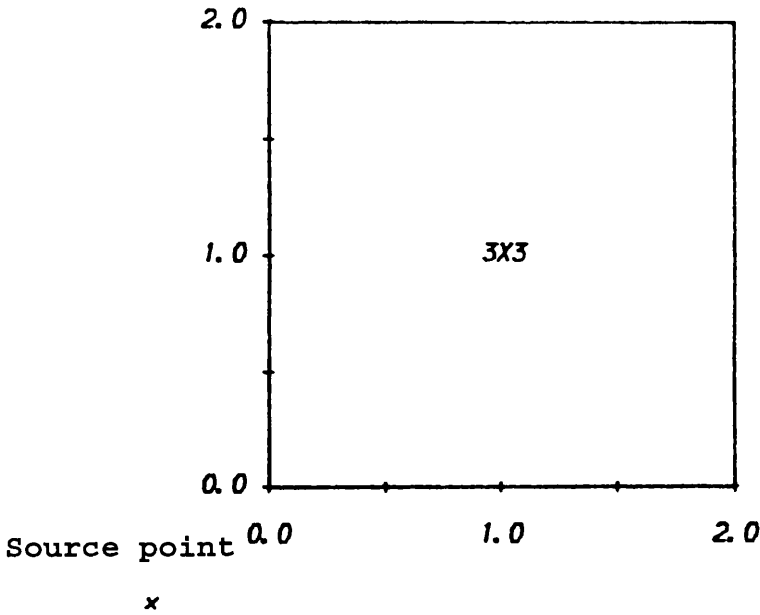
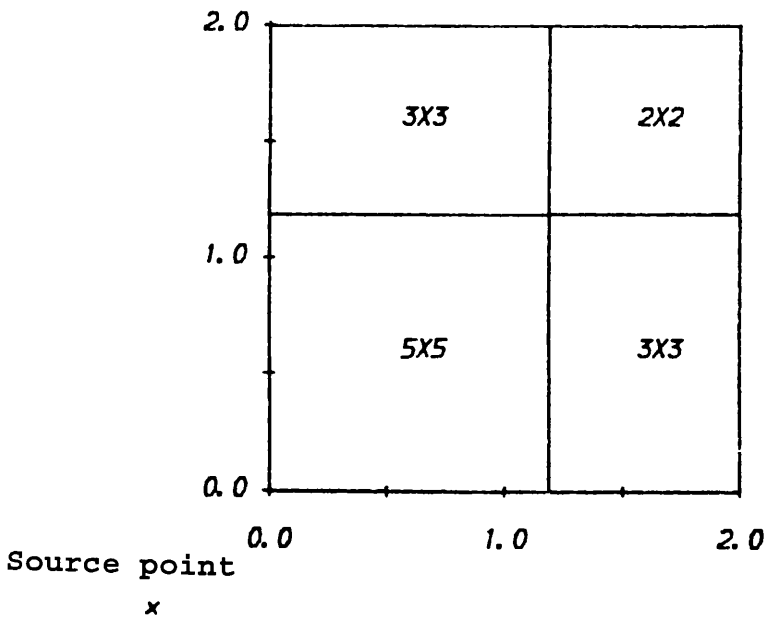


Figure 3.7: Numerical Example

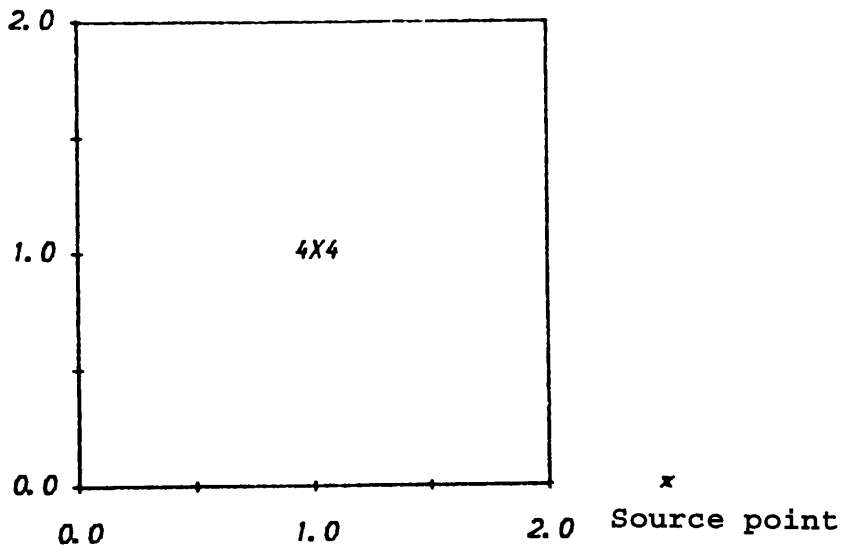


Present study: Computed Value = 1.98307 1516, $\epsilon=0.36 \times 10^{-3}$

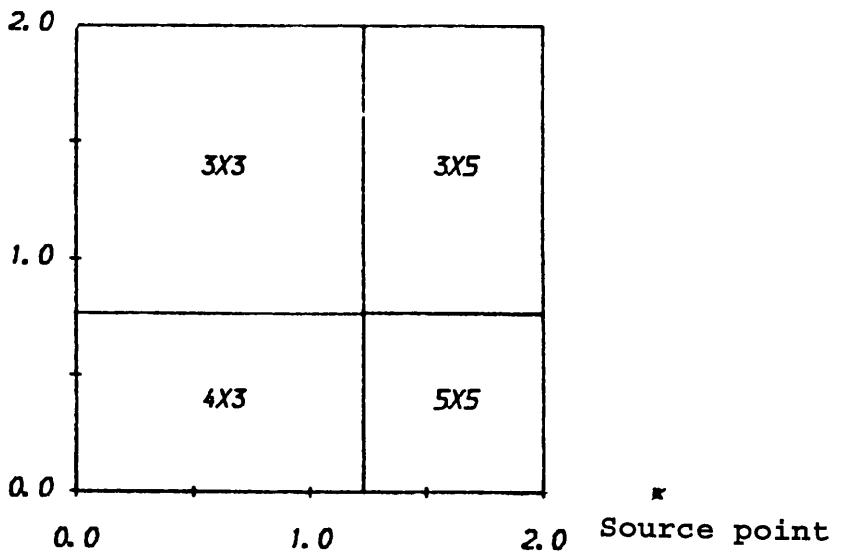


Lachat's Method: Computed Value = 1.98235 6533, 47 Gauss points, $\epsilon=0.2 \times 10^{-5}$

Figure 3.8a Adaptive Integration Scheme
 Integrand = $1/r$, Source Point x at $(-0.5, -0.5)$
 Analytical Solution = 1.98235 2629; $\epsilon_a = 10^{-3}$

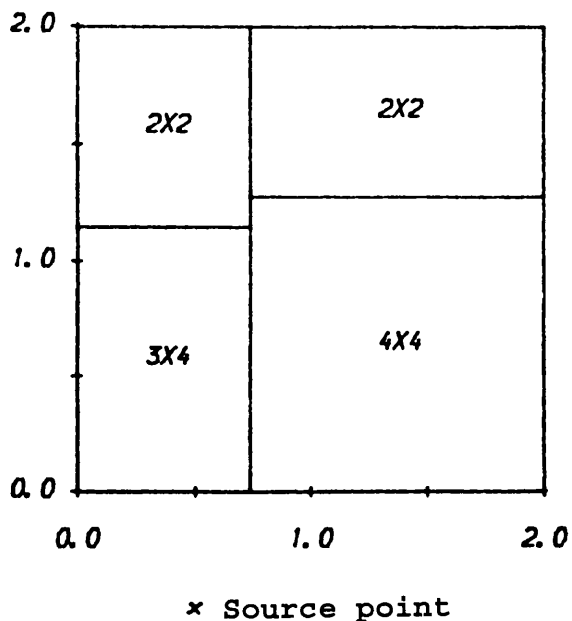


Present study: Computed Value = 2.38410 9896, $\epsilon = 0.2 \times 10^{-3}$

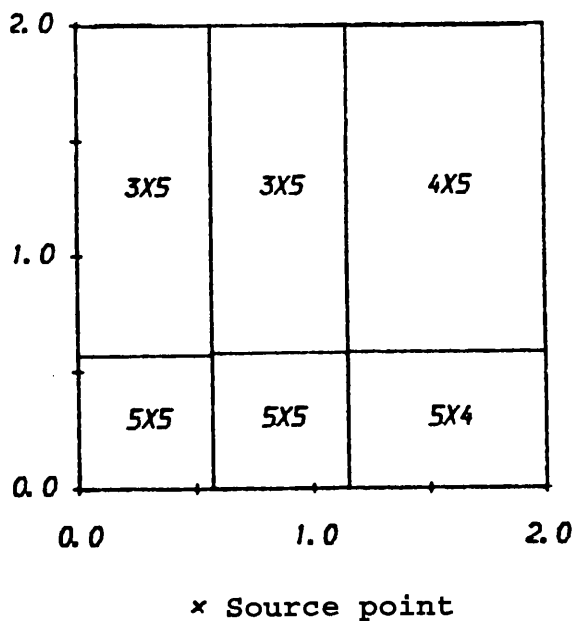


Lachat's Method: Computed Value = 2.38456 8890, 61 Gauss points, $\epsilon = 0.7 \times 10^{-6}$

Figure 3.8b Adaptive Integration Scheme
 Integrand = $1/r$, Source Point x at (2.5,0.0)
 Analytical Solution = 2.38456 7146; $\epsilon_a = 10^{-3}$

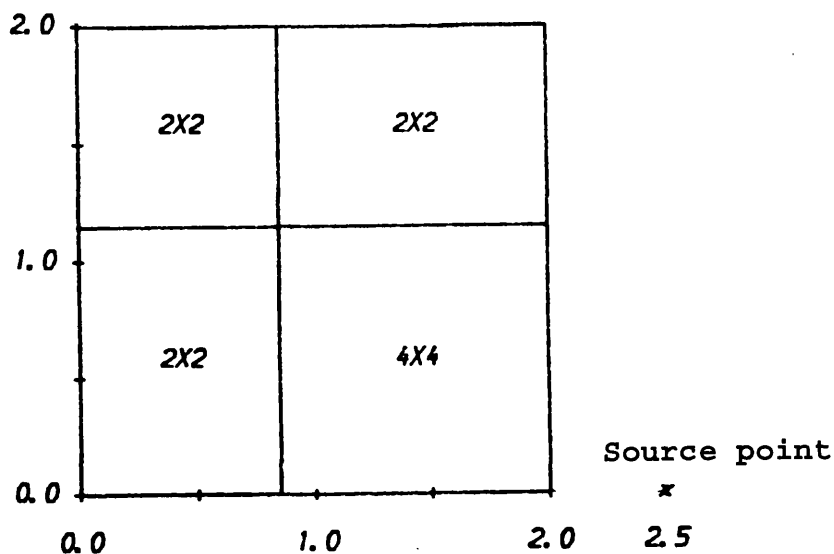


Present study: Computed Value = 2.19299 3365, 36 Gauss points, $\epsilon=0.13 \times 10^{-3}$

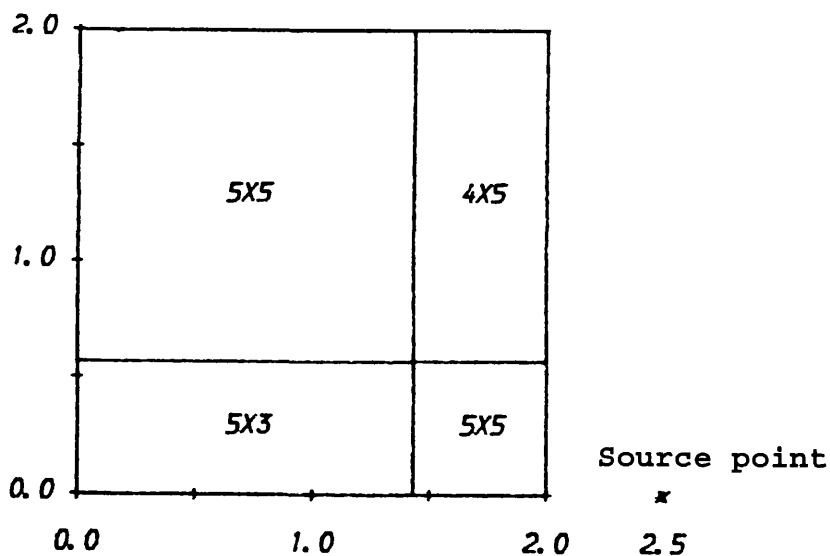


Lachat's Method: Computed Value = 2.19327 2092, 120 Gauss points, $\epsilon=0.4 \times 10^{-6}$

Figure 3.9a Adaptive Integration Scheme
 Integrand = $1/r^2$, Source Point x at $(0.5, -0.5)$
 Analytical Solution = 2.19327 2957; $\epsilon_a = 10^{-3}$



Present study: Computed Value = 1.67259 5468, 28 Gauss points, $\epsilon = 0.11 \times 10^{-3}$



Lachat's Method: Computed Value = 1.67278 1491, 85 Gauss points, $\epsilon = 0.5 \times 10^{-6}$

Figure 3.9b Adaptive Integration Scheme
 Integrand = $1/r^2$, Source Point x at (2.5,0.0)
 Analytical Solution = 1.67278 0609; $\epsilon_a = 10^{-3}$

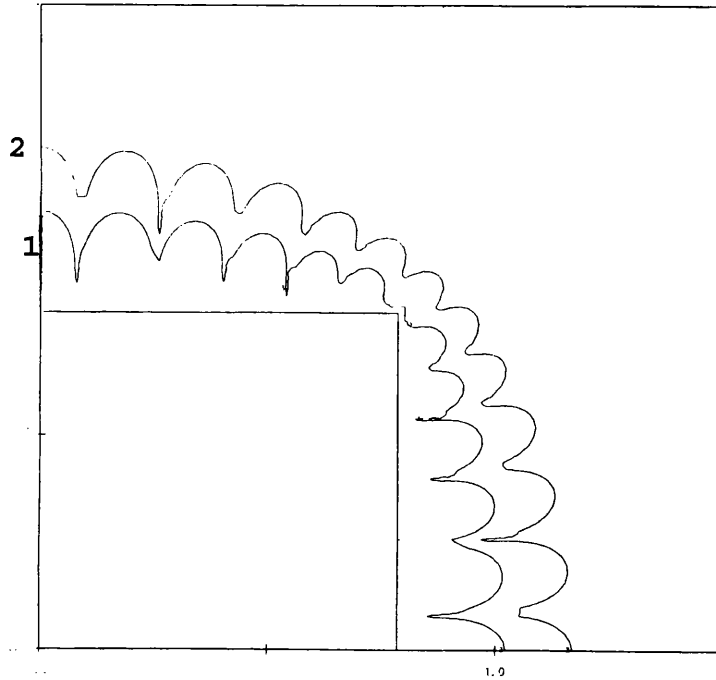


Figure 3.10a Error Contour Of Numerical Integration
Integrand = e^{ikr}/r , $k=1$, Integration Order =7.

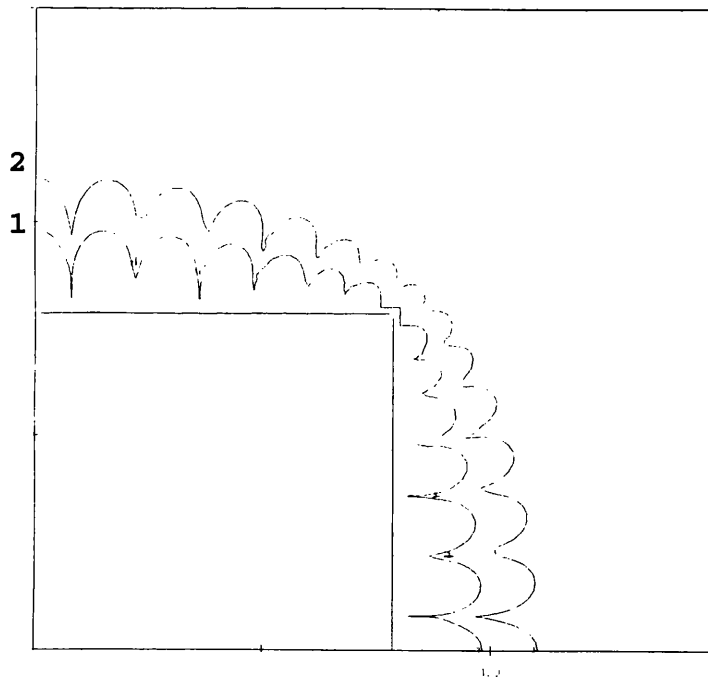


Figure 3.10b Error Contour Of Numerical Integration
Integrand = e^{ikr}/r , $k=1$, Integration Order =8.

Contour 1: $\epsilon=10^{-3}$
Contour 2: $\epsilon=10^{-4}$

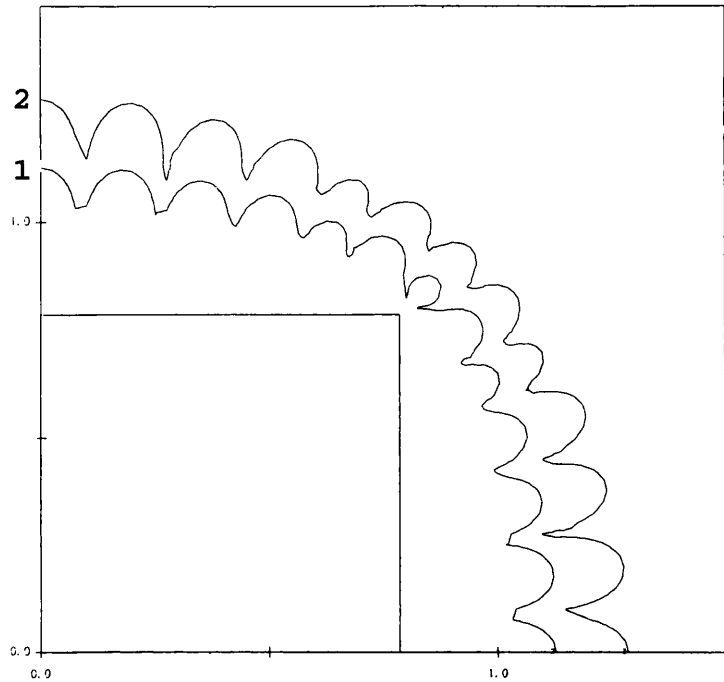


Figure 3.11a Error Contour Of Numerical Integration
Integrand = e^{ikr}/r^2 , $k=1$, Integration Order =7.

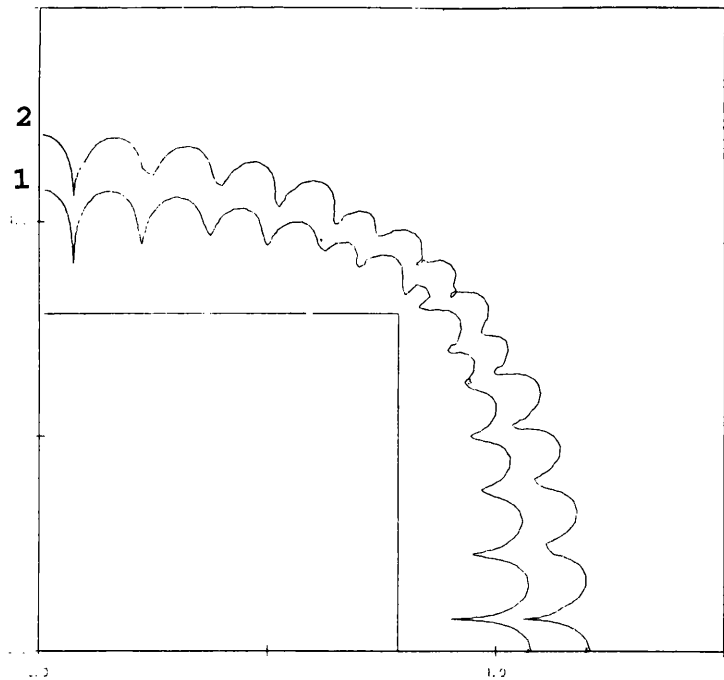


Figure 3.11b Error Contour Of Numerical Integration
Integrand = e^{ikr}/r^2 , $k=1$, Integration Order =8.

Contour 1: $\epsilon=10^{-3}$
Contour 2: $\epsilon=10^{-4}$

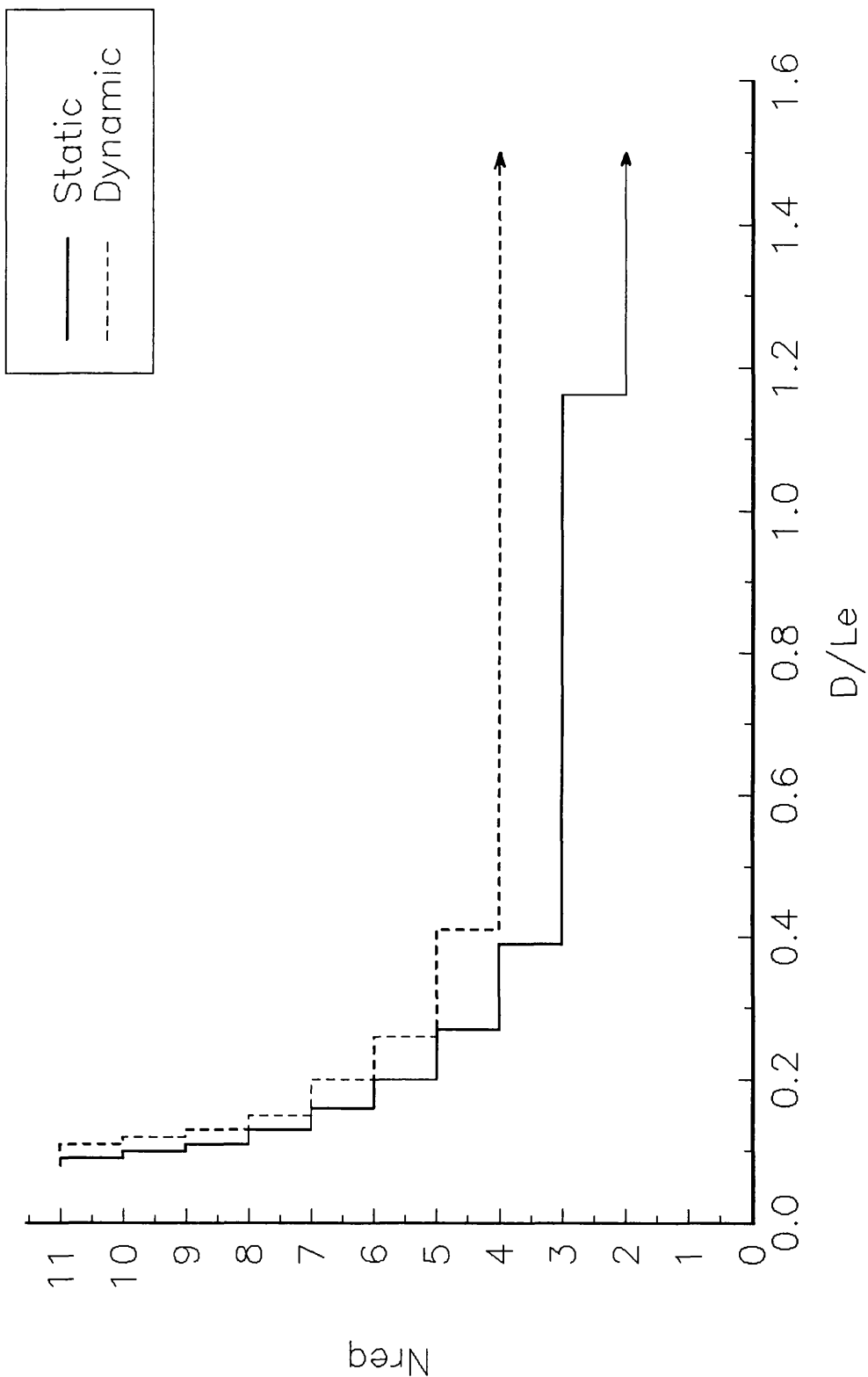


Figure 3.12 Comparisons of the results for static integrals and dynamic integrals, integrand=1/r, $\epsilon_a=0.1\%$.

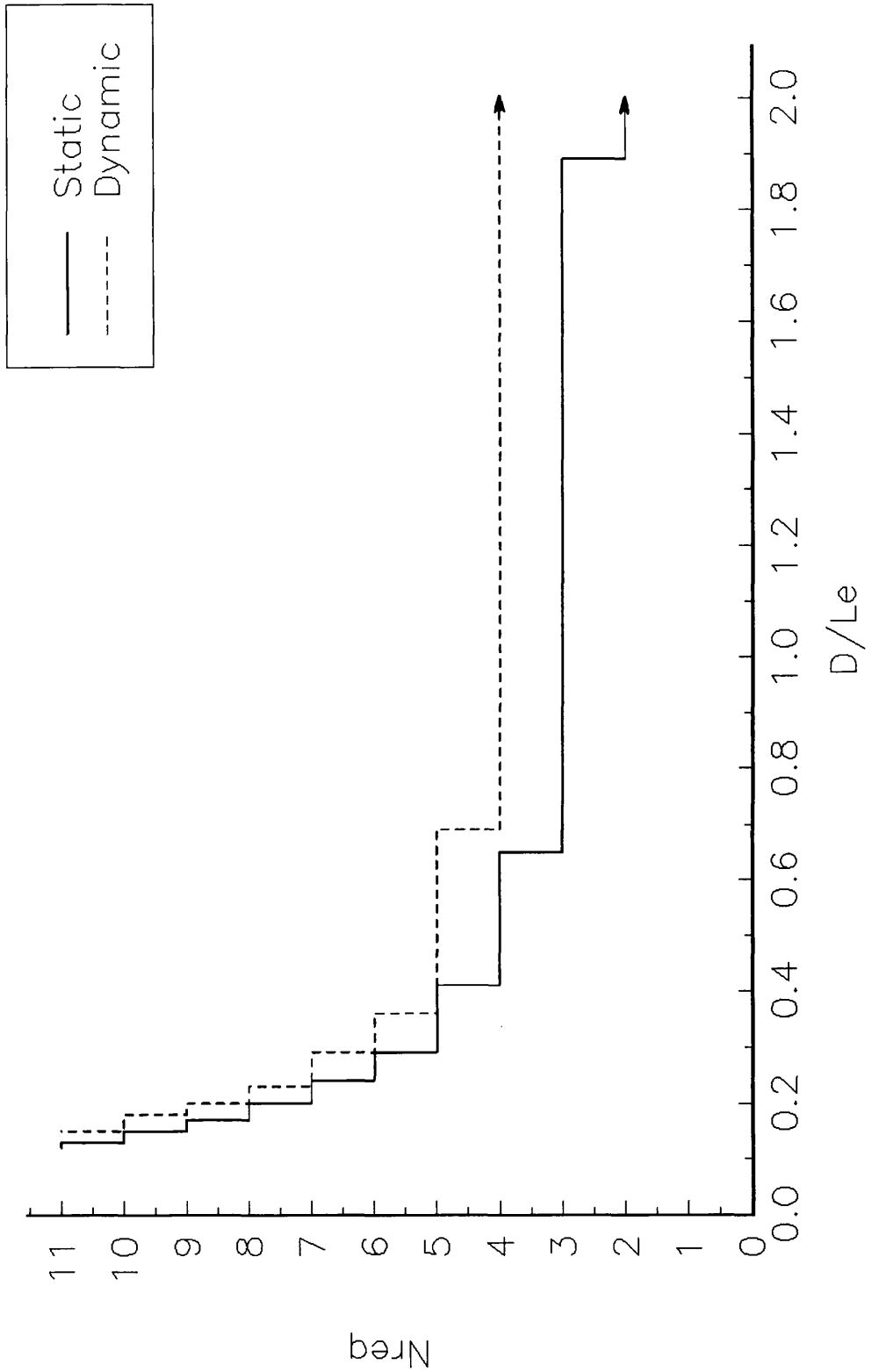


Figure 3.13 Comparisons of the results for static integrals and dynamic integrals, integrand= $1/r^2$, $\epsilon_a=0.1\%$.

CHAPTER 4

INTEGRATION SCHEMES (II) SINGULAR INTEGRALS

4.1 Introduction

Accurate evaluation of singular integrals is an essential, but difficult problem which must be overcome in any implementation of the boundary element method. Although these singularities are difficult to deal with, it is necessary to evaluate them accurately since the contributions from these integrals are generally of greatest numerical size in the coefficient matrices. A general approach for the interpretation and integration of singular integrals in the boundary element method has been presented by Rosen and Cormack(1993).

In the boundary element analysis, the singularity arises when the source point is on the element being integrated. As will be elaborated later, singular integrals can be classified as weakly singular (integrable) integrals and strongly singular integrals. For example, if the source point is at node 1 of an eight noded element (Figure 4.1), then the following singular integrals

$$\int_S G_{ij} N_\alpha dS \quad (4.1)$$

and

$$\int_S T_{ij} N_{\alpha'} dS \quad (4.2)$$

are weakly singular, while the integrals

$$\int_S T_{ij} N_{\alpha^*} dS \quad (4.3)$$

are strongly singular; in which N_{α} are the shape functions, $\alpha=1\sim 8$; the prime and asterisk denote non-singular ($\alpha'=2\sim 7$) and singular ($\alpha^*=1$) quantities, respectively.

The objective of this chapter is to describe the effective numerical methods used in the present study for evaluating singular integrals in the boundary element analysis. Weakly singular integrals are computed by means of a sub-division and transformation method, which is based on the analytical technique used for the computation of singular integrals over a triangular region in polar coordinates. The jump term C_{ij} and the strongly singular integrals of elastostatic problems have been calculated in an indirect manner using the procedure based on rigid body motion (e.g., Lachat and Watson, 1976) and, in this thesis, this method is extended to dynamic problems. An efficient method for dealing with halfspace problems by semi-analytical means has also been developed in the present study. The numerical results have been verified, whenever possible, by analytical methods.

4.2 Weakly Singular Integrals

4.2.1 Introduction

Analytical methods have been used to evaluate weakly singular integrals over constant elements (e.g., Jaswon and Ponter, 1963; Cruse, 1969; Jaswon and Symm, 1977; Sofianos, 1987; and Kim and

Papageorgiou, 1993) and linear elements (Cruse, 1974). However, extension of analytical integration to quadratic elements, especially for three-dimensional analyses, is difficult, if not impossible. The use of numerical integration is therefore essential.

Theoretical studies of numerical integration of singular integrals have been summarized by Davis and Rabinowitz (1984) and Mori and Piessens (1987), but only few of these lead to worthwhile practical applications. During the past two decades, enormous effort has been made by researchers to develop effective integration techniques suitable for the boundary element method. Three methods for the evaluation of integrable singular integrals have been intensively studied in the literature: the subtraction method (Jeng and Wexler, 1977; Berger and Bernard, 1983; and Aliabadi et al, 1985), the weighted Gauss quadrature method (Aliabadi and Hall, 1987a), and the sub-division and transformation method (Lachat and Watson, 1976). For detailed discussion of these methods, reference is made to Aliabadi and Rooke (1991).

The present study adopts the sub-division and transformation technique because, as has been shown by Lean and Wexler (1985), Mustoe (1984), and Watson (1979), it is capable of producing accurate numerical solutions for weakly singular integrals. Furthermore, the sub-division and transformation schemes are equally applicable to weakly singular integrals with oscillatory integrands. Based on the results of extensive numerical studies carried out during the course of this study, optimal integration rules for each sub-element have been obtained in order to provide the best combination of accuracy and efficiency.

4.2.2 Sub-element Mapping

The sub-division and transformation method is based on the well-known analytical technique used for the computation of singular integrals over the triangular region in polar coordinates. After dividing singular elements into triangular sub-elements, Lachat and Watson(1976) and Li and Han(1985) transform the triangular sub-elements into unit squares. The Jacobian of this transformation is of order r and consequently reduces the strength of the singularity. Gauss-Legendre quadrature can then be applied without special difficulty. Alternatively, Rizzo and Shippy(1977), Banerjee et al(1992), Manolis et al(1986), and Hayami and Brebbia(1988) integrate numerically each triangular sub-element in polar coordinates. This is essentially the same process.

Following the work of Lachat and Watson(1976), the general process of sub-division and transformation is schematically given as follows:

(A) The eight-node element(Figure 4.2a) in the global Cartesian system (x,y) is mapped onto a $(-1,+1)$ square in the intrinsic coordinate system (s,t) , as in Figure 4.2b. The Jacobian relating the transformation from the (x,y) system to the (s,t) system is J_n .

(B) The singular element is divided into two or four triangular sub-elements. The common apex of all sub-elements is the singular node α^* , as in Figure 4.2c.

(C) Each sub-element is mapped onto a flat right triangle with sides of unit length, Figure 4.2d. The singularity must be centred on node 3 in order to obtain a consistent mapping scheme. The Jacobian

matrix relating the transformation from the (s,t) system to the (η, ξ) system is J_m .

(D) A further mapping is then performed by transforming the singularity (node 3) into one side of a square and the three sides of the triangle into the remaining three sides of the square, as in Figure 4.2e. The Jacobian J_1 relating the transformation from the (η, ξ) system to the (p,q) system is

$$J_1 = (1-p) \tag{4.4}$$

and

$$\xi = p \tag{4.5}$$

$$\eta = q(1-p) \tag{4.6}$$

It should be noted that the integration points are clustered around the singularity as a result of the sub-division and transformation procedure (Figure 4.3). Consequently, the accuracy of numerical integration is improved. It will be shown in the following that the Jacobian J_1 and the shape functions N_α (except for $\alpha = \alpha^*$) provide factors which cancel singularities of order r^{-1} .

4.2.3 Weakly Singular Functions

Aliabadi et al (1987) show that exact cancelling of the weak singularity occurs for triangular elements with linear, quadratic, or cubic shape function representations. The analytical removal of weak singularities has also been shown by Aliabadi and Hall (1987b) and Guiggiani (1992) using the subtraction method. The approach of Aliabadi et al (1987) is reviewed here for completeness.

CHAPTER 4 INTEGRATION SCHEMES (II) : SINGULAR INTEGRALS

To show the Jacobian $J_1=(1-p)$ can cancel the $1/r$ singularity in the (p,q) system, a rectangular element is considered (Figure 4.1). In this case, the Jacobian J_N and J_M are constants and the Cartesian coordinates of an arbitrary point on this element are

$$x=0.5[(1-s)x_1+(1+s)x_5] \quad (4.7)$$

$$y=0.5[(1-t)y_1+(1+t)y_5] \quad (4.8)$$

where x_i and y_i are the coordinates of node i in the global Cartesian system.

Assuming that the source point is at node 1, it is easy to demonstrate, after some manipulations, that s and t can be expressed as

$$s=2\eta-1 \quad (4.9)$$

$$t=1-2\xi \quad (4.10)$$

in the (η, ξ) system, and

$$s=2q-2pq-1 \quad (4.11)$$

$$t=1-2p \quad (4.12)$$

in the (p,q) system.

Introducing equation (4.11) and (4.12) into equation (4.7) and (4.8) yields

$$x=(1-q+pq)x_1+(q-pq)x_5 \quad (4.13)$$

$$y=py_1+(1-p)y_5 \quad (4.14)$$

Consequently, the distance r between an arbitrary point and the source point (node 1) in the (p,q) system is

$$\begin{aligned} r &= \sqrt{(x-x_1)^2 + (y-y_1)^2} \\ &= (1-p) \sqrt{q^2 (x_5-x_1)^2 + (y_5-y_1)^2} \end{aligned} \tag{4.15}$$

It should be noted that the term $(1-p)$ represents the singularity of function $1/r$, because the second square root in the above equation is non-zero. Written in this way, the exact cancelling of the $1/r$ singularity in the $(p-q)$ coordinate system by the $(1-p)$ term arising from the Jacobian of transformation, Equation (4.4), is apparent.

If s and t are also introduced into the shape functions, the resulting equations are of the form:

$$N_1 = p(2pq-1)(1-2q+pq)$$

$$N_2 = 2(1-p)(q-q^2+q^2p)$$

$$N_3 = (1-p)(2p+2q-2pq-3)pq$$

$$N_4 = 4pq(1-p)^2 \tag{4.16}$$

$$N_5 = q(1-p)(2q-2pq-2p-1)$$

$$N_6 = 4p(1-p)^2$$

$$N_7 = (1-p)(1+pq-q)(1+2pq-2p-2q)$$

$$N_8 = 4p(1-p)(1+pq-q)$$

It is evident in this case that the shape functions provide an

additional factor $(1-p)$ to cancel the $1/r$ singularity, except for the singular quantity $N_{\alpha^*} = N_1$.

As has been shown in Chapter 2, the asymptotic behaviour of the singularities of the fundamental solutions are

$$G_{ij} \sim O\left(\frac{1}{r}\right)$$
$$T_{ij} \sim O\left(\frac{1}{r^2}\right)$$

Based on the above discussions it is apparent that, if the source point is at node α^* of the singular element, the following integrals

$$\int_s G_{ij} N_{\alpha} dS \quad (4.1, \text{ repeated})$$

and

$$\int_s T_{ij} N_{\alpha} dS \quad (4.2, \text{ repeated})$$

are weakly singular (integrable), while

$$\int_s T_{ij} N_{\alpha^*} dS \quad (4.3, \text{ repeated})$$

are strongly singular. This classification of singular integrals can be further clarified by the fundamental property of the shape functions: the value of N_{α^*} is unity at node α^* and is zero at all other nodes while the values of N_{α} are zero at node α^* .

4.2.4 Numerical Study

To verify the accuracy of the sub-division and transformation

method, a comprehensive numerical study has been carried out. Without loss of generality, the following analogous integrals

$$\int_s \frac{N_\alpha}{r} dS \quad (4.17)$$

and

$$\int_s \frac{N_{\alpha'}}{r^2} dS \quad (4.18)$$

are considered in the present study. The integration regions are assumed to be squares of dimension two units. The behaviour of these analogous integrals are illustrated in Figures 4.4 and 4.5, and these display various degrees of smoothness. As elaborated in the previous sub-section, the singularities of most weakly singular integrands have been eliminated by the shape functions. On the other hand, the behaviour of integrands N_α^*/r and N_α^*/r^2 , e.g., figure 4.4a, shows the unbounded function value at the singularity. It is significant to note that the degree of smoothness of these integrands has considerable influence on the accuracy of the integration method. Consequently, a complete study of the various integrands is required to reach a useful conclusion.

Singular integrals (Equations 4.17 and 4.18) have been evaluated by analytical techniques and by the sub-division and transformation method. The former are performed by subdividing the region into triangles and integrating each triangle in the polar coordinate system; see Appendix 4.1 for more details. On the other hand, each sub-element is computed numerically by the sub-division and transformation method using a sequence of Gauss-Legendre formula of order n in each direction, where $n=2\sim 8$.

Analytical solutions and numerical results for a wide range of

singular integrals are summarized in Tables 4.1 and 4.2. These analytical solutions can be used for checking quadrature programs and subroutines. The numerical results illustrate the very fast rate of convergence of the sub-division and transformation method. It is observed that the quality of the numerical integration depends on the type (smoothness) of integrands. Based on the computed relative errors, however, the use of 5x5 integration rule for each sub-element provides sufficient precision for engineering purpose (the results agree to five digits and relative error $\leq 10^{-3}$).

4.2.5 Effects of singular vertex angle

In the boundary element analysis, the magnitude of the vertex angles of triangular sub-elements depend on the discretization scheme. It is useful, both theoretically and practically, to study the effect of singular vertex angle on the accuracy of the subdivision and transformation method. In this thesis. the singular integral

$$\int \frac{1}{r} dA$$

over a triangular region is considered. As shown in Figure 4.6, the range of the singular vertex angle α_s is $10^\circ \sim 80^\circ$.

Analytical solutions and numerical solutions are obtained, respectively, by integrating this integral in polar coordinates and by using a sequence of numerical integrations of order n for each direction, where $n=2 \sim 20$. The analytical solutions and computed numerical results (which agree to five digits) are given in Table 4.3. It is observed that sub-elements with larger vertex angles α_s require higher integration orders to maintain acceptable accuracy. However, the influence of the singular vertex angle on the numerical results obtained by the

sub-division and transformation method is moderate, in comparison with those obtained by weighted Gauss quadrature method (Aliabadi and Hall, 1987a) or the Taylor series expansions (Aliabadi et al, 1985).

The maximum possible vertex angles α_s of sub-elements of rectangular elements are depicted in Figure 4.7. Singular vertex angles of up to 76° are found in rectangular elements of aspect ratio equal to four. As a consequence, for analyses using elements of aspect ratio not greater than two, the use of 5x5 integration rule for each sub-element is sufficient for practical purposes. Otherwise, further sub-division of triangular sub-elements into sectors are required.

4.2.6 Integrals With Oscillatory Integrands

Because of the wavy nature of the oscillatory integrands, the evaluation of weakly singular integrals in dynamic problems is much more complicated. However, by imposing appropriate constraints on element size, the sub-division and transformation method is equally applicable to oscillatory singular integrals. In the present study, the following analogous singular integrals

$$\int_s \frac{N_\alpha}{r} e^{i\kappa r} dS \quad (4.19)$$

and

$$\int_s \frac{N_{\alpha'}}{r^2} e^{i\kappa r} dS \quad (4.20)$$

are considered. The characteristics of these integrals depend on the wave number κ , defined as

$$\kappa = \frac{\omega}{C_2} \quad (3.18; \text{repeated})$$

where C_2 is the velocity of the shear wave. As mentioned in Chapter 2, in the present study the maximum dimension of the largest element employed in the discretization scheme is limited to 1/4 Rayleigh wavelengths.

In order to obtain benchmark solutions, the integrals (equations 4.19 and 4.20) over a triangular region have been evaluated analytically in the radial direction (Appendix 4.2) and high order numerical integration ($n=11$) has been used in the circumferential direction. On the other hand, these integrals are computed numerically by the sub-division and transformation method using a sequence of integration order n for each direction, where $n=2\sim 7$. A wide range of integrands has been studied in order to obtain sufficient information on this problem. Preliminary numerical studies for a wide range of frequencies revealed that the constraint on element size eliminates the need to modify the integration order for different frequencies. Numerical results and relative errors in relation to these semi-analytical benchmark solutions are given in Table 4.4 and 4.5.

These results illustrate the rapid rate of convergence of the sub-division and transformation method. It should be noted that, beyond the integration order=6x6, the accuracy of the numerical results for some integrals deteriorates, due to round-off. Clearly, the performance of the sub-division and transformation method depends on the type of integrand. The use of 5x5 integration rules for each sub-element is recommended for practical purpose.

4.3 STRONGLY SINGULAR INTEGRALS

4.3.1 Introduction

The importance of accurate evaluation of strongly singular integrals has been recognized since the very beginning of the development of boundary element methods (Rizzo, 1967). These integrals are Cauchy integrals and their principal values exist only if the adjacent elements are taken together. Analytical integration can be used for constant boundary elements, while special numerical techniques are required for higher order elements. Methods of dealing with Cauchy principal value integrals in boundary element methods have been summarized by Guiggiani (1991).

Explicit evaluation of the free terms and the Cauchy principal values of the integrals is tedious (Manolis et al, 1986; Guiggiani and Casalini, 1987; and Guiggiani, 1992). In most elastostatic boundary element analyses, the strongly singular integrals have been determined by considering rigid body translation of the problem region, eg, Brebbia (1980). In this way, the jump terms C_{ij} and the sum of all the strongly singular integrals, which constitute the diagonal block of the [T] matrix, can be computed indirectly. However, this indirect scheme is not immediately applicable to dynamic boundary element analyses (Rizzo et al, 1985; Manolis, et al, 1986; and Guiggiani, 1992). Accordingly, this section describes a rigorous method which exploits the constraint equation of rigid body translation (for static problems) to evaluate the singularities of strongly singular integrals arising in dynamic analyses.

4.3.2 Evaluation Of The Diagonal Block For Static Problems

It has been shown (Cruse, 1969) that the traction-free problem:

$$C_{ij}(y) u_i(y) = - \int_S T_{ij}^{st}(x, y) u_i(x) dS \quad (4.21)$$

admits non-trivial rigid body displacement solutions. If unit rigid body translations of the body, $u_i = 1$, are imposed, then:

$$C_{ij} = - \int_S T_{ij}^{st}(x, y) dS \quad (4.22)$$

The discretized form of Equation(4.22) can be written as:

$$C_{ij} = - \sum_{M^*} \int T_{ij}^{st} dS - \sum_{M'} \int T_{ij}^{st} dS \quad (4.23)$$

in which, M refers to elements and the prime and the asterisk superscripts refer to non-singular and singular quantities, respectively. The integrals over a singular element can of course be classified as weakly singular integrals and a strongly singular integral. Consequently, after the introduction of the shape functions, equation(4.23) becomes:

$$C_{ij} = - \sum_{M^*} \int T_{ij}^{st} N_{\alpha^*} dS - \sum_{M^*} \sum_{\alpha'} \int T_{ij}^{st} N_{\alpha'} dS - \sum_{M'} \int T_{ij}^{st} dS \quad (4.24)$$

or

$$[C_{ij} + \sum_{M^*} \int T_{ij}^{st} N_{\alpha^*} dS] = - \sum_{M^*} \sum_{\alpha'} \int T_{ij}^{st} N_{\alpha'} dS - \sum_{M'} \int T_{ij}^{st} dS \quad (4.25)$$

in which α refers to nodes.

It should be noted that, on the left hand side of Equation (4.25), the summation of singular elements represents the set of all adjacent elements connected to the source point y(the singularity). This equation shows that the diagonal block can be obtained by the sum of the off-diagonal blocks, which can be computed numerically. In addition, this approach avoids the

explicit computation of the jump term C_{ij} . This indirect scheme have been successfully used in the past to compute the diagonal block of elastostatic problems (Lachat and Watson, 1976; Watson, 1979; Mustoe, 1984) and potential problems (Brebbia, 1980).

4.3.3 Evaluation Of The Diagonal Block For Dynamic Problems

The diagonal block of the $[T]$ matrix in the elastodynamic boundary element formulation is

$$C_{ij} + \sum_{M^*} \int T_{ij} N_{\alpha^*} dS \quad (4.26)$$

It should be noted that the rigid-body translation is not an elementary solution of the dynamic boundary integral equation. Consequently, the application of the indirect scheme described in the previous sub-section is not straightforward.

Because C_{ij} is the same for both static and harmonic loading cases, it is possible to remove the strongly singular integrals from dynamic boundary integral equations. The central idea behind the process is that the diagonal block of dynamic problems can be expressed in terms of its static counterpart and a non-singular integral. Substitution of Equation(4.25) into Equation(4.26), after some manipulations, the diagonal block is of the form:

$$\begin{aligned} & C_{ij} + \sum_{M^*} \int T_{ij} N_{\alpha^*} dS \\ &= C_{ij} + \sum_{M^*} \int T_{ij}^{st} N_{\alpha^*} dS + \sum_{M^*} \int (T_{ij} - T_{ij}^{st}) N_{\alpha^*} dS \\ &= \sum_{M^*} \int (T_{ij} - T_{ij}^{st}) N_{\alpha^*} dS - \sum_{M^*} \sum_{\alpha'} T_{ij}^{st} N_{\alpha'} dS - \sum_{M'} \int T_{ij}^{st} dS \end{aligned} \quad (4.27)$$

in which, all the integrals can be readily evaluated by

numerical integration.

This method is the simplest scheme to implement, in comparison with directly computing the jump term and the strongly singular integrals, and a significant factor in the success of the boundary element analysis. Similar approaches have been presented by Rizzo et al(1985); Manolis et al(1986); and Guiggiani(1992).

4.3.4 Halfspace problems

Many geotechnical engineering problems are idealized by the halfspace model(Figure 4.8), which presents no particular difficulties for boundary element methods. In general, the (infinite) hemispherical surface of the region can be neglected since the displacements and tractions on this infinite boundary are zero(regular conditions). However, the azimuthal integral in equation(4.22) over the unbounded hemispherical boundary must be considered in order to evaluate the diagonal block properly.

Recently, several researchers(Ahmad and Banerjee, 1988b; Wang and Banerjee, 1990; Hirose, 1991; Israil and Banerjee, 1992) use "enclosing" elements(Figure 4.9) to deal with the azimuthal integral over the infinite hemisphere of halfspace models. The displacements and tractions on the enclosing elements are finite but small. In two dimensional analyses, the use of enclosing elements is evidently feasible, although at some computational cost. However, in three dimensional problems, this approach increases the computational effort considerably.

In the present study, the azimuthal integral over the unbounded hemisphere is computed analytically. As illustrated in Appendix 4.3, the azimuthal integral is independent of the radius of the hemisphere and can be written as

$$S_{ij} = -\frac{1}{2} \delta_{ij} \quad (4.28)$$

For halfspace problems, the azimuthal integral S_{ij} is therefore significant and must be incorporated into the boundary element formulation.

4.4 CONCLUSIONS

The results of boundary element analyses are very sensitive to the computed values of singular elements since they represent contributions generally of greatest numerical size to the coefficient matrices. For this reason, particular attention must be paid to the implementation of accurate integration techniques. This chapter describes methods used in the present study for the evaluation of weakly singular integrals and strongly singular integrals; the "strictly diagonal block".

The sub-division and transformation scheme for integrable singular integrals is straightforward, in principle, because it requires only the implementation of basic concepts involving geometrical transformations and Gauss-Legendre quadrature. In addition, perhaps more importantly, this method is capable of producing satisfactory results for singular integrals with oscillatory integrands. The results of a rigorous numerical study demonstrate the accuracy and efficiency of the method. It is concluded that the use of the 5x5 integration rule for each sub-element provides sufficient precision (relative errors less than 10^{-3}). The analytical solutions of some typical integrals (given in Appendices 4.1 and 4.2 and Tables 4.1, 4.2, 4.3 and 4.4) can be used for checking quadrature programs and subroutines.

Explicit evaluations of strongly singular integrals is

extremely difficult. The strictly diagonal block of elastostatic problems can be calculated in an indirect manner using the procedure based on rigid body motion and this method can be extended to elastodynamic problems as shown here. An efficient method for dealing with halfspace problems by semi-analytical means has also been presented in this chapter. Using these methods, the singular integrals in the discretized boundary element formulation can now be evaluated numerically without special difficulty.

APPENDIX 4.1: ANALYTICAL INTEGRATION OF

$$I = \int \frac{N_1}{r_1} dA$$

over a 2x2 square.

The value r_1 is the distance between an arbitrary point at the square and the source point, node 1. As shown in Figure A4-1, the square is transformed into s-t system and subdivided into sub-elements. It should be noted that, in this particular case, $J_n = 1$, $r_1(x,y) = r_1(s,t)$, and the integral can be written as

$$I = \int_{-1}^{+1} \int_{-1}^{+1} \frac{N_1(s,t)}{r_1(s,t)} ds dt \tag{A4-1}$$

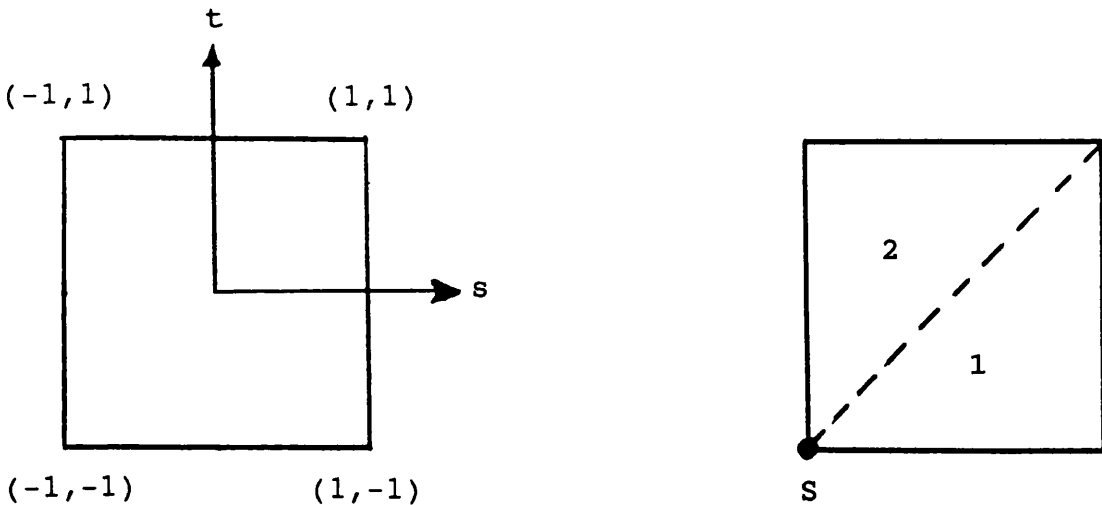


Figure A4-1: The transformation from x-y system to s-t system

Sub-element 1:

As shown in Figure(A4-2), the triangle is mapped into polar coordinates.

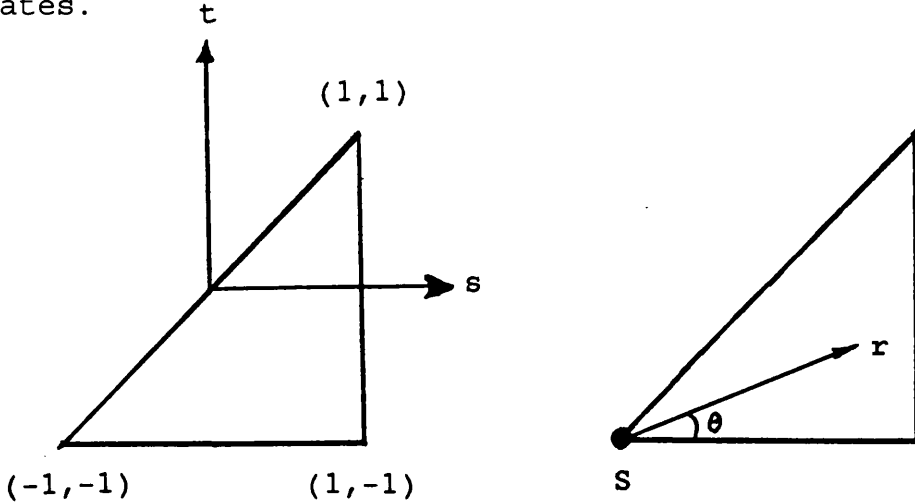


Figure A4-2: The transformation of triangular sub-elements

After some manipulations, the variables s and t can be expressed in terms of the polar coordinates:

$$\begin{aligned} s &= r \cos \theta - 1 \\ t &= r \sin \theta - 1 \\ ds dt &= r_1 dr d\theta \end{aligned} \tag{A4-2}$$

and the integral can be written as

$$\begin{aligned} I &= \int_0^{\frac{\pi}{4}} \int_0^{r(\theta)} \frac{N_1(r, \theta)}{r_1(r, \theta)} r_1 dr d\theta \\ &= \int_0^{\frac{\pi}{4}} \int_0^{2 \sec \theta} N_1(r, \theta) dr d\theta \end{aligned} \tag{A4-3}$$

Substituting Equation(A4-2) into the shape function N_1 , leads to

$$\begin{aligned}
 N_1 &= -.25(1-s)(1-t)(1+s+t) \\
 &= -.25(2-r\cos\theta)(2-r\sin\theta)(r\cos\theta+r\sin\theta-1) \\
 &= -.25(4+2r^2-6r\cos\theta-6r\sin\theta+5r^2\cos\theta\sin\theta \\
 &\quad -r^3\cos^2\theta\sin\theta-r^3\cos\theta\sin^2\theta)
 \end{aligned} \tag{A4-4}$$

Consequently, the inner integral becomes

$$\begin{aligned}
 &\int_0^{2\sec\theta} N_1 dr \\
 &= \frac{1}{4} \left[4r + \frac{2}{3}r^3 - 3r^2\cos\theta - 3r^2\sin\theta + \frac{5}{3}r^3\cos\theta\sin\theta \right. \\
 &\quad \left. - \frac{r^4}{4}\cos^2\theta\sin\theta - \frac{r^4}{4}\cos\theta\sin^2\theta \right]_0^{2\sec\theta} \\
 &= -\sec\theta - \frac{2}{3}\sec^2\theta\sin\theta + \frac{4}{3}\sec^3\theta - \sec^3\theta\sin^2\theta
 \end{aligned} \tag{A4-5}$$

and

$$\begin{aligned}
 &\int_0^{\frac{\pi}{4}} \left[-\sec\theta - \frac{2}{3}\sec^2\theta\sin\theta + \frac{4}{3}\sec^3\theta - \sec^3\theta\sin^2\theta \right] d\theta \\
 &= \left[-\ln|\sec\theta + \tan\theta| - \frac{2}{3}\sec\theta + \frac{2}{3}(\tan\theta\sec\theta + \ln|\sec\theta + \tan\theta|) \right. \\
 &\quad \left. - \left(\frac{\sin\theta}{2\cos^2\theta} - \frac{1}{2}\ln|\sec\theta + \tan\theta| \right) \right]_0^{\frac{\pi}{4}} \\
 &= 0.106455474
 \end{aligned} \tag{A4-6}$$

In an analogous manner, it can be shown that the integral over sub-element II is 0.10645 5474.

The same process can be used to compute other weakly singular integrals.

APPENDIX 4.2: Analytical Integration Of

$$\int \frac{N_{\alpha} \cdot e^{ikr}}{r} dS$$

over a triangle in the radial direction.

In a similar manner (to Appendix 4.1), this integral over a triangular region can be written as

$$I = \int_0^{\frac{\pi}{4}} \int_0^{2\sec\theta} N_{\alpha}(r, \theta) e^{ikr} dr d\theta \quad (\text{A4-7})$$

and, for illustrative purpose, $N_1(r, \theta)$ is

$$\begin{aligned} N_1 &= -.25(1-s)(1-t)(1+s+t) \\ &= -.25(2-r\cos\theta)(2-r\sin\theta)(r\cos\theta+r\sin\theta-1) \\ &= -.25(4+2r^2-6r\cos\theta-6r\sin\theta+5r^2\cos\theta\sin\theta \\ &\quad -r^3\cos^2\theta\sin\theta-r^3\cos\theta\sin^2\theta) \end{aligned}$$

Consequently, the integral relating to the radial direction can be expressed as

$$\begin{aligned} I_r &= \int_0^{2\sec\theta} N_{\alpha}(r, \theta) e^{ikr} dr \\ &= A \int e^{ikr} dr + B \int r e^{ikr} dr + C \int r^2 e^{ikr} dr \end{aligned} \quad (\text{A4-8})$$

in which, coefficients A, B, and C are functions of θ or constant.

Analytical solutions for these integrals are given as follows:

$$\int e^{ikr} dr = \frac{e^{ikr}}{ik} \quad (\text{A4-9})$$

$$\int r e^{ikr} dr = \frac{r e^{ikr}}{ik} - \frac{1}{ik} \int e^{ikr} dr \quad (\text{A4-10})$$

$$\int r^2 e^{ikr} dr = \frac{r^2 e^{ikr}}{ik} - \frac{2}{ik} \int r e^{ikr} dr \quad (\text{A4-11})$$

**Appendix 4.3 Analytical Integration Of The Azimuthal Integral
Over An Infinite Hemisphere**

Spherical coordinates (Figure A4.3) are used to study this particular case. The relationship between the Cartesian coordinates and the spherical coordinates are given as follows:

$$\begin{aligned}x_1 &= r \sin \phi \cos \theta \\x_2 &= r \sin \phi \sin \theta \\x_3 &= r \cos \phi\end{aligned}\tag{A4.12}$$

and the Jacobian J_s

$$J_s(r, \phi, \theta) = r^2 \sin \phi\tag{A4-13}$$

Consequently, the following quantities arising in the fundamental solutions can be obtained:

$$\begin{aligned}r_{,1} = n_1 &= \sin \phi \cos \theta \\r_{,2} = n_2 &= \sin \phi \sin \theta \\r_{,3} = n_3 &= r \cos \phi\end{aligned}\tag{A4-14}$$

and

$$\frac{\partial r}{\partial n} = \sum_{i=1}^3 n_i r_{,i} = \sin^2 \theta \cos^2 \phi + \sin^2 \theta \sin^2 \phi + \cos^2 \theta = 1\tag{A4-15}$$

Without loss of generality, in the following the source point is placed at the origin (Figure A4.4). By introducing equations

(A4.12) - (A4.15) into the static traction fundamental solution, after some mathematical manipulations, the integral of equation(4.22) over the hemisphere can then be written as

$$S_{ij} = \int_S T_{ij}^{st}(x, y) dS \quad (A4-16)$$

$$= \frac{-1}{8\pi(1-\nu)} \int_0^{2\pi} \int_0^{\frac{\pi}{2}} [(1-2\nu)\delta_{ij} + 3r_{,i}r_{,j}] \sin\theta d\phi d\theta$$

This equation may now be integrated analytically. It is easy to show that, for example,

$$\int_0^{2\pi} \int_0^{\frac{\pi}{2}} \sin\theta d\phi d\theta = 2\pi \quad (A4-17)$$

and, for $i=j=1$,

$$3 \int_0^{2\pi} \int_0^{\frac{\pi}{2}} r_{,i}r_{,j} \sin\theta d\phi d\theta = 3 \int_0^{2\pi} \int_0^{\frac{\pi}{2}} \sin^3\theta \cos^2\phi d\phi d\theta = 2\pi \quad (A4-18)$$

Consequently,

$$S_{11} = \frac{-1}{8\pi(1-\nu)} [(1-2\nu) \cdot 2\pi + 2\pi] = -\frac{1}{2} \quad (A4-19)$$

In brief, it can be concluded that

$$S_{ij} = -\frac{1}{2} \delta_{ij} \quad (A4-20)$$

and S_{ij} is independent of the radius of the hemisphere.

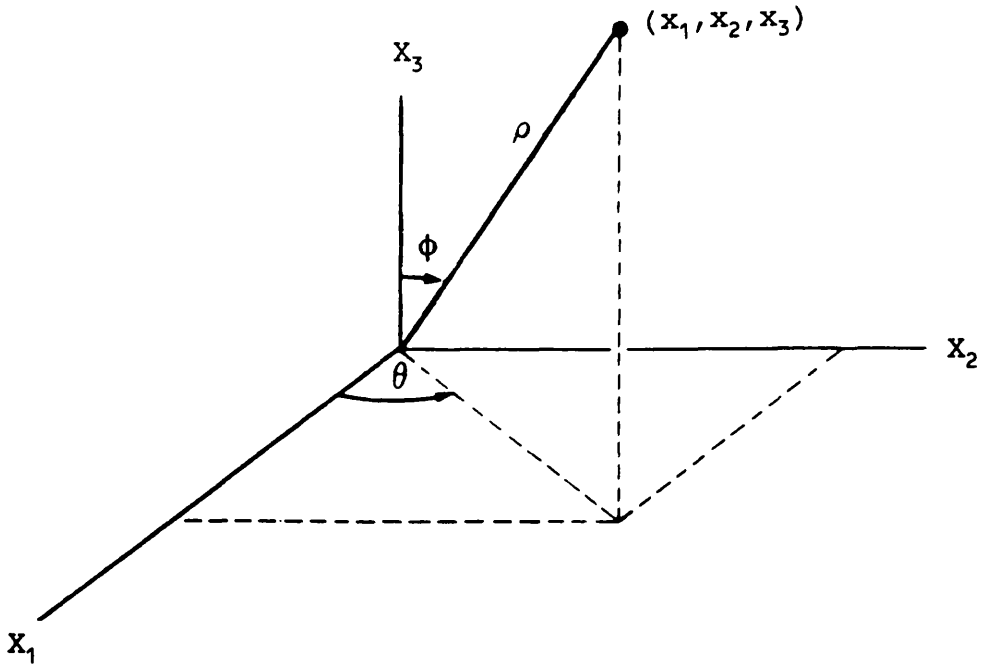


Figure A4.3: Spherical Coordinate System

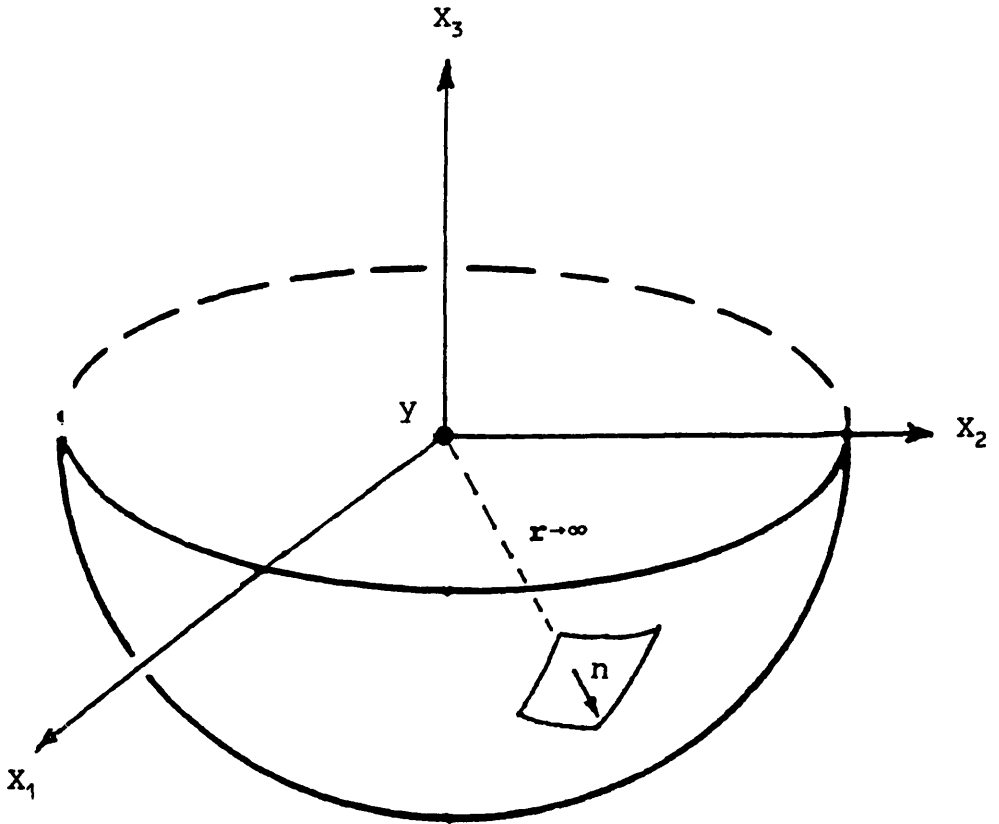


Figure A4.4: Integration Over The Unbounded Hemisphere

TABLE 4.1 NUMERICAL EVALUATION OF SINGULAR INTEGRALS

$$\int_{-1}^{+1} \int_{-1}^{+1} \frac{N_1}{r} d\eta d\zeta$$

Gauss point per subelement	Singularity at node 1 $\iota = 1$ $V_{\text{analytical}} = 0.21291\ 0948$	
	Computed value	relative error(%)
2x2	0.21454 4391	7.67 E-1
3x3	0.21289 2072	8.87 E-3
4x4	0.21290 9502	6.79 E-4
5x5	0.21291 1081	6.25 E-5
6x6	0.21291 0963	7.05 E-6
7x7	0.21291 0967	8.92 E-6
8x8	0.21291 0967	8.92 E-6

Gauss point per subelement	Singularity at node 1 $\iota = 2$ $V_{\text{analytical}} = 1.27369\ 3832$	
	Computed value	relative error(%)
2x2	1.27369 6387	2.01 E-4
3x3	1.27361 6002	6.11 E-3
4x4	1.27369 7942	3.23 E-4
5x5	1.27369 3741	7.15 E-6
6x6	1.27369 3830	1.57 E-7
7x7	1.27369 3833	7.85 E-8
8x8	1.27369 3833	7.85 E-8

TABLE 4.1 NUMERICAL EVALUATION OF SINGULAR INTEGRALS

$$\int_{-1}^{+1} \int_{-1}^{+1} \frac{N_i}{r} d\eta d\zeta$$

Gauss point per subelement	Singularity at node 1 $\iota = 3$ $V_{\text{analytical}} = -0.31748\ 0464$	
	Computed value	relative error(%)
2x2	-0.31503 1608	7.71 E-1
3x3	-0.31746 9894	3.33 E-3
4x4	-0.31748 4718	1.34 E-3
5x5	-0.31748 0249	6.77 E-5
6x6	-0.31748 0470	1.89 E-6
7x7	-0.31748 0466	6.30 E-7
8x8	-0.31748 0466	6.30 E-7

Gauss point per subelement	Singularity at node 1 $\iota = 4$ $V_{\text{analytical}} = 0.84787\ 1898$	
	Computed value	relative error(%)
2x2	0.84460 7606	3.85 E-1
3x3	0.84783 1859	4.72 E-3
4x4	0.84787 8938	8.30 E-4
5x5	0.84787 1579	3.76 E-5
6x6	0.84787 1905	8.26 E-7
7x7	0.84787 1900	2.36 E-7
8x8	0.84787 1899	2.36 E-7

TABLE 4.1 NUMERICAL EVALUATION OF SINGULAR INTEGRALS

$$\int_{-1}^{+1} \int_{-1}^{+1} \frac{N_i}{r} d\eta d\zeta$$

Gauss point per subelement	Singularity at node 1 $\iota = 5$ $V_{\text{analytical}} = -0.29558 \ 7149$	
	Computed value	relative error(%)
2x2	-0.29392 9936	5.61 E-1
3x3	-0.29552 3199	2.16 E-2
4x4	-0.29559 2935	1.96 E-3
5x5	-0.29558 6939	7.11 E-5
6x6	-0.29558 7151	6.77 E-7
7x7	-0.29558 7150	3.38 E-7
8x8	-0.29558 7149	0

Gauss point per subelement	Singularity at node 2 $\iota = 2$ $V_{\text{analytical}} = 2.52638 \ 3842$	
	Computed value	relative error(%)
2x2	2.54404 4362	6.99 E-1
3x3	2.52619 3549	7.53 E-3
4x4	2.52620 2185	7.19 E-3
5x5	2.52639 5620	4.66 E-4
6x6	2.52638 5397	6.16 E-5
7x7	2.52638 3615	8.99 E-6
8x8	2.52638 3836	2.38 E-7

TABLE 4.1 NUMERICAL EVALUATION OF SINGULAR INTEGRALS

$$\int_{-1}^{+1} \int_{-1}^{+1} \frac{N_i}{r} d\eta d\zeta$$

Gauss point per subelement	Singularity at node 2 $\iota = 3$ $V_{\text{analytical}} = -0.33382 \ 8436$	
	Computed value	relative error(%)
2x2	-0.33103 5092	8.37 E-1
3x3	-0.33298 4305	2.53 E-1
4x4	-0.33390 0038	2.15 E-2
5x5	-0.33383 3957	1.65 E-3
6x6	-0.33382 7324	3.33 E-4
7x7	-0.33382 8441	1.50 E-6
8x8	-0.33382 8462	7.79 E-6

Gauss point per subelement	Singularity at node 2 $\iota = 4$ $V_{\text{analytical}} = 1.37293 \ 3664$	
	Computed value	relative error(%)
2x2	1.37655 2585	2.64 E-1
3x3	1.37132 1303	1.17 E-1
4x4	1.37297 5321	3.03 E-3
5x5	1.37294 9191	1.13 E-3
6x6	1.37293 2388	9.29 E-5
7x7	1.37293 3543	8.81 E-6
8x8	1.37293 3686	1.60 E-6

TABLE 4.1 NUMERICAL EVALUATION OF SINGULAR INTEGRALS

$$\int_{-1}^{+1} \int_{-1}^{+1} \frac{N_i}{r} d\eta d\zeta$$

Gauss point per subelement	Singularity at node 2 $l = 5$ $V_{analytical} = -0.45415\ 3166$	
	Computed value	relative error(%)
2x2	-0.45615 9461	4.42 E-1
3x3	-0.45351 8252	1.40 E-1
4x4	-0.45416 3318	2.24 E-3
5x5	-0.45415 9548	1.41 E-3
6x6	-0.45415 2723	9.75 E-5
7x7	-0.45415 3112	1.19 E-5
8x8	-0.45415 3174	1.76 E-6

Gauss point per subelement	Singularity at node 2 $l = 6$ $V_{analytical} = 1.11583\ 0306$	
	Computed value	relative error(%)
2x2	1.11507 9559	6.73 E-2
3x3	1.11548 8160	3.07 E-2
4x4	1.11585 1697	1.92 E-3
5x5	1.11583 3068	2.48 E-4
6x6	1.11582 9916	3.50 E-5
7x7	1.11583 0293	1.17 E-6
8x8	1.11583 0311	4.48 E-7

TABLE 4.2 NUMERICAL EVALUATION OF SINGULAR INTEGRALS

$$\int_{-1}^{+1} \int_{-1}^{+1} \frac{N_i}{r^2} d\eta d\zeta$$

Gauss point per subelement	Singularity at node 1 $\iota = 2$ $V_{\text{analytical}} = 1.88982\ 6556$	
	Computed value	relative error(%)
2x2	1.89071 0383	4.68 E-2
3x3	1.88950 2762	1.71 E-2
4x4	1.88984 4862	9.69 E-4
5x5	1.88982 6147	2.16 E-5
6x6	1.88982 6540	8.47 E-7
7x7	1.88982 6558	1.06 E-7
8x8	1.88982 6556	0

Gauss point per subelement	Singularity at node 1 $\iota = 3$ $V_{\text{analytical}} = -0.47854\ 5343$	
	Computed value	relative error(%)
2x2	-0.47540 9836	6.55 E-1
3x3	-0.47845 3039	1.93 E-2
4x4	-0.47855 8363	2.72 E-3
5x5	-0.47854 4740	1.26 E-4
6x6	-0.47854 5352	1.88 E-6
7x7	-0.47854 5345	4.18 E-7
8x8	-0.47854 5344	2.09 E-7

TABLE 4.2 NUMERICAL EVALUATION OF SINGULAR INTEGRALS

$$\int_{-1}^{+1} \int_{-1}^{+1} \frac{N_i}{r^2} d\eta d\zeta$$

Gauss point per subelement	Singularity at node 1 $\nu = 4$ $V_{\text{analytical}} = 0.63806\ 0459$	
	Computed value	relative error(%)
2x2	0.63387 9781	6.55 E-1
3x3	0.63793 7385	1.93 E-2
4x4	0.63807 7818	2.72 E-3
5x5	0.63805 9654	1.26 E-4
6x6	0.63806 0470	1.72 E-6
7x7	0.63806 0460	1.57 E-7
8x8	0.63806 0459	0

Gauss point per subelement	Singularity at node 1 $\nu = 5$ $V_{\text{analytical}} = -0.29148\ 6868$	
	Computed value	relative error(%)
2x2	-0.28961 7486	6.41 E-1
3x3	-0.29134 4383	4.89 E-2
4x4	-0.29150 0124	4.55 E-3
5x5	-0.29148 6364	1.73 E-4
6x6	-0.29148 6870	6.86 E-7
7x7	-0.29148 6869	3.43 E-7
8x8	-0.29148 6868	0

TABLE 4.2 NUMERICAL EVALUATION OF SINGULAR INTEGRALS

$$\int_{-1}^{+1} \int_{-1}^{+1} \frac{N_i}{r^2} d\eta d\zeta$$

Gauss point per subelement	Singularity at node 2 $\iota = 3$ $V_{\text{analytical}} = -0.60146\ 4285$	
	Computed value	relative error(%)
2x2	-0.60148 8561	4.04 E-3
3x3	-0.59741 4382	6.73 E-1
4x4	-0.60170 0796	3.93 E-2
5x5	-0.60151 0050	7.61 E-3
6x6	-0.60145 8216	1.01 E-3
7x7	-0.60146 3968	5.27 E-5
8x8	-0.60146 4390	1.75 E-5

Gauss point per subelement	Singularity at node 2 $\iota = 4$ $V_{\text{analytical}} = 2.09030\ 7488$	
	Computed value	relative error(%)
2x2	2.11638 0868	1.25 E0
3x3	2.08325 8115	3.37 E-1
4x4	2.09033 3384	1.24 E-3
5x5	2.09040 9420	4.48 E-3
6x6	2.09030 1266	2.98 E-4
7x7	2.09030 6367	5.36 E-5
8x8	2.09030 7643	7.42 E-6

TABLE 4.2 NUMERICAL EVALUATION OF SINGULAR INTEGRALS

$$\int_{-1}^{+1} \int_{-1}^{+1} \frac{N_i}{r^2} d\eta d\zeta$$

Gauss point per subelement	Singularity at node 2 $\iota = 5$ $V_{\text{analytical}} = -0.86256\ 4064$	
	Computed value	relative error(%)
2x2	-0.87451 6418	1.39 E0
3x3	-0.85962 1725	3.41 E-1
4x4	-0.86255 7847	7.21 E-4
5x5	-0.86260 7588	5.05 E-3
6x6	-0.86256 1659	2.79 E-4
7x7	-0.86256 3571	5.72 E-5
8x8	-0.86256 4127	7.30 E-6

Gauss point per subelement	Singularity at node 2 $\iota = 6$ $V_{\text{analytical}} = 1.36683\ 4813$	
	Computed value	relative error(%)
2x2	1.37065 4458	2.80 E-1
3x3	1.36450 3388	1.71 E-1
4x4	1.36691 1632	5.62 E-3
5x5	1.36686 4575	2.18 E-3
6x6	1.36683 1988	2.07 E-4
7x7	1.36683 4543	1.98 E-5
8x8	1.36683 4869	4.10 E-6

TABLE 4.3 EFFECT OF THE SINGULAR VERTEX ANGLE
(For results accurate to five digits)

α°	Analytical solutions	Required Gauss order	Numerical Values
10	0.17542 59	2x2	0.17542 55
20	0.35637 85	3x3	0.35637 86
30	0.54930 62	3x3	0.54930 59
40	0.76290 98	4x4	0.76291 03
50	1.01068 33	5x5	1.01068 35
60	1.31695 81	5x5	1.31696 38
70	1.73541 55	7x7	1.73541 64
80	2.43624 69	10x10	2.43624 76

TABLE 4.4 NUMERICAL EVALUATION OF SINGULAR INTEGRALS

$$\int_{-1}^{+1} \int_{-1}^{+1} \frac{N_i e^{ikr}}{r} d\eta d\zeta$$

Gauss point per subelement	Singularity at node 1, $\iota = 1$ $\kappa = 1$. $V_{\text{semi-analytical}}$ $= (0.30631\ 0343, -0.13899\ 0273)$	
	Computed value	relative error(%)
2x2	(0.32031 2799, -0.07266 7596)	4.57
3x3	(0.30696 9582, -0.14083 3567)	2.15 E-1
4x4	(0.30629 5990, -0.13897 1237)	4.69 E-3
5x5	(0.30631 0526, -0.13899 0369)	5.96 E-5
6x6	(0.30631 0333, -0.13899 0266)	3.34 E-6
7x7	(0.30631 0336, -0.13899 0266)	2.19 E-6

TABLE 4.4 NUMERICAL EVALUATION OF SINGULAR INTEGRALS

$$\int_{-1}^{+1} \int_{-1}^{+1} \frac{N_i e^{i\kappa r}}{r} d\eta d\zeta$$

Gauss point per subelement	Singularity at node 1, $\iota = 2$ $\kappa = 1.$ $V_{\text{semi-analytical}}$ $= (0.63139\ 1437, 0.67694\ 8836)$	
	Computed value	relative error(%)
2x2	(0.63551 7187, 0.60999 6826)	6.53 E-1
3x3	(0.63039 2743, 0.67869 1667)	1.58 E-1
4x4	(0.63140 9780, 0.67693 0990)	2.91 E-3
5x5	(0.63139 1239, 0.67694 8910)	3.13 E-5
6x6	(0.63139 1417, 0.67694 8813)	3.16 E-6
7x7	(0.63139 1419, 0.67694 8814)	2.90 E-6

TABLE 4.4 NUMERICAL EVALUATION OF SINGULAR INTEGRALS

$$\int_{-1}^{+1} \int_{-1}^{+1} \frac{N_i e^{ikr}}{r} d\eta d\zeta$$

Gauss point per subelement	Singularity at node 1, $\iota = 3$ $\kappa = 1$. $V_{\text{semi-analytical}}$ $= (-0.15561\ 5611, -0.16512\ 1654)$	
	Computed value	relative error(%)
2x2	(-0.14096 1784, -0.14712 2817)	9.42
3x3	(-0.15583 3511, -0.16542 8900)	1.40 E-1
4x4	(-0.15561 7661, -0.16511 9335)	1.32 E-3
5x5	(-0.15561 5419, -0.16512 1651)	1.23 E-4
6x6	(-0.15561 5608, -0.16512 1641)	1.36 E-6
7x7	(-0.15561 5604, -0.16512 1641)	4.00 E-6

TABLE 4.4 NUMERICAL EVALUATION OF SINGULAR INTEGRALS

$$\int_{-1}^{+1} \int_{-1}^{+1} \frac{N_i e^{ikr}}{r} d\eta d\zeta$$

Gauss point per subelement	Singularity at node 1, $\iota = 4$ $\kappa = 1$. $V_{\text{semi-analytical}}$ $= (0.20084\ 7584, 0.58227\ 8758)$	
	Computed value	relative error(%)
2x2	(0.14891 1821, 0.59520 2300)	2.59 E+1
3x3	(0.20252 5964, 0.58154 6900)	8.36 E-1
4x4	(0.20083 3229, 0.58228 8506)	7.15 E-3
5x5	(0.20084 7415, 0.58227 8668)	8.43 E-5
6x6	(0.20084 7582, 0.58227 8729)	1.10 E-6
7x7	(0.20084 7577, 0.58227 8729)	3.28 E-6

TABLE 4.4 NUMERICAL EVALUATION OF SINGULAR INTEGRALS

$$\int_{-1}^{+1} \int_{-1}^{+1} \frac{N_i e^{i\kappa r}}{r} d\eta d\zeta$$

Gauss point per subelement	Singularity at node 1, $\iota = 5$ $\kappa = 1.$ $V_{\text{semi-analytical}}$ $= (-0.14361\ 3290, -0.18521\ 8569)$	
	Computed value	relative error(%)
2x2	(-0.09408 4170, -0.18500 4901)	3.45 E+1
3x3	(-0.14530 9974, -0.18474 0700)	1.18 E+0
4x4	(-0.14359 7383, -0.18522 6296)	1.11 E-2
5x5	(-0.14361 3215, -0.18521 8518)	5.22 E-5
6x6	(-0.14361 3281, -0.18521 8570)	6.11 E-6
7x7	(-0.14361 3280, -0.18521 8570)	6.75 E-6

TABLE 4.4 NUMERICAL EVALUATION OF SINGULAR INTEGRALS

$$\int_{-1}^{+1} \int_{-1}^{+1} \frac{N_i e^{ikr}}{r} d\eta d\zeta$$

Gauss point per subelement	Singularity at node 2, $\iota = 1$ $\kappa = 1$. $V_{\text{semi-analytical}}$ $= (-0.17043\ 8433, -0.17024\ 6303)$	
	Computed value	relative error(%)
2x2	(-0.16097 7542, -0.15558 4219)	5.55
3x3	(-0.16978 6843, -0.17047 4383)	3.82 E-1
4x4	(-0.17049 8602, -0.17024 4876)	3.53 E-2
5x5	(-0.17044 2767, -0.17024 6337)	2.54 E-3
6x6	(-0.17043 7561, -0.17024 6332)	5.12 E-4
7x7	(-0.17043 8464, -0.17024 6332)	1.78 E-5

TABLE 4.4 NUMERICAL EVALUATION OF SINGULAR INTEGRALS

$$\int_{-1}^{+1} \int_{-1}^{+1} \frac{N_i e^{i\kappa r}}{r} d\eta d\zeta$$

Gauss point per subelement	Singularity at node 2, $\iota = 2$ $\kappa = 1.$ $V_{\text{semi-analytical}}$ $= (1.73354 \ 9433, \ 0.75276 \ 7741)$	
	Computed value	relative error(%)
2x2	(1.76056 6879, 0.73798 8718)	1.56
3x3	(1.73312 9957, 0.75298 6414)	2.42 E-2
4x4	(1.73340 7128, 0.75276 6255)	8.21 E-3
5x5	(1.73355 8850, 0.75276 7762)	5.43 E-4
6x6	(1.73355 0668, 0.75276 7756)	7.12 E-5
7x7	(1.73354 9262, 0.75276 7756)	9.85 E-6

TABLE 4.4 NUMERICAL EVALUATION OF SINGULAR INTEGRALS

$$\int_{-1}^{+1} \int_{-1}^{+1} \frac{N_i e^{i\kappa r}}{r} d\eta d\zeta$$

Gauss point per subelement	Singularity at node 2, $\iota = 4$ $\kappa = 1.$ $V_{\text{semi-analytical}}$ $= (0.73516 \ 8170, \ 0.70106 \ 5735)$	
	Computed value	relative error(%)
2x2	(0.71622 3731, 0.67977 3108)	2.58
3x3	(0.73410 7269, 0.70135 4687)	1.44 E-1
4x4	(0.73520 4387, 0.70106 4143)	4.93 E-3
5x5	(0.73518 0582, 0.70106 5755)	1.69 E-3
6x6	(0.73516 7148, 0.70106 5750)	1.39 E-4
7x7	(0.73516 8093, 0.70106 5750)	1.04 E-5

TABLE 4.5 NUMERICAL EVALUATION OF SINGULAR INTEGRALS

$$\int_{-1}^{+1} \int_{-1}^{+1} \frac{N_i e^{ikr}}{r^2} d\eta d\zeta$$

Gauss point per subelement	Singularity at node 1, $\iota = 2$ $\kappa = 1$. $V_{\text{semi-analytical}}$ $= (1.51597\ 5022, 0.87138\ 6032)$	
	Computed value	relative error(%)
2x2	(1.54543 6331, 0.87100 3473)	1.94
3x3	(1.51520 4053, 0.87113 9976)	5.09 E-2
4x4	(1.51599 6473, 0.87139 1482)	1.43 E-3
5x5	(1.51597 4554, 0.87138 5919)	3.09 E-5
6x6	(1.51597 4961, 0.87138 6003)	4.03 E-6
7x7	(1.51597 4979, 0.87138 6005)	2.87 E-6

TABLE 4.5 NUMERICAL EVALUATION OF SINGULAR INTEGRALS

$$\int_{-1}^{+1} \int_{-1}^{+1} \frac{N_i e^{i\kappa r}}{r^2} d\eta d\zeta$$

Gauss point per subelement	Singularity at node 1, $\iota = 3$ $\kappa = 1.$ $V_{\text{semi-analytical}}$ $= (-0.38623 \ 1404, -0.21622 \ 2096)$	
	Computed value	relative error(%)
2x2	(-0.38787 5544, -0.20880 5922)	4.26 E-1
3x3	(-0.38608 5410, -0.21626 9350)	3.78 E-2
4x4	(-0.38624 4708, -0.21622 5260)	3.45 E-3
5x5	(-0.38623 0785, -0.21622 1907)	1.60 E-4
6x6	(-0.38623 1398, -0.21622 2087)	1.52 E-6
7x7	(-0.38623 1390, -0.21622 2084)	3.46 E-6

TABLE 4.5 NUMERICAL EVALUATION OF SINGULAR INTEGRALS

$$\int_{-1}^{+1} \int_{-1}^{+1} \frac{N_i e^{i\kappa r}}{r^2} d\eta d\zeta$$

Gauss point per subelement	Singularity at node 1, $\iota = 4$ $\kappa = 1.$ $V_{\text{semi-analytical}}$ $= (0.28932\ 5593, 0.49875\ 9941)$	
	Computed value	relative error(%)
2x2	(0.27070 4900, 0.47817 3725)	6.44
3x3	(0.28947 3675, 0.49909 7173)	5.12 E-2
4x4	(0.28934 0794, 0.49876 2566)	5.25 E-3
5x5	(0.28932 4786, 0.49875 9669)	2.79 E-4
6x6	(0.28932 5593, 0.49875 9922)	1.14 E-7
7x7	(0.28932 5583, 0.49875 9918)	3.55 E-6

TABLE 4.5 NUMERICAL EVALUATION OF SINGULAR INTEGRALS

$$\int_{-1}^{+1} \int_{-1}^{+1} \frac{N_i e^{ikr}}{r^2} d\eta d\zeta$$

Gauss point per subelement	Singularity at node 1, $\iota = 5$ $\kappa = 1.$ $V_{\text{semi-analytical}}$ $= (-0.19351\ 2907, -0.20273\ 4553)$	
	Computed value	relative error(%)
2x2	(-0.18110 9879, -0.18214 6574)	6.41
3x3	(-0.19359 4933, -0.20307 0287)	4.24 E-2
4x4	(-0.19352 4281, -0.20273 6089)	5.88 E-3
5x5	(-0.19351 2401, -0.20273 4390)	2.62 E-4
6x6	(-0.19351 2899, -0.20273 4550)	4.34 E-6
7x7	(-0.19351 2898, -0.20273 4549)	4.64 E-6

TABLE 4.5 NUMERICAL EVALUATION OF SINGULAR INTEGRALS

$$\int_{-1}^{+1} \int_{-1}^{+1} \frac{N_i e^{i\kappa r}}{r^2} d\eta d\zeta$$

Gauss point per subelement	Singularity at node 2, $\iota = 1$ $\kappa = 1$. $V_{\text{semi-analytical}}$ $= (-0.50771\ 7330, -0.23020\ 9938)$	
	Computed value	relative error(%)
2x2	(-0.51292 7808, -0.22508 0052)	1.03
3x3	(-0.50361 7454, -0.22954 8717)	8.08 E-1
4x4	(-0.50795 4150, -0.23026 7467)	4.66 E-2
5x5	(-0.50776 3174, -0.23021 4300)	9.03 E-3
6x6	(-0.50771 1341, -0.23020 9090)	1.18 E-3
7x7	(-0.50771 7092, -0.23020 9976)	4.68 E-5

TABLE 4.5 NUMERICAL EVALUATION OF SINGULAR INTEGRALS

$$\int_{-1}^{+1} \int_{-1}^{+1} \frac{N_i e^{-i\kappa r}}{r^2} d\eta d\zeta$$

Gauss point per subelement	Singularity at node 2, $\iota = 4$ $\kappa = 1.$ $V_{\text{semi-analytical}}$ $= (1.71009\ 8888, 0.95942\ 4431)$	
	Computed value	relative error(%)
2x2	(1.74170 0991, 0.95383 5700)	1.85
3x3	(1.70299 9810, 0.95819 7033)	4.15 E-1
4x4	(1.71012 5039, 0.95945 8556)	1.53 E-3
5x5	(1.71020 0868, 0.95943 6715)	5.96 E-3
6x6	(1.71009 2715, 0.95942 3440)	3.61 E-4
7x7	(1.71009 7816, 0.95942 4360)	6.27 E-5

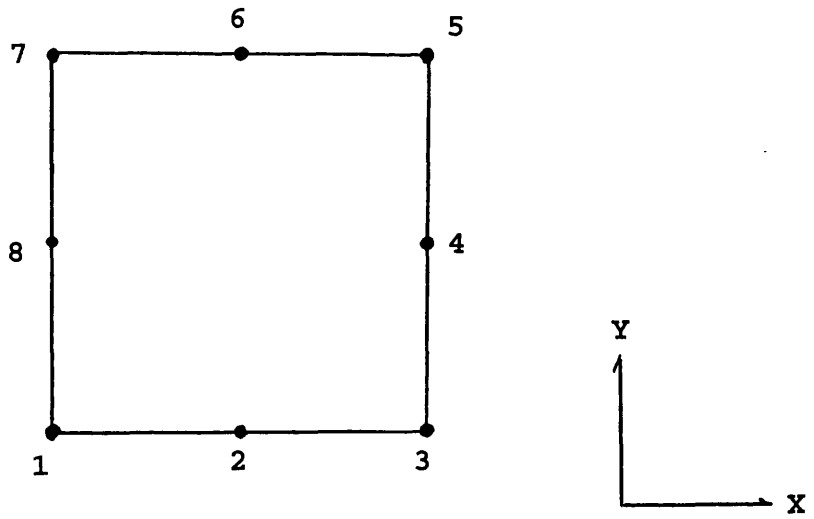


Figure 4.1: Eight-noded rectangular element

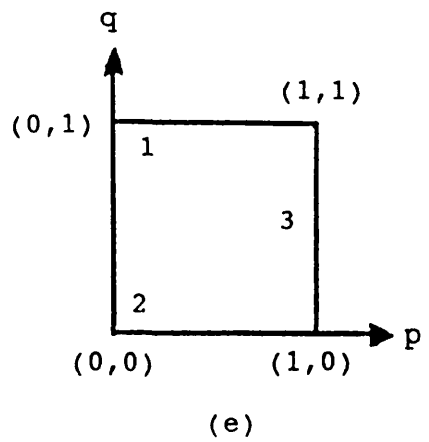
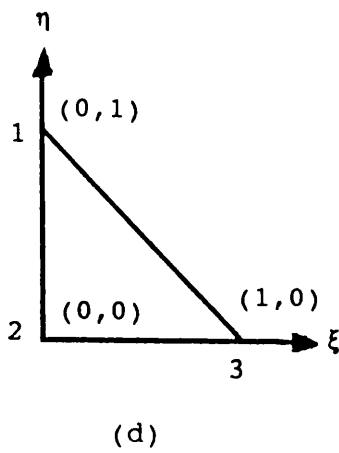
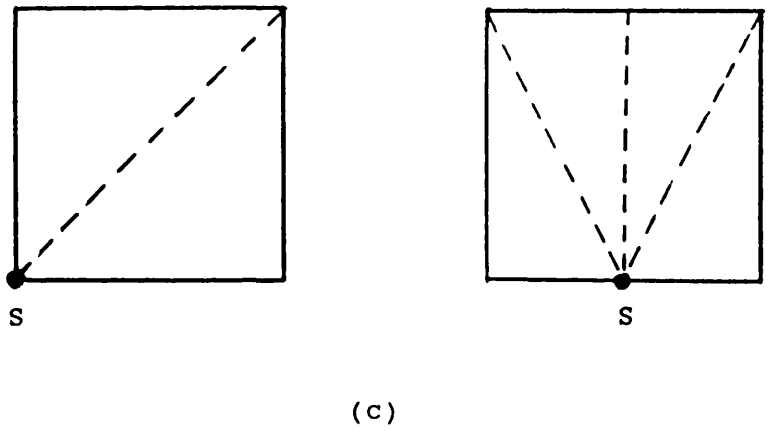
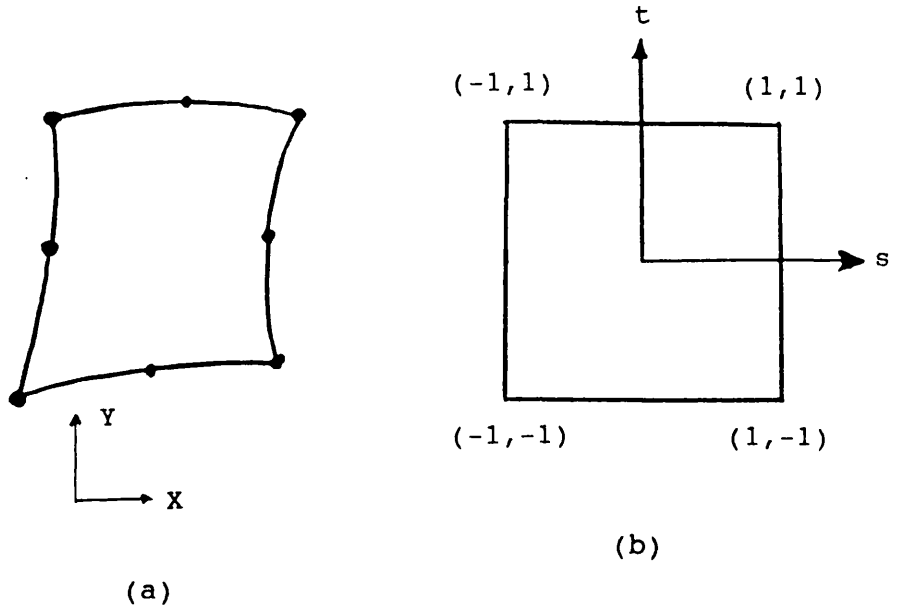


Figure 4.2: Sub-division and transformation method

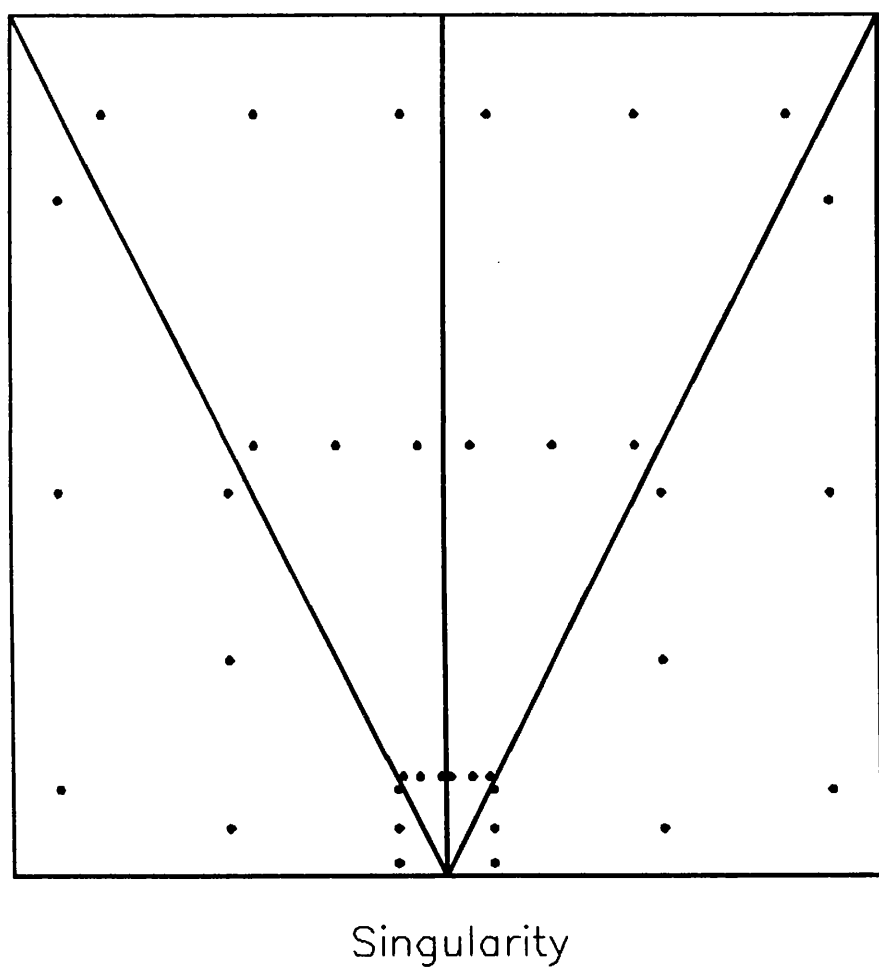


Figure 4.3: The distribution of integration points

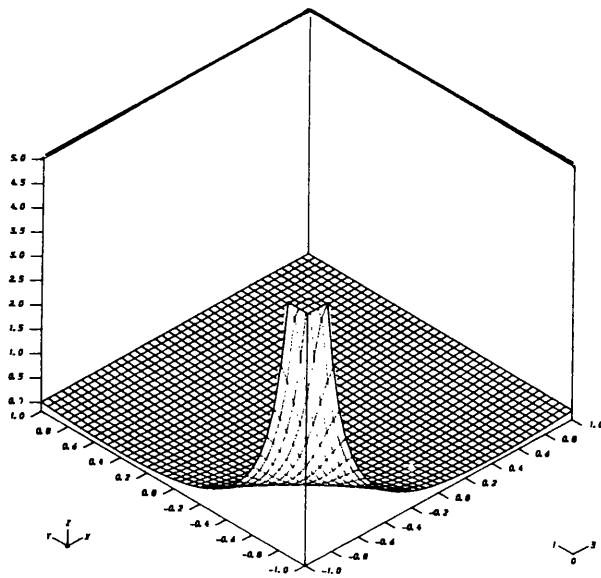


Figure 4.4a: The behaviour of integrand N_1/r_1

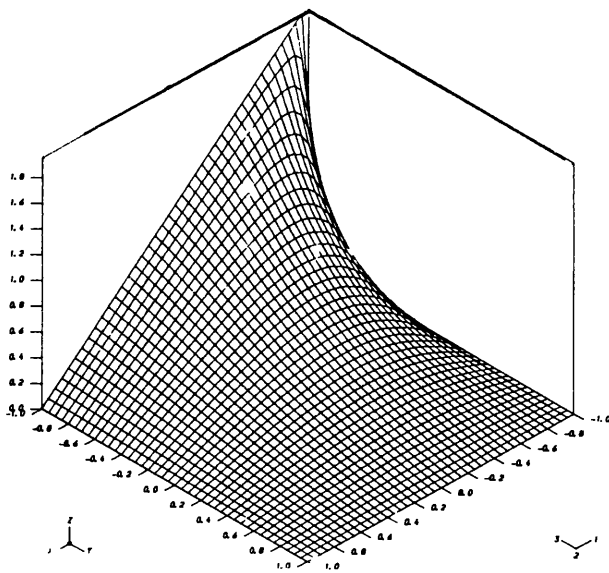


Figure 4.4b: The behaviour of integrand N_2/r_1

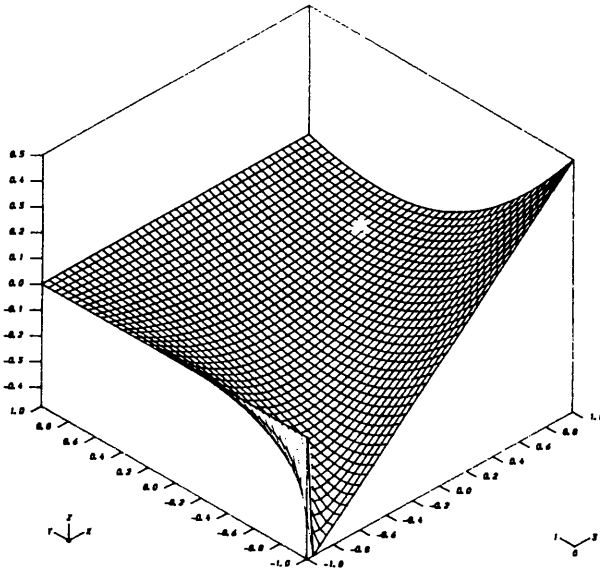


Figure 4.4c: The behaviour of integrand N_3/r_1

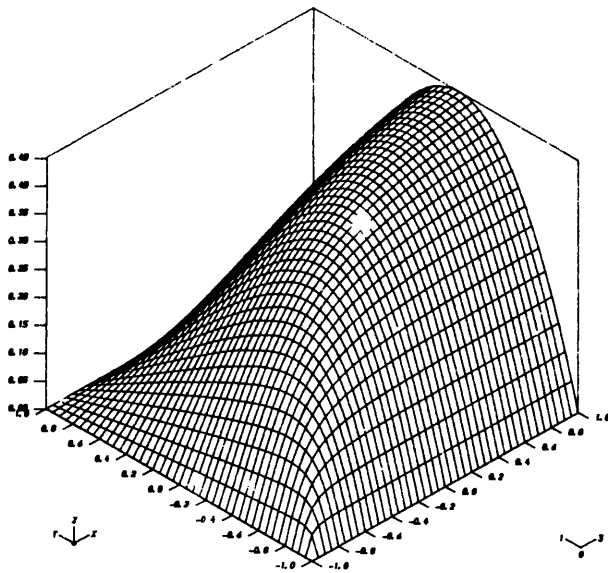


Figure 4.4d: The behaviour of integrand N_4/r_1

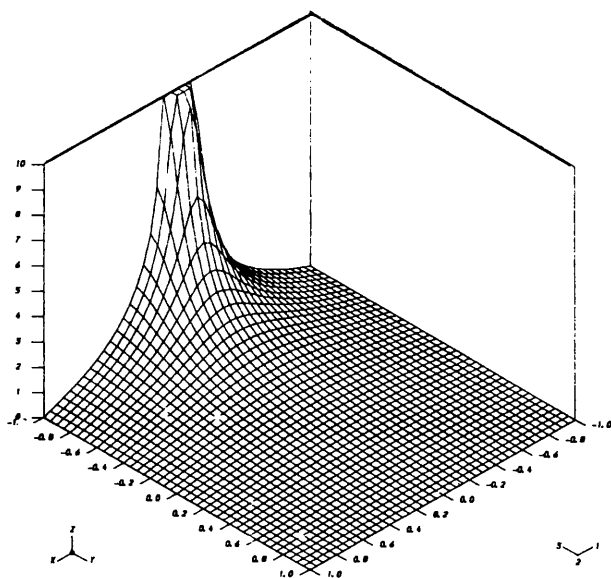


Figure 4.4e: The behaviour of integrand N_2/r_2

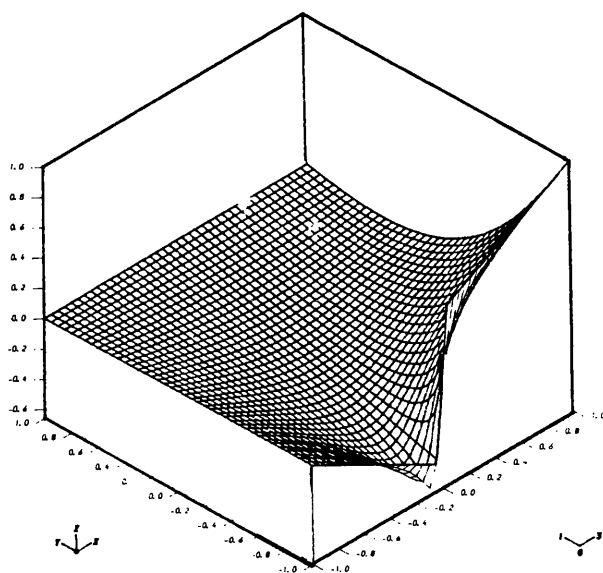


Figure 4.4f: The behaviour of integrand N_3/r_2

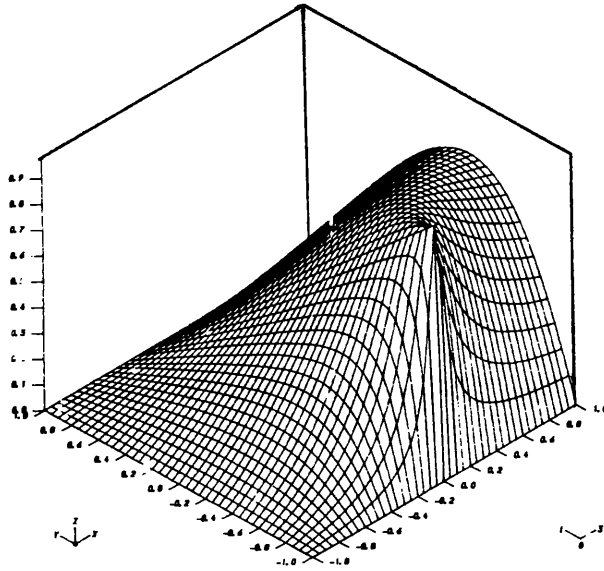


Figure 4.4g: The behaviour of integrand N_4/r_2

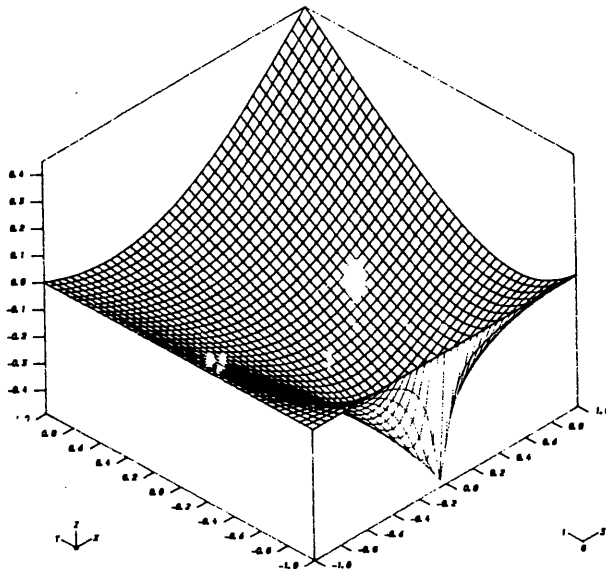


Figure 4.4h: The behaviour of integrand N_5/r_2

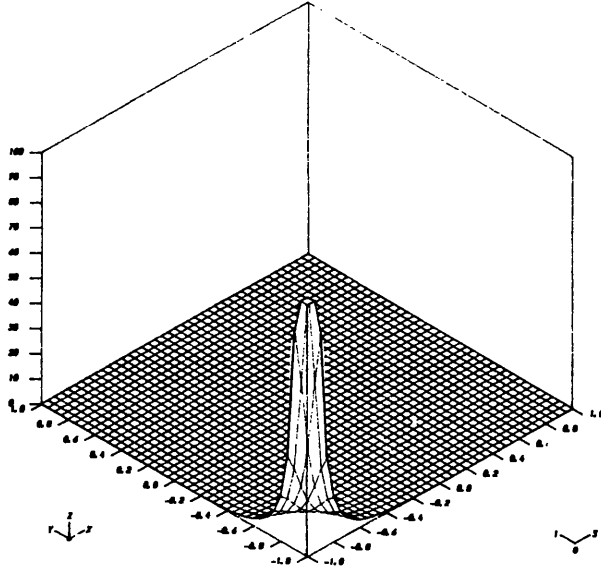


Figure 4.5a: The behaviour of integrand N_1/r_1^2

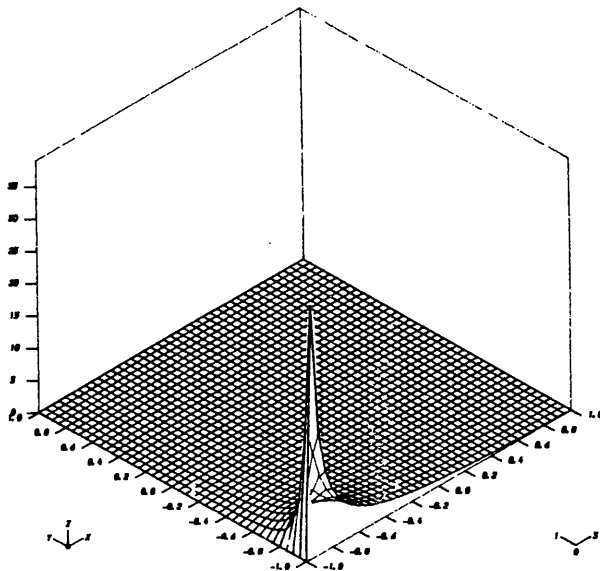


Figure 4.5b: The behaviour of integrand N_2/r_1^2

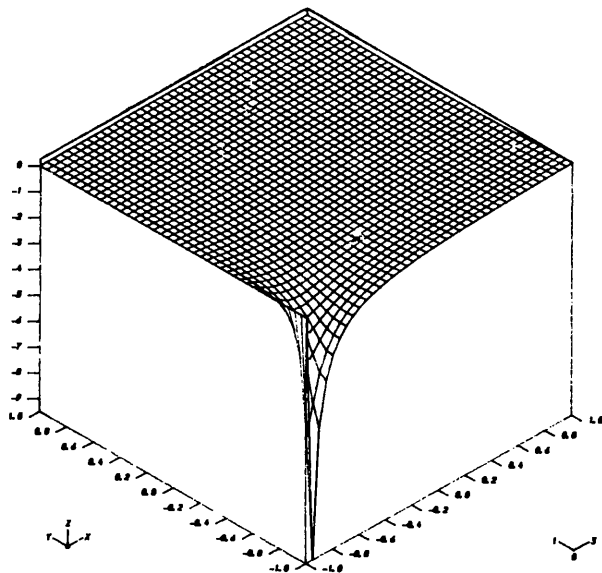


Figure 4.5c: The behaviour of integrand N_3/r_1^2

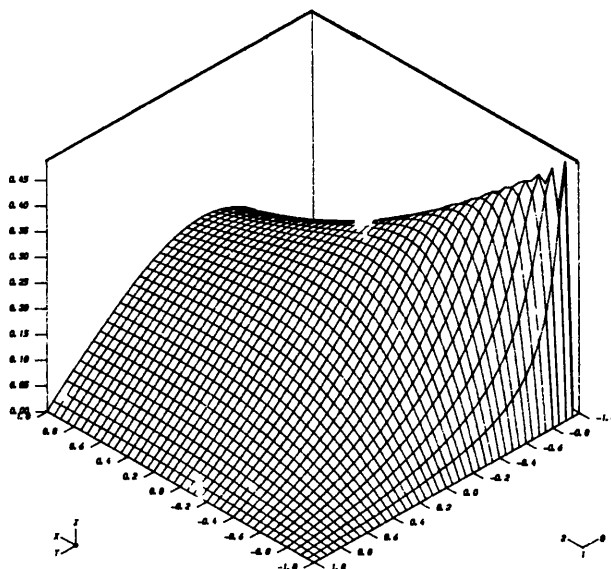


Figure 4.5d: The behaviour of integrand N_4/r_1^2

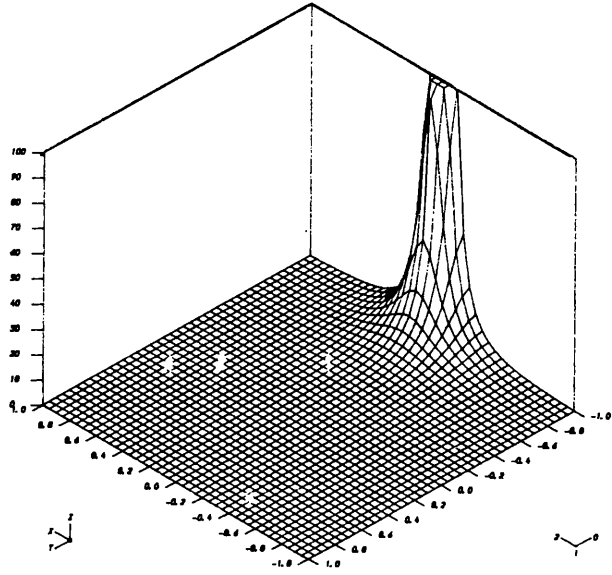


Figure 4.5e: The behaviour of integrand N_2/r_2^2

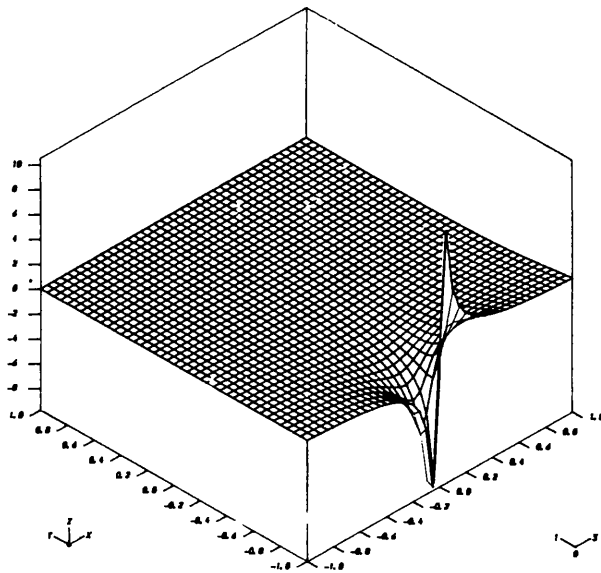


Figure 4.5f: The behaviour of integrand N_3/r_2^2

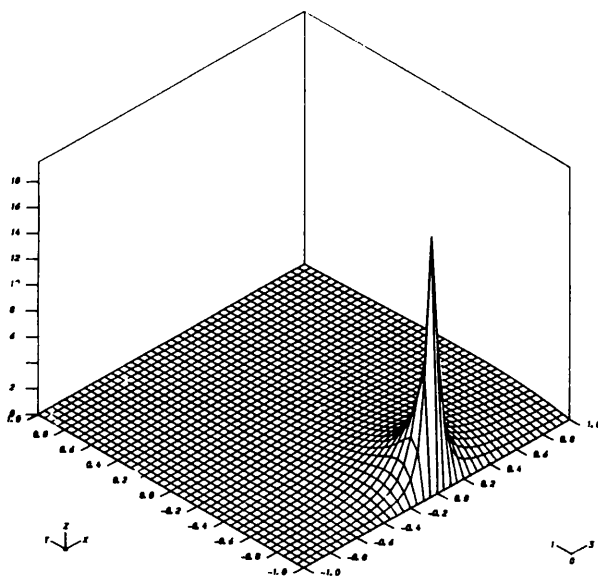


Figure 4.5g: The behaviour of integrand N_4/r_2^2

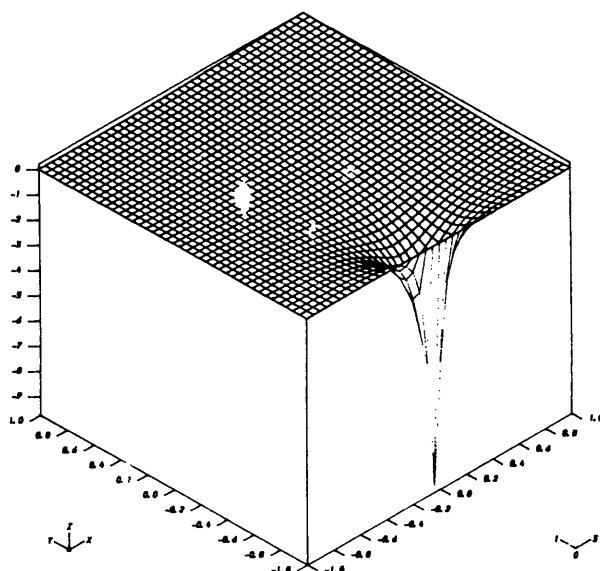


Figure 4.5h: The behaviour of integrand N_5/r_2^2

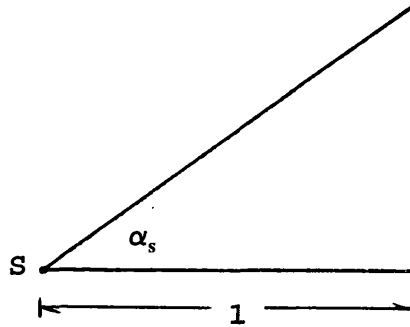
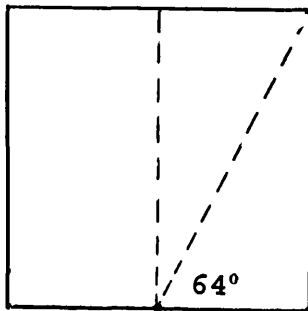
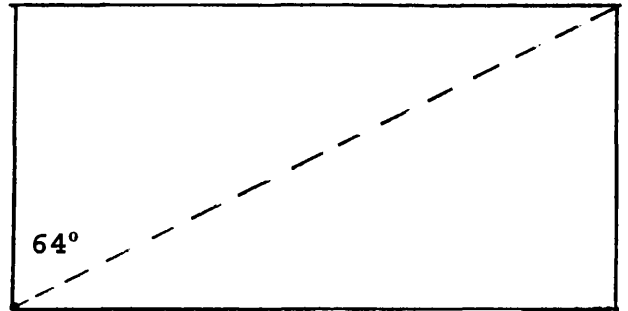


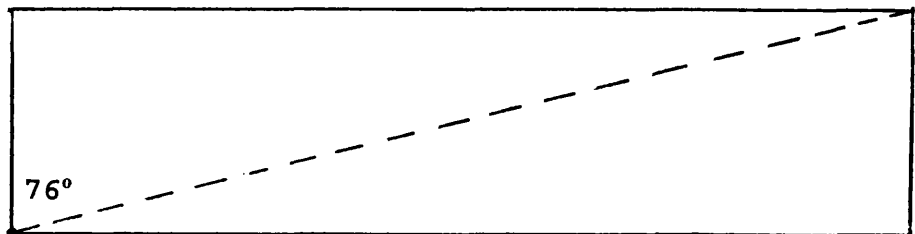
Figure 4.6 : Study of singular vertex angle



aspect ratio = 1



aspect ratio = 2



aspect ratio = 4

Figure 4.7: Maximum possible vertex angles

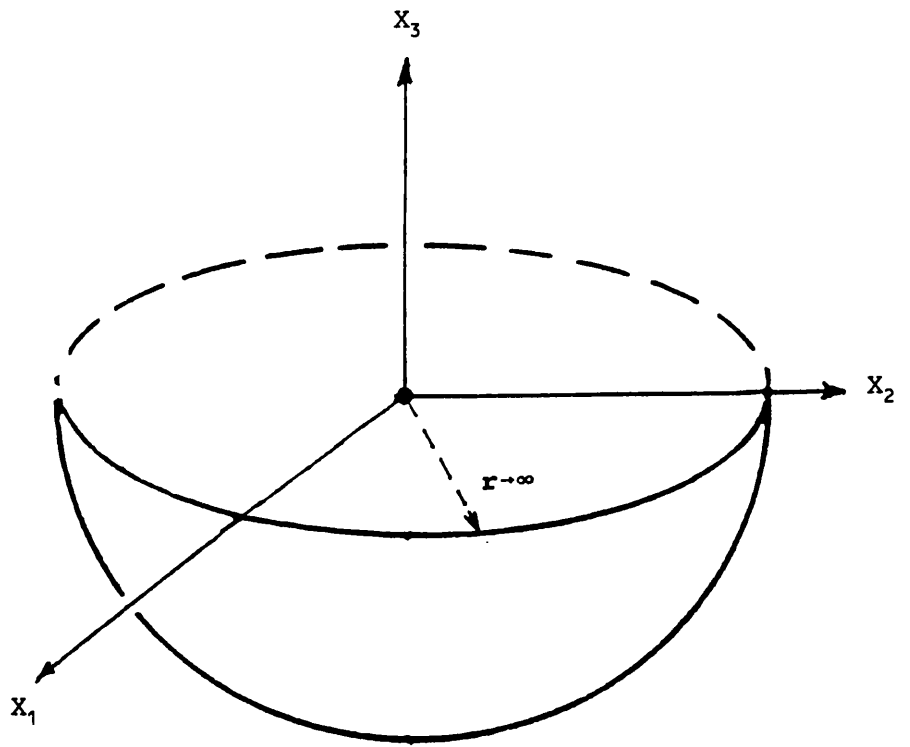
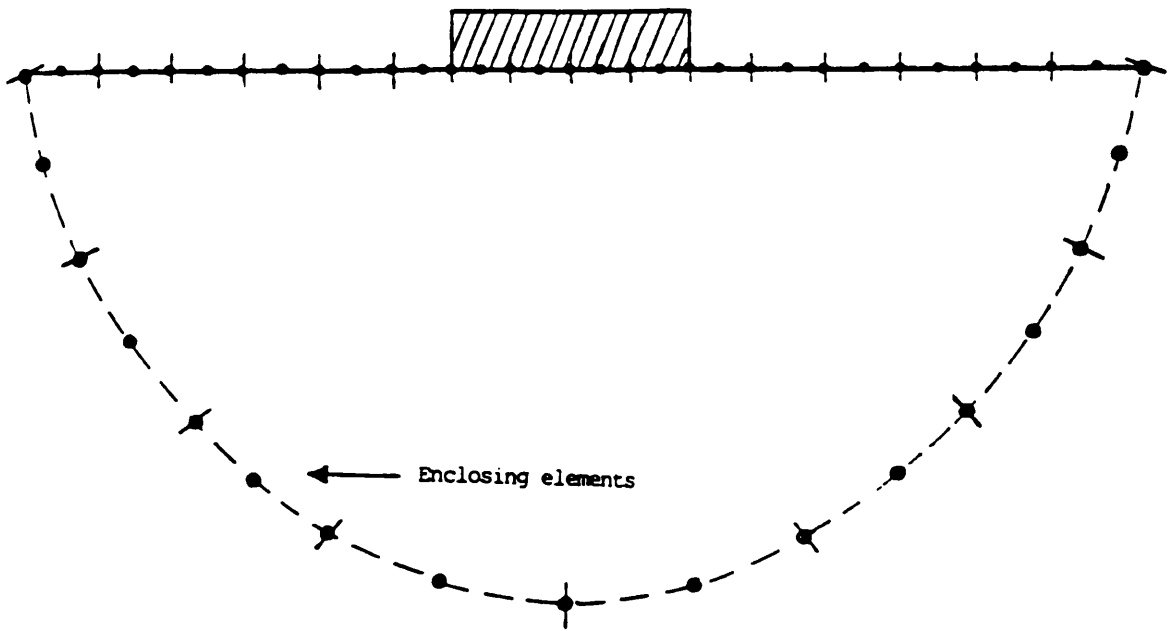


Figure 4.8: Halfspace model



Boundary element discretization of a half-space problem

Figure 4.9: Enclosing elements (from Ahmad and Banerjee, 1988)

CHAPTER 5

INFINITE BOUNDARY ELEMENTS

5.1 INTRODUCTION

Many geotechnical problems can be idealized by assuming that the regions remote from the area of interest extend to infinity; the problem of soil-structure interaction is a typical example of this. Most boundary element analyses of machine foundations use the full-space fundamental solution (e.g., Emperador and Dominguez, 1989; Gazetas and Tassoulas, 1987a and b) and, consequently, require the discretization of the free surface of the halfspace. As the capacity of computers is finite, the semi-infinite surface must then be truncated to a bounded region of manageable size. For example, the truncated discretization scheme used by Israil and Banerjee (1990) was confined to a region within $5B$ and $18B$ (B is the half-width of the rectangular foundation) around surface and embedded foundations, respectively. However, higher-order elements with dimensions smaller than $1/4$ Rayleigh wavelengths are essential for modelling wave fields accurately. Consequently, in order to obtain results of acceptable accuracy, this method of analysis requires considerable computational resources, particularly for high frequency (small wavelength) problems. In the literature, very few results have been obtained for dimensionless frequencies (a_0) greater than two.

A more effective method is to incorporate "infinite elements",

based on finite element ideas, into the boundary element analysis. The idea of infinite boundary elements was first proposed by Watson(1979) in connection with static halfspace problems. However, as noted by Watson himself, rules for the use of infinite elements in boundary element analyses required further research. Watson's formulation contained an error which was only corrected in a much later paper(Beer and Watson, 1989). Recently, the use of infinite boundary elements to analyze unbounded geotechnical problems has received considerable attention. Beer et al(1987) employ infinite boundary elements to model a tunnel which is assumed to extend to infinity. Later, Beer and Watson(1989) discussed the application of special types of boundary elements for the modelling of surfaces which extend to infinity. Chuhan et al(1991) developed shape functions for describing far-field behaviour associated with multiple wave propagation. Davies and Bu(1993) describe infinite boundary element solutions for high frequency response of machine foundations, based on the work described in this thesis.

This chapter presents details of the infinite boundary elements for static and dynamic halfspace problems. The basis of the method, for static problems, is that the far-field displacements can be reasonably described by a (real) function, called the decay function. A mapping technique is then developed to transform the infinite element onto a unit square. Because integrands of static problems decrease monotonously with the distance and approach zero as the distance becomes infinite, Gauss-Legendre quadrature can be used for evaluating integrals over infinite boundary elements. Based on the results of numerical tests, an order-adaptive integration criterion was developed in order to obtain accurate numerical results with minimum cost. A series of static foundation problems were then analyzed to demonstrate the applicability and accuracy of the formulation and excellent agreement with analytical solutions was obtained.

The development of infinite element techniques for dynamic problems is very much more complicated. The dynamic (complex valued) decay function assumed in the development of infinite boundary elements for elastodynamic analyses is based on Rayleigh wave attenuation away from a source located at the centroid of the loaded area. The integrals over the infinite elements are then computed between successive zeros of the integrands. Numerical studies reveal that the slowly convergent infinite series sum of these integrals can be calculated very efficiently by means of the Euler transformation. Illustrative results for foundations subjected to harmonic loads are presented in order to illustrate the potential of the formulation.

5.2 ASYMPTOTIC BEHAVIOUR OF THE FAR-FIELD

5.2.1 Introduction

The displacements and tractions at an arbitrary point in a finite boundary element can be described in terms of element nodal values and the shape functions. Evidently, conventional shape functions are not capable of describing the behaviour of field variables over an infinite region. Special shape functions can however be developed for this purpose, based on analytical solutions for halfspace problems.

In the analysis of halfspace problems, the boundary element method involves integrations, in the far-field, over only the surface of the semi-infinite domain. In general, these unbounded surfaces are traction-free in most geotechnical problems. This observation makes it possible to eliminate the displacement kernel integrals

$$\int_s G_{ij} t_i dS$$

over free surfaces outside the loaded area. Consequently, in addition to the significant reduction of computational effort that this implies, the traction behaviour of the far-field need not be considered further.

5.2.2 Static Displacement Behaviour

Analytical solutions for smooth circular foundations resting on an elastic halfspace subjected to various types of loadings have been collected by Poulos and Davis(1974). For example, the displacements at an arbitrary point y on the surface of an elastic halfspace due to a uniformly distributed vertical load p_v acting on a circular area(radius= r_c) can be obtained from the following equations:

Vertical displacement at y($r > r_c$)

$$u_z = p_v \cdot r_c \cdot \frac{1 - \nu^2}{E} \cdot \frac{H}{r} \tag{5.1}$$

Radial horizontal displacement at y($r > r_c$)

$$u_r = p_v \cdot r_c \cdot \frac{(1 + \nu)(1 - 2\nu)}{E} \cdot \frac{1}{2r} \tag{5.2}$$

in which E is the modulus of elasticity, r is the distance between the point y and the centre of the circular foundation, and H is a function of some constants and r^2 (see Poulos and Davis, 1974; integrals I₂₀₀, p. 349).

Careful examination of the above solutions indicates that,

neglecting terms associated with higher order reciprocal powers of r , the asymptotic far-field displacements on the halfspace surface are as follows:

$$\begin{aligned} u_z &\sim O\left(\frac{1}{r}\right) \\ u_r &\sim O\left(\frac{1}{r}\right) \end{aligned} \tag{5.3}$$

Asymptotic displacements corresponding to various types of loadings are summarized in Table 5.1.

It should be further noted that the displacement field outside the immediate loaded area is practically identical for both welded and smooth contact conditions between soil and foundation (Schiffman, 1969). Accordingly, appropriate decay functions D_s can be established to describe the displacement field in the (infinite) radial direction. For example, for uniform vertical stresses or displacements on a finite area, the far-field vertical displacement u_z can be evaluated from the equation:

$$u_z = u_{0z} \frac{r_0}{r} = u_{0z} \cdot D_s \tag{5.4}$$

where r_0 and r are the distances from the centre of the loaded area to some convenient reference point and an arbitrary colinear point in the far-field, respectively; u_{0z} is the vertical displacement at the reference point (Figure 5.2a).

The analytical and predicted vertical displacements outside a circular foundation, subjected to uniformly distributed loads, are illustrated in Figure 5.2b, respectively, in which all the displacements have been normalized by the factor $p_v r_c (1-\nu^2)/E$. It is observed that excellent agreement with analytical solutions can be achieved by using a reference point in the

near vicinity of the foundation ($r_0/r_c=1.5$). This example clearly shows the effectiveness of the proposed decay function.

5.2.3 Dynamic Displacement Behaviour

Some knowledge of elastic wave propagation in halfspaces is necessary in order to replicate the asymptotic displacement behaviour of the far-field. The three characteristic waves on the surface of a homogeneous isotropic elastic halfspace, namely the dilatation, shear, and Rayleigh waves, all contribute to the displacement field, which makes closed-form analytical solutions impractical. However, a number of studies (e.g., Miller and Pursey, 1954; Gazetas and Yegian, 1979) have shown that Rayleigh waves are predominant in the propagation of energy on the surface of elastic halfspaces. For practical purposes, it seems reasonable to assume that the displacement behaviour of the far-field is the same as the Rayleigh wave field. A detailed description of the Rayleigh wave field has been given by, for example, Eringen and Suhubi (1975).

Based on the geometrical ray theory, Hudson (1980) and Achenbach et al (1982) show that the orthogonal trajectories of the family of wavefronts in a homogeneous material are straight lines. Consequently, a one-dimensional decay function D_d is developed in this thesis by using an exponential term to describe approximately the oscillatory behaviour of the Rayleigh wave, namely,

$$u = u_0 \cdot D_d \quad (5.5)$$

$$D_d = \left(\frac{r_0}{r} \right)^{1/2} \cdot \exp \frac{i\omega r}{c_r} \quad (5.6)$$

in which, c_r is the Rayleigh wave velocity. This equation implies that the amplitude of the displacement waves decays at

the same spatial rate as the Rayleigh waves, namely, $r^{1/2}$. In this thesis, the velocity of Rayleigh wave is calculated from the (approximate) expression given by Achenbach(1976) :

$$C_R = \frac{0.862 + 1.14\nu}{1 + \nu} \cdot C_2 \quad (5.7)$$

in which, C_2 is the velocity of the shear waves.

Because the displacements in dynamic analyses are usually complex-valued numbers, it is necessary to ensure the continuity and compatibility of displacement phase at the interface between the near-field and far-field, and its continuance into the far-field. An explicit boundary condition is that the decay function should be unity at $r=r_0$. However, the use of equation(5.6) leads to

$$D_d = \exp \frac{i\omega r_0}{C_r}$$

Accordingly, a factor

$$D_d^* = \exp \frac{-i\omega r_0}{C_r} \quad (5.8)$$

is introduced into Equation(5.6) in order to eliminate the undesirable term, ie.,

$$D_d = \left(\frac{r_0}{r}\right)^{1/2} \cdot \exp \frac{i\omega(r-r_0)}{C_r} \quad (5.9)$$

Two types of bonding between soil and foundation, i.e. welded and smooth contact, have been investigated in the analysis of machine foundations as well as various simplified "relaxed" boundary conditions. It seems reasonable to suppose that the

decay function described above is valid, outside the immediate loaded area, for all these cases. As mentioned earlier, under static loading conditions, the analogous result has been demonstrated.

5.3 DISCRETIZATION AND MAPPING THEORY

5.3.1 Discretization Of The Far Field

In this thesis, the boundary of the halfspace model is subdivided into a core region S_F , the far-field S_I and the hemispherical surface S_H with radius approaching infinity, shown schematically in Figure 5.3. The core region is discretized with finite-sized boundary elements, in which tractions and displacements are described by quadratic shape functions N_α over eight-noded boundary elements.

The discretization of the semi-infinite surface of the halfspace by infinite boundary elements can be variously accomplished. It is worth noting that the infinite boundary elements proposed by Beer et al (1987) and Beer and Watson (1989) do not lie radially from the decay centre. This results in many difficulties in geometrical definition of the infinite element and the interpolation of far-field variables. The former requires additional nodes in the infinite direction to define the infinite element. In practice, the latter problem has been resolved, approximately, by moving the decay centre to a "fictitious" decay centre (Figure 5.4). In the present study, the far-field is modelled by means of infinite elements whose edges, in the radial direction, are defined by straight lines radiating from the centre of the loaded area (Figure 5.5). Because a novel mapping technique has been developed in the present study, no additional degrees-of-freedom are needed to model the infinite region of the halfspace problem. Consequently, as described later, the far-field displacements

can then be easily calculated. A similar discretization has been presented by Chuhan et al (1991). However, they use extra nodes in the infinite direction to define the geometry of the infinite boundary element.

The hemispherical surface need not be discretized since the azimuthal integral over this infinite boundary due to local loading can be shown to be zero. However, as described in Chapter 4, the azimuthal integral over S_H is significant if the traction singularities in the near-field are to be evaluated by means of the indirect procedure based on rigid-body displacement.

5.3.2 Interpolation Of Displacements

Over each infinite element, the variation of displacements with respect to the radial direction are described by the decay functions, while the variation in the circumferential direction is described by quadratic shape functions. As shown in Figure (5.6), the displacement at an arbitrary reference point, $u_{i\alpha 0}$ on the boundary between the core region and the far-field, can be expressed, in terms of nodal displacements $U_{i\alpha}$, as

$$u_{i\alpha 0} = \sum_{\alpha=1}^3 M_{\alpha} U_{i\alpha} \quad (5.10)$$

in which,

$$\begin{aligned} M_1 &= \frac{\xi(\xi-1)}{2} \\ M_2 &= 1-\xi^2 \\ M_3 &= \frac{\xi(1+\xi)}{2} \end{aligned} \quad (5.11)$$

The far-field displacements $u_{i\alpha}$ can then be obtained from the equation:

$$u_{i\alpha} = u_{i\alpha 0} \cdot D_{s/d} = \sum_{\alpha=1}^3 M_{\alpha} U_{i\alpha} \cdot D_{s/d} \quad (5.12)$$

5.3.3 Geometric Representation

Static Analyses

The integrands in static analyses are well-behaved in the far-field and, consequently, Gauss-Legendre quadrature is capable of producing satisfactory results without special difficulty. To facilitate numerical integration, it is necessary to transform the infinite element onto a unit square. Owing to the use of additional nodes in the infinite direction to define infinite elements, mapping methods developed by Beer et al (1987), Beer and Watson(1989), and Chuhan et al(1991) are inefficient. A novel mapping technique for elastostatic problems is developed in this thesis.

As shown in Figure 5.7a, the type of infinite element used in this thesis is a three-node element defined by using rays originating from the decay origin(the centre of the foundation) to infinity. Without loss of generality, the decay centre is chosen as the origin. An infinite shape function, $(1+\eta)/2$, is used to describe the one-dimensional variation in the infinite direction(Figure 5.7b). The infinite sector is then mapped onto a rectangle with the η -direction extending to infinity (Figure 5.7c). The geometry is defined by

$$\begin{aligned}
 x &= \frac{1+\eta}{2} \sum_{i=1}^3 M_i(\xi) x_i \\
 y &= \frac{1+\eta}{2} \sum_{i=1}^3 M_i(\xi) y_i
 \end{aligned}
 \tag{5.13}$$

where x_i and y_i are the global nodal coordinates.

Clearly, $\eta = -1$ represents the decay origin while $\eta = +1$ represents the interface between the near-field and the far-field. A further mapping of the infinite area ($\eta \geq +1$) is then performed from the (η, ξ) system to the (a, b) system, as shown in Figure 5.7d. The corresponding transformation, after some manipulations, can be written as

$$\begin{aligned}
 \eta &= \frac{(3a+5)}{(1-a)} \\
 \xi &= b
 \end{aligned}
 \tag{5.14}$$

By substituting Equation (5.14) into Equation (5.13), the appropriate coordinate transformation, from the (x, y) system to the (a, b) system, for the infinite boundary element is given by

$$\begin{aligned}
 x &= \frac{(3+a)}{(1-a)} \sum_{i=1}^3 M_i(b) x_i \\
 y &= \frac{(3+a)}{(1-a)} \sum_{i=1}^3 M_i(b) y_i
 \end{aligned}
 \tag{5.15}$$

The Jacobian matrix J_1 for the transformation from the (x, y)

coordinate system to the (a,b) coordinate system can be computed without special difficulty. This mapping means that the integration points lie radially from the origin and are concentrated near to the origin(Figure 5.8). As a consequence, the accuracy of numerical integration is improved because most integration points are distributed in the region where the contribution to the integrals is the largest.

The distances r_0 and r in Equation(5.4) can be found from the equations:

$$r_0 = \sqrt{\left(\sum_{i=1}^3 M_i(b) x_i\right)^2 + \left(\sum_{i=1}^3 M_i(b) y_i\right)^2} \quad (5.16)$$

$$r = \frac{(3+a)}{(1-a)} \sqrt{\left(\sum_{i=1}^3 M_i(b) x_i\right)^2 + \left(\sum_{i=1}^3 M_i(b) y_i\right)^2} \quad (5.17)$$

In terms of local coordinates, the decay function can be expressed as:

$$D_s = \frac{r_0}{r} = \frac{(1-a)}{(3+a)} \quad (5.18)$$

Thus, when evaluating integrals over static infinite elements the value of the decay function at any arbitrary integration point can be readily calculated in the local coordinate system.

Dynamic Analyses

In dynamic analyses, integrals over infinite boundary elements are oscillatory integrals:

$$\int_I T_{ij} M_{\alpha} D_d dS$$

The direct use of conventional numerical integration method is impractical in these cases and special integration schemes become necessary. In this thesis, numerical integration of oscillating functions was carried out between the zeros of the integrand. As a consequence, each infinite element has been sub-divided into six-noded curvilinear patches by determining the zeros of the integrand along the rays, shown schematically in Figure 5.9. The present study considers only the first few (less than six) sub-elements because an extrapolation technique, as described later, is used to compute the infinite integral.

The Cartesian coordinates of an arbitrary point on a patch can be obtained in terms of the nodal coordinates. The shape functions for six-noded elements have been presented by, for example, Bathe(1982). However, the displacement at an arbitrary point on a patch is described by the decay function D_d .

It should be further noted that, to each source point, the locations of zeros depend on the individual component of the complex-valued function $T_{ij}D_d$, which has nine components. In addition, for each component of $T_{ij}D_d$, the zeros of the real part and the imaginary part are at different positions. However, careful examination of the function $T_{ij}D_d$ indicates that, for each pair of the following integrands, the zeros for the real (or imaginary) part are the same:

$$\begin{aligned} &T_{13}D_d \text{ and } T_{23}D_d, \\ &T_{31}D_d \text{ and } T_{32}D_d, \text{ and} \\ &T_{21}D_d \text{ and } T_{12}D_d. \end{aligned}$$

Clearly, the search for the zeros requires considerable computational resources. There are many numerical methods to find zeros of a function; see, for example, Chapra and Canale (1989). In the present study the zeros along a ray were determined by the "regula falsi" method exploiting the fact that functions change sign in the vicinity of a root. As shown in Figure 5.10, a straight line is used to join the two initial (guess) points x_l and x_r . The intersection of this line with the x-axis is x_i :

$$x_i = x_r - \frac{f(x_r)(x_l - x_r)}{f(x_l) - f(x_r)} \quad (5.19)$$

which represents an improved estimate of the root. The value x_i then replaces whichever of the two guesses, x_l or x_r , yields a function value with the same sign as $f(x_i)$. The process is repeated until the absolute value of $f(x_i)$ falls below 10^{-5} (in the present study, less than six iterations are needed). The search then continues to find the next zero along that particular ray. Once sufficient zeros have been found on all rays, the subelement patches are then constructed through these zeros.

5.3.4 Boundary Element Formulation For Halfspace Problems

In the numerical solution of the boundary integral equation, it is necessary to categorize the boundary elements and integrals needed in the computer program. In the previous two chapters these integrals are classified as non-singular integrals, integrable singular integrals, and the strictly diagonal block. In this chapter, the boundary elements are classified as finite size elements and infinite elements. These distinctions are introduced into the boundary integral equations in order to make the discretized terms more clear in programming practice. This systematic strategy makes the numerical implementation of boundary element formulation

relatively straightforward.

Based on this philosophy, the complete discretized boundary element formulation for dynamic halfspace problems can be developed (see Appendix 5.0 for detail):

$$\begin{aligned}
 & \left\{ \frac{\delta_{ij}}{2} - \sum_{M'} \int_F T_{ij}^{st} dS - \sum_{M^*} \sum_{\alpha'} \int_F T_{ij}^{st} N_{\alpha'} dS + \sum_{M^*} \int_F (T_{ij} - T_{ij}^{st}) N_{\alpha^*} dS \right. \\
 & \left. - \sum_{M'} \int_I T_{ij}^{st} dS - \sum_{M^*} \sum_{\alpha'} \int_I T_{ij}^{st} M_{\alpha'} dS + \sum_{M^*} \int_I (T_{ij} D_d - T_{ij}^{st}) M_{\alpha^*} dS \right\} \cdot u_i \quad (5.20) \\
 & = \sum_{M'} \sum_{\alpha=1}^8 t_{i\alpha} \int_F G_{ij} N_{\alpha} dS + \sum_{M^*} \sum_{\alpha=1}^8 t_{i\alpha} \int_F G_{ij} N_{\alpha} dS - \sum_{M'} \sum_{\alpha=1}^8 u_{i\alpha} \int_F T_{ij} N_{\alpha} dS \\
 & - \sum_{M^*} \sum_{\alpha'} u_{i\alpha'} \int_F T_{ij} N_{\alpha'} dS - \sum_{M'} \sum_{\alpha=1}^3 u_{i\alpha} \int_I T_{ij} M_{\alpha} D_d dS - \sum_{M^*} \sum_{\alpha'} u_{i\alpha'} \int_I T_{ij} M_{\alpha'} D_d dS
 \end{aligned}$$

The discretized formulation for static analyses can be obtained by replacing the dynamic fundamental solutions and decay function with their static counterparts:

$$\begin{aligned}
 & \left\{ \frac{\delta_{ij}}{2} - \sum_{M'} \int_F T_{ij}^{st} dS - \sum_{M^*} \sum_{\alpha'} \int_F T_{ij}^{st} N_{\alpha'} dS \right. \\
 & \left. - \sum_{M'} \int_I T_{ij}^{st} dS - \sum_{M^*} \sum_{\alpha'} \int_I T_{ij}^{st} M_{\alpha'} dS + \sum_{M^*} \int_I T_{ij}^{st} M_{\alpha^*} \cdot (D_s - 1) dS \right\} \cdot u_i \quad (5.21) \\
 & = \sum_{M'} \sum_{\alpha=1}^8 t_{i\alpha} \int_F G_{ij}^{st} N_{\alpha} dS + \sum_{M^*} \sum_{\alpha=1}^8 t_{i\alpha} \int_F G_{ij}^{st} N_{\alpha} dS - \sum_{M'} \sum_{\alpha=1}^8 u_{i\alpha} \int_F T_{ij}^{st} N_{\alpha} dS \\
 & - \sum_{M^*} \sum_{\alpha'} u_{i\alpha'} \int_F T_{ij}^{st} N_{\alpha'} dS - \sum_{M'} \sum_{\alpha=1}^3 u_{i\alpha} \int_I T_{ij}^{st} M_{\alpha} D_s dS - \sum_{M^*} \sum_{\alpha'} u_{i\alpha'} \int_I T_{ij}^{st} M_{\alpha'} D_s dS
 \end{aligned}$$

in which, all the integrals are integrable and can be evaluated by means of numerical integration.

Similar equation for unbounded static problems has been presented by Beer and Watson(1989). However, the formulation proposed by Watson(1979) did not include the integral

$$\int_I T_{ij}^{st} M_a \cdot (D_s - 1) dS$$

This omission has, as expected, significant consequence for the accuracy of the analysis, since the contributions of this integral are of greatest numerical size to the strictly diagonal block.

5.4 INTEGRATION OVER INFINITE BOUNDARY ELEMENTS

5.4.1 Non-singular Static Integrals

To develop an order adaptive integration rule for the numerical integration of non-singular static integrals over infinite elements, an extensive series of numerical tests has been performed by considering the analogous integral

$$\int_I \frac{D_s}{r^2} dS$$

For an arbitrary source, the integral is computed numerically using a sequence of Gauss-Legendre formula of order n, where n=2~11. This integral can also be evaluated analytically in the radial direction although numerical integration has to be used in the circumferential direction(see Appendix 5.1). Once these computations have been done for the whole core region S_F ,

the relative error contours can be drawn, as shown in Figure 5.11. These test results indicate that the criterion for selecting the optimal number of integration point with respect to the infinite(radial) direction is as follows:

allowable error $\leq 10^{-2}$

$$N_{req} = \text{INTEGER} \left[4 \cdot \left(\frac{L}{D_{min}} \right)^{1/2} + 1 \right] \geq 4 \quad (5.22)$$

allowable error $\leq 10^{-3}$

$$N_{req} = \text{INTEGER} \left[6 \cdot \left(\frac{L}{D_{min}} \right)^{1/2} + 1 \right] \geq 5 \quad (5.23)$$

where D_{min} is the minimum distance between the infinite boundary element being integrated and the source point; L is the length of the interface between finite and infinite boundary elements. However, an integration order equal to three is sufficient in the circumferential direction. As an example, with a uniform discretization scheme of the core region, the smallest value of D_{min} is $L/2$. Consequently, the maximum required integration point in the infinite direction are six and nine, respectively, for maximum allowable errors of 10^{-2} and 10^{-3} .

5.4.2 Non-singular Oscillatory Integrals

Evaluations of integrals with oscillatory integrands over unbounded domains are beset with difficulties. Since the fundamental solutions and decay function used in the dynamic analysis contain complex exponential terms, the integrand consists of positive and negative quantities. Gauss-Legendre quadrature is clearly inadequate for such problems because of the large number of sampling points required and, consequently, excessive computational time. In the present study, integrals over infinite boundary elements were computed in a piecewise

manner between successive zeros of the integrand, as described earlier. For this purpose, the spatial integration was carried out over six-noded curvilinear patches, as shown in Figure 5.12. Consequently, the value of oscillatory integral over an infinite element can be expressed as a series:

$$\begin{aligned}
 I &= I_0 - I_1 + I_2 - I_3 \dots\dots\dots \\
 &= \sum_{j=0}^{\infty} (-1)^j \cdot I_j
 \end{aligned}
 \tag{5.24}$$

in which, I_j represents the absolute value of j th patch. The characteristic of this series is that all the terms are positive and slowly decrease in numerical value as j increases.

For illustration purpose, the analogous integral

$$\int T_{ij} D_d dS
 \tag{5.25}$$

over an infinite element is considered. It should be noted that the integrands are complex-valued numbers. As mentioned earlier, for each component of $T_{ij} D_d$, the zeros of the real part and the imaginary part are at different positions. For the sake of brevity, the example presented here is limited to the real part of $T_{13} D_d$. The integrals over an individual sub-element are alternating positive and negative, as illustrated in Table 5.2. Numerical studies revealed that by normal means the sum of more than 1000 terms is needed to obtain a convergent result, accurate to within 0.1% (Figure 5.13). The upper and the lower bounds are the envelopes of the sum of the infinite series. Clearly, this approach is impractical.

An efficient and accurate integration scheme based on the Euler transformation (Bromwich, 1908) has been used in the present study to accelerate this process. According to this

transformation, the infinite series, Equation (5.24), can be written formally

$$\begin{aligned}
 I &= I_0 - I_1 + I_2 \dots\dots\dots \\
 &= \frac{1}{2} I_0 - \frac{1}{4} \Delta I_0 + \frac{1}{8} \Delta^2 I_0 \dots\dots + \frac{(-1)^{p+1}}{2^p} \Delta^{p-1} I_0
 \end{aligned}
 \tag{5.26}$$

where

$$\Delta I_j = I_{j+1} - I_j
 \tag{5.27}$$

$$\Delta^{L+1} I_j = \Delta^L I_{j+1} - \Delta^L I_j
 \tag{5.28}$$

In order to illustrate the merit of the Euler transformation, the integral, Equation(5.25), is reconsidered. It should be noted that, in order to improve the accuracy of this method, it is not necessary to begin the Euler transformation with the first term. When the transformation starts from the third term, the sums obtained are given in Table 5.2. This example emphasizes that highly accurate results can be achieved, with dramatically reduced computational effort, by integration over only five patches, using this method. The difference between the result of the Euler transformation and a thousand terms of the original series, Equation(5.24), is approximately 0.1%.

5.4.3 Singular Integrals

Singular integrals over infinite elements can be computed by subdividing the integration domain into a singular finite region and an infinite non-singular region. The former can be carried out by means of the sub-division and transformation method, while the latter can be computed by the method described above.

An important feature to point out in the discretized boundary element formulation is that, as shown by Beer and Watson(1989), the integral

$$\int_I T_{ij}^{st} dS$$

over an infinite boundary element is unbounded. This difficulty has been solved semi-analytically in this thesis by exploiting the anti-symmetry of the traction kernel over the complete semi-infinite surface, rather than considering individual infinite elements. As shown in Figure 5.14, the principal idea is to zone the far-field into two regions, S_A and S_B , defined by a circle of radius δ centred at the current source point. It is essential that S_A contains S_F . Each infinite element is then divided into a finite subelement and an infinite region; the union of the latter is S_B . Integrals over each finite subelement can then be computed without special difficulty, while the geometrical symmetry of S_B enables us to carry out the integration analytically with respect to polar coordinates(See Appendix 5.2). After some rather lengthy manipulations, it is found that only the diagonal terms of the solutions, a 3x3 matrix, are different from zero. The non-zero elements of this matrix(Q_{ij}) are as follows:

$$Q_{11}=Q_{22}=\frac{(y_3-x_3) \cdot (4\nu-5)}{8\delta(1-\nu)}$$

$$Q_{33}=\frac{-1 \cdot (y_3-x_3)^3 - 3\delta^2(y_3-x_3) \cdot (1-2\nu)}{12 \cdot \delta^3(1-\nu)} \quad (5.29)$$

Clearly these values are bounded and for surface foundations they are identically zero.

5.5 ILLUSTRATIVE NUMERICAL EXAMPLES

5.5.1 Displacements Due To Uniformly Distributed Load

The applicability of the infinite static boundary element is verified by calculating the vertical displacements at the smooth surface of an elastic halfspace due to a uniformly distributed vertical load p acting on a square area ($2a \times 2a$). Analytical solutions for points beneath the foundation have been given by Giroud (1968).

Three approaches have been used to analyze this problem:

- 1) Analysis based on the assumption of "relaxed" boundary (for example, Mohammadi and Karabalis, 1990), which neglects the contributions of the free surface and the horizontal displacements at the soil-foundation interface;
- 2) The conventional boundary element analysis, using a truncated mesh of size $12a \times 12a$; and
- 3) The infinite boundary element analysis, using single rings of finite boundary elements and infinite boundary elements, respectively, to model the free surface of the halfspace.

Preliminary numerical studies of this particular problem reveal that the computed values are practically insensitive to the number of elements for the discretization of the foundation. In the present study the foundation is discretized by 2×2 finite boundary elements. Results of these three sets of studies are given in Table 5.3.

Excellent agreement with analytical solutions are achieved by using infinite boundary elements at very low computational cost. Smaller displacements (by comparison with analytical solutions) are predicted by analyses using a truncated mesh and the relaxed boundary. The reason is that, in these two approaches, additional constraints have been imposed on the boundary of the mesh and the interface between the soil and

foundation, respectively.

Of particular interest is that the three sets of numerical results for incompressible medium are identical with the analytical solution. This is because, for this particular case, integrals over the free surface are zero and no shear stresses exist on the soil-foundation interface. Thus the truncation of the mesh introduces no error to the results. Consequently, for surface foundation problems, the contribution of the free surface of the elastic halfspace can be neglected for incompressible material. However, as the material becomes more compressible the error of numerical results increases, for both studies of the relaxed boundary and the truncated mesh. This observation suggests that analyses based on mesh truncation or relaxed boundary should be used only for problems when the material is incompressible or nearly so.

5.5.2 Vertical Static Stiffnesses Of Square Foundations

The calculation of static stiffnesses of rigid foundations forms an essential step in the analysis of machine foundations. However, analytical solutions to three dimensional problems are limited to the circular foundation resting on a smooth halfspace, Poulos and Davis(1974). Approximate solutions for smooth rectangular foundations have been presented in the literature. Gorbunov-Possadov and Serebrjanyi(1961) compute static stiffnesses of rectangular foundations by using a double power series to approximate the distribution of traction along the soil-foundation interface. Goodier and Hodge(1958) present upper and lower bounds for the vertical stiffness of rigid square foundations. The lower bound is equivalent to the well-known "equivalent circle approximation". Analytical solutions for perfectly welded foundations are not available in the literature.

In the present study, the truncated discretization scheme and the infinite boundary element, respectively, are used for evaluating the vertical stiffness of a 2Bx2B square foundation. The Poisson's ratio of the soil is 0.25. Smooth soil-foundation contact is assumed.

The effect of the size of finite boundary element mesh in both approaches was considered by using the same discretization scheme for the foundation and increasing the mesh-foundation ratio M_r :

$$\frac{\text{(The dimension of the mesh)}}{\text{(The dimension of the foundation)}}$$

As shown in Figure 5.15, it is apparent that the mesh-foundation ratio has negligible influence on the infinite element analysis. However, this study reveals the very slow rate of convergence of the truncated mesh approach. In the truncated meshes studied, the increase of mesh size does not reduce the significant difference between results of these two approaches. This observation suggests that special care must be exercised in interpreting the results of convergence studies.

Figure 5.16 shows the variation of the computed stiffnesses with the number of elements, $N_f \times N_f$, used for the discretization of soil-foundation interface. For smaller values of N_f , the interface discretization has significant effects on both approaches using finite boundary elements and infinite elements. The main reason is that rigid foundation problems have a solution with singularities in the traction field and, consequently, the usual shape functions are not able to describe the sharp variation of traction in the solution. However, Figure 5.16 reveals that numerical values computed with at least 6x6 elements are reasonably accurate.

The values computed by the infinite element analysis using $N_f = 8$ are presented in Figure 5.17. Excellent agreement with the above mentioned solutions are obtained. This example clearly demonstrates the merit of infinite elements since finer interface discretization is possible (few elements are needed to model the free surface).

5.5.3 Vertical Dynamic Stiffnesses Of Square Foundations

The vertical stiffnesses of rigid square surface foundations (of dimensions $2B$) resting on an elastic halfspace were determined to illustrate the applicability of the infinite element formulation. Perfect bond between the foundation and the soil is assumed. The contact area was uniformly discretized with square elements with dimensions less than $1/4$ Rayleigh wavelengths (a minimum of 8×8 elements). Single rings of finite boundary elements and infinite elements were used to model the near field and far field, respectively. The minimum number of degrees of freedom in these analyses is 1443. Symmetry conditions were taken into account to save computational time, and a Poisson's ratio of $1/3$ was used throughout.

The computed impedance functions are referred to the centre of the foundation and can be written as:

$$K_v = GB(k_v + ia_0 c_v) \quad (5.30)$$

in which, k_v and c_v are the dimensionless stiffness and damping coefficients, respectively, of the impedance functions. Figure 5.18 and 5.19, respectively, depict the variation of stiffness coefficients and damping coefficients with respect to a_0 . The numerical results obtained by Dominguez and Roesset (1978) and by Mita and Luco (1989b) are also indicated. The former is based on the full-space fundamental solutions and a truncated

model. Because halfspace Green's functions were used in the latter study, no free surface discretization was needed but considerable calculation was necessary to compute the Green's functions since they are not in closed form. Both studies employed a simple discretization scheme based on assumed constant field variables over each element. For these frequency problems the agreement between their results and those obtained here is good. In general, the stiffness coefficient of the present study are closer to those obtained by Mita and Luco (less than 5%) than to those obtained by Dominguez and Roesset. For $a_0 \geq 1$, larger discrepancies exist between the damping coefficient of Dominguez and Roesset and those of Mita and Luco, which are close to the results of the present study.

An illustrative example of the spatial variation of the vertical displacements outside the immediate vicinity of the foundation for a dimensionless frequency of 3.0 is given in Figure 5.20. The continuity of the magnitudes and phase of the displacement between the finite and infinite domains is evident.

5.6 CONCLUSIONS

This chapter describes a novel boundary element solution of the response of machine foundations using infinite boundary elements to describe the far-field displacement behaviour outside the immediate vicinity of the loaded area, coupled with the full-space fundamental solution for harmonic point loading. Based on analytical solutions for halfspace problems, the static decay functions have been presented in this chapter. A novel mapping technique is then developed to transform the infinite element onto a unit square. An order adaptive integration criterion was also developed in order to obtain accurate numerical results with minimum cost. The dynamic

decay function assumed in the analysis is based on Rayleigh wave attenuation away from the centre of the foundation. Integrals over the infinite boundary elements are computed between successive zeros of the integrand and an Euler transformation has been used to accelerate this slowly convergent procedure.

Because of its simplicity, the infinite element has great potential advantages in analyzing unbounded problems by the boundary element method. In particular, two-dimensional infinite elements are capable of modelling the unbounded surface of three dimensional problems. In this study, the near field can be modelled by finite boundary elements surrounding by a single ring of infinite elements. Because the displacement behaviour of far field was described by the nodal values of finite boundary elements, no additional degrees-of-freedom are introduced to model the infinite region of the halfspace problem. Consequently, the use of infinite elements makes it more feasible to analyze high frequency problems since small size quadratic elements are needed to discretize the core region only.

Illustrative results for square foundations have been presented to demonstrate that the infinite element described here is capable of producing accurate and efficient boundary element solutions for the response of machine foundations.

Appendix 5.0: Derivation of The Discretized Boundary Element Formulation

The discretized boundary element formulation involving infinite boundary elements is given as follows:

$$\begin{aligned}
 C_{ij}u_i = & \sum_{M'} \sum_{\alpha=1}^8 t_{i\alpha} \int_F G_{ij} N_{\alpha} dS + \sum_{M^*} \sum_{\alpha=1}^8 t_{i\alpha} \int_F G_{ij} N_{\alpha} dS - \sum_{M'} \sum_{\alpha=1}^8 u_{i\alpha} \int_F T_{ij} N_{\alpha} dS \\
 & - \sum_{M^*} \sum_{\alpha'} u_{i\alpha'} \int_F T_{ij} N_{\alpha} dS - \sum_{M^*} u_{i\alpha^*} \int_F T_{ij} N_{\alpha^*} dS - \sum_{M'} \sum_{\alpha=1}^3 u_{i\alpha} \int_I T_{ij} M_{\alpha} D_{\alpha} dS \\
 & - \sum_{M^*} \sum_{\alpha'} u_{i\alpha'} \int_I T_{ij} M_{\alpha} D_{\alpha} dS - \sum_{M^*} u_{i\alpha^*} \int_I T_{ij} M_{\alpha^*} D_{\alpha^*} dS \quad (A5.0-1)
 \end{aligned}$$

in which, F and I refer to finite and infinite regions, respectively; the superscripted prime and asterisk denote non-singular and singular quantities. It should be noted that integrals involving the displacement fundamental solution over the infinite boundary elements have been discarded since, as described earlier, these are identically zero.

Because node α^* of each strongly singular element corresponds to the source point, i.e., $u_{i\alpha^*} = u_i$, the discretized boundary integral equations can be written as

$$\begin{aligned}
 & \{C_{ij} + \sum_{M^*} \int_F T_{ij} N_{\alpha^*} dS + \sum_{M^*} \int_I T_{ij} M_{\alpha^*} D_{\alpha^*} dS\} u_i \\
 = & \sum_{M'} \sum_{\alpha=1}^8 t_{i\alpha} \int_F G_{ij} N_{\alpha} dS + \sum_{M^*} \sum_{\alpha=1}^8 t_{i\alpha} \int_F G_{ij} N_{\alpha} dS - \sum_{M'} \sum_{\alpha=1}^8 u_{i\alpha} \int_F T_{ij} N_{\alpha} dS \\
 & - \sum_{M^*} \sum_{\alpha'} u_{i\alpha'} \int_F T_{ij} N_{\alpha} dS - \sum_{M'} \sum_{\alpha=1}^3 u_{i\alpha} \int_I T_{ij} M_{\alpha} D_{\alpha} dS \\
 & - \sum_{M^*} \sum_{\alpha'} u_{i\alpha'} \int_I T_{ij} M_{\alpha} D_{\alpha} dS \quad (A5.0-2)
 \end{aligned}$$

The strictly diagonal block, the left hand side of Equation (A5.0-2), can be indirectly determined by considering the rigid body motion. Under static conditions, the rigid body translation leads to the result:

$$C_{ij} = -\int T_{ij}^{st} dS$$

$$= -\int_{S_F} T_{ij}^{st} dS - \int_{S_I} T_{ij}^{st} dS - \int_{S_H} T_{ij}^{st} dS \quad (A5.0-3)$$

in which, refer to Figure 5.3, S_F represents the core region, S_I the far-field, and S_H the hemispherical surface with radius approaching infinity. It should be noted that decay functions are not incorporated into equation (A5.0-3) because they are incompatible with the rigid body translation technique.

The discretized form of Equation (A5.0-3) can be written as:

$$C_{ij} = -\sum_{M^*} \sum_{\alpha'} \int_F T_{ij}^{st} N_{\alpha'} dS - \sum_{M^*} \int_F T_{ij}^{st} N_{\alpha} \cdot dS - \sum_{M'} \int_F T_{ij}^{st} dS$$

$$- \sum_{M'} \int_I T_{ij}^{st} dS - \sum_{M^*} \sum_{\alpha'} \int_I T_{ij}^{st} M_{\alpha'} dS - \sum_{M^*} \int_I T_{ij}^{st} M_{\alpha} \cdot dS + \frac{1}{2} \delta_{ij} \quad (A5.0-4)$$

or, by moving strongly singular integrals to the left hand side,

$$C_{ij} + \sum_{M^*} \int_F T_{ij}^{st} N_{\alpha} \cdot dS + \sum_{M^*} \int_I T_{ij}^{st} M_{\alpha} \cdot dS$$

$$= -\sum_{M^*} \sum_{\alpha'} \int_F T_{ij}^{st} N_{\alpha'} dS - \sum_{M'} \int_F T_{ij}^{st} dS$$

$$- \sum_{M'} \int_I T_{ij}^{st} dS - \sum_{M^*} \sum_{\alpha'} \int_I T_{ij}^{st} M_{\alpha'} dS + \frac{1}{2} \delta_{ij} \quad (A5.0-5)$$

in which, $1/2\delta_{ij}$ is the analytical value of the azimuthal integral over S_H .

Because C_{ij} is the same for both static and harmonic loading cases, Equation (A5.0-5) can be introduced into Equation (A5.0-2). After some manipulations the boundary element formulation

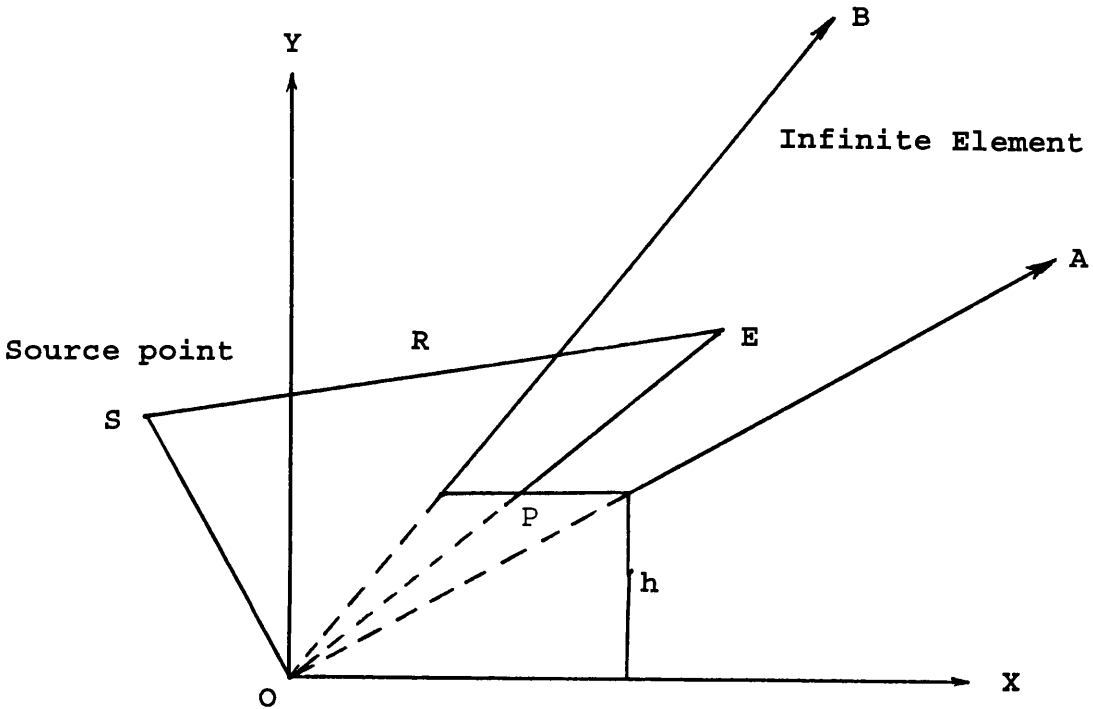
is of the form:

$$\begin{aligned}
 & \left\{ \frac{\delta_{ij}}{2} - \sum_{M'} \int_F T_{ij}^{st} dS - \sum_{M^*} \sum_{\alpha'} \int_F T_{ij}^{st} N_{\alpha'} dS + \sum_{M^*} \int_F (T_{ij} - T_{ij}^{st}) N_{\alpha} dS \right. \\
 & \left. - \sum_{M'} \int_I T_{ij}^{st} dS - \sum_{M^*} \sum_{\alpha'} \int_I T_{ij}^{st} M_{\alpha'} dS + \sum_{M^*} \int_I (T_{ij} D_d - T_{ij}^{st}) M_{\alpha} dS \right\} \cdot u_i \\
 & = \sum_{M'} \sum_{\alpha=1}^8 t_{i\alpha} \int_F G_{ij} N_{\alpha} dS + \sum_{M^*} \sum_{\alpha=1}^8 t_{i\alpha} \int_F G_{ij} N_{\alpha} dS - \sum_{M'} \sum_{\alpha=1}^8 u_{i\alpha} \int_F T_{ij} N_{\alpha} dS \\
 & - \sum_{M^*} \sum_{\alpha'} u_{i\alpha'} \int_F T_{ij} N_{\alpha'} dS - \sum_{M'} \sum_{\alpha=1}^3 u_{i\alpha} \int_I T_{ij} M_{\alpha} D_d dS - \sum_{M^*} \sum_{\alpha'} u_{i\alpha'} \int_I T_{ij} M_{\alpha'} D_d dS
 \end{aligned}
 \tag{A5.0-6}$$

The discretized formulation for static analyses can be obtained by replacing dynamic fundamental solutions and decay function with their static counterparts:

$$\begin{aligned}
 & \left\{ \frac{\delta_{ij}}{2} - \sum_{M'} \int_F T_{ij}^{st} dS - \sum_{M^*} \sum_{\alpha'} \int_F T_{ij}^{st} N_{\alpha'} dS \right. \\
 & \left. - \sum_{M'} \int_I T_{ij}^{st} dS - \sum_{M^*} \sum_{\alpha'} \int_I T_{ij}^{st} M_{\alpha'} dS + \sum_{M^*} \int_I T_{ij}^{st} M_{\alpha} (D_s - 1) dS \right\} \cdot u_i \\
 & = \sum_{M'} \sum_{\alpha=1}^8 t_{i\alpha} \int_F G_{ij}^{st} N_{\alpha} dS + \sum_{M^*} \sum_{\alpha=1}^8 t_{i\alpha} \int_F G_{ij}^{st} N_{\alpha} dS - \sum_{M'} \sum_{\alpha=1}^8 u_{i\alpha} \int_F T_{ij}^{st} N_{\alpha} dS \\
 & - \sum_{M^*} \sum_{\alpha'} u_{i\alpha'} \int_F T_{ij}^{st} N_{\alpha'} dS - \sum_{M'} \sum_{\alpha=1}^3 u_{i\alpha} \int_I T_{ij}^{st} M_{\alpha} D_s dS - \sum_{M^*} \sum_{\alpha'} u_{i\alpha'} \int_I T_{ij}^{st} M_{\alpha'} D_s dS
 \end{aligned}
 \tag{A5.0-7}$$

Appendix 5.1: Semi-Analytical Integration of $\int D_s/R^2 dS$ Over Infinite Elements



Angle AOX = β_1 , Angle BOX = β_2 , Angle SOX = ϕ , Angle EOX = θ ,
 SO = α , OE = r , OP = r_0 .

Figure A5.1-1 Semi-Analytical Integration Over Infinite Element

As shown in Figure A5.1-1, α , ϕ and h are known for each source point S and

$$D_s = \frac{r_0}{r} \quad (5.1)$$

$$r_0 = \frac{h}{\sin\theta} \quad (A5.1-1)$$

According to the Law of cosines, the following relationship can be obtained:

$$R^2 = \alpha^2 + r^2 - 2r\alpha \cos(\phi - \theta) \quad (A5.1-2)$$

The integral can be written as

$$\int \frac{D_s}{R^2} dS = \int \frac{D_s}{R^2} r dr d\theta = \int \frac{h}{R^2 \sin\theta} dr d\theta \quad (A5.1-3)$$

Substituting Equation (A5.1-2) into Equation (A5.1-3) will give

$$I = \int_{\beta_1}^{\beta_2} \frac{h}{\sin\theta} \int_{r_0}^{\infty} \frac{1}{r^2 - 2r\alpha \cos(\phi - \theta) + \alpha^2} dr d\theta \quad (A5.1-4)$$

It should be noted that the integral

$$\int_{r_0}^{\infty} \frac{1}{r^2 - 2r\alpha \cos(\phi - \theta) + \alpha^2} dr$$

can be analytically evaluated. Based on the analytical solution of Integral 109 (page 246), provided by Beyer (1987), this integral becomes

$$\begin{aligned} & \left[\frac{1}{\alpha \sin(\phi - \theta)} \tan^{-1} \frac{2r - 2\alpha \cos(\phi - \theta)}{2\alpha \sin(\phi - \theta)} \right]_{r_0}^{\infty} \\ & = \left[\frac{\pi}{2} - \tan^{-1} \frac{\frac{h}{\sin\theta} - \alpha \cos(\phi - \theta)}{\alpha \sin(\phi - \theta)} \right] \frac{1}{\alpha \sin(\phi - \theta)} \quad (A5.1-5) \end{aligned}$$

Consequently, integral (A5.1-4) can be written as

$$\int_{\beta_1}^{\beta_2} \frac{h}{\alpha \sin \theta \sin(\phi - \theta)} \left[\frac{\pi}{2} - \tan^{-1} \frac{\frac{h}{\sin \theta} - \alpha \cos(\phi - \theta)}{\alpha \sin(\phi - \theta)} \right] d\theta \quad (\text{A5.1.6})$$

which can be computed numerically by Gauss-Legendre quadrature.

Reference:

Beyer, W.H. (1987), *CRC Standard Mathematical Tables*, CRC Press, Inc., Florida.

Appendix 5.2: Integration of $\int T_{ij}^{st} dS$ over S_B

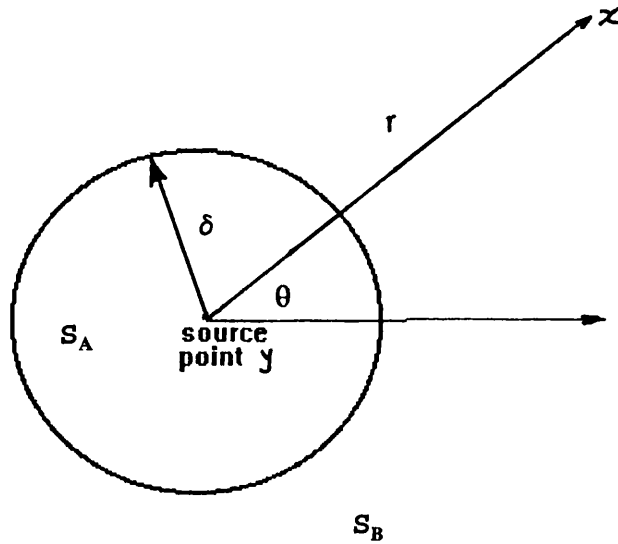


Figure A5.2-1 : The Polar Coordinate System

The traction fundamental solution can be simplified if polar coordinates is used. As shown in Figure A5.2-1, the origin of the coordinate system is the source point. It should be noted that $n_1=n_2=0$ and $n_3=1$ for points on the far-field and

$$r_{,1} = (x_1 - y_1) = r \cos \theta \quad (A5.2-1)$$

$$r_{,2} = (x_2 - y_2) = r \sin \theta \quad (A5.2-2)$$

$$r_{,3} = \frac{\Delta x_3}{r} \quad (A5.2-3)$$

where

$$\Delta x_3 = x_3 - y_3 \quad (A5.2-4)$$

Substituting Equations (A5.2-1) ~ (A5.2-4) into Equation (2.24) will give the following expressions for the traction fundamental solution:

$$T_{11} = \frac{C\Delta x_3}{r^3} \{3\cos^2\theta + (1-2\nu)\} \quad (\text{A5.2-5})$$

$$T_{22} = \frac{C\Delta x_3}{r^3} \{3\sin^2\theta + (1-2\nu)\} \quad (\text{A5.2-6})$$

$$T_{33} = \frac{C\Delta x_3}{r^3} \left\{ \frac{(\Delta x_3)^2}{r^2} + (1-2\nu) \right\} \quad (\text{A5.2-7})$$

$$T_{12} = T_{21} = \frac{3C\Delta x_3 \cos\theta \sin\theta}{r^3} \quad (\text{A5.2-8})$$

$$T_{13} = \frac{C}{r^2} \left\{ 3\cos\theta \frac{(\Delta x_3)^2}{r^2} + (1-2\nu) \cos\theta \right\} \quad (\text{A5.2-9})$$

$$T_{31} = \frac{C}{r^2} \left\{ 3\cos\theta \frac{(\Delta x_3)^2}{r^2} - (1-2\nu) \cos\theta \right\} \quad (\text{A5.2-10})$$

$$T_{23} = \frac{C}{r^2} \left\{ 3\sin\theta \frac{(\Delta x_3)^2}{r^2} + (1-2\nu) \sin\theta \right\} \quad (\text{A5.2-11})$$

$$T_{32} = \frac{C}{r^2} \left\{ 3\sin\theta \frac{(\Delta x_3)^2}{r^2} - (1-2\nu) \sin\theta \right\} \quad (\text{A5.2-12})$$

where

$$C = \frac{-1}{8\pi(1-\nu)} \quad (\text{A5.2-13})$$

For this particular case, the integrals over S_B can be computed by analytical integration:

$$\begin{aligned}
 \int_{s_2} T_{11} dS &= C \Delta x_3 \int_0^{2\pi} [3 \cos^2 \theta + (1-2\nu)] \int_{\delta}^{\infty} \frac{1}{r^3} r dr d\theta \\
 &= \frac{C \Delta x_3}{\delta} \int_0^{2\pi} [3 \cos^2 \theta + (1-2\nu)] d\theta \\
 &= \frac{\Delta x_3 (4\nu - 5)}{8\delta (1-\nu)} \qquad (A5.2-14)
 \end{aligned}$$

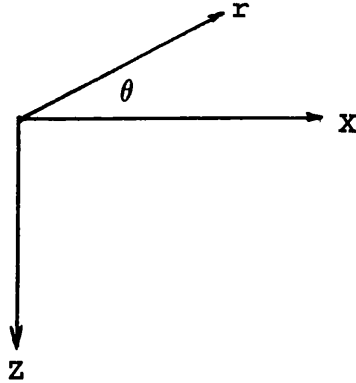
$$\begin{aligned}
 \int_{s_2} T_{22} dS &= C \Delta x_3 \int_0^{2\pi} [3 \sin^2 \theta + (1-2\nu)] \int_{\delta}^{\infty} \frac{1}{r^3} r dr d\theta \\
 &= \frac{C \Delta x_3}{\delta} \int_0^{2\pi} [3 \sin^2 \theta + (1-2\nu)] d\theta \\
 &= \frac{\Delta x_3 (4\nu - 5)}{8\delta (1-\nu)} \qquad (A5.2-15)
 \end{aligned}$$

$$\begin{aligned}
 \int_{s_2} T_{33} dS &= \int_0^{2\pi} \int_{\delta}^{\infty} \left[\frac{C(\Delta x_3)^3}{r^5} + \frac{C \Delta x_3 (1-2\nu)}{r^3} \right] r dr d\theta \\
 &= \int_0^{2\pi} \left[\frac{C(\Delta x_3)^3}{3\delta^3} + \frac{(1-2\nu) C \Delta x_3}{\delta} \right] d\theta \\
 &= \frac{-1 \cdot (\Delta x_3)^3 - 3\delta^2 \Delta x_3 \cdot (1-2\nu)}{12 \cdot \delta^3 (1-\nu)} \qquad (A5.2-16)
 \end{aligned}$$

It is easy to show that the off-diagonal terms are zero, for example,

$$\int_{s_2} T_{12} dS = C \Delta x_3 \int_0^{2\pi} \int_{\delta}^{\infty} \frac{3 \cos \theta \sin \theta}{r^3} r dr d\theta$$
$$= \frac{3 C \Delta x_3}{\delta} \int_0^{2\pi} \cos \theta \sin \theta d\theta = 0 \quad (\text{A5.2-17})$$

TABLE 5.1 : Asymptotic Static Far-Field Behaviour At The Surface Of A Homogeneous Halfspace



LOAD/DISPLACEMENT TYPES (Figure 5.1)	DISPLACEMENTS (in cylindrical coordinates)		
	RADIAL u_r	TANGENTIAL u_θ	VERTICAL u_z
UNIFORM VERTICAL PRESSURE/DISPLACEMENT	$1/r$	-	$1/r$
UNIFORM UNIDIRECTIONAL SHEAR STRESS/DISPLACEMENT	$\cos\theta/r$	$\sin\theta/r$	$\cos\theta/r$
LINEAR TORSIONAL SHEAR STRESS/DISPLACEMENT	-	$1/r^2$	-
LINEAR VERTICAL PRESSURE/DISPLACEMENT	$\cos\theta/r^2$	$\sin\theta/r^2$	$\cos\theta/r^2$

TABLE 5.2 EULER INTEGRATION OF OSCILLATORY FUNCTION

$$\int_{\infty} T_{13} D_d dS$$

$$\sum_{j=1}^{1000} I_j = 0.708220 \cdot 10^{-3}$$

j-th patch	$I_j \times 10^{-3}$	Sum $\times 10^{-3}$	Sum by Euler Transformation $\times 10^{-3}$
1	0.939790	0.939790	
2	-0.440216	0.499574	
3	0.391252	0.890826	0.695199
4	-0.344214	0.546612	0.7069585
5	0.299656	0.846268	0.7072685

Euler Transformation:

$$I = I_0 - I_1 + I_2 \dots \dots \dots$$

$$= \frac{1}{2} I_0 - \frac{1}{4} \Delta I_0 + \frac{1}{8} \Delta^2 I_0 \dots \dots + \frac{(-1)^{p+1}}{2^p} \cdot \Delta^{p-1} I_0$$

where

$$\Delta I_j = I_{j+1} - I_j$$

$$\Delta^{L+1} I_j = \Delta^L I_{j+1} - \Delta^L I_j$$

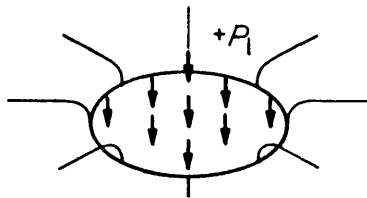
TABLE 5.3 Values of Dimensionless Displacement, G_u/pa

[CORNER]

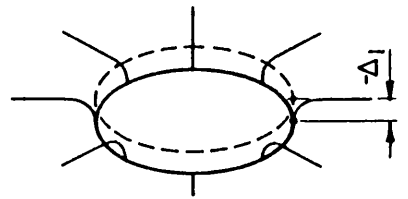
ν	Relaxed Boundary	Finite Boundary Element	Infinite Boundary Element	Analytical solution
0.0	0.4208	0.5147	0.5609	0.5611
0.1	0.4052	0.4729	0.5047	0.5050
0.2	0.3857	0.4292	0.4486	0.4489
0.3	0.3607	0.3831	0.3926	0.3928
0.4	0.3273	0.3340	0.3366	0.3367
0.5	0.2806	0.2806	0.2806	0.2806

[CENTRE]

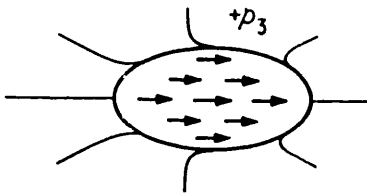
ν	Relaxed Boundary	Finite Boundary Element	Infinite Boundary Element	Analytical solution
0.0	0.8415	1.0298	1.1265	1.1222
0.1	0.8105	0.9471	1.0131	1.0100
0.2	0.7714	0.8598	0.8998	0.8978
0.3	0.7213	0.7672	0.7866	0.7855
0.4	0.6545	0.6684	0.6736	0.6733
0.5	0.5611	0.5611	0.5611	0.5611



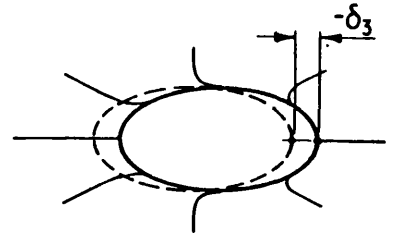
UNIFORM VERTICAL PRESSURE



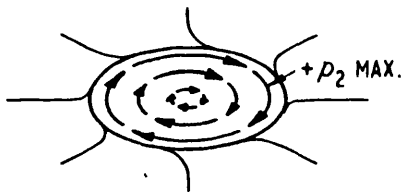
UNIFORM VERTICAL DISPLACEMENT



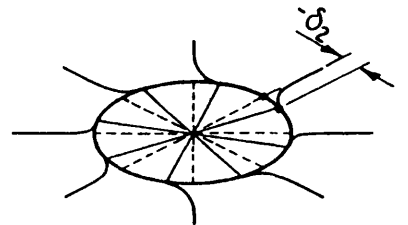
UNIFORM UNIDIRECTIONAL SHEAR STRESS



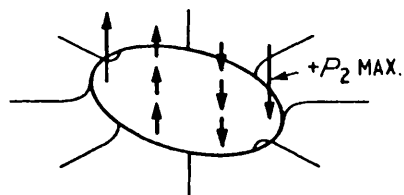
UNIFORM UNIDIRECTIONAL SHEAR DISPLACEMENT



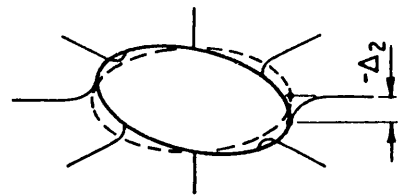
LINEAR TORSIONAL SHEAR STRESS



LINEAR TORSIONAL SHEAR DISPLACEMENT



LINEAR VERTICAL PRESSURE



LINEAR VERTICAL DISPLACEMENT

Figure 5.1 Load/Displacement Types (from Poulos and Davis, 1974)

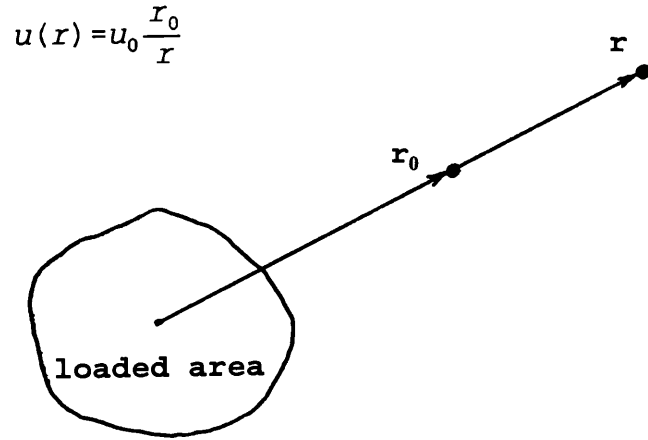


Figure 5.2a: The static decay function

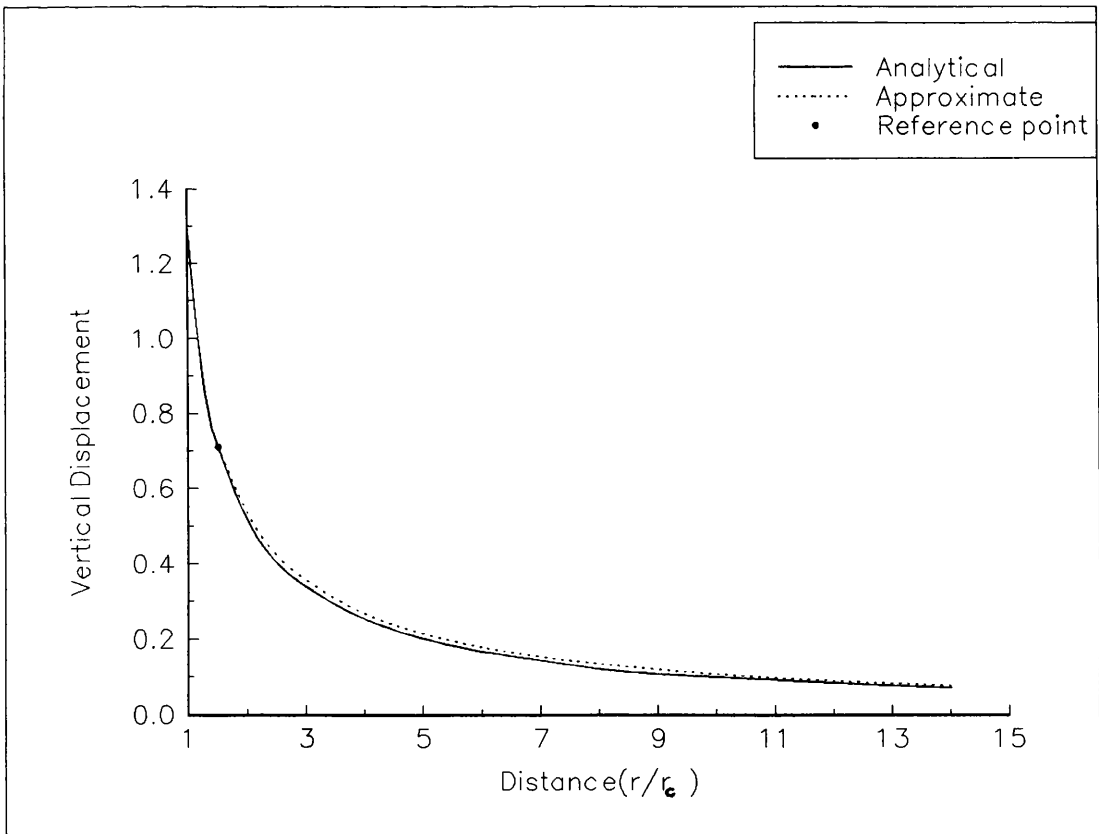


Figure 5.2b: The Far Field Displacement Behaviour

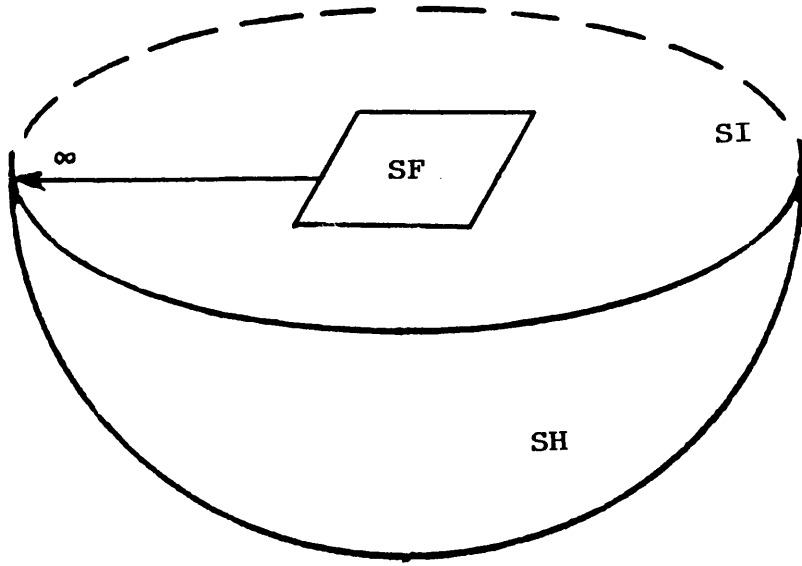


Figure 5.3 The Boundary of The Halfspace Model

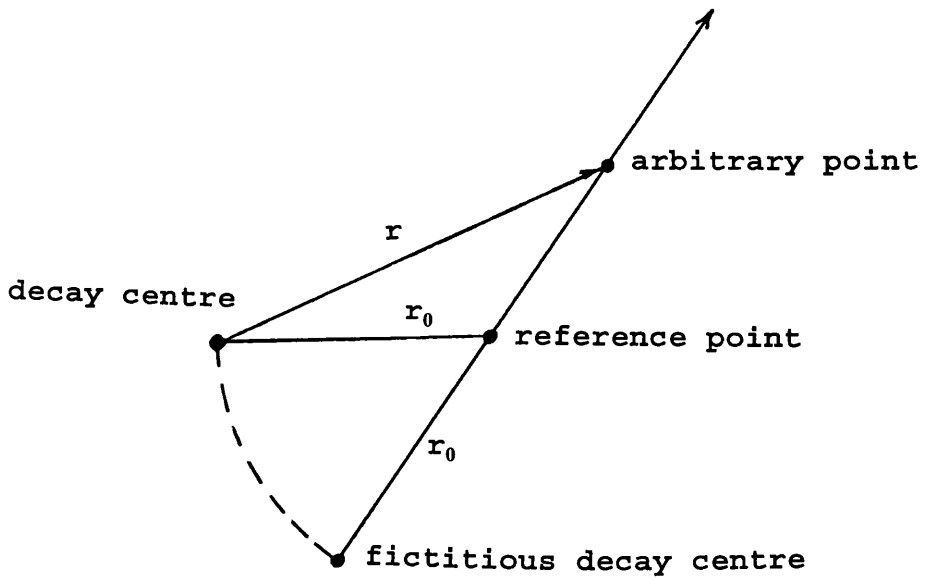


Figure 5.4 Fictitious Decay Centre

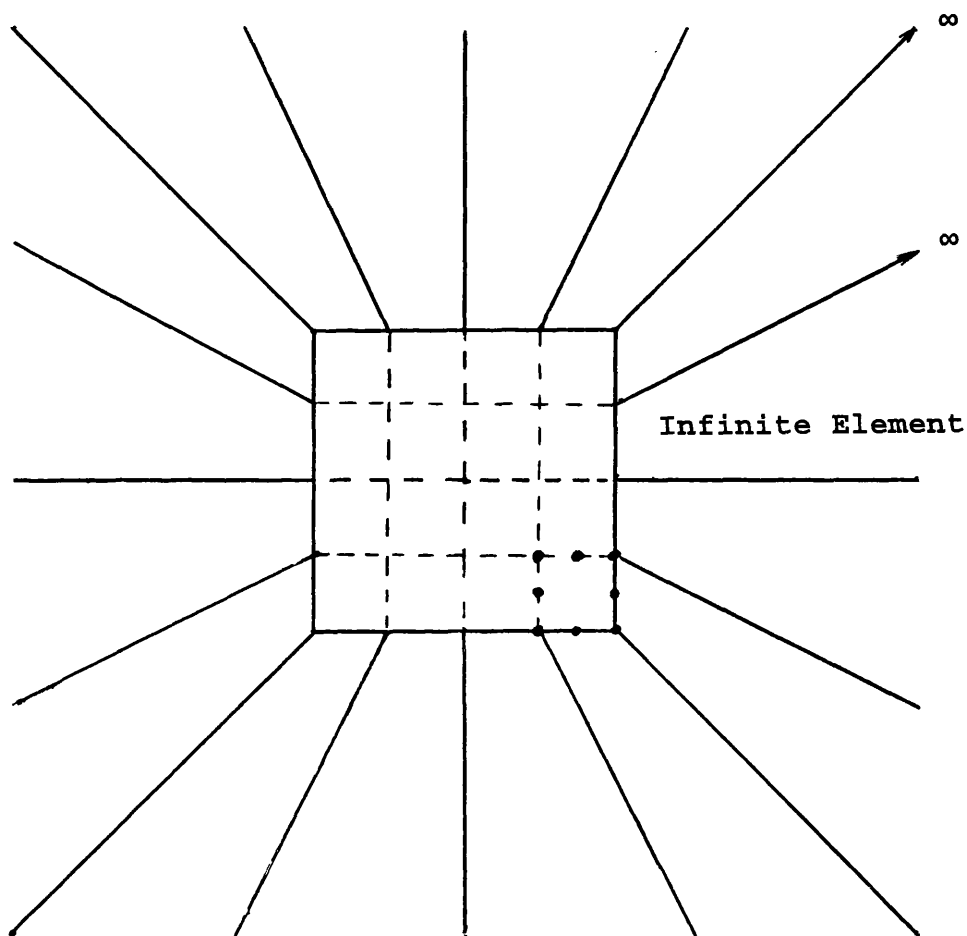


Figure 5.5 The Infinite Boundary Element

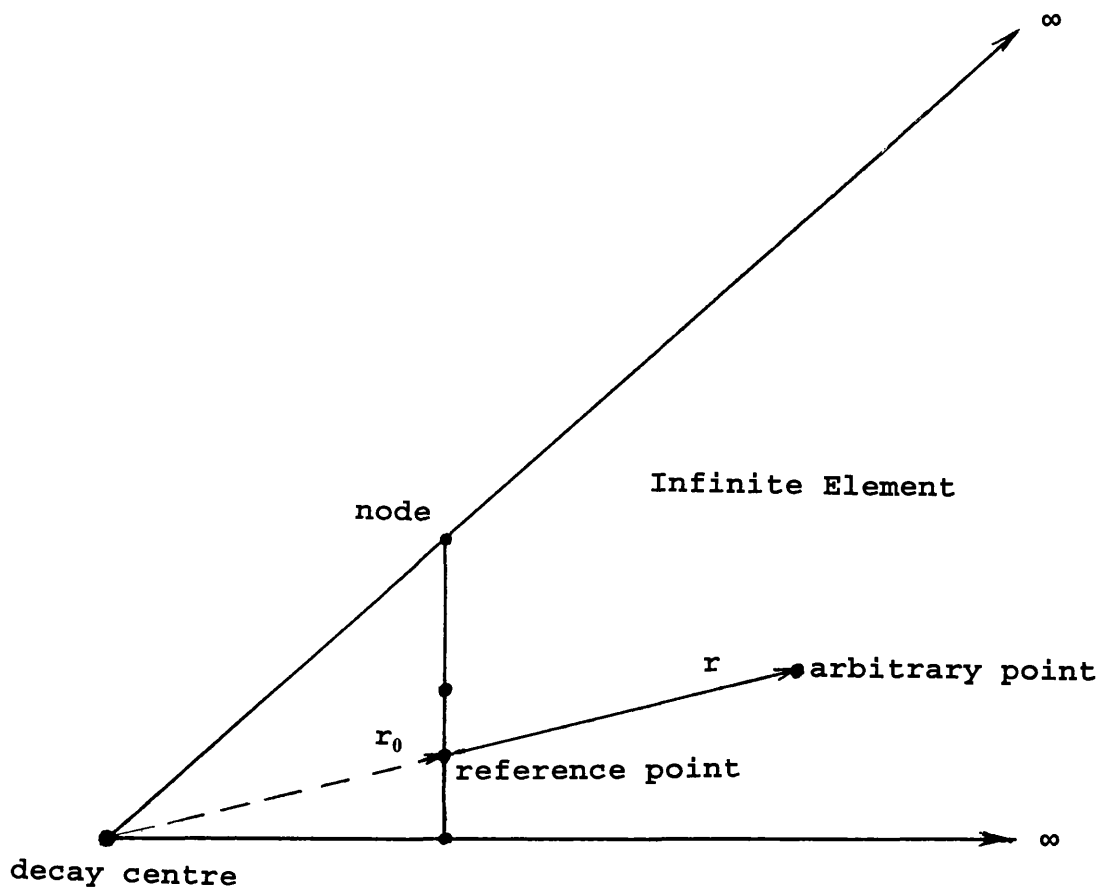
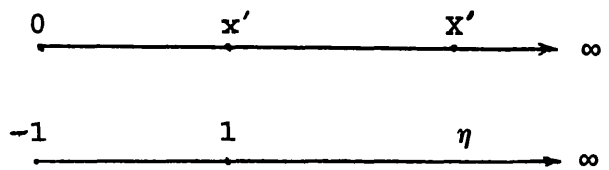
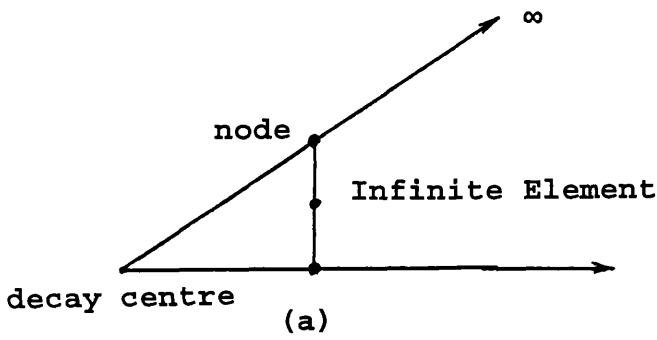


Figure 5.6: Interpolation of displacement over an infinite element



(b) $\eta = \frac{1+\eta}{2} x'$

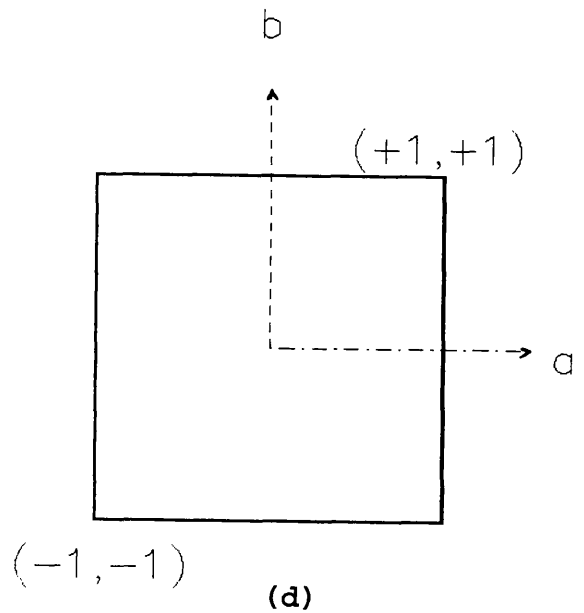
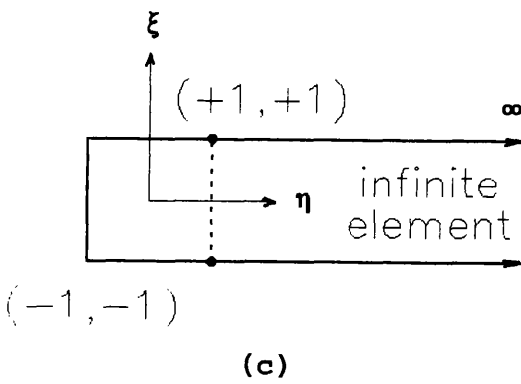


Figure 5.7: Transformation of the infinite element into an unit square

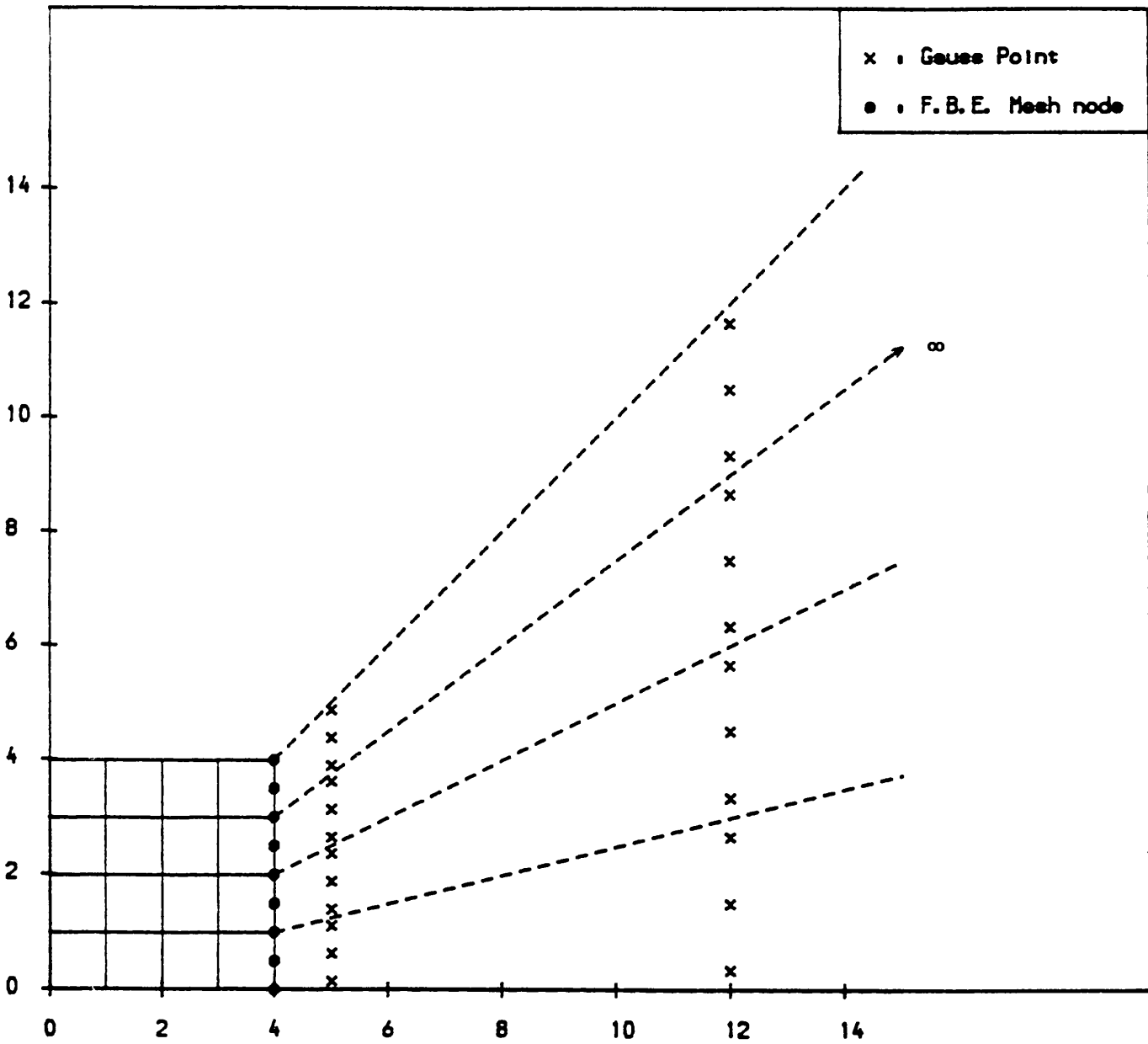


Figure 5.8 Distribution of Gauss Points, 3x3 Integration Rule, The third row of Gauss points are located at 140.

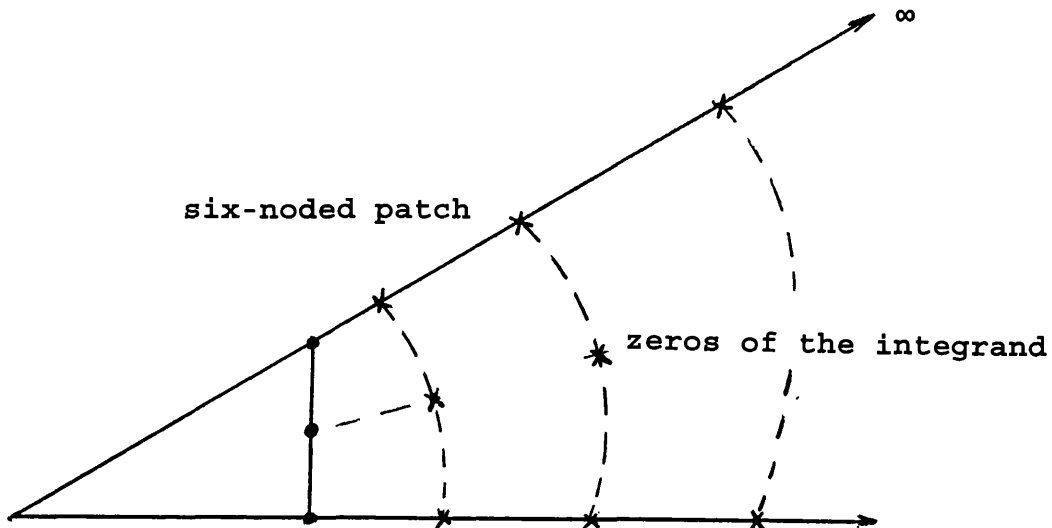


Figure 5.9: Sub-division of infinite elements

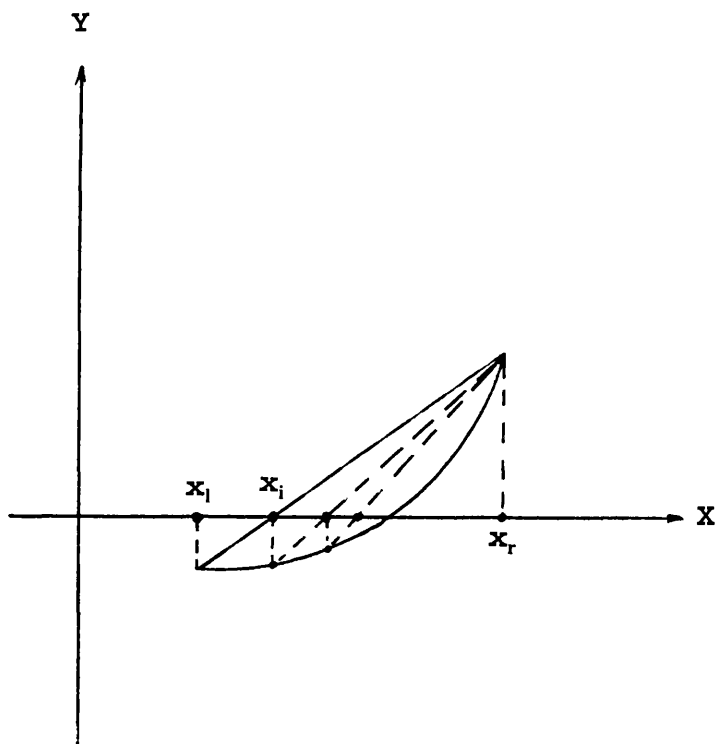


Figure 5.10: Regula Falsi Method

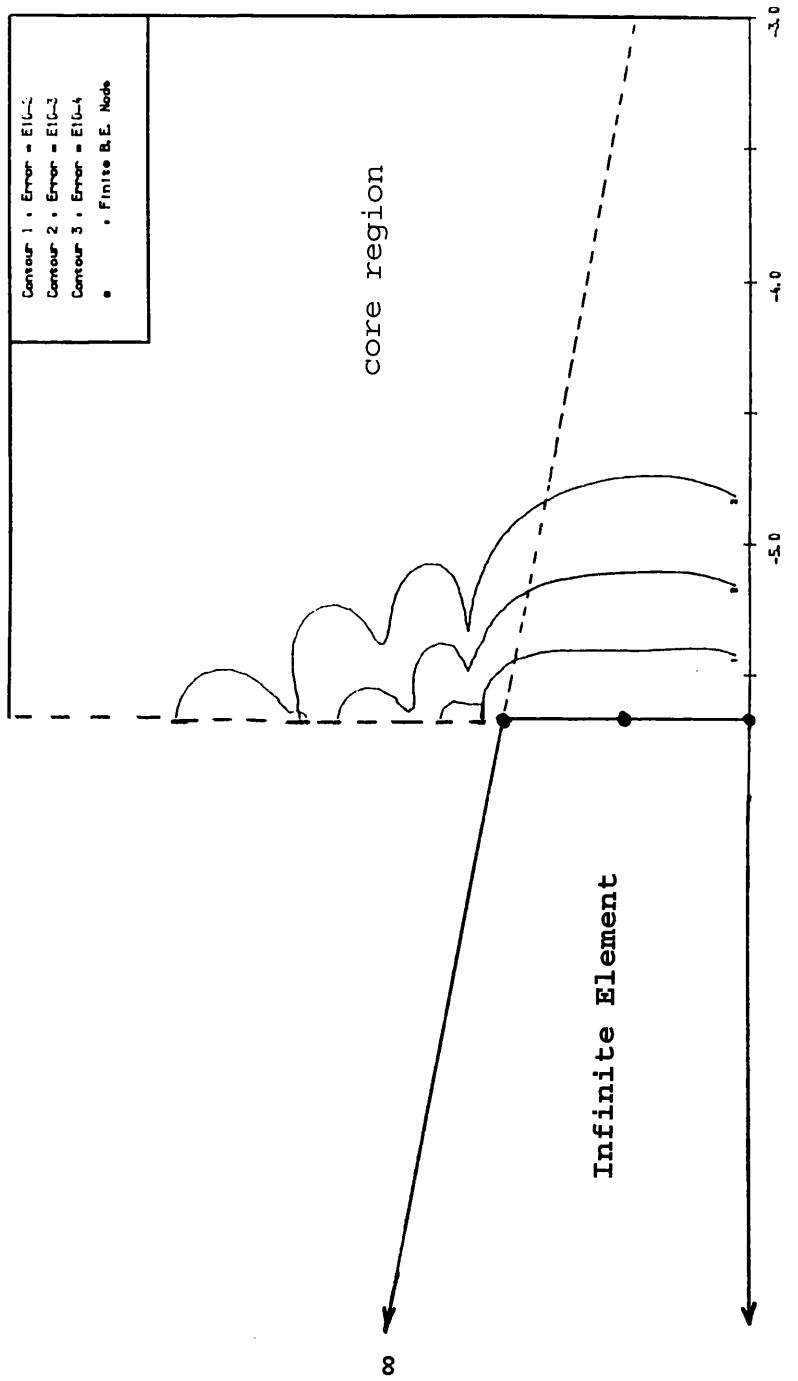


Figure 5.11 Error Contours Of Numerical Integration Over Infinite Elements, 3 and 10 Integration Orders In The Circumferential and Radial Directions, respectively.

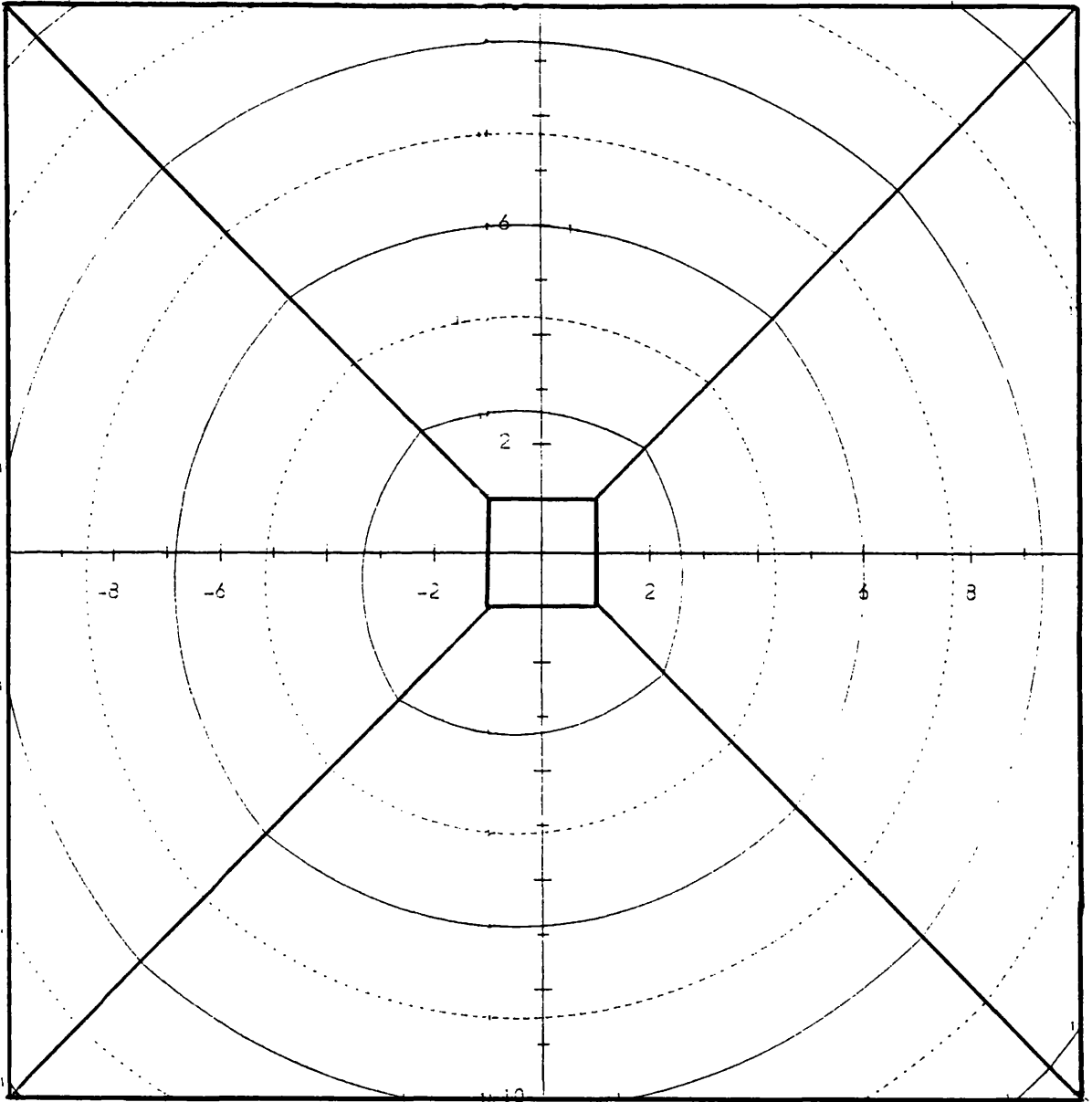


Figure 5.12 Zeros Of Integrands $T_{31}D_d$ and $T_{32}D_d$, $V_s = 141$ m/s,
 Frequency= 70 rad/s, Field Point at $(-1,-1)$, Full Lines:
 Real Part, Broken Lines: Imaginary Part.

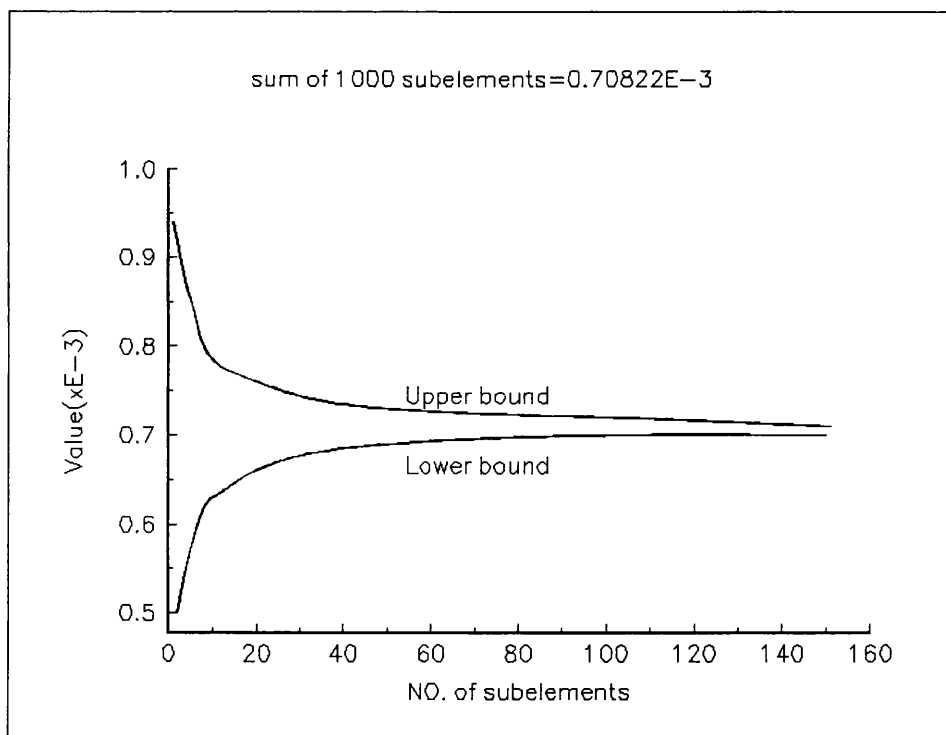
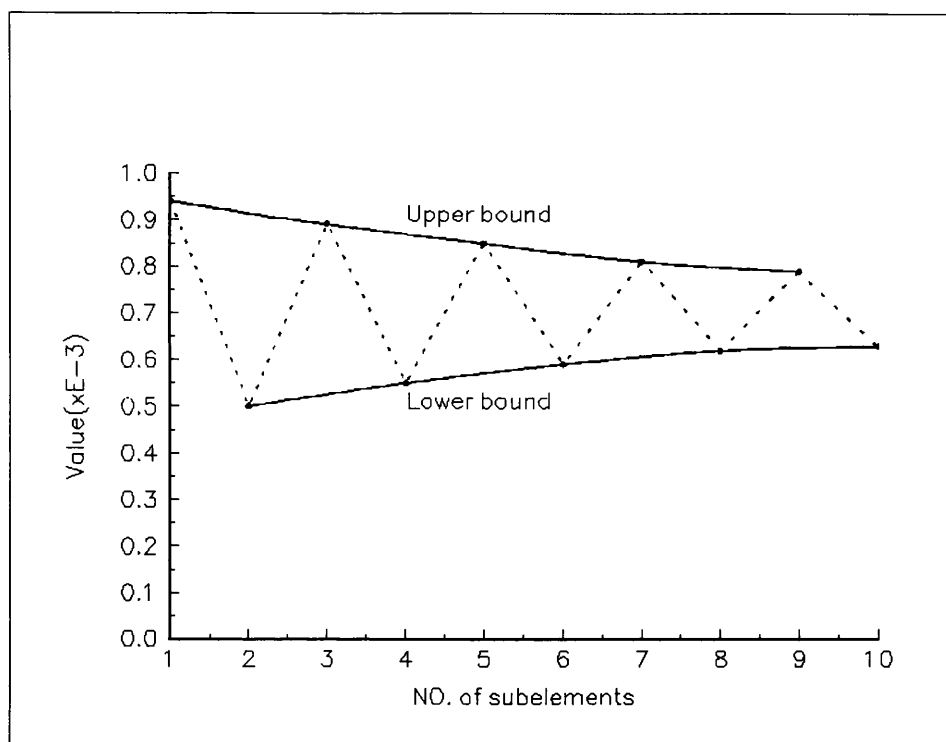


Figure 5.13: Bounds Of Integration Values, $a_0 = 0.5$, Integrand=Real Part of $T_{13}D_d$

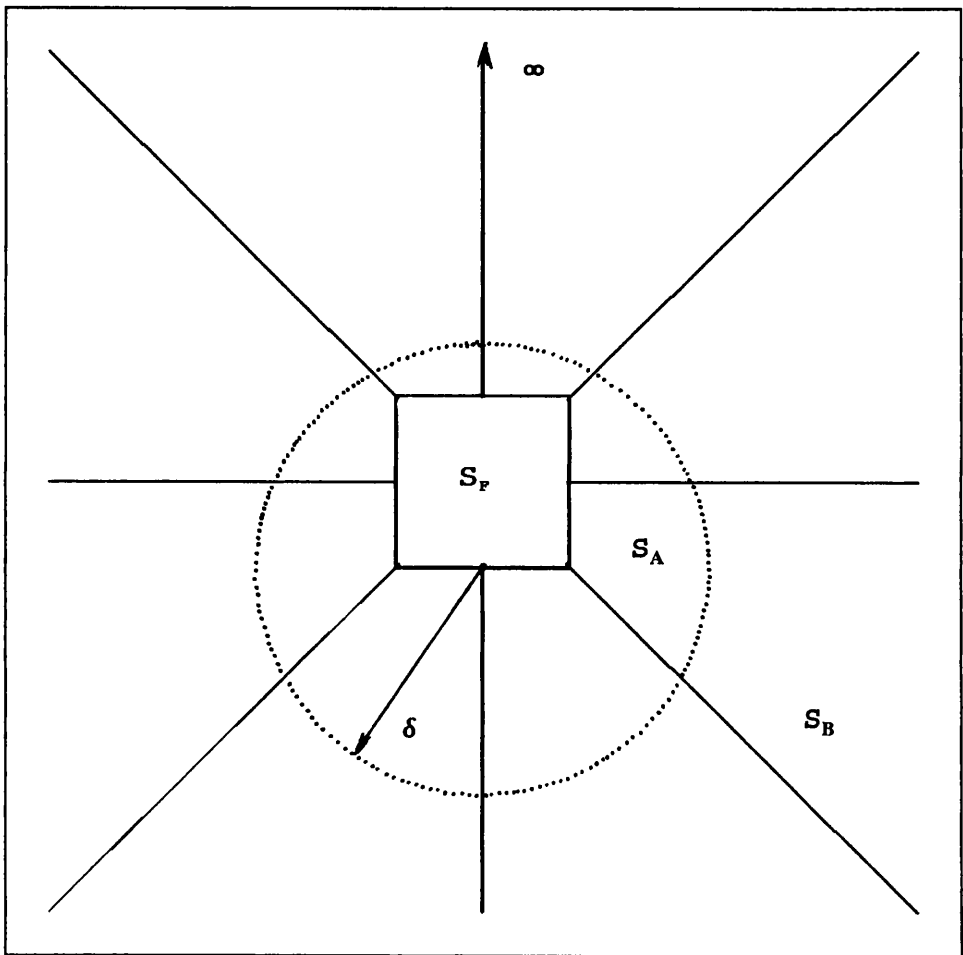


Figure 5.14: Zoning Of The Far Field

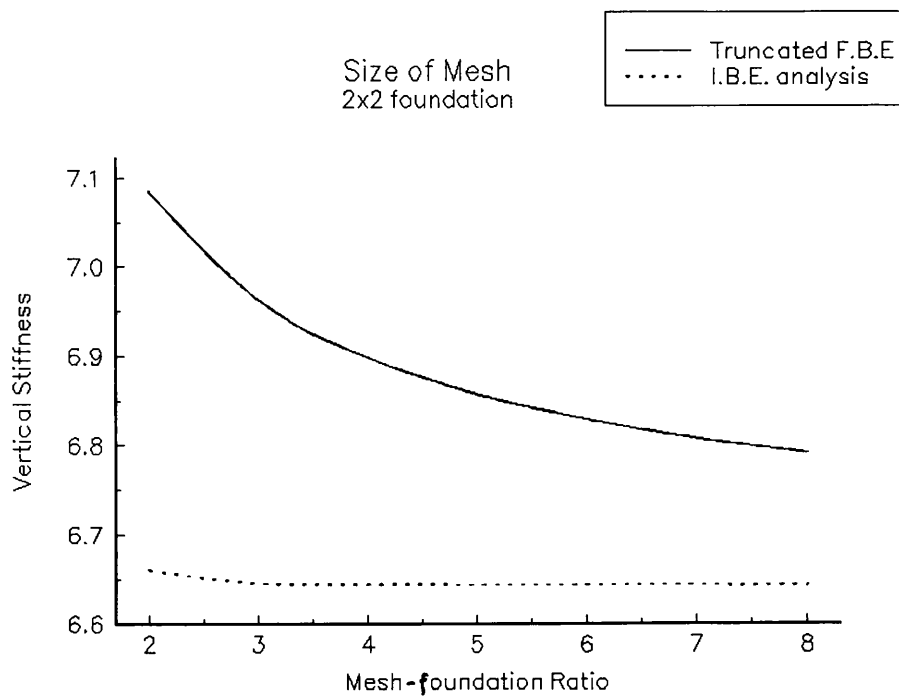


Figure 5.15: Effect of the size of mesh

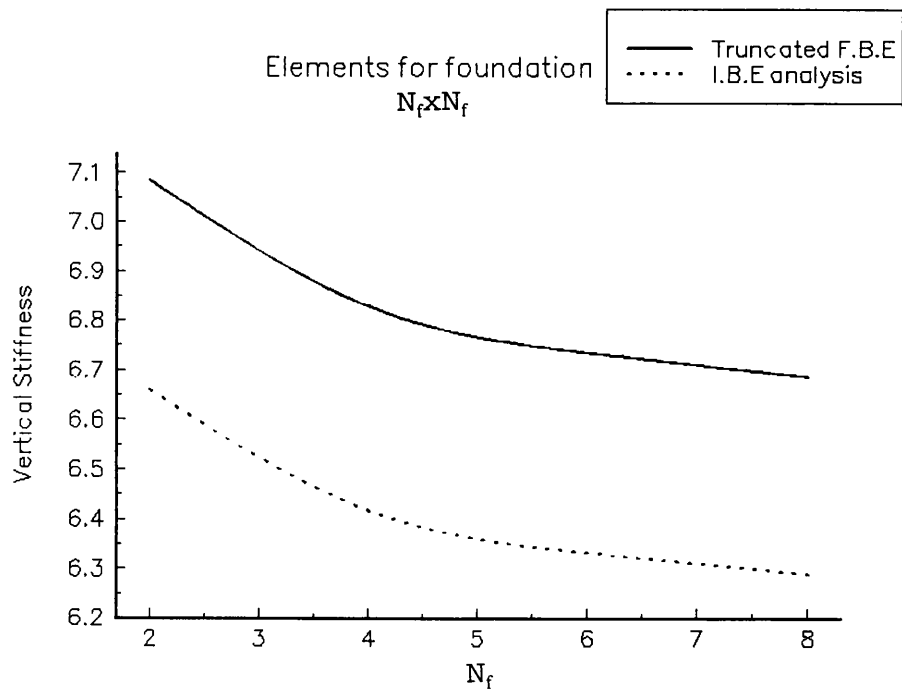


Figure 5.16: Effect of the discretization of foundation

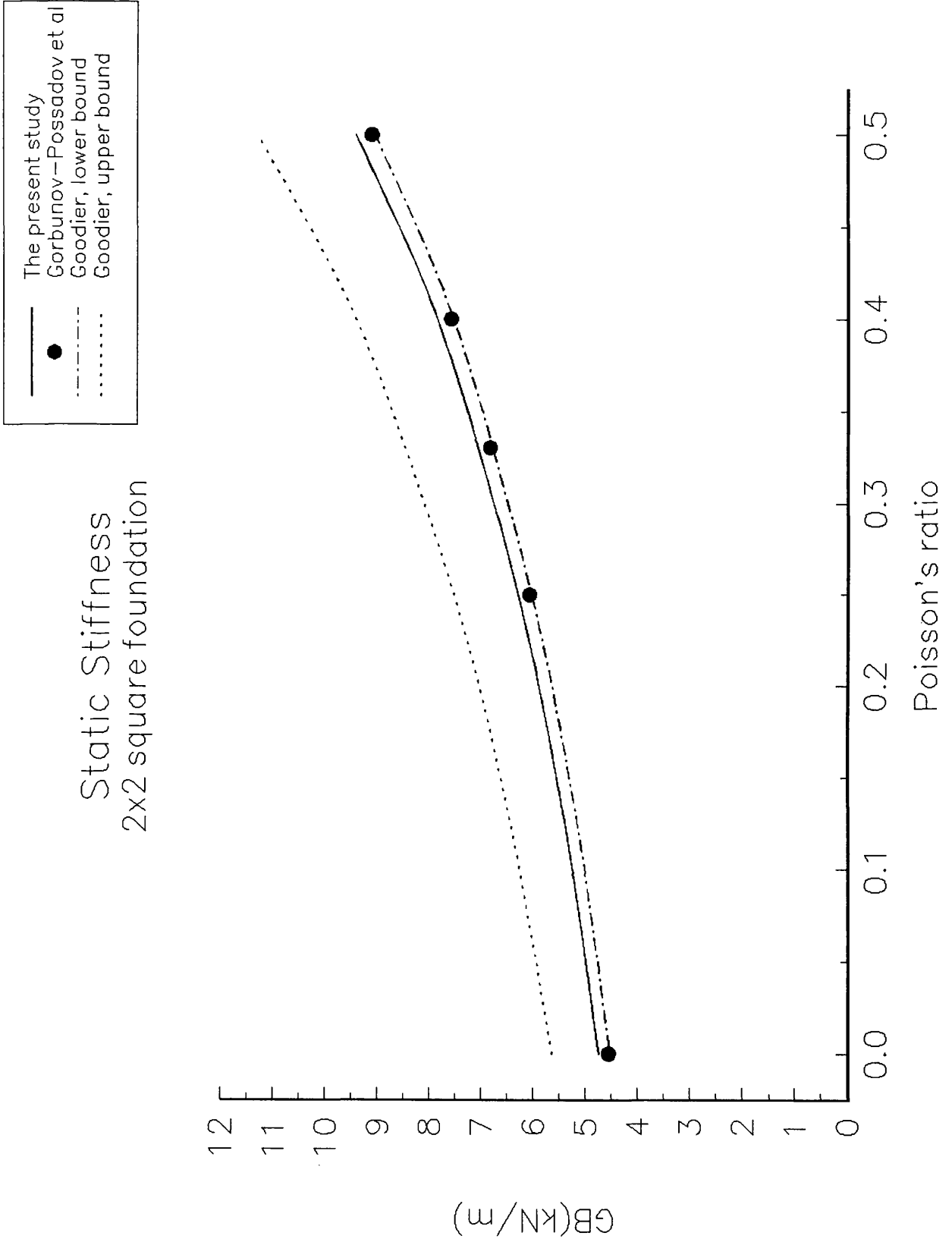


Figure 5.17: Static stiffness of square foundation

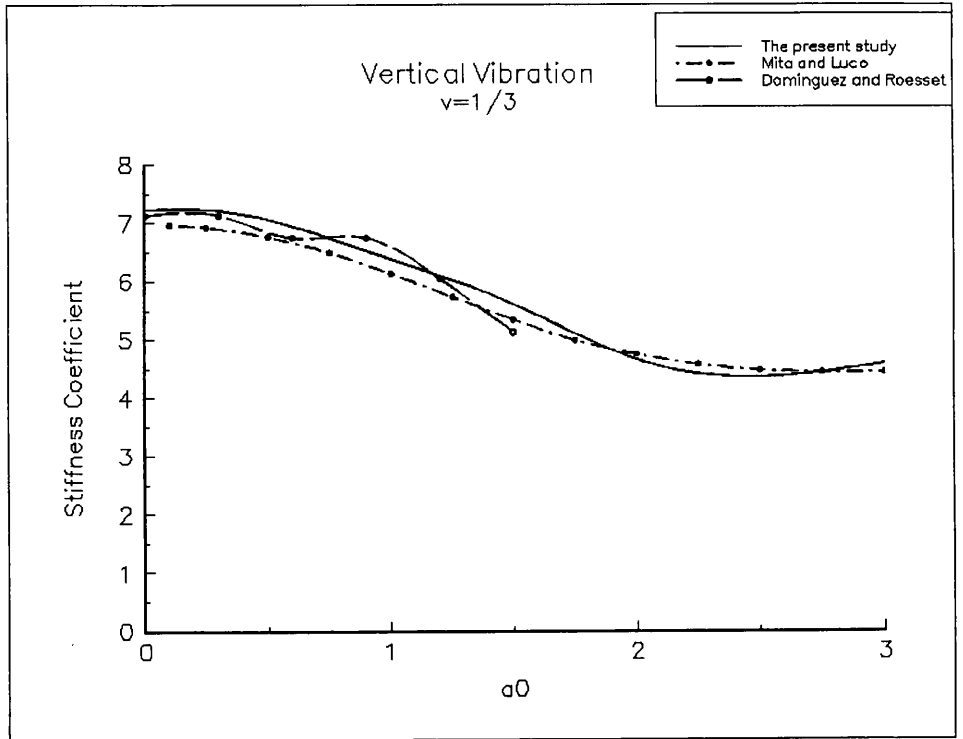


Figure 5.18: The Variation Of K_v With Respect To a_0

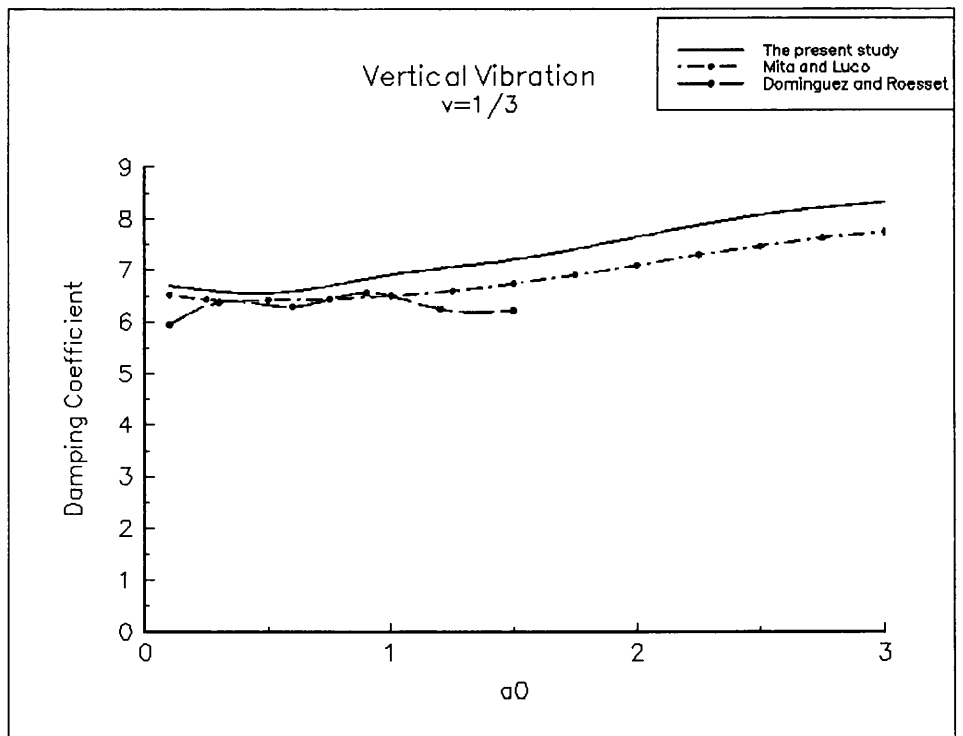


Figure 5.19: The Variation Of C_v With Respect To a_0

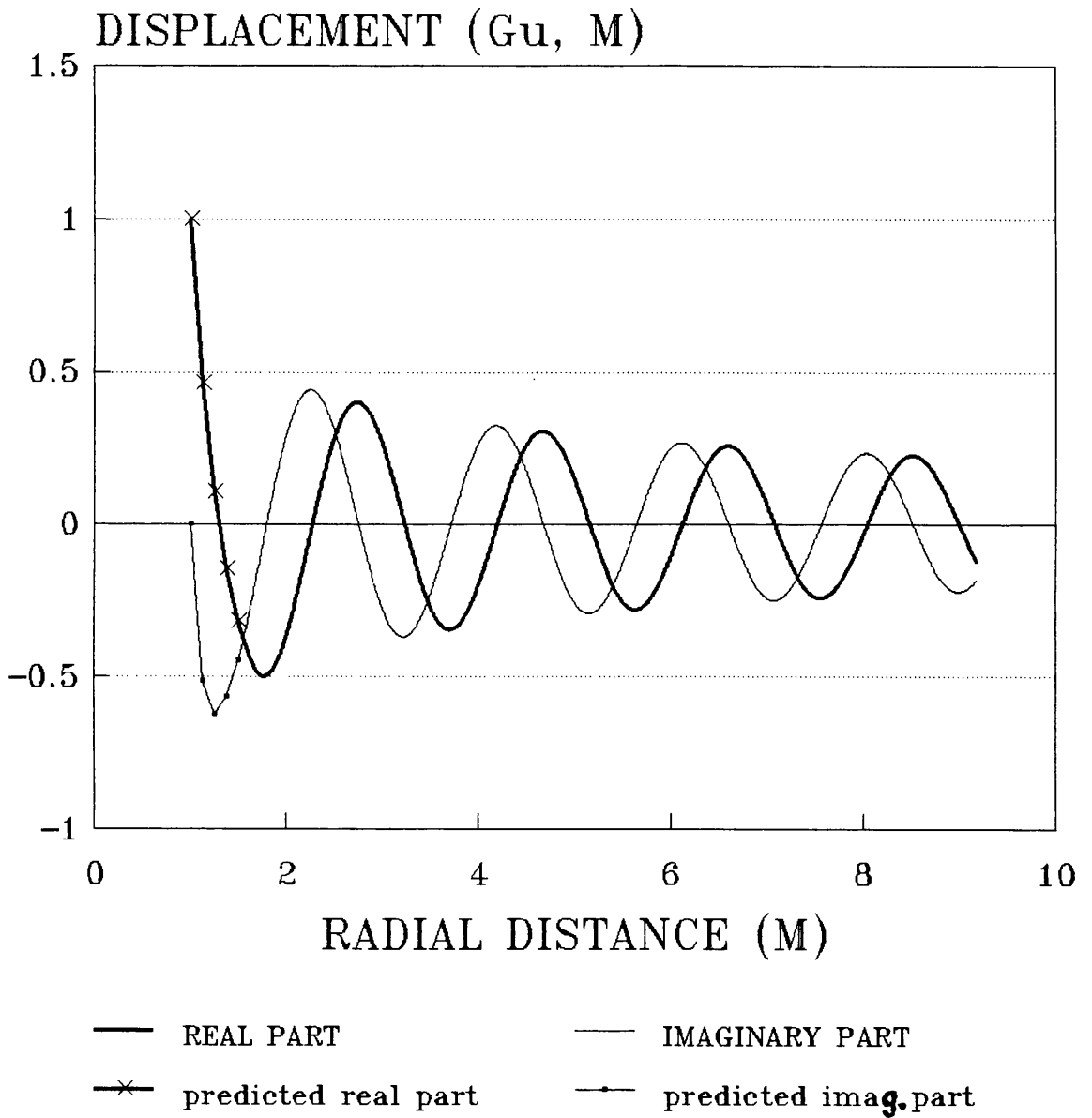


Figure 5.20: Vertical Displacement Fields, $a_0=3$, 12x12 Finite Size Mesh, 8x8 Elements For The Foundation.

CHAPTER 6

NUMERICAL IMPLEMENTATION

6.1 Introduction

The general theory and discretized formulation of the boundary element method for elastodynamics has been presented in previous chapters. The numerical integration techniques and infinite boundary elements proposed are shown to be capable of providing reliable results but, in practice, the merit of boundary element methods can only be fully recognized when they are implemented efficiently. This chapter describes the special purpose FORTRAN program for the steady-state dynamic analysis of three-dimensional rigid rectangular foundations, which was developed for the purposes of this study. This program can analyze problems of flexible foundations as well by prescribing appropriate (traction) boundary conditions at the soil-foundation interface; however, the work in this thesis concentrates on the more difficult rigid foundation case.

Rather than giving explicit programming details of the program (which now contains over 6000 lines of FORTRAN code), some important aspects pertaining to efficient programming techniques in boundary element methods are discussed further. Attention here is focused on the generation of the system matrices, which consumes the major part of the computational effort. In the present study, the prescribed boundary conditions are incorporated during the assembly of the system equations. The advantage of this approach is that the cost of analyses and the required computer storage can be significantly

reduced, which enables the program to analyze larger problems, that is, more degrees of freedom. Furthermore, this scheme provides an effective method to deal with a well-known difficulty in the boundary element analysis, namely, problems with traction discontinuities at corners and edges. The program takes advantage of symmetry conditions, if any, in order to reduce the size of the system equations.

Computational efficiency of computers has been significantly improved by recent developments in computer technology-vectorization and parallelization. Vectorization can greatly increase the speed of program execution (by pipelining instructions), without requiring multiple independent (i.e., parallel) processors (Polychronopoulos, 1988). Since it is more convenient to convert a scalar-series FORTRAN program into vectorized form, attention in this study was given to vectorization. Experience of vectorizing the boundary element program using the IBM 3090-150 Vector Facility is described. In general, speed-up due to vectorization reduces computational times by a factor of about three.

6.2 Structure Of The Program

The numerical implementation of various boundary element analyses has been presented by Banerjee and Butterfield (1981), Brebbia (1980), Manolis (1989), and Becker (1992). The main steps are, in general:

(a) Initialization

This is essentially an input operation.

(b) Discretization

Representation of the geometry and field variables by a finite number of (nodal) values, together with an assumption of spatial interpolation between nodes.

(c) Numerical evaluation of integrals

This leads to the generation of the system equations:

$$[U]\{t\} = [T]\{u\} \quad (6.1)$$

where [U] and [T] contain the coefficients obtained by calculating the integrals involving the fundamental solutions G_{ij} and T_{ij} , respectively. Arrays {t} and {u} represent the nodal tractions and displacements.

(d) Solution of the system matrices

This can be performed by transferring all the unknown nodal values in Equation(6.1) on the left and the known ones to the right, namely,

$$[A]\{X\} = [B]\{Y\} = \{b\} \quad (6.2)$$

where matrix [A] is composed of the columns of [U] and [T] which multiply the unknowns; and, {X} and {Y} represent the unknown and known nodal quantities, respectively. The solution of these sets of simultaneous linear algebraic equations can usually be obtained without special difficulty in boundary element analyses.

(e) Post-processing

This step includes computations of displacements and tractions at each boundary node and, for example, internal results at selected points.

The program developed in the present study does not follow these steps in precisely this way. The major difference occurs in the procedure used to establish the system equations. In practice, the matrix [A] has been formed without the need to generate the system matrix in its entirety. The elements of matrix [B] are also immediately multiplied by the known quantities as they are generated and stored in array {b}. A

simplified flow chart depicting the program structure is given in Figure 6.1. The primary subroutines used in the program, together with their functions are listed in Table 6.1. The general algorithm of the program is directed by a MAIN program and several independent modules and MAIN links these modules during the execution of the program. The character of this modular program makes it possible to facilitate further expansion and development. Many common subroutines have also been developed to perform specialized tasks, such as standard matrix operations and computations of the shape functions, fundamental solutions, and the calculations necessary to compute the minimum distance between a node and an element. In order to obtain highly accurate results, the calculations in this program are carried out in double precision arithmetic.

6.3 Pre-Processing

The relatively simplicity of the input data files (by comparison for example with FEM files) is one of the significant advantages of boundary element methods. The program has been consciously implemented to minimize the size of input data file. As elaborated in Appendix 6.1, the input data of this boundary element program can be divided into the following categories:

(1) Title

The title describes the subject of the analysis and appears on the start of the output.

(2) Dimensionless frequency a_0

(3) Geometrical information related to discretization

The geometrical data which the user must supply the program are as follows (see Appendix 6.1 for full details):

- i) the dimensions of the foundation, i.e., XL, YL, and EMB;
- ii) the discretization of the foundation, i.e., NFX, NFY, and NLAYER; and
- iii) the discretization of the free surface, i.e., NLX, NLY, NEW, SRAT, and JINF.

The program uses quadratic rectangular elements. It should be noted that major changes in the size of two adjacent elements or the use of high aspect ratio elements (greater than four) may result in numerical instability. In general, best results are obtained when element dimensions are gradually increased with distance away from singularities (Yokoyama and Zaita, 1992; and Karamanoglu and Beswick, 1991).

(4) Material properties

The properties of homogeneous soil deposits can be defined by the shear modulus of elasticity, the Poisson's ratio, and the mass density.

(5) Boundary conditions

One of the important steps in the boundary element analysis is the description of the boundary conditions. The prescribed displacements at the centre of the rigid foundation are given by the array DISP. Two types of contact between soil and foundation, namely, the welded contact and the smooth contact, can be considered in the present study and will be discussed further in the next section. Furthermore, the parameter NPART can be used to simulate two extreme cases relating to embedded foundations, i.e., full height sidewall contact foundations and trench foundations (no wall contact).

A subroutine DATGEN has been developed in order to read the input file and detect certain types of data error in the input file. This subroutine automatically establishes the boundary element mesh with non-equal size rectangular elements and, if required, infinite boundary elements (Figure 6.2). Further

more, it generates additional data (see Appendix 6.2) for the three-dimensional analysis of rectangular machine foundations.

It is worth noting that a large amount of data is generated during the execution of a boundary element program. In particular, the system matrix $[A]$, which occupies significant memory, needs to be accessed many times during program execution. In order to save execution time, all data are stored in high-speed in-core memory. This is the simplest and most effective method to manage data, although it is limited by the capacity of the computer being used. For the purposes of this study, this limits the maximum dimensions of the program to 256 boundary elements (or 2500 degrees of freedom). It is of course possible to employ auxiliary memory but this will incur computational cost.

6.4 Boundary Conditions

6.4.1 Contact Condition At Soil-Foundation Interfaces

The boundary conditions needed for the machine foundation problem are zero tractions on the free surface of the halfspace and the contact condition between the soil-foundation interface S_c . Two different (rigorous) contact conditions are considered, namely, perfectly smooth contact and perfectly welded contact. The former condition implies zero shear stresses over the contact area, while the latter restricts the lateral displacements along the interface. In addition, in the literature, so-called "relaxed" boundary are often invoked in which certain degrees of freedom are simply ignored (e.g., Karabalis and Beskos, 1986; and Mohammadi and Karabalis, 1990). These (approximate) analyses result in substantial reductions in complexity and computational costs but at the expense of sacrificing rigour; they do not conform to any real (physical) boundary conditions and are not, in general, considered further

here. Without loss of generality, in the following a rigid embedded foundation subjected to vertical displacement, w_z , is assumed in order to show the nature of contact conditions (Figure 6.3a).

Welded contact

In general, assuming there is no separation and sliding, the displacements $\{u^p\}$ of a point at the welded contact area S_c must satisfy the compatibility requirement:

$$\{u^p\} = [S^T] \{U^F\} \tag{6.3}$$

where

$$\{u^p\} = \{u_x, u_y, u_z\}^T \tag{6.4}$$

$$\{U^F\} = \{\Delta_x, \Delta_y, \Delta_z, \Theta_x, \Theta_y, \Theta_z\}^T \tag{6.5}$$

in which Δ_i are the translational components i at the centre of the foundation and θ_i are the (small) rotational components with respect to the i -axis. The transformation matrix $[S^T]$ is:

$$[S^T] = \begin{bmatrix} 1 & 0 & 0 & 0 & d_3 & -d_2 \\ 0 & 1 & 0 & -d_3 & 0 & d_1 \\ 0 & 0 & 1 & d_2 & -d_1 & 0 \end{bmatrix} \tag{6.6}$$

where

$$d_i = x_{ni} - x_{ci} \tag{6.7}$$

in which, x_{ni} and x_{ci} are the coordinates of the node and the centre of the foundation, respectively.

As shown in Figure 6.3b, if $\{U^F\} = \{0, 0, w_z, 0, 0, 0\}$, the boundary

conditions of any point at the soil-foundation interface can be prescribed as:

$$\begin{aligned} u_x &= 0 \\ u_y &= 0 \\ u_z &= w_z \end{aligned} \tag{6.8}$$

Boundary conditions at the soil-foundation interface resulting from the assumption of welded contact can be rigorously modelled by boundary element methods. However, because it is difficult to deal with these boundary conditions, the application of analytical methods to machine foundations problems with welded contact conditions has received little attention in the literature.

Smooth contact

As shown in Figure 6.3c, since no friction exists in the smooth soil-foundation interface, the boundary conditions at the base mat are

$$\begin{aligned} t_x &= 0 \\ t_y &= 0 \\ u_z &= w_z \end{aligned} \tag{6.9}$$

and, for the sidewalls with outward normal $|n_1|=1$,

$$\begin{aligned} u_x &= 0 \\ t_y &= 0 \\ t_z &= 0 \end{aligned} \tag{6.10}$$

while for the sidewalls with outward normal $|n_2|=1$,

$$\begin{aligned}t_x &= 0 \\ u_y &= 0 \\ t_z &= 0\end{aligned}\tag{6.11}$$

Analytical solutions for the response of surface foundations on smooth halfspaces have been reported in the literature (eg., Arnold, et al, 1955; Pak and Gobert, 1991). Boundary element methods can of course analyze machine foundation problems with smooth soil-foundation interfaces without difficulty.

6.4.2 Difficulties In Modelling The Traction Discontinuity

In general, traction discontinuities occur where the shape of the boundary changes abruptly, or when the boundary conditions change suddenly, or when both of these factors apply. The boundary condition for a smooth embedded foundation (Figure 6.4) is a typical example of such traction discontinuities. It is worth noting that the use of higher order elements in boundary element methods implies continuous function values between two adjacent elements. Consequently, as shown in Figure 6.4b and 6.4c, the tractions at nodes j and k produce anomalous tractions over the traction free element b and the smooth sidewall element g. The difficulty arises in the definition of boundary conditions at nodes j and k, because obviously it is impossible to impose two contradictory boundary conditions at one node. Many practical problems involve corners and edges so this is a common difficulty. Special procedures are needed to deal with the traction discontinuity; otherwise numerical techniques will produce inaccurate results.

Similar difficulties are encountered in a large class of boundary element analyses, for example, potential problems, as described by Banerjee and Butterfield (1981); Becker (1992); Davies (1993); and many others. Often, this problem is treated

by using double nodes (Ayala and Gomez, 1979; Crotty and Wardle, 1985; and Mitra and Ingber, 1993). Using this concept of double nodes, it is then possible to assign different traction values at nodes 3 and 3' (see Figure 6.5); while these two boundary nodes have the same coordinates. In two dimensional problems, the use of double nodes is evidently feasible, although at some computational cost. However, it is more cumbersome to use this technique (multiple nodes) to describe the traction discontinuities in three dimensional analyses.

Several alternative methods have also been reported in the literature to treat this problem. Jaswon and Symm (1977) "round off" corners to obtain a smooth boundary in the analysis of potential problems. Watson (1979) used small elements to model the region in the vicinity around the corner in order to localize the error. Rego Silva, et al (1993), like many others, use discontinuous elements (non-conforming elements) to solve this difficulty. Some techniques (e.g., the use of small elements in the vicinity of corners) must be used with great care since they may be a potential source of numerical instability. For more details, reference is made to Davies (1993).

6.4.3 The Elimination Method

In the present study, the problem of traction discontinuity is circumvented by the apparently novel method of directly imposing the boundary conditions on each boundary element during the assembly of the system equations. This numerical technique is in essence a refinement of the multiple node method but without increasing the number of degrees of freedom. Without loss of generality, a simple example is given to demonstrate the basis of the technique. As shown in Figure 6.6a, linear elements A and B are utilized to model a welded contact area and the free surface, respectively. Since the

nature of boundary conditions changes at the interface between two elements, a double node 2' is introduced to circumvent the problem of traction discontinuity (Figure 6.6b). However, nodes 2 and 2' have the same displacement because the displacement field is continuous across the elements. This implies that the traction discontinuity does not raise any problem in the assembly of [T] matrix. As a consequence, the resulting system equations for this simple case are

$$[U]_{6 \times 8}^* \{t\}_{8 \times 1}^* = [T]_{6 \times 6} \{u\}_{6 \times 1} \quad (6.12)$$

in which,

$$[U]^* = \begin{bmatrix} |U_{11} & U_{12} & U_{13} & U_{14} & U_{15} & U_{16} & U_{17} & U_{18}| \\ |U_{21} & \cdot & \cdot & \cdot & \cdot & \cdot & \cdot & U_{28}| \\ |U_{31} & \cdot & \cdot & \cdot & \cdot & \cdot & \cdot & U_{38}| \\ |U_{41} & \cdot & \cdot & \cdot & \cdot & \cdot & \cdot & U_{48}| \\ |U_{51} & \cdot & \cdot & \cdot & \cdot & \cdot & \cdot & U_{58}| \\ |U_{61} & U_{62} & U_{63} & U_{64} & U_{65} & U_{66} & U_{67} & U_{68}| \end{bmatrix} \quad (6.13)$$

$$[T] = \begin{bmatrix} |T_{11} & T_{12} & T_{13} & T_{14} & T_{15} & T_{16}| \\ |T_{21} & \cdot & \cdot & \cdot & \cdot & T_{26}| \\ |T_{31} & \cdot & \cdot & \cdot & \cdot & T_{36}| \\ |T_{41} & \cdot & \cdot & \cdot & \cdot & T_{46}| \\ |T_{51} & \cdot & \cdot & \cdot & \cdot & T_{56}| \\ |T_{61} & T_{62} & T_{63} & T_{64} & T_{65} & T_{66}| \end{bmatrix} \quad (6.14)$$

$$\{t\}^* = \{t_{1x}, t_{1y}, t_{2x}, t_{2y}, t_{3x}, t_{3y}, t_{2'x}, t_{2'y}\}^T \quad (6.15)$$

and

$$\{u\} = \{u_{1x}, u_{1y}, u_{2x}, u_{2y}, u_{3x}, u_{3y}\}^T \quad (6.16)$$

The extra two columns in $[U]^*$ matrix, i.e., columns 7 and 8, arise from the tractions defined at the double node 2'.

It should be noted that if the tractions at the fictitious double node 2' are known, then after some mathematical manipulation, the system equations can be written as follows:

$$[U]^* \{t\}^* = [U] \{t\} + \{M\} = [T] \{u\} \quad (6.17)$$

where

$$[U] = \begin{bmatrix} U_{11} & U_{12} & U_{13} & U_{14} & U_{15} & U_{16} \\ U_{21} & \cdot & \cdot & \cdot & \cdot & U_{26} \\ U_{31} & \cdot & \cdot & \cdot & \cdot & U_{36} \\ U_{41} & \cdot & \cdot & \cdot & \cdot & U_{46} \\ U_{51} & \cdot & \cdot & \cdot & \cdot & U_{56} \\ U_{61} & U_{62} & U_{63} & U_{64} & U_{65} & U_{66} \end{bmatrix} \quad (6.18)$$

$$\{t\} = \{t_{1x}, t_{1y}, t_{2x}, t_{2y}, t_{3x}, t_{3y}\}^T \quad (6.19)$$

and the constant array is

$$\{M\} = \{m_1, m_2, m_3, m_4, m_5, m_6\}^T \quad (6.20)$$

in which

$$m_k = U_{k7} \times t_{2'/x} + U_{k8} \times t_{2'/y} \quad (6.21)$$

In this simple example, $\{M\}$ can be eliminated since quantities t_{2x} and t_{2y} are zero. Furthermore, in most analyses with double nodes, the array $\{M\}$ can be computed without special difficulty. On the other hand, it is significant to note that elements of the 3rd and 4th columns in $[U]$ are associated with

node 2 and element A only, i.e., they are independent of element B. In addition, the contributions of node 1 to matrix [U], i.e., U_{11} and U_{12} , are of no importance because $U_{11} \times t_{1x}$ and $U_{12} \times t_{1y}$ are zero (traction free element). This implies that zeros can be imposed in the columns in [U] matrix, which corresponds to the zero traction components. Consequently, the resulting system matrices [U] and {t} will be:

$$[U] = \begin{bmatrix} 0 & 0 & U_{13} & U_{14} & U_{15} & U_{16} \\ 0 & 0 & . & . & . & U_{26} \\ 0 & 0 & . & . & . & U_{36} \\ 0 & 0 & . & . & . & U_{46} \\ 0 & 0 & . & . & . & U_{56} \\ 0 & 0 & U_{63} & U_{64} & U_{65} & U_{66} \end{bmatrix} \quad (6.22)$$

and

$$\{t\} = \{0., 0., t_{2x}, t_{2y}, t_{3x}, t_{3y}\}^T \quad (6.23)$$

In view of the above discussion, these characteristics suggest that the principal ideas of the double node method can be achieved simply by omitting the integrals involving the displacement fundamental solution

$$\int G_{ij} t_k dS \quad (6.24)$$

over particular boundary elements, over which tractions in the k-direction are zero. Clearly, incorporation of prescribed boundary conditions into the assembly of the system equations simulates the traction discontinuities in a rigorous manner. The application of the method to three-dimensional boundary element analyses is a relatively straightforward operation. Although in the case described above, one set of tractions at

the double node is zero, this is by no means a limitation of the method, which is quite general. In addition, where one traction set is zero, the omission of some integrals during the collocation procedure can save significant CPU time.

6.4.4 Treatment of Corners and Edges

The method described above is applicable to problems of corners and edges. For reasons of simplicity, as shown in Figure 6.7, a two-dimensional rigid embedded foundation subjected to vertical displacement w_z is considered. Linear elements are used in this example. Smooth contact is assumed at the soil-foundation interface. The boundary conditions at the basemat, i.e., element C, are:

$$\begin{aligned} u_z &= w_z \\ t_x &= 0 \end{aligned} \tag{6.25}$$

while at the sidewalls:

$$\begin{aligned} u_x &= 0 \\ t_z &= 0 \end{aligned} \tag{6.26}$$

It should be noted that the boundary conditions of boundary element analyses are prescribed at boundary nodes. The treatment of nodes 2 and 5 has been described in the previous sub-section. However, the proper prescription of boundary conditions at the corners, i.e., nodes 3 and 4, creates difficulties in the analysis. Clearly, any attempt to impose single-valued traction boundary conditions at the corners will result in erroneous solutions, although the displacement boundary conditions are, of course, unique. Consequently, the appropriate boundary conditions at nodes 3 and 4 are:

$$\begin{aligned} u_x &= 0 \\ u_z &= w_z \end{aligned} \tag{6.27}$$

The number of degrees of freedom for this particular problem is twelve. It should be noted that the (ix2-1) and (ix2)-th columns of the system matrices represent the contribution of node i in the X and Z directions, respectively. For example, the contribution of element B, which contains nodes 2 and 3, will be assembled into the 3~6-th columns of the system matrices. However, zeros can be imposed on the 4 and 6-th columns in [U] matrix, since $t_z=0$ over element B. Consequently, contributions of element B to the [U] matrix can be written as:

$$[U]_{12 \times 12}^B = \begin{bmatrix} 0 & 0 & U_{13} & 0 & U_{15} & 0 & 0 & 0 & 0 & 0 & 0 & 0 \\ 0 & 0 & . & 0 & . & 0 & 0 & 0 & 0 & 0 & 0 & 0 \\ 0 & 0 & . & 0 & . & 0 & 0 & 0 & 0 & 0 & 0 & 0 \\ 0 & 0 & . & 0 & . & 0 & 0 & 0 & 0 & 0 & 0 & 0 \\ . & . & . & . & . & . & . & . & . & . & . & . \\ 0 & 0 & U_{j3} & 0 & U_{j5} & 0 & 0 & 0 & 0 & 0 & 0 & 0 \end{bmatrix} \tag{6.28}$$

Similarly, the contributions of element C and D, respectively, are:

$$[U]_{12 \times 12}^C = \begin{bmatrix} 0 & 0 & 0 & 0 & 0 & U_{16} & 0 & U_{18} & 0 & 0 & 0 & 0 \\ 0 & 0 & 0 & 0 & 0 & . & 0 & . & 0 & 0 & 0 & 0 \\ 0 & 0 & 0 & 0 & 0 & . & 0 & . & 0 & 0 & 0 & 0 \\ 0 & 0 & 0 & 0 & 0 & . & 0 & . & 0 & 0 & 0 & 0 \\ . & . & . & . & . & . & . & . & . & . & . & . \\ 0 & 0 & 0 & 0 & 0 & U_{j6} & 0 & U_{j8} & 0 & 0 & 0 & 0 \end{bmatrix} \tag{6.29}$$

and

$$[U]_{12 \times 12}^D = \begin{array}{c} | 0 \ 0 \ 0 \ 0 \ 0 \ 0 \ U_{17} \ 0 \ U_{19} \ 0 \ 0 \ 0 | \\ | 0 \ 0 \ 0 \ 0 \ 0 \ . \ 0 \ . \ 0 \ 0 \ 0 \ 0 | \\ | 0 \ 0 \ 0 \ 0 \ 0 \ . \ 0 \ . \ 0 \ 0 \ 0 \ 0 | \\ | 0 \ 0 \ 0 \ 0 \ 0 \ . \ 0 \ . \ 0 \ 0 \ 0 \ 0 | \\ | . \ . \ . \ . \ . \ . \ . \ . \ . \ . \ . \ . | \\ | 0 \ 0 \ 0 \ 0 \ 0 \ 0 \ U_{j7} \ 0 \ U_{j9} \ 0 \ 0 \ 0 | \end{array} \quad (6.30)$$

As described in the previous sub-section, contributions of element A and E to [U] matrix can be neglected. Eventually, the system matrix [U] can be obtained as follows:

$$[U]_{12 \times 12} = [U]_{12 \times 12}^B + [U]_{12 \times 12}^C + [U]_{12 \times 12}^D \quad (6.31)$$

It is significant that all the steps leading to Equation(6.31) are rigorous and satisfy all the specified boundary conditions.

The performance of the method is demonstrated by analyzing a three-dimensional embedded square foundation(of dimensions 2B) subjected to vertical static loads. The base mat was uniformly discretized with 8x8 square elements. Two layers of same size elements were used to discretize the sidewalls. Single rings of finite boundary elements and infinite elements were used to model the free surface of the halfspace. Several embedment depths were considered, and a Poisson's ratio =0.25 was used in the analysis. The effect of embedment on the static stiffness is given in Figure 6.8. It is observed that embedment increases the vertical static stiffness of the foundation. Corresponding results obtained by Mita and Luco (1989b) and Gazetas(1991) are also indicated. The former solved this problem by using a coupled BE-FE method while the latter presented engineering approximations. The numerical results plotted in Figure 6.8 compare favourably with those predicted by Mita and Luco(1989b) and Gazetas(1991).

6.5 Matrix Assembly

6.5.1 Numerical Integration Modules

In order to form the system matrices, it is necessary to evaluate the integrals in the discretized boundary integral equations (Equation 5.20). The structure of the numerical integration module is given in Figure 6.9.

6.5.2 Assembly of System Matrices

The system matrices are constructed sequentially for each source point/nodal point on the boundary. It should be noted that the $3 \times j - 2$, $3 \times j - 1$, and $3 \times j$ -th rows of the system matrices are formed by collocation with respect to node j . Without loss of generality, given a source point j , the contribution of an eight noded element k to the system matrix $[U]$ may be stored in matrix $[u^{jk}]_{3 \times 24}$. In general, it consists of eight 3×3 submatrices, namely,

$$[u^{jk}] = [[a]_1, [a]_2, \dots, [a]_8] \quad (6.32)$$

where submatrix $[a]_n$ contains the coefficients relating to the node with local nodal number n . Based on the source identification number j and the index between local node numbers and global node numbers, these submatrices can be summed and assembled into the appropriate location within the system matrices.

It should be noted that the coefficients of the system matrices $[U]$ and $[T]$ may differ by several orders of magnitude, for practical problems. In order to avoid excessive round-off error, it is important to ensure proper conditioning of the matrices by means of appropriate scaling. In the present study all the elements of the matrix $[U]$ and the vector $\{u\}$ have been scaled by the shear modulus of the soil, G .

Since boundary element analyses generate non-symmetric fully populated matrices (for single zone problems), limitations on computer memory may constrain the use of a large numbers of elements. The frontal solvers (Zienkiewicz and Taylor, 1989) common to many major finite element codes cannot be used to overcome this problem (because they assume symmetry) and in consequence it has been necessary to develop special purpose codes. For each source point j , there are two submatrices, $[U^j]_{3 \times 3n}$ and $[T^j]_{3 \times 3n}$, where n is the number of nodes, obtained by summing the integrals derived from the fundamental solutions G_{ij} and T_{ij} , respectively. Because half of the boundary conditions at each nodal point is known, it is necessary to move the coefficients relating to the unknown values to the left and the known ones to the right, namely,

$$[A^j]_{3 \times 3n} \{x\}_{3n \times 1} = [B^j]_{3 \times 3n} \{y\}_{3n \times 1} = \{b^j\}_{3 \times 1} \quad (6.33)$$

The elements of matrix $[B^j]$ can be immediately multiplied by the known boundary quantities $\{y\}$ as they are generated and, subsequently, stored in the array $\{b^j\}$. This technique obviates the need to store the entire system matrix $[B]$, see Equation (6.2). This procedure permits rapid assembly of the system matrix $[A]$. In addition, as described in the previous section, problems relating to the traction discontinuities can be dealt with sequentially. This procedure provides an important improvement in computational efficiency.

6.5.3 Symmetry

The order of the system matrices can be greatly reduced if there is symmetry of the problem with respect to one or more axes. For homogeneous, isotropic materials, geometric and loading symmetries can be easily incorporated, with significant computational gains.

In general, it is best to take account of symmetry during assembly of the system matrices. This can be accomplished by a condensation process which integrates the contributions of reflected elements and performs the assembly of the matrix [A] of reduced size. For simplicity, the general procedure is illustrated by considering the following matrix equation:

$$[A]_{4 \times 4} \{B\}_{4 \times 1} = \{C\}_{4 \times 1} \quad (6.34)$$

where

$$[A] = \begin{bmatrix} a_{11} & a_{12} & a_{13} & a_{14} \\ a_{21} & a_{22} & a_{23} & a_{24} \\ a_{31} & a_{32} & a_{33} & a_{34} \\ a_{41} & a_{42} & a_{43} & a_{44} \end{bmatrix} \quad (6.35)$$

$$\{B\} = \{b_1, b_2, b_3, b_4\}^T \quad (6.36)$$

and the constant array

$$\{C\} = \{c_1, c_2, c_3, c_4\}^T \quad (6.37)$$

If b_3 is the corresponding symmetrical quantity of b_1 , namely, $b_1 = b_3$, then the following reduced-sized matrices are sufficient for the solution of {B}:

$$[A]^R = \begin{bmatrix} a_{11} + a_{13} & a_{12} & a_{14} \\ a_{21} + a_{23} & a_{22} & a_{24} \\ a_{31} + a_{33} & a_{32} & a_{34} \end{bmatrix} \quad (6.38)$$

$$\{B\}^R = \{b_1, b_2, b_4\}^T \quad (6.39)$$

and

$$\{C^R = \{c_1, c_2, c_3\}^T \quad (6.40)$$

The integrations over boundary elements are still carried out over the entire surface with respect to a source point. However, collocation is only required on the "object" nodes since the field values at the image nodes are known through symmetry. It should be noted that sign changes in some columns of the system matrices may be needed before condensation. This procedure can reduce significantly the CPU time required to compute and solve the system matrices. For machine foundation problems with several hundred degrees of freedom, the "speed-up" due to quadrantal symmetry is approximately four.

6.6 Solution of System Matrix

It is well known that the system matrix [A] is a non-symmetrical fully populated matrix for single-zone problems. In general, the CPU time taken for the solution of this type of matrix is approximately proportional to N_A^3 (Fox, 1964), where N_A is the dimension of [A]. The overall efficiency of boundary element analyses depends to a far lesser degree than FE analyses on the numerical procedure used for the solution of the system matrix. The solver's share of the total CPU-time, especially for problems with many degrees of freedom, has been discussed by many researchers, for example, Brebbia(1989) and Rezayat(1992), among others. In the present study, the system matrices are solved by NAG library subroutines, ie. F04ATF and F04ADF for static analyses and dynamic analyses, respectively. It is worth noting that these subroutines have been written utilising Assembler for maximum speed(Ellersick, 1987). For the analyses described in this thesis, accurate solutions can be achieved with relatively little computational effort(less than 3% of the total CPU time), with respect to the time taken

to assemble the system equations.

6.7 Calculation Of Foundation Stiffnesses

The computation of the dynamic stiffnesses (impedances) of rigid foundations has been described by various researchers, for example, Karabalis and Rizos (1993). In general, once the system matrix has been solved, the foundation stiffnesses can be calculated by straightforward operations.

Let the soil-foundation contact area S_c be discretized into M_{sc} elements. The dynamic stiffnesses are obtained by integrating the tractions developed over the contact area, namely,

$$\sum_{M=1}^{M_{sc}} \int_{\Delta_{sc}} [S^T]^T \{t\}_p dS \quad (6.41)$$

in which, $[S^T]^T$ is the transpose of the transformation matrix (see Equation 6.6). The traction array at any point on an element, $\{t\}_p = \{t_x, t_y, t_z\}_p^T$, can be expressed in terms of the corresponding nodal values, $\{t\}_\alpha = \{t_x, t_y, t_z\}_\alpha^T$, as

$$\{t\}_p = \sum_{\alpha=1}^8 N_\alpha \{t\}_\alpha \quad (6.42)$$

6.8 Vectorization of Program

6.8.1 Introduction

The increasing demand for computational power in many areas of science and engineering has led to major advances in vector

computer architectures, vectorization techniques and compilers, and parallel processing. It is conceivable that these developments will become an essential part of the computing environment for boundary element analyses.

The generation of system matrices in the boundary element method is not "data dependent" and, consequently, is particularly suitable for parallel machines (Kumar et al, 1989; and Ciskowski et al, 1989). However, program restructuring is needed to run most existing scalar programs on parallel machines. At the time this research was started, parallel processing was not readily available at Glasgow University and hence this thesis focuses on the vectorization of the boundary element program.

During program vectorization, a compiler identifies the parts of a program that can take advantage of the architectural characteristics of the vector machine. Consequently, without major modification, existing scalar programs can be converted into vectorized mode for vector machines (Kobayashi et al 1989; Min and Gupta, 1991; Zucchini and Mukherjee, 1991). The vector facility on the IBM 3090 150-E has been utilized in the present study to give substantial efficiency gains as described below.

6.8.2 Vectorization Technique

General vectorization techniques has been discussed in detail by Polychronopoulos (1988) and Ellersick (1987). A key to achieve effective vectorization is to properly implement DO loops in FORTRAN programs. In practice, re-writing of some of the code is needed to remove possible obstacles that can hamper vectorization, eg., by replacing divisions with multiplications wherever possible within DO loops. It should be noted, possibly because of the overhead involved in calling library routines, that in many cases the use of codes developed by

users may be more efficient than using certain simple NAG subroutines, e.g., matrix operations. The NAG matrix solver (F04ATF and F04ADF) are currently used in the present study. Details of vectorization status for each DO loop can be obtained from the compile-time report.

In order to improve the performance of the vectorized program, a study of program performance was carried out at execution time. This analysis gave the percentage of the total CPU time spent in each subroutine during a complete run in order to identify the program "hot spots". The results of these execution analyses for a problem with 675 degrees of freedom are given in Figure 6.10, in which the item "Others" refers mainly to the subroutines for pre-processing, post-processing, matrix operations, etc. As expected, the most time-consuming subroutine is that for the evaluation of the fundamental solutions. Based on these results, considerable effort was expended to implement efficient vectorized code in these routines.

6.8.3 Results

In order to evaluate the efficiency gains due to vectorization, the static stiffness of a square surface foundation was analyzed by scalar and vector version algorithms, respectively. Various boundary element meshes were used to model the near field. All runs were carried out in a multiple user environment. In order to assess the influence of multiple users, the program was run three times for each case and the average CPU times were recorded. The performance of the scalar and the vector programs in various modules is given in Table 6.2. It should be noted that the CPU time spent in the matrix solver is the same for both scalar and vectorized programs. As would be expected, the computation of system matrices takes up the most computational effort in the boundary element

analysis. For the problem analyzed, the assembly of the system matrices consumed 92~97 per cent and 96~99 percent of the total CPU time, using vectorized and scalar programs, respectively. In general, the scalar/vector "speed-up" is about three. As shown in Figure 6.11, the significance of vectorization depends upon the number of degrees of freedom of the problem being solved. Boundary element programs, coupled with vectorization, enable large complex three-dimensional problems to be solved at relatively low cost.

6.9 Summary

This chapter describes some features of the boundary element program for the steady-state dynamic analysis of three-dimensional rigid rectangular foundations. Some important aspects pertaining to efficient programming techniques of boundary element methods are discussed in detail. A novel method is described for incorporating boundary conditions during the assembly of the system equations. It can deal with problems of traction discontinuities at corners and edges without increasing the number of degrees of freedom. Consequently, the cost of analyses and memory demands can be significantly reduced, which enables the program to analyze larger problems. This technique alone brings worthwhile improvements to the computational efficiency of the boundary element analyses.

This program has been vectorized by using the IBM 3090-150 Vector Facility. Problems of various size (degrees of freedom) have been analyzed using both the scalar and the vectorized programs. In general, the assembly of the system matrices takes between 92% to 99% of the total CPU time. Consequently, subroutines relevant to these calculations require careful coding. The improvement of efficiency due to vectorization is (typically) three.

Appendix 6.1 Input Specification

The data for this program is free format. Individual data items are separated from each other by a comma.

Record 1:

TITLE

TITLE : The title of the problem.

Record 2:

GS XUN RW a ₀

GS - Shear Modulus of soil, kN/m²
XUN - Poisson's ratio of soil
RW - bulk unit weight of soil, kN/m³
a₀ - Dimensionless frequency

Record 3:

XL YL

XL - The width of the foundation, m
YL - The length of the foundation, m

Record 4:

NLX NLY NFX NFY

NLX - Number of elements in the mesh(X-direction)
NLY - Number of elements in the mesh(Y-direction)
NFX - Number of equal-size elements for the foundation(X-direction)
NFY - Number of equal-size elements for the foundation(Y-direction)

Record 5:

NEW

The number of rings of finite boundary elements around the

foundation.

Record 6:

SRAT

SRAT is an array used to set up the ring dimensions, eg., SRAT(i) is the dimension of the ith ring of elements(Figure 6.2).

Record 7:

KS

KS - type of contact between soil and foundation and consideration of symmetrical conditions:

- 1 - Smooth contact.
- 2 - Smooth contact, consider symmetry conditions.
- 3 - Welded contact.
- 4 - Welded contact, consider symmetry conditions.

Record 8:

DISP

array DISP - The prescribed translations and rotation of the foundation.

Record 9:

NLAYER

NLAYER - number of layers of elements used to discretize the sidewall

- 0 - surface foundations

Record 10: omit if NLAYER = 0

EMB NPART

EMB - depth of the embedment, m
NPART - sidewall contact parameter
0 - full height contact
2 - no sidewall contact

Record 11:

JINF

JINF - Use of Infinite Boundary Elements:
1 - With Infinite Elements
2 - Without Infinite Elements

Appendix 6.2 DATA GENERATED BY SUBROUTINE DATGEN

1) The general variables used by the program are given below:

NELEM = Number of elements
NODE = Number of nodes
NCK = number of soil-foundation contact nodes
NEF = number of soil-foundation contact elements
C1 = Velocity of compression wave
C2 = Velocity of shear wave
CR = Velocity of Rayleigh wave

2) Matrices for Nodes and Elements:

CORDS = nodal coordinates
NCON = node numbers for each elements(element connectivity)
VJACOB = Jacobian of elements
TN = outward normal vectors of elements
LIST = soil-foundation contact nodes
LEED = soil-foundation contact elements
LET = Element types array, soil-foundation contact element,
traction free element, etc.
KEXY = nodes in the analyzed area and their corresponding
symmetrical nodes

3) Gauss Integration:

GSX = Gauss Points.
GSW = Gauss Weights.

TABLE 6.1 SUBROUTINE FUNCTIONS

MODULE	SUBROUTINE	TASK
Pre-processing	DATGEN	reads input data file and generates geometrical information related to discretization
	SIDE	generates elements for the sidewalls
	BSYM	generates the "object" nodes and the "image" nodes with respect to symmetry
	INFA	generates geometrical information related to infinite elements
Set-up System Matrices	NON	controls the evaluation of non-singular integrals over finite boundary elements
	SING	controls the evaluation of singular integrals over finite boundary elements
	INFC	controls the evaluation of integrals over infinite boundary elements
	BMATA	controls the assembly of sub-matrices of [A] and {b}
	BMAT	controls the assembly of the system matrices [A] and {b}
	RIGID	imposes the appropriate boundary conditions

TABLE 6.1(continued) SUBROUTINE FUNCTIONS

MODULE	SUBROUTINE	TASK
Computation of integrals	GAUSS	generates Gauss points and weights of Gauss-Legendre quadrature
	KERN	computes values of G_{ij} and T_{ij}
	DIST	computes the distance between a point and an element
	FGPR	finds the required integration points
	SUBDIV	sub-divides elements
	CALK	performs Gauss-Legendre quadrature
	RS	performs the sub-division and transformation method
	ZERO	finds the zeros along a ray
	INFB1	evaluates static integrals over infinite elements
	INFB2	evaluates non-singular dynamic integrals over infinite elements
	INFB3	evaluates singular dynamic integrals over infinite elements
	FNODE	performs the Regula Falsi method
Solution of [A]	F04ATF	solves real-value [A]
	F04ADF	solves complex-value [A]
Post- processing	STIF	computes foundation stiffnesses and prints both input information and results given by the program

TABLE 6.2 CPU-TIME FOR VECTORIZED AND SCALAR PROGRAMS

$$\frac{\text{(Vectorized)}}{\text{(Scalar)}}$$

Unit: sec.

Degree of Freedom	Pre-Process	Set Up Equations	Solution of Matrix	Post-Process	Total
24	0.004	0.297	0.012	0.010	0.323
	0.006	0.918		0.023	0.959
63	0.004	1.373	0.037	0.014	1.428
	0.006	4.007		0.027	4.077
120	0.005	4.475	0.099	0.020	4.598
	0.007	13.064		0.036	13.207
195	0.005	11.518	0.277	0.029	11.829
	0.008	34.009		0.052	34.347
288	0.005	25.320	0.700	0.041	26.066
	0.010	74.996		0.080	75.786
399	0.006	49.228	1.549	0.058	50.841
	0.012	147.560		0.124	149.245
528	0.006	87.832	3.195	0.082	91.115
	0.014	264.660		0.189	268.058
675	0.007	146.538	5.944	0.112	152.601
	0.017	443.905		0.284	450.150

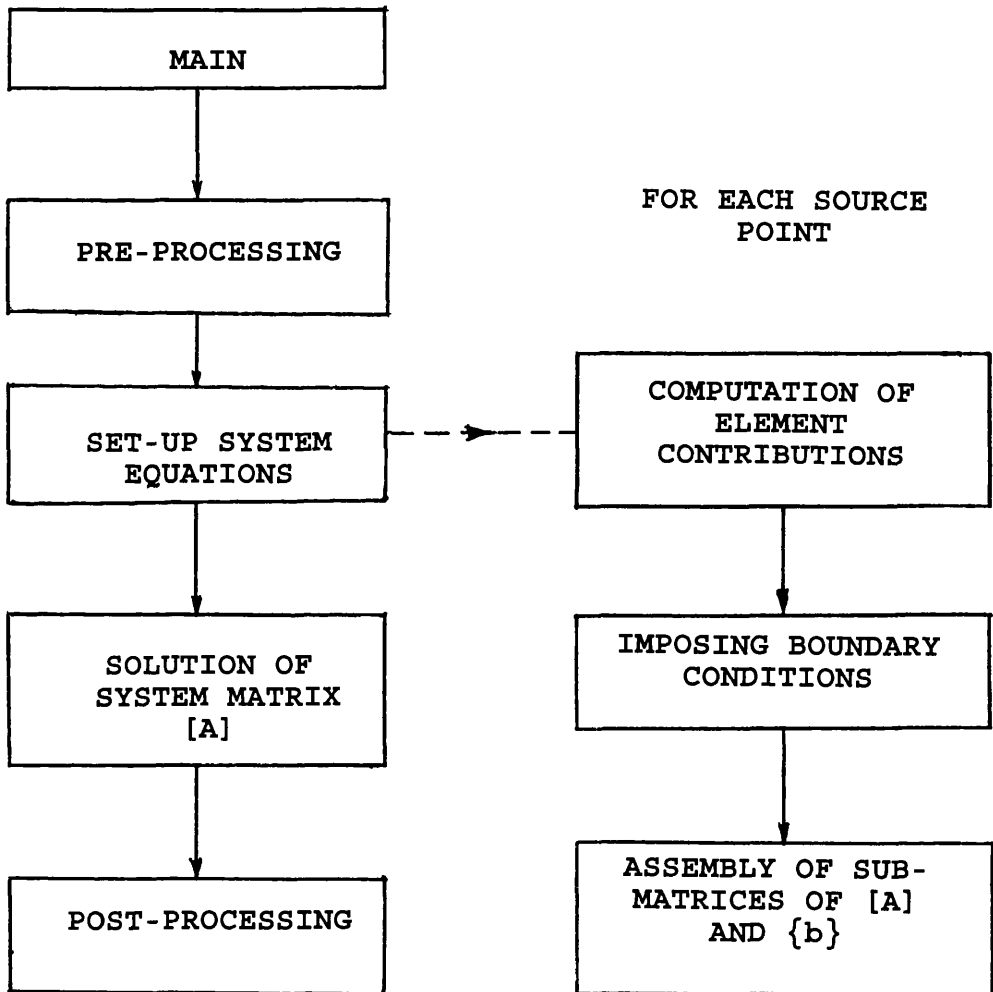


FIGURE 6.1: ORGANIZATION OF THE PROGRAM

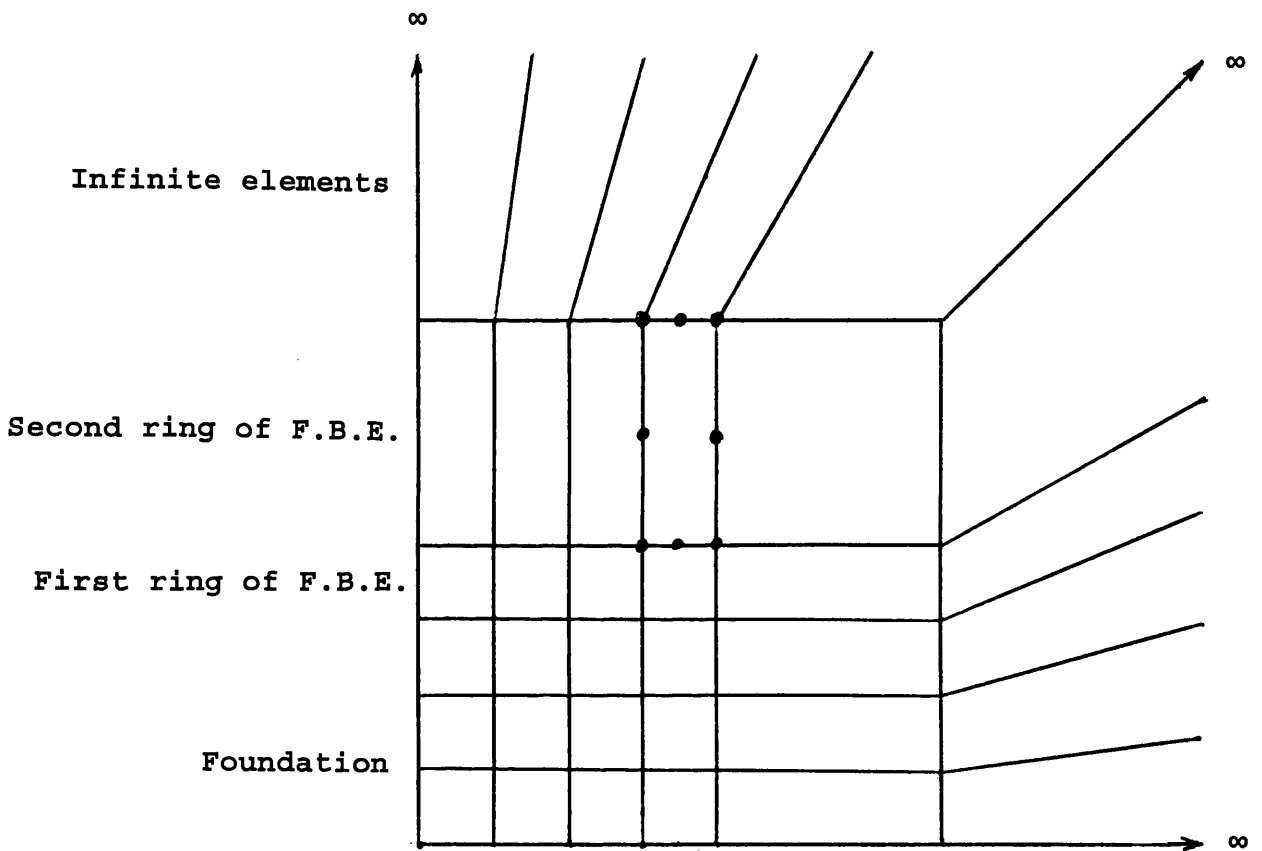
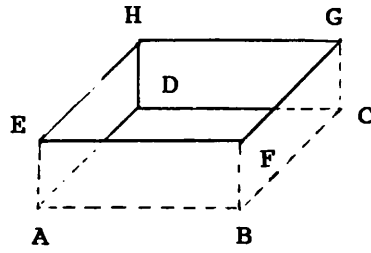
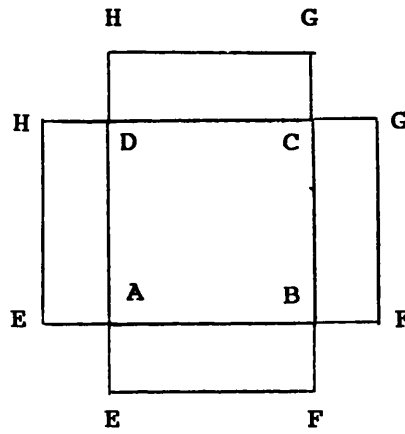


Figure 6.2: Boundary Element Mesh(Quadrantal Symmetry)

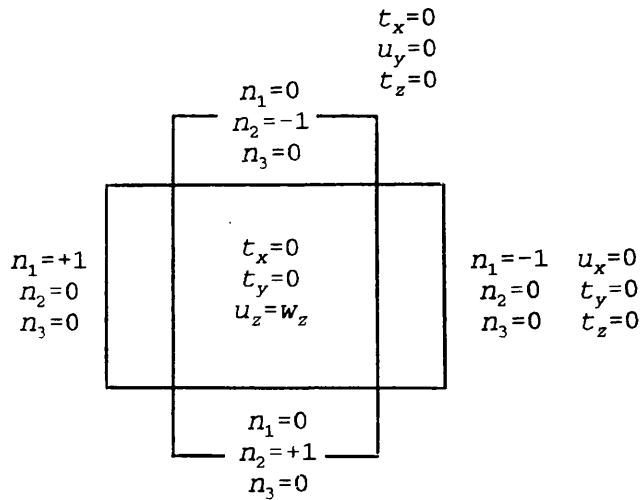


(a) Rigid embedded foundation



$$\begin{aligned} u_x &= 0 \\ u_y &= 0 \\ u_z &= w_z \end{aligned}$$

(b) Welded boundary conditions



$$\begin{aligned} t_x &= 0 \\ u_y &= 0 \\ t_z &= 0 \end{aligned}$$

$$\begin{aligned} n_1 &= +1 \\ n_2 &= 0 \\ n_3 &= 0 \end{aligned}$$

$$\begin{aligned} n_1 &= 0 \\ n_2 &= -1 \\ n_3 &= 0 \end{aligned}$$

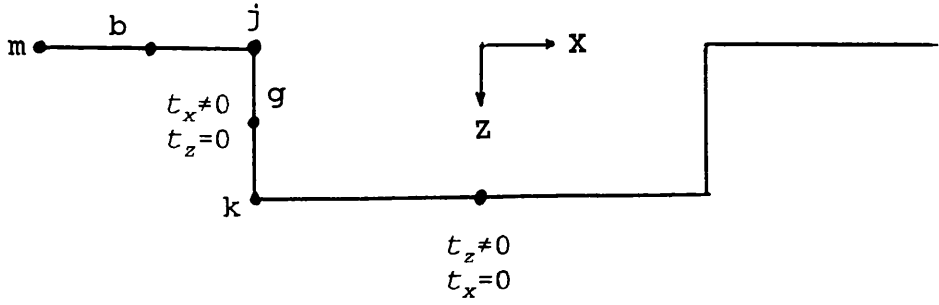
$$\begin{aligned} t_x &= 0 \\ t_y &= 0 \\ u_z &= w_z \end{aligned}$$

$$\begin{aligned} n_1 &= -1 & u_x &= 0 \\ n_2 &= 0 & t_y &= 0 \\ n_3 &= 0 & t_z &= 0 \end{aligned}$$

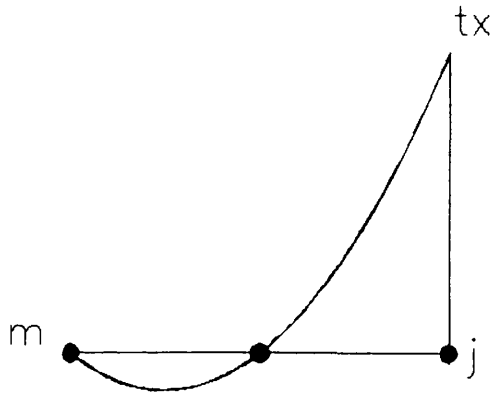
$$\begin{aligned} n_1 &= 0 \\ n_2 &= +1 \\ n_3 &= 0 \end{aligned}$$

(c) Smooth boundary conditions

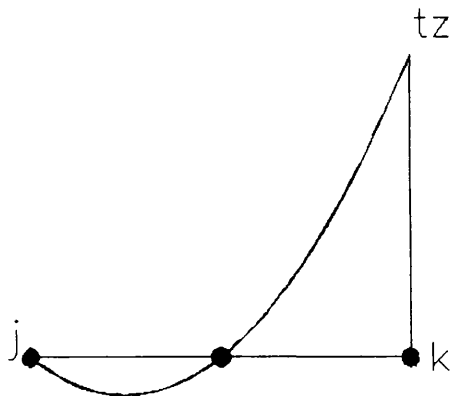
Figure 6.3: Contact Conditions At Soil-Foundation Interface



(a) Smooth embedded foundation



(b) The distribution of traction t_x over element b



(c) The distribution of traction t_z over element g

Figure 6.4: Traction Discontinuities Of Embedded Foundations

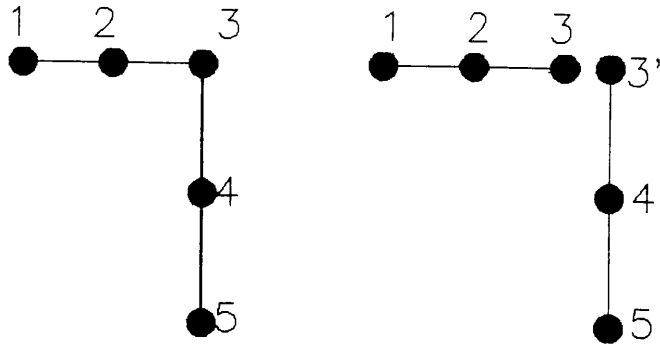


Figure 6.5: Double nodes at a corner

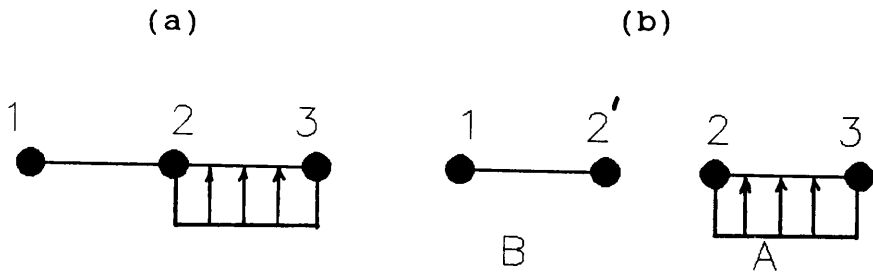


Figure 6.6: Traction boundary condition changes at the interface between two elements

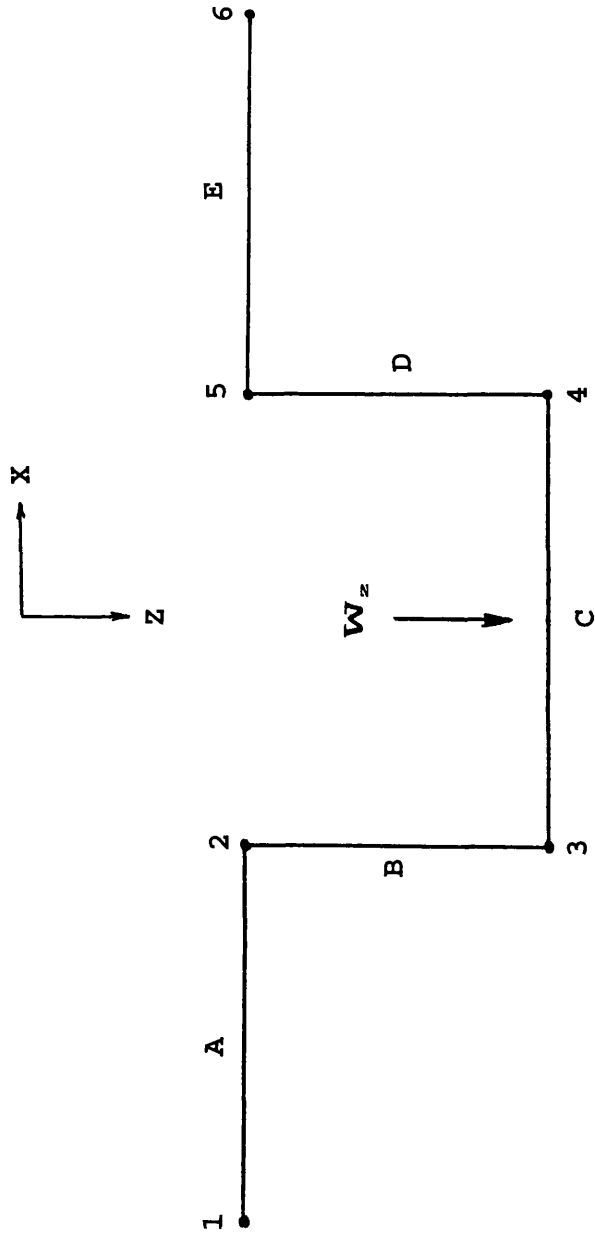


Figure 6.7: 2-D embedded foundation

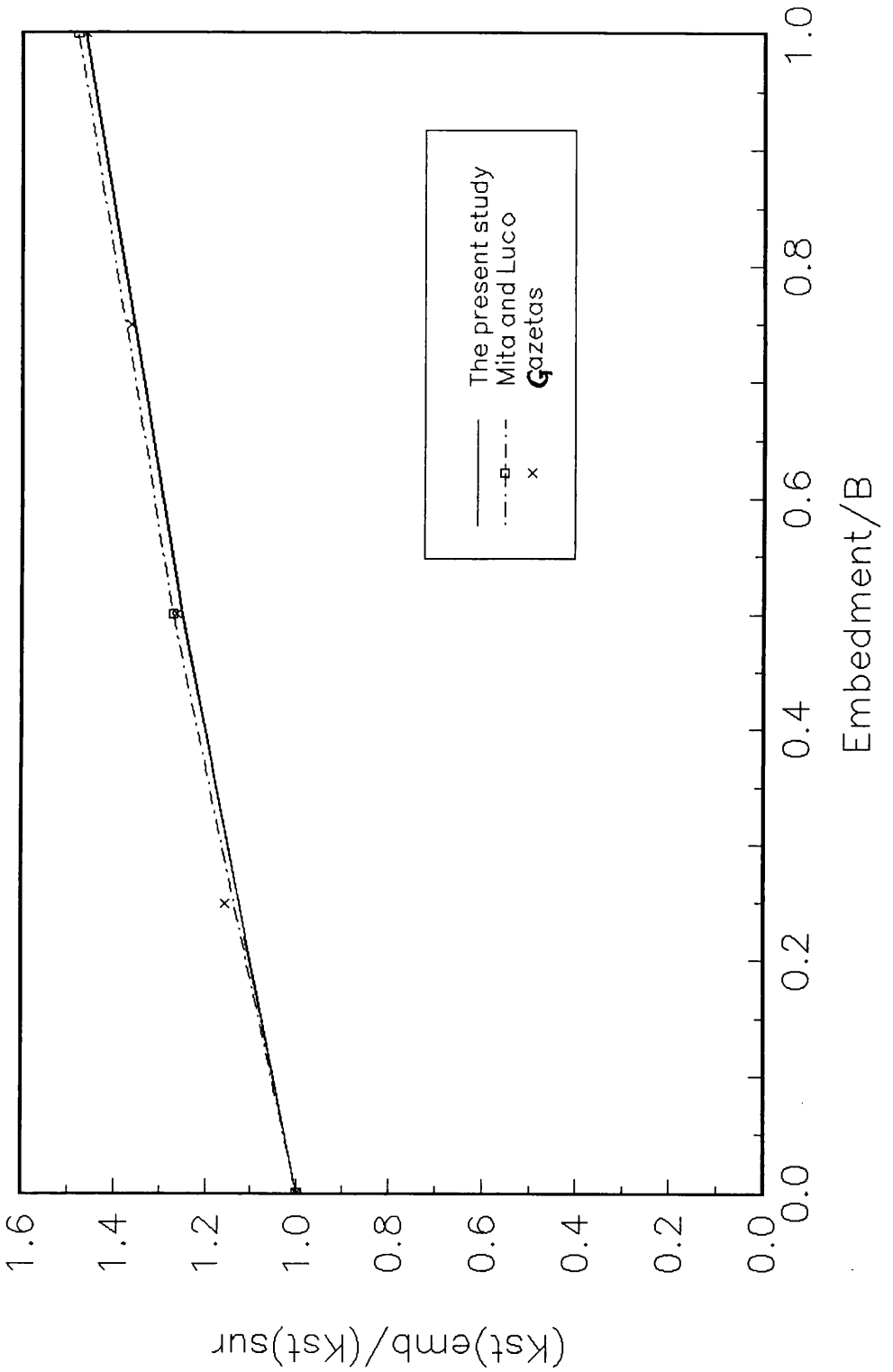


Figure 6.8: The effect of embedment on static vertical foundation stiffness

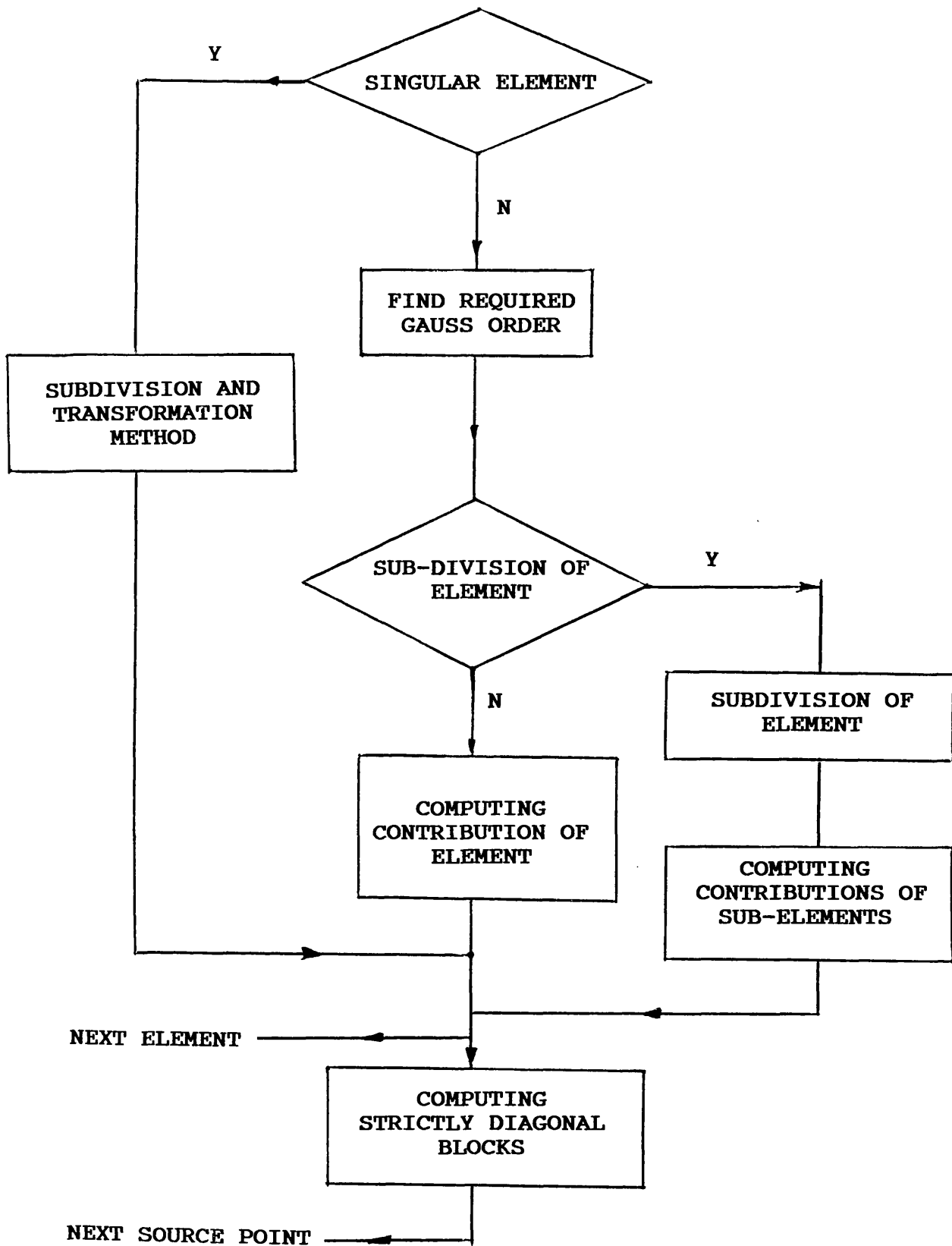


Figure 6.9: Organization of integration module

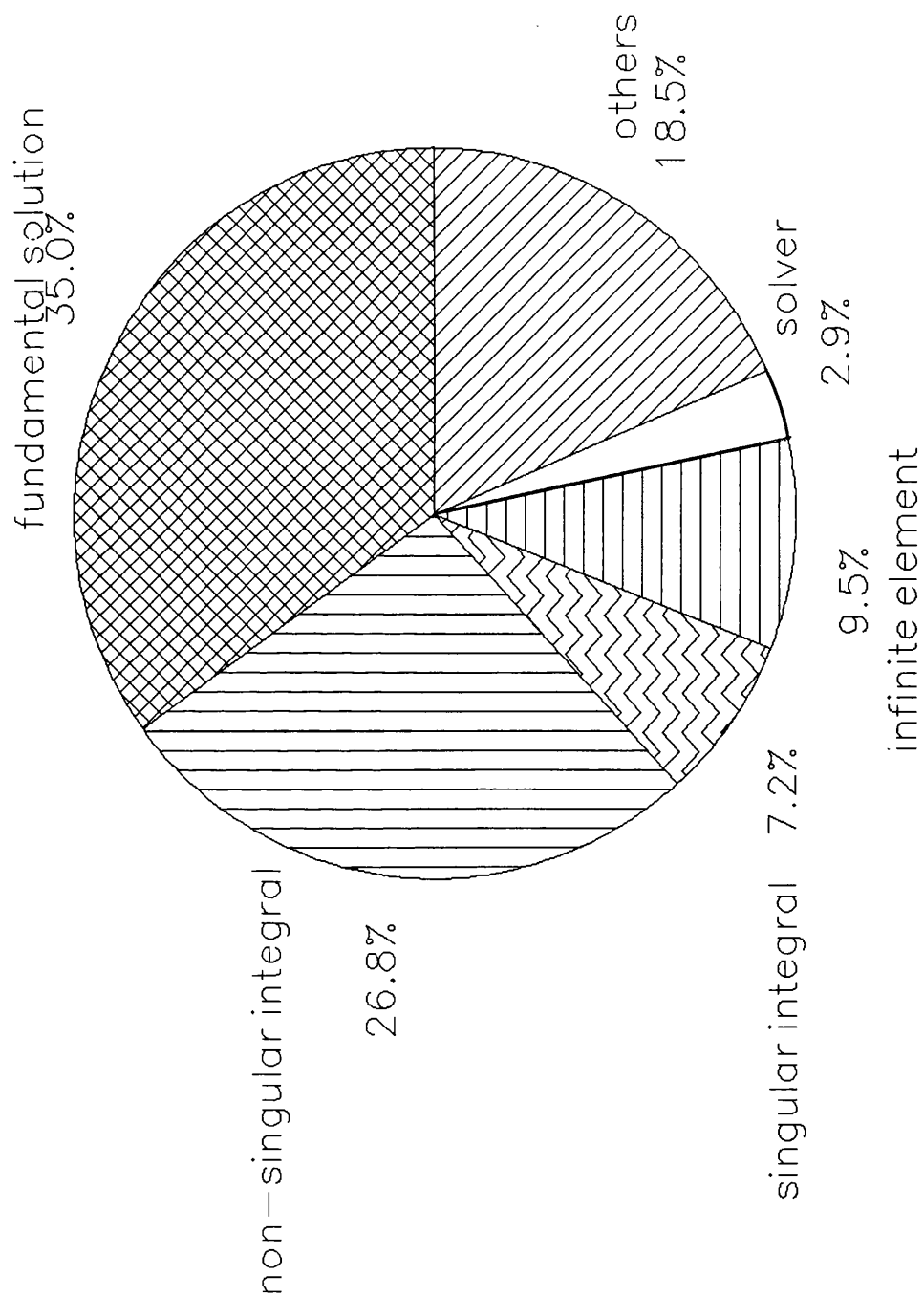


Figure 6.10: Percentage of CPU time spent in subroutines

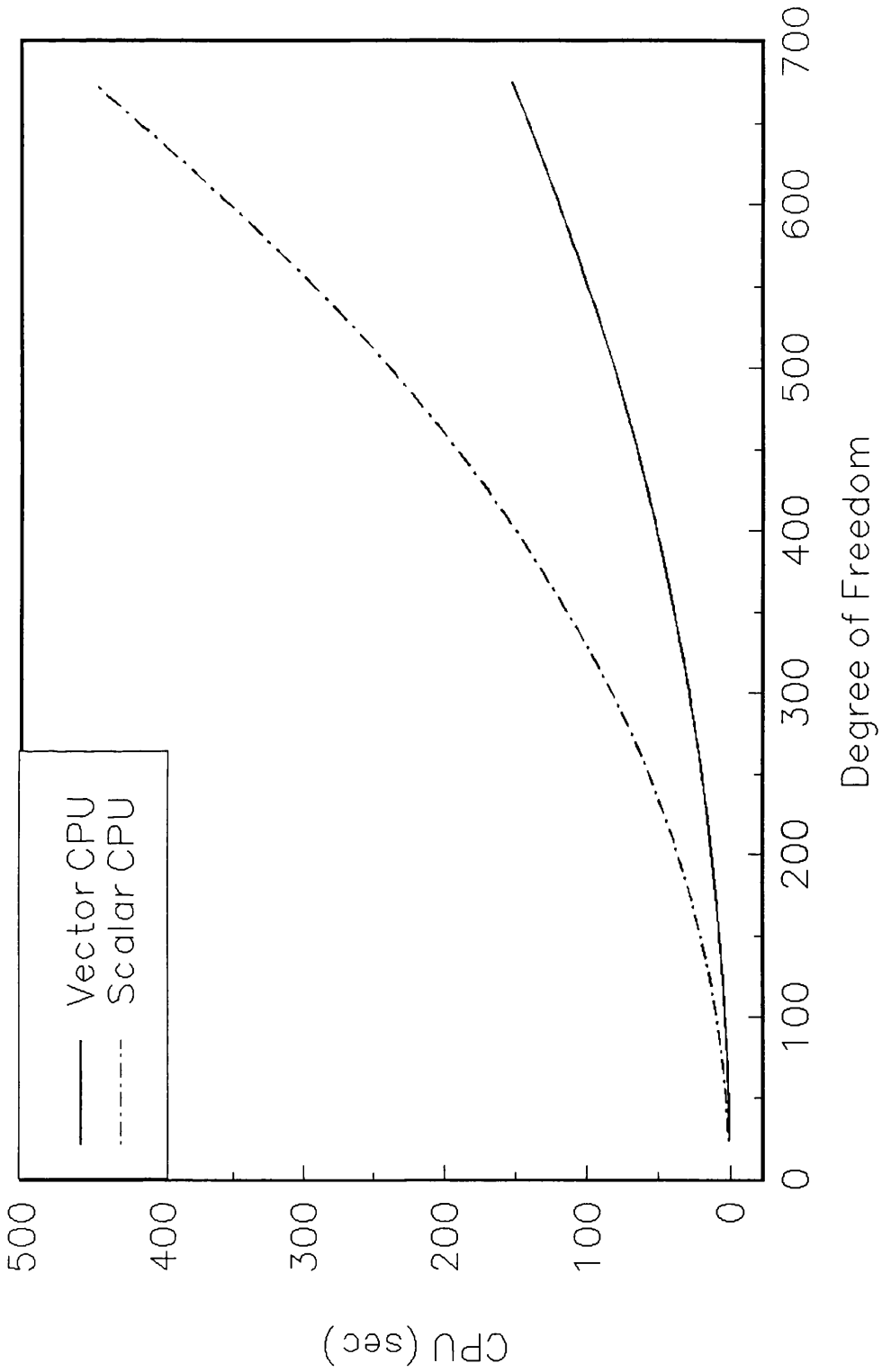


Figure 6.11: The performance of the scalar and vector programs

CHAPTER 7

DYNAMIC RESPONSE OF MACHINE FOUNDATIONS

7.1 Introduction

The purpose of this chapter is to demonstrate the versatility of the boundary-element technique developed in this thesis for the three-dimensional analysis of embedded rectangular machine foundations. Vertical and coupled horizontal-rocking vibrations are considered. Referring to Figure 7.1, the plane of horizontal translation and rocking is defined by the X- and Y-axes, and the aspect ratio N is defined as follows:

$$N = \frac{L}{B} \quad (7.1)$$

The impedance functions are referred to the centre of the base mat and can be written as follows:

vertical vibration:

$$K_v = GL(k_v + ia_0 c_v) \quad (7.2)$$

horizontal vibration, along longitudinal (x) direction:

$$K_{hx} = GL(k_{hx} + ia_0 c_{hx}) \quad (7.3)$$

horizontal vibration, along lateral (y) direction:

$$K_{hy} = GL(k_{hy} + ia_0 c_{hy}) \quad (7.4)$$

rocking vibration, about the longitudinal (x) axis:

$$K_{Ix} = GI_{bx}^{0.75} (k_{Ix} + ia_0 c_{Ix}) \quad (7.5)$$

rocking vibration, about the lateral (y) axis:

$$K_{Iy} = GI_{by}^{0.75} (k_{Iy} + ia_0 c_{Iy}) \quad (7.6)$$

and the cross-coupling term:

$$K_c = GBL(k_c + ia_0 c_c) \quad (7.7)$$

in which, k_α and c_α ($\alpha = v, hx, hy, rx, ry, \text{ or } c$) are the dimensionless stiffness and damping coefficients, respectively, of the impedance functions; I_{bx} and I_{by} are the second moments of area about the x and y axes of the base mat.

In the numerical model, the base mat is uniformly discretized by square elements, and the size of the elements is limited to 1/4 Rayleigh wavelengths. For embedded foundations, two layers of boundary elements are used to discretize the sidewalls (Preliminary calculations revealed that one layer of elements was not sufficient to obtain accurate results). A single ring of finite boundary elements is used to model the near field, and infinite elements are used to model the remainder of the free surface of the halfspace. Perfect bond between the foundation and the soil is assumed. A Poisson's ratio of 0.25 is used, except where indicated otherwise.

Typical results are given for very high frequencies ($a_0 \gg 2$) and for foundations on incompressible soil ($\nu=1/2$). These should be of considerable interest in practical applications but have received scant attention in the published literature. In addition, some important questions in machine foundation analyses are addressed for the first time: i.e., effect of the foundation shape (aspect ratio) and the characteristics of embedment (surface, trench, or fully embedded foundations) on the impedance functions, in the high frequency range. It should be noted that these problems have been addressed by Dominguez and Roesset (1978), Mita and Luco (1989b), Israil and Banerjee (1990), and many others, only for low to moderate frequencies ($a_0 \leq 3$). Some of the results obtained in this study are also compared with published experimental measurements.

7.2 Dynamic Stiffnesses At Very High Frequencies

The published literature is rich in results for the response of machine foundations for low frequencies, usually for a_0 values less than two (Gazetas, 1983; Roesset, 1980a,b; and Novak, 1987). The paucity of results for high-frequency vibrations is largely due to the practical limitations of rigorous numerical techniques and the costs of computation. However, foundation designers require knowledge of the response of foundations to high frequency excitations, since the serviceability criterion for high frequency vibration becomes increasingly stringent. From an academic point of view, it is of interest to know to what extent the dispersion of waves in elastic media generates damping, and thus limits the amplitude response of foundations, at high frequencies. The need for such studies of machine foundation response at high frequencies has been identified by, for example, Awojobi (1971); Luco and Westmann (1972); Crouse et al (1990); Roesset (1980b).

The development of the infinite element methodology in this thesis provides the means to obtain rigorous results at high frequencies. The impedance functions (non-dimensional stiffness and damping coefficients) for rigid square foundations, for dimensionless frequencies up to ten, are given in Figures 7.2~7.5. The numerical results given by Mita and Luco (1989b) for $a_0 \leq 3$ are also indicated. These are retrieved from their viscoelastic results by using the correspondence principle of viscoelasticity (Lysmer, 1980). The discrepancies between the two sets of results at these low frequencies, less than 5% in general, may arise from the intrinsic difference between the quadratic elements used in this thesis and the simple constant elements used by Mita and Luco (1989b). Although the high frequency results can not be verified against the work of other authors (since the results described in this thesis are new), it is believed, by extension, that they are accurate.

The impedance functions for horizontal translation (Figure 7.3) are practically independent of frequency and require no further comment.

For vertical vibration (Figure 7.2), there is a general trend of decreasing stiffness with frequency although this is obscured by an oscillatory component. The reason for this complicated pattern is unclear, although this pattern can also be just discerned in the results obtained by Mita and Luco (1989b). This coefficient is strongly dependent on Poisson's ratio, here taken to be equal to 0.25. The damping coefficient reaches a maximum at $a_0 = 3$ and is practically constant thereafter, a result perhaps suggested by the data obtained by Mita and Luco (1989b).

The results for rocking vibration (Figure 7.4) are more interesting. Here, the results obtained by Mita and Luco (1989b) fail to indicate the form of the impedance functions

at high frequencies, which at $a_0 = 3$ and beyond are essentially constant.

The cross-coupling coefficients (Figure 7.5) are relatively small and are rather complicated functions of frequency. It appears that their high frequency asymptotic values are zero. The physical source of these complex functions of frequency is unclear. The relatively small values for (intrinsic) cross-coupling terms is supported by the numerical studies (Gazetas, 1983) and experimental measurements (Crouse et al, 1990). However, cross-coupling is of course important in the design of real foundations because of the additional terms arising from real foundation geometry.

The general observation that the impedance functions are sensibly constant at high frequencies ($a_0 > 4$) verifies the analytical radiation damping model proposed by Gazetas and Dobry (1984). This important phenomenon can not be discerned in general from the results of Mita and Luco (1989b).

7.3 Effects Of Foundation Shape

Machine foundations are generally not square in shape. Several researchers (e.g., Gazetas, et al, 1985; Dobry and Gazetas, 1986, have shown that foundation shape has significant influence on the impedance functions, and that the "equivalent circle" approximation may produce inaccurate results for rectangular foundations with aspect ratios greater than three. In the present study, surface foundations with aspect ratios of $N=2$ and 4 are used to illustrate the effect of foundation shape. The responses of rectangular foundations for dimensionless frequencies up to five are given in Figures 7.6~7.10.

For rectangular foundations, Figure 7.6 shows that the vertical impedance decreases faster with frequency as the aspect ratio increases. The results shown in Figures 7.7 and 7.8 reveal that the horizontal static stiffness in the lateral direction is greater than the stiffness in the longitudinal direction. The horizontal impedances are relatively insensitive to changes in frequency. Consequently, the adoption of constant stiffness coefficients for horizontal vibration may be a reasonable approximation for a wide range of frequencies. The rocking static stiffness about the lateral axis is greater than the stiffness about the longitudinal axis (Figures 7.9 and 7.10). These impedances are strongly dependent on frequency but exhibit broadly similar trends for all values of aspect ratio up to (at least) four.

For each vibration mode, the general trend is that although the variation of damping coefficient is sensitive to frequency, it is insensitive to aspect ratio. At high frequencies, and for all foundation shapes, constant damping is a good approximation. However, the foundations with the higher values of aspect ratio produce the largest damping per unit contact area or area moment of inertia, at all frequencies. Experimental studies (Dobry et al, 1986; Gazetas and Stokoe, 1991) and analytical studies (Gazetas, 1983) provide strong support for this predicted influence of aspect ratio on radiation damping.

It is significant to note that, although damping usually varies with frequency, the damping coefficients c_v , c_{hx} , and c_{hy} asymptotically approach constant values, at high frequencies irrespective of foundation shape. As illustrated in Figure 7.11, similar asymptotic behaviour can be observed in rocking vibration, if the imaginary parts of K_{rx} and K_{ry} are normalized with respect to GI_{bx} and GI_{by} rather than the normalisation of Equations 7.5 and 7.6. The results (Figure 7.11) of this

normalisation imply that, at high frequencies, foundations produce approximately the same amount of damping per unit second moment of area. This observation supports the simple analytical radiation damping model proposed by Gazetas and Dobry(1984).

The numerical results obtained in Figures 7.6~7.10 are compared with those predicted by the engineering models proposed by Gazetas (1991). It should be noted that his models for dynamic stiffness and radiation damping are compiled from published numerical results for perfectly welded contact foundations. However, his algebraic formulas for static stiffnesses of surface foundations are appropriate only for smooth contact condition. Based on the assumption that the effects of aspect ratio on the static stiffnesses are independent of the contact conditions, approximate impedance functions for $a_0 \leq 2$ can be obtained and have been indicated in figures 7.6~7.10. In general, the agreement between the two sets of results is reasonable and the important trends observed at low frequencies can be predicted by these engineering models. The discrepancies observed in Figures 7.6~7.10, are generally less than 10%.

7.4 Effects Of Embedment

In practice, machine foundations are usually partially or fully embedded into the soil. Theoretical predictions and experimental measurements(eg, Novak, 1970; Anandakrishnan and Krishnaswamy, 1972) indicate that foundation embedment reduces the amplitude of vibration and increases the resonant frequency. In addition, the effect of embedment is generally dependent upon the soil-sidewall contact area. However, separation and slippage may occur near the ground surface, where the confining pressures are small. Field experiments,

Stokoe and Richart (1974) and Richart (1975), indicate that, for certain types of soil and vibration modes, soil-foundation contact may be reduced or eliminated completely from the vertical sidewalls of embedded foundations. Consequently, before counting on the effect of embedment, the engineer must estimate the quality of the sidewall-soil contact.

As schematically illustrated by Figure 7.12, the numerical studies refer to cast-in-place foundations (complete sidewall contact) and trench foundations (no sidewall contact at all). In other words, the two limiting conditions for embedment are studied. Numerical results relating to effect of deep embedment (embedment equal to the half-width of the foundation) for dimensionless frequencies up to five on square foundations are given in Figures 7.13~7.16. The results for perfect sidewall-soil contact (only) given by Mita and Luco (1989b), for lower frequencies are also indicated. Inspection of Figures 7.13~7.15 reveals good agreement between the two sets of results at these low frequencies. However, significant differences can be observed for the stiffness coefficient of the cross-coupling term (Figure 7.16). The new high-frequency results obtained here and the results obtained for the intermediate cases should prove useful for design purposes.

It is evident that, if the sidewalls are in perfect contact with the surrounding soil, part of the applied load is equilibrated by tractions along the sidewalls. As a consequence, the impedance functions for embedded foundations are generally larger than those of surface foundations and trench foundations (This is not true in cases of nearly incompressible soils). In general, the stiffness coefficients for horizontal and rocking vibrations of embedded foundations, with perfect sidewall contact, monotonously decreases with increasing frequency. The stiffness coefficient for vertical vibration is a more complicated function of frequency. The

influence of embedment on the stiffness coefficients for horizontal vibration (and the cross-coupling mode) tend to be reduced at higher frequencies. Regardless of frequency and vibration mode, the damping coefficients increase significantly with increasing contact area or second moment of area. Similar conclusions (Gazetas and Stokoe, 1991) have been drawn from experimental data. It is worth noting that the damping coefficient for rocking vibration does not tend to zero at low frequencies for embedded foundations (i.e., unlike surface foundations). All the damping coefficients for embedded foundations are practically constant at high frequencies ($a_0 > 4$).

When the sidewall of the foundation is not in contact with the surrounding soil deposit then, throughout the frequency range, the stiffness coefficients are only slightly higher than those for surface foundations. In addition, the trench effect is insignificant for radiation damping, especially for higher frequencies ($a_0 \geq 2$), and may be neglected. Experimental evidence, eg, Novak (1970); Beredugo and Novak (1972); Stokoe and Richart (1974); Richart (1975), tends to support these predictions: embedment with no sidewall contact has little effect on the dynamic response of foundations.

The interpretation of the difference between the predicted damping coefficients of the two limiting cases is that waves emanating from the base mat-soil interface propagate predominantly downwards and are unaffected by the presence of over-burden soil, unlike waves propagating in the horizontal direction. This argument, which has also been verified by Chen (1984), provides strong support for the engineering approximations developed by Gazetas et al (1985) and Fotopoulou et al (1989).

7.5 Incompressible Media

Incompressible soils are frequently encountered in engineering practice but their analysis can be fraught with difficulties, particularly for dynamic problems. Veletsos and Wei(1971) and Veletsos and Verbic(1974) indicated that, for values of Poisson's ratio close to $1/2$, vertical and rocking stiffness coefficients of circular surface foundations decrease with increasing frequency and may be negative in the high frequency range. Such negative values imply a phase difference between load and displacement response of more than 90 degrees. On the other hand, it is well known that as Poisson's ratio approaches $1/2$, the dilatational wave velocity tends to infinity. This has caused serious difficulty in the analysis of machine foundations by numerical methods for many years and no rigorous numerical results for foundations embedded in incompressible soil are currently available in the literature. The present study is unique in that it is capable of analyzing this problem by using the special fundamental solutions for incompressible soil developed in Chapter 2.

7.5.1 Surface Foundations On Incompressible Halfspace

Results for the vertical response of a square foundations resting on an incompressible halfspace are presented in Figure 7.17, along with the experimental data measured by Nii(1987). In general, the predicted stiffness coefficient is in excellent agreement with the experimental measurements. The discrepancy between the predicted damping coefficient and experimental data is only about 10%, and this small discrepancy may well be due to the assumption of perfect soil-foundation contact in the experiment study(or a number of other factors).

A simple approximation can be developed to describe the

decrease of the vertical stiffness coefficient as a quadratic function of frequency:

$$K=K_{st}(1-\alpha a_0^2) \quad (7.8)$$

in which, K_{st} is the static stiffness of the foundation. The function $(1-\alpha a_0^2)$ is plotted in Figure 7.18 and suggests that the value of the coefficient α is 0.25. The performance of this approximation is excellent in the range of frequency examined ($a_0 \leq 6$). The maximum error (at $a_0=6$) is less than 10%.

It should be noted that, for $\nu=1/2$, the parabolic variation in the stiffnesses of circular foundations has been explained by adding a fictitious ("participating") mass m_f to the actual foundation mass (Barkan, 1962; Crockett and Hammond, 1948; Pauw, 1953; Hsieh, 1962). The fictitious mass is assumed to oscillate (as a rigid body) in phase with the machine and foundation. Consequently, the effect of this fictitious mass on the frequency-independent spring stiffness of the mass-spring-dashpot analog (Gazetas, 1983) can be expressed as

$$\begin{aligned} K &= K_{st} - m_f \omega^2 \\ &= K_{st} \left(1 - \frac{m_f}{K_{st}} \omega^2 \right) \end{aligned} \quad (7.9)$$

Several values for this fictitious mass have been reported in the literature; for example, $m_f=2\rho r^3$ ($=0.64\rho A_0 r_0$) and $m_f=0.4\rho A_0 r_0$, respectively, are suggested by Hsieh (1962) and Meek and Wolf (1993) for the vertical vibration of circular foundations with area A_0 and radius r_0 .

Evidently, equations (7.8) and (7.9) imply that

$$\alpha a_0^2 \approx \frac{m_f}{k_{st}} \omega^2 \quad (7.10)$$

Now, for a rectangular foundation the dimensionless frequency is

$$a_0^2 = \frac{\rho \omega^2 B^2}{G} \quad (7.11)$$

where B is the half-width. Based on the equivalent circle approximation the equivalent radius r_e is then 1.13B. The static stiffness K_{st} for a square foundation resting on an incompressible halfspace can be written as

$$K_{st} = \frac{4Gr_e}{1-\nu}$$

$$\approx 9GB \quad (7.12)$$

By substituting Equations (7.11) and (7.12) into (7.10), it is easy to show that

$$\frac{0.25\rho\omega^2 B^2}{G} = \frac{m_f}{9GB} \omega^2 \quad (7.13)$$

Consequently, the fictitious mass for a square foundation is

$$m_f = 0.56\rho AB$$

$$= 0.5\rho A r_e \quad (7.14)$$

This value is intermediate between those values obtained by Hsieh(1962) and Meek and Wolf(1993), cited earlier. It should be noted that the "participating mass" concept is applicable only to incompressible soils.

7.5.2 Embedded Foundations In Incompressible Halfspace

The analysis of rectangular foundations embedded in nearly incompressible soils($0.5 > \nu \geq 0.4$) has generated considerable interest throughout the past decade, eg, Gazetas and Tassoulas (1987a,b); Tohdo et al(1986); Mita and Luco(1989b), among others. However, results for Poisson's ratio equal to 1/2 are not available in the published literature. In the present study, rigorous results for square foundations deeply embedded in incompressible soils are presented in order to provide further insight into this problem.

It is significant, as shown in Figures 7.19~7.22, that the stiffness coefficients of embedded foundations(embedment equal to the half width of the foundation) in incompressible soils(in all modes) are highly frequency dependent. The effect of Poisson's ratio on the horizontal and cross-coupling stiffness coefficients for embedded foundations is substantially different from those for surface foundations. The horizontal stiffness coefficient of surface foundations is practically constant while the horizontal stiffness coefficient of embedded foundations decreases significantly with frequency. Some earlier workers(Elsabee and Moray, 1977) recommend use of the same frequency variation of k_h for both surface foundations and embedded foundations. This approach may be satisfactory for low values of Poisson's ratio but will cause serious errors for nearly incompressible soils.

The stiffness coefficients in the moderate to high frequency

range indicate lower values for embedded foundation than for surface foundations. These results contradict the general rule that embedment increases the impedance functions. Comparisons between the results for $\nu=1/4$ with those for $\nu=1/2$ indicate that the decrease in the stiffness coefficients as a function of frequency for embedded foundations is more pronounced in the later case. Poisson's ratio has little effect on the damping coefficients.

7.6 Conclusions

This chapter presents results for several practical problems in machine foundations to illustrate the potential of the boundary element technique developed in this thesis. In particular, the results obtained by means of the high-frequency analysis, which have been unattainable by numerical methods hitherto, should be of value in practice. Also, reported on here are results pertaining to the dynamic behaviour of foundations resting on, or embedded in, the incompressible halfspace; a problem which has not been solved in the literature, but has been rigorously investigated in the present study. The computer program developed in this study can be used for further investigation of this and other related problems. Some of these possibilities are outlined in the following chapter.

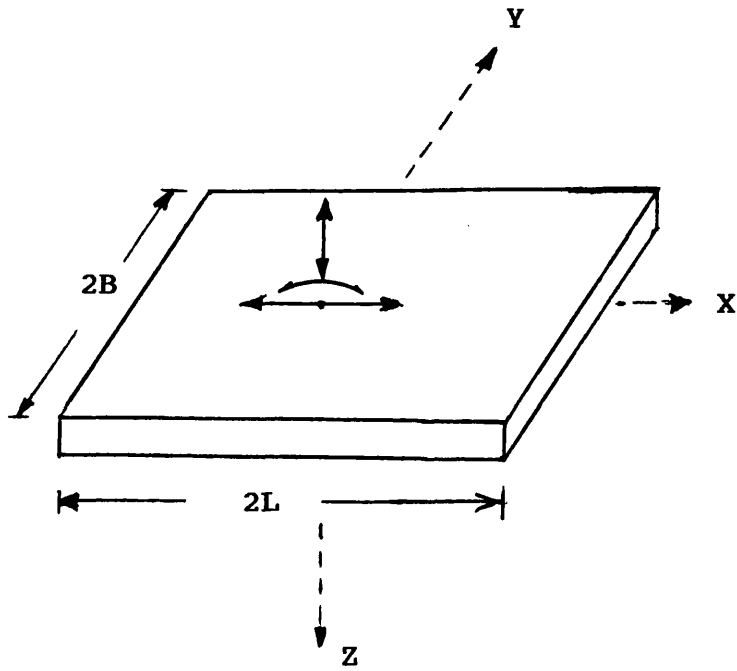


Figure 7.1: The rectangular foundation

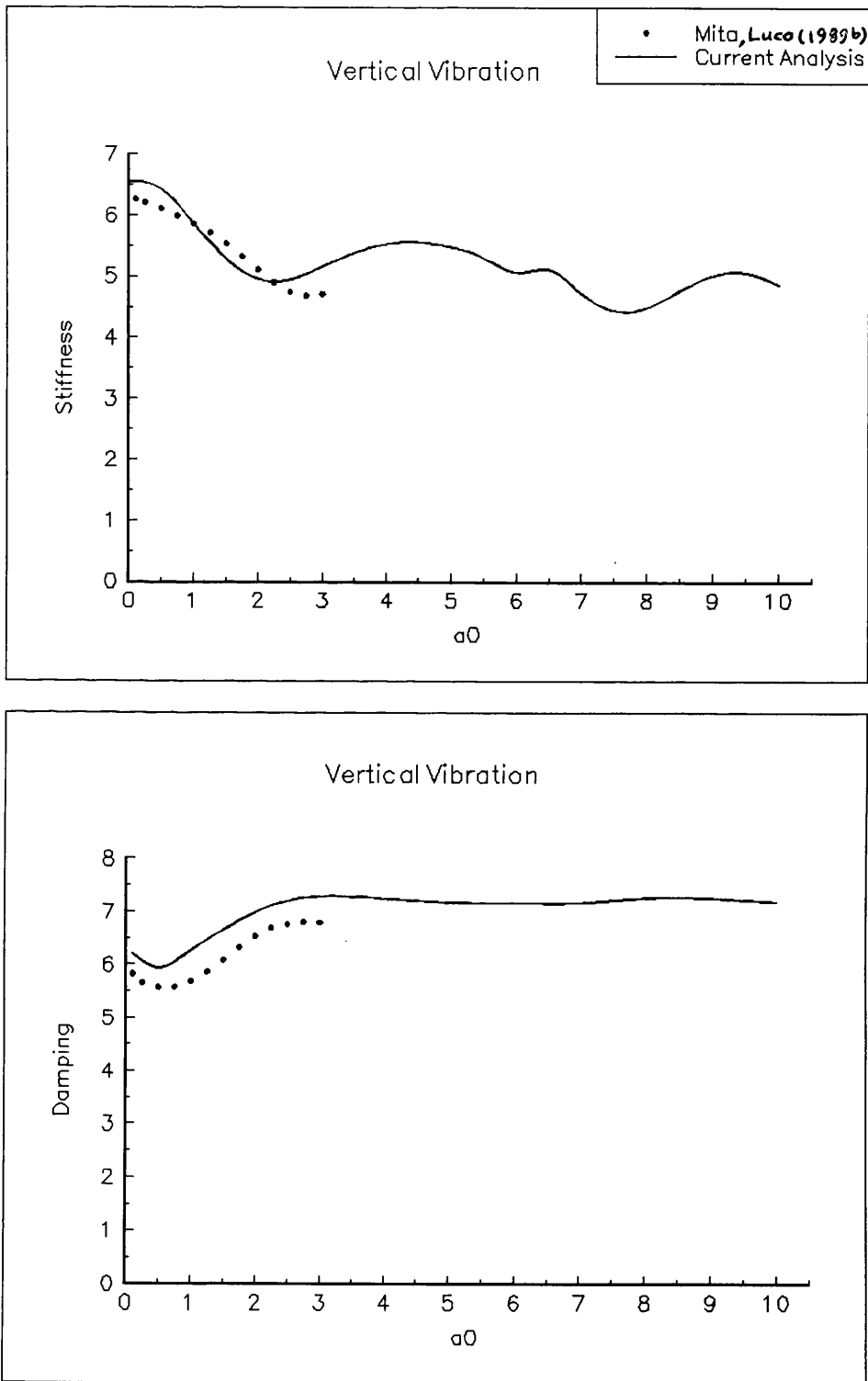


Figure 7.2: Vertical impedance at high frequencies

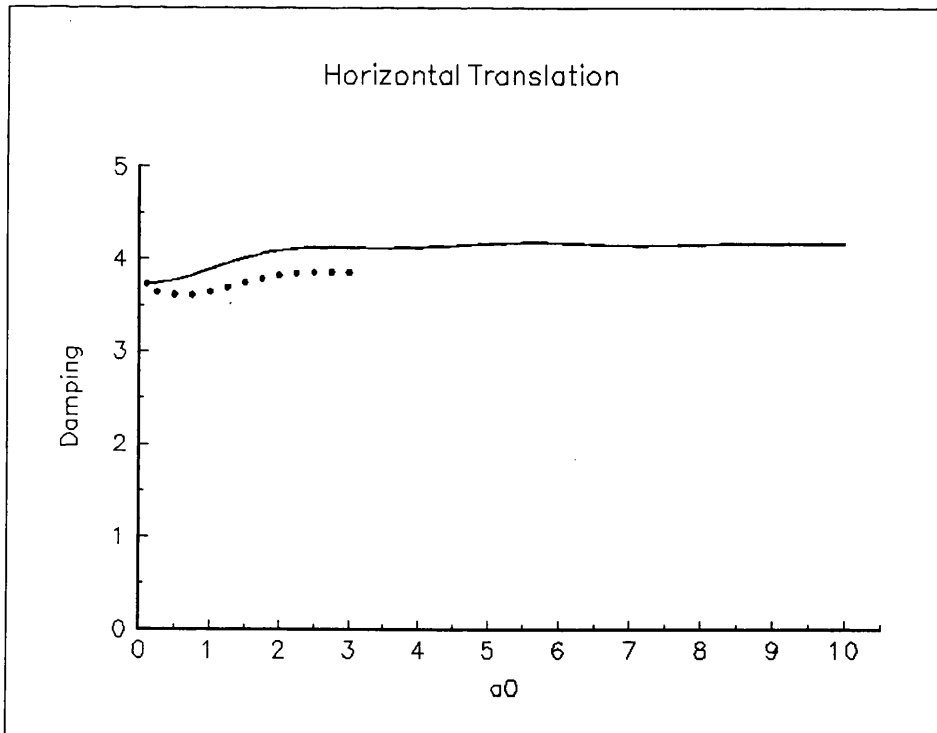
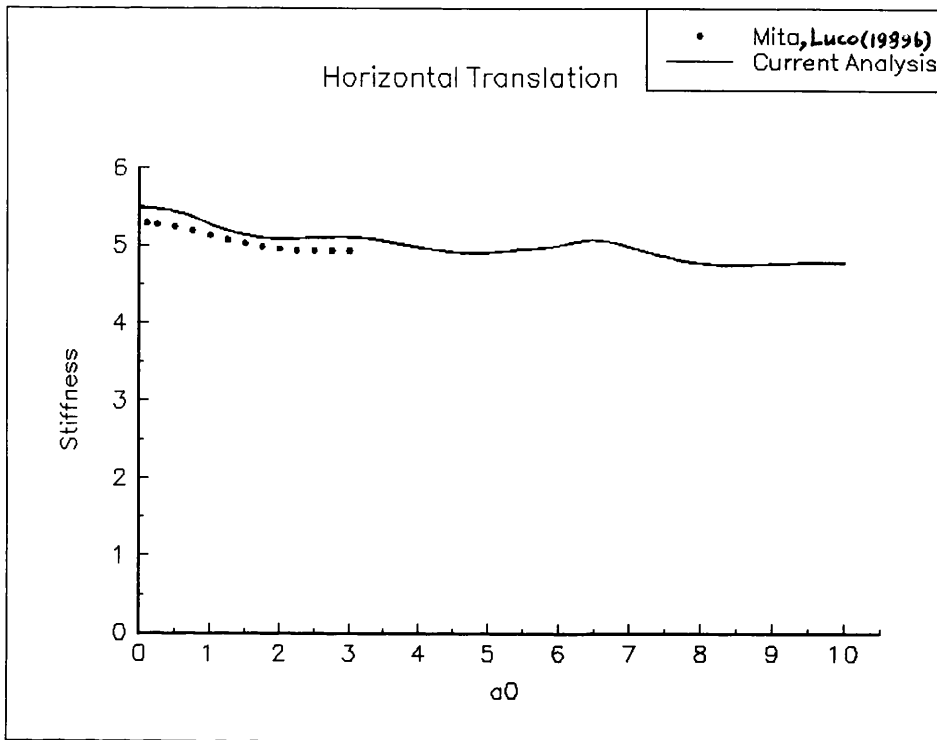


Figure 7.3: Horizontal impedance at high frequencies

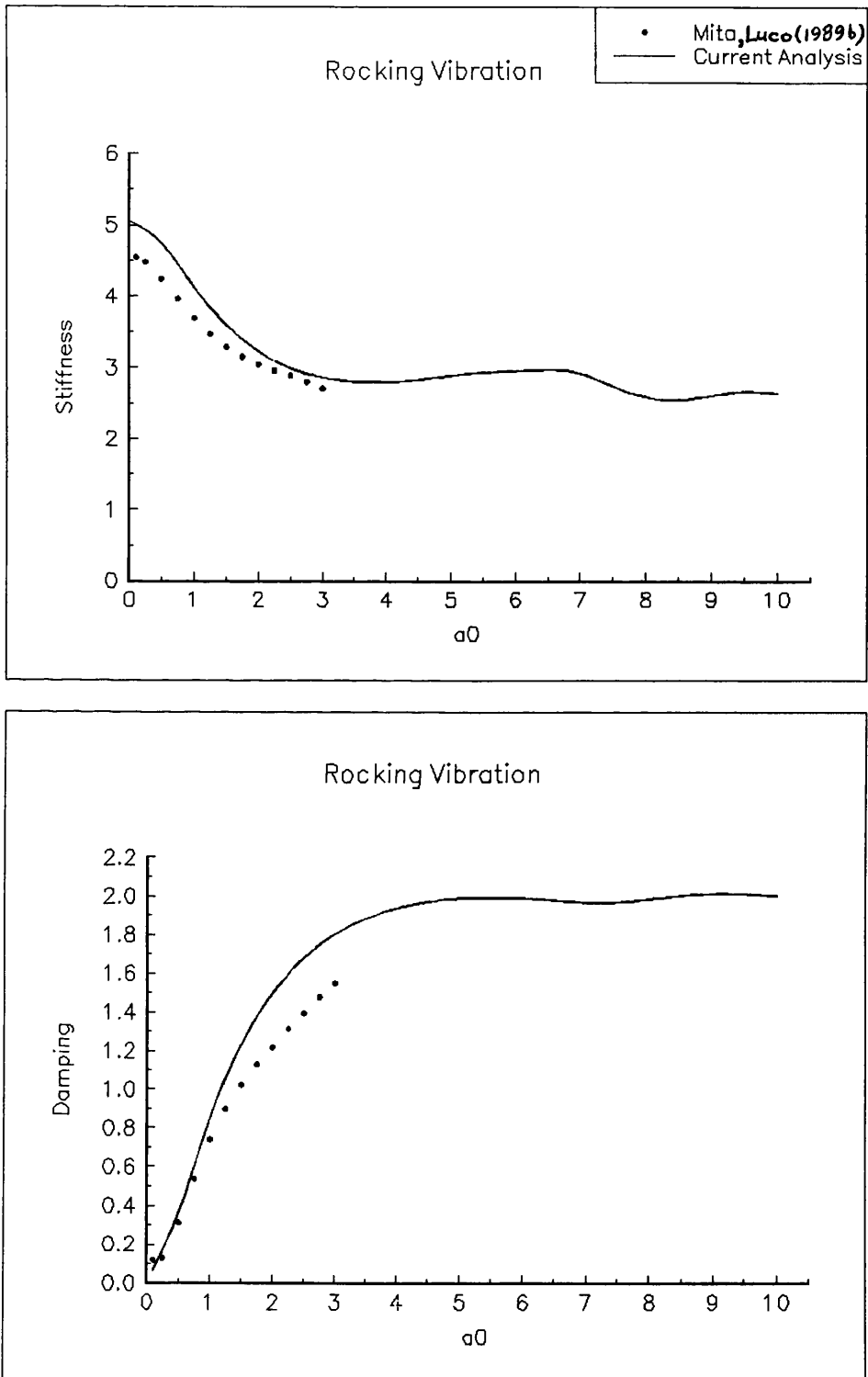


Figure 7.4: Rocking impedance at high frequencies

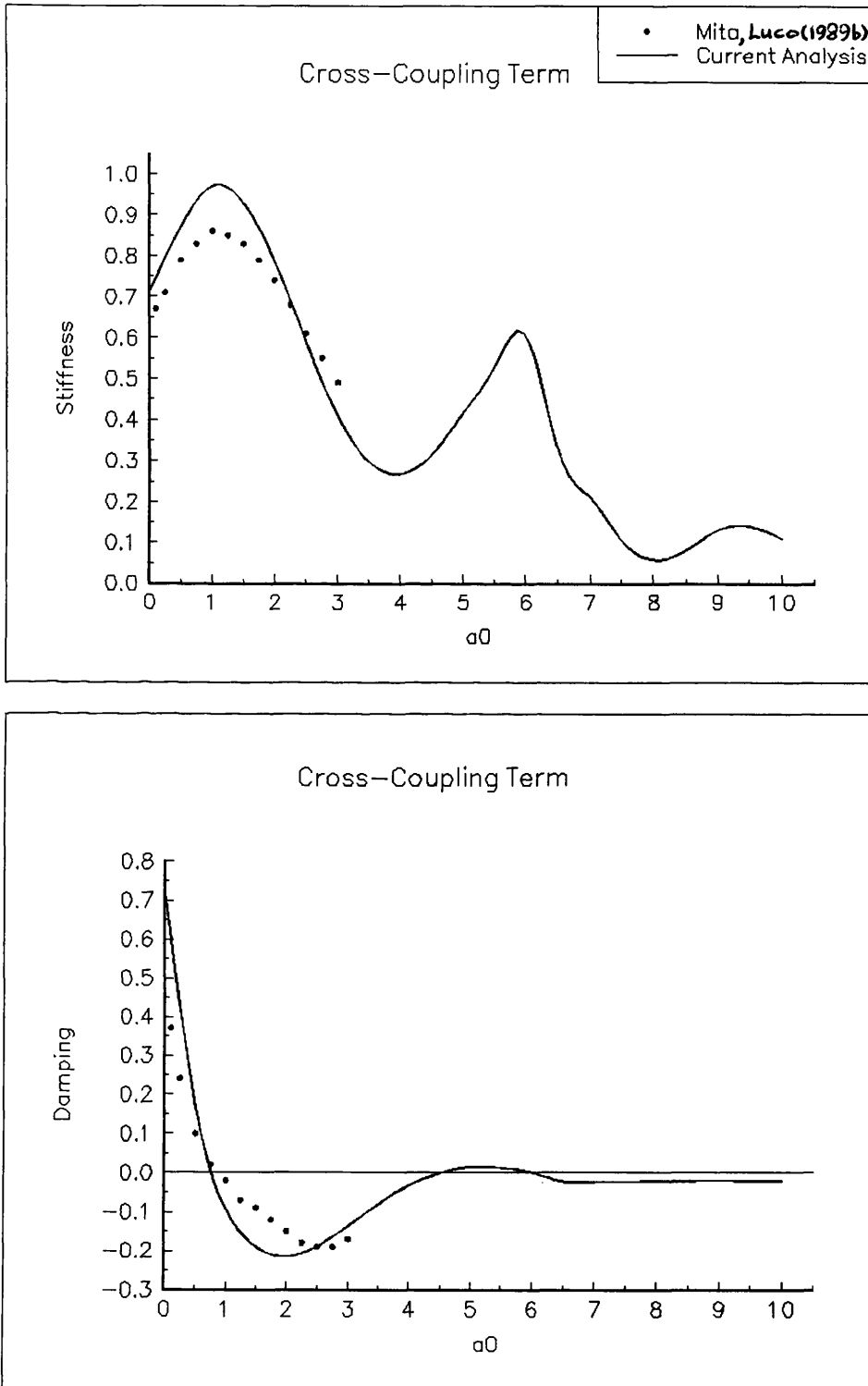


Figure 7.5: Cross-coupled impedance at high frequencies

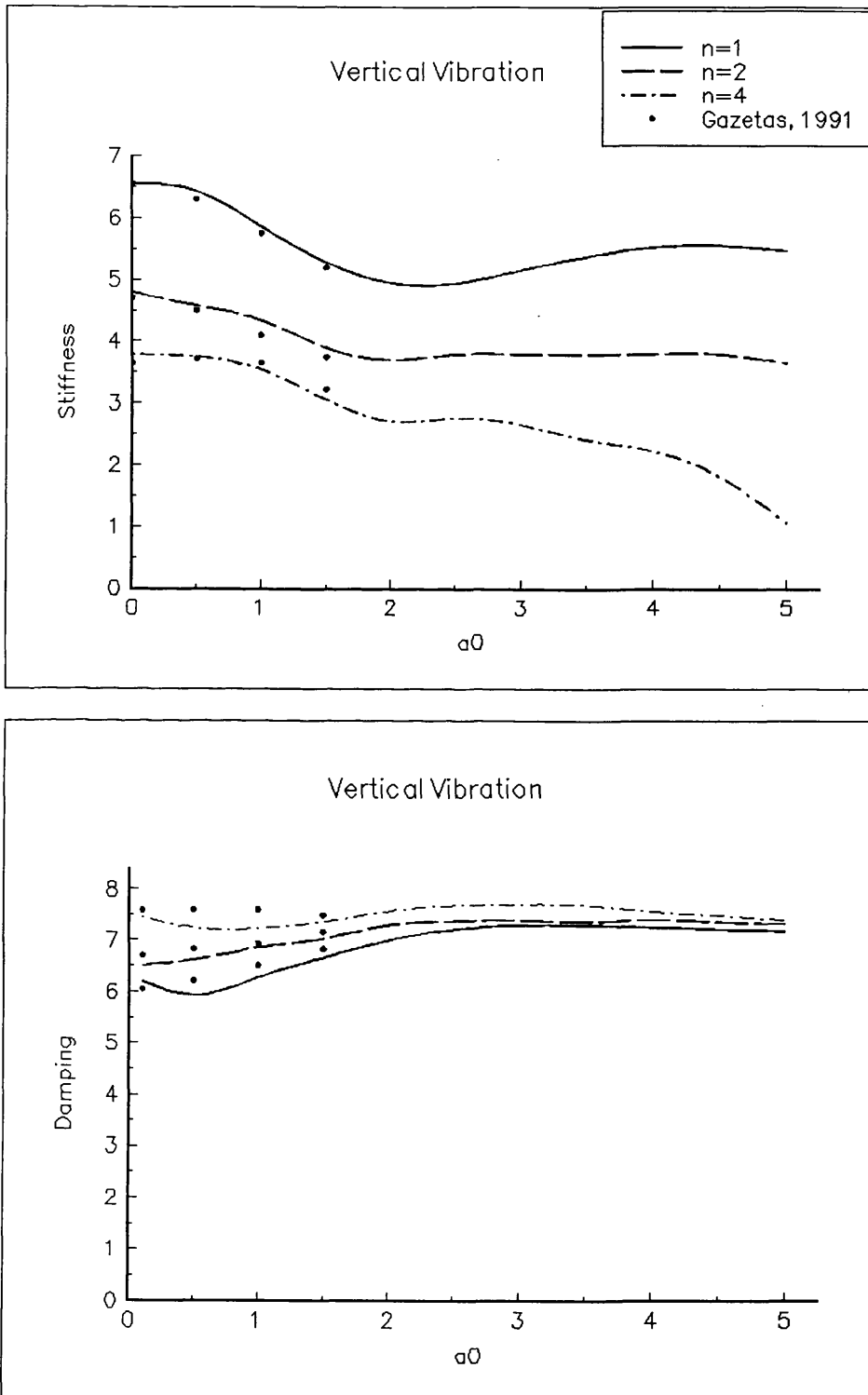


Figure 7.6: Effect of aspect ratio on vertical impedance

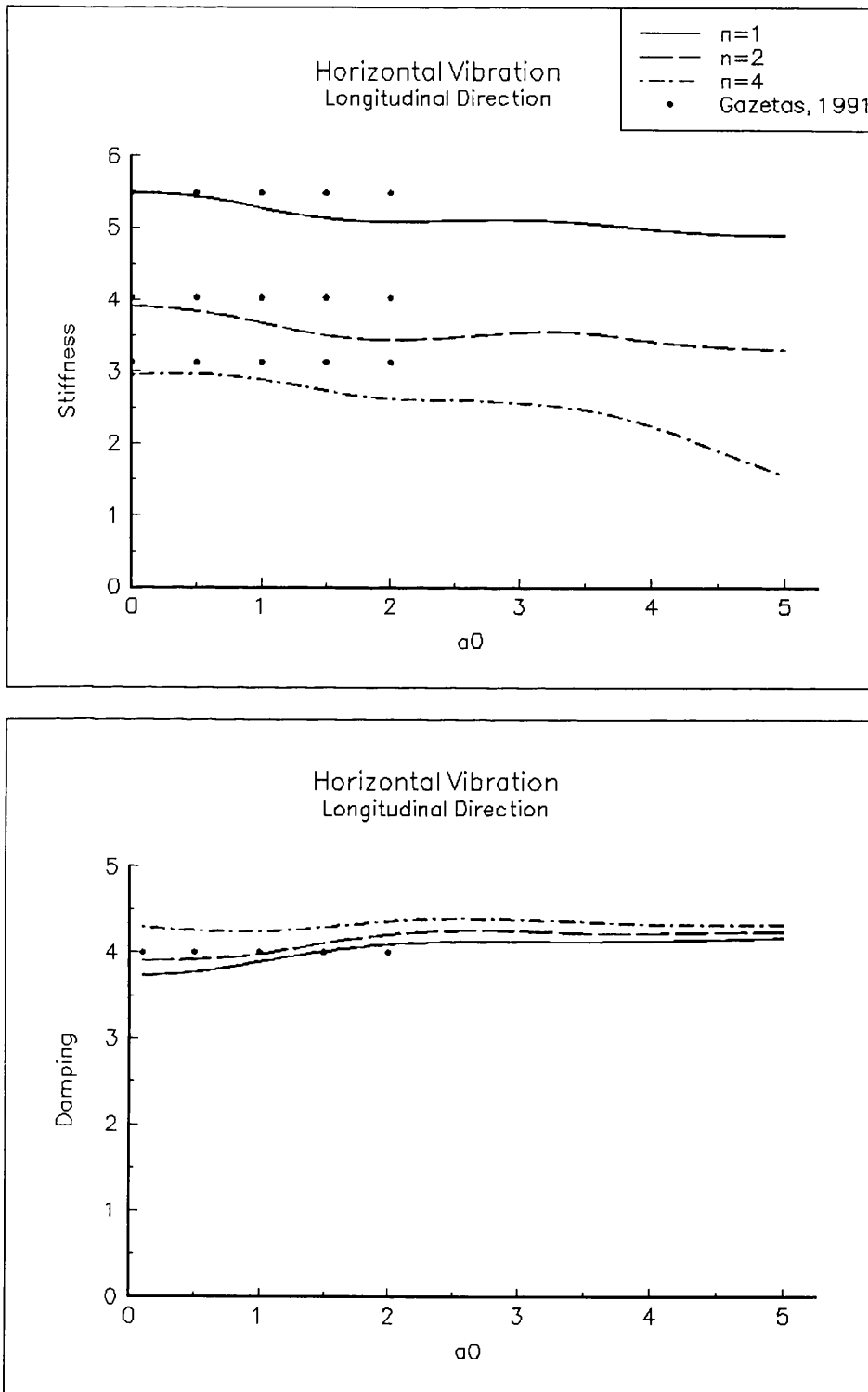


Figure 7.7: Effect of aspect ratio on horizontal impedance (longitudinal direction)

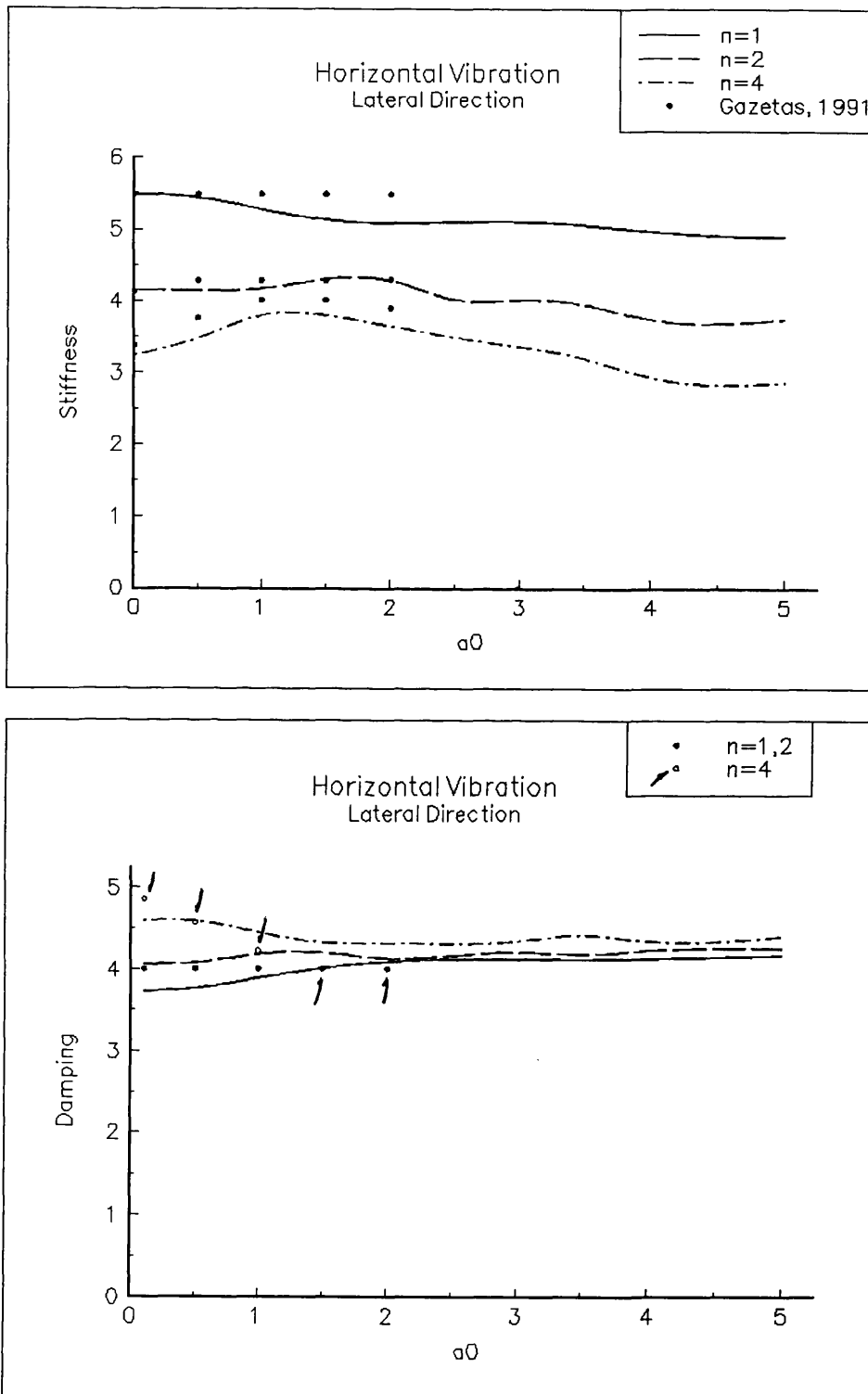


Figure 7.8: Effect of aspect ratio on horizontal impedance (lateral direction)

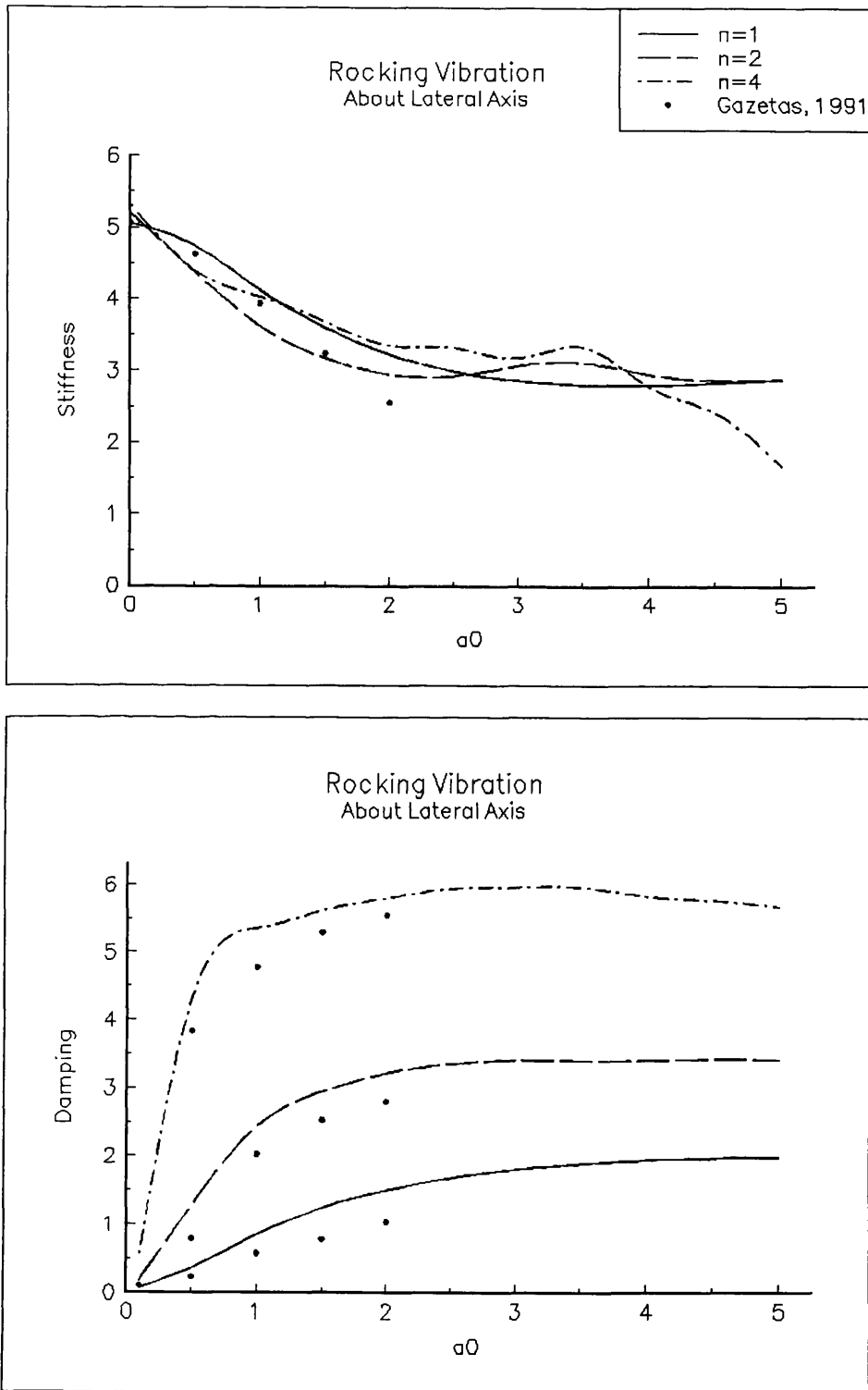


Figure 7.9: Effect of aspect ratio on rocking impedance (about lateral axis)

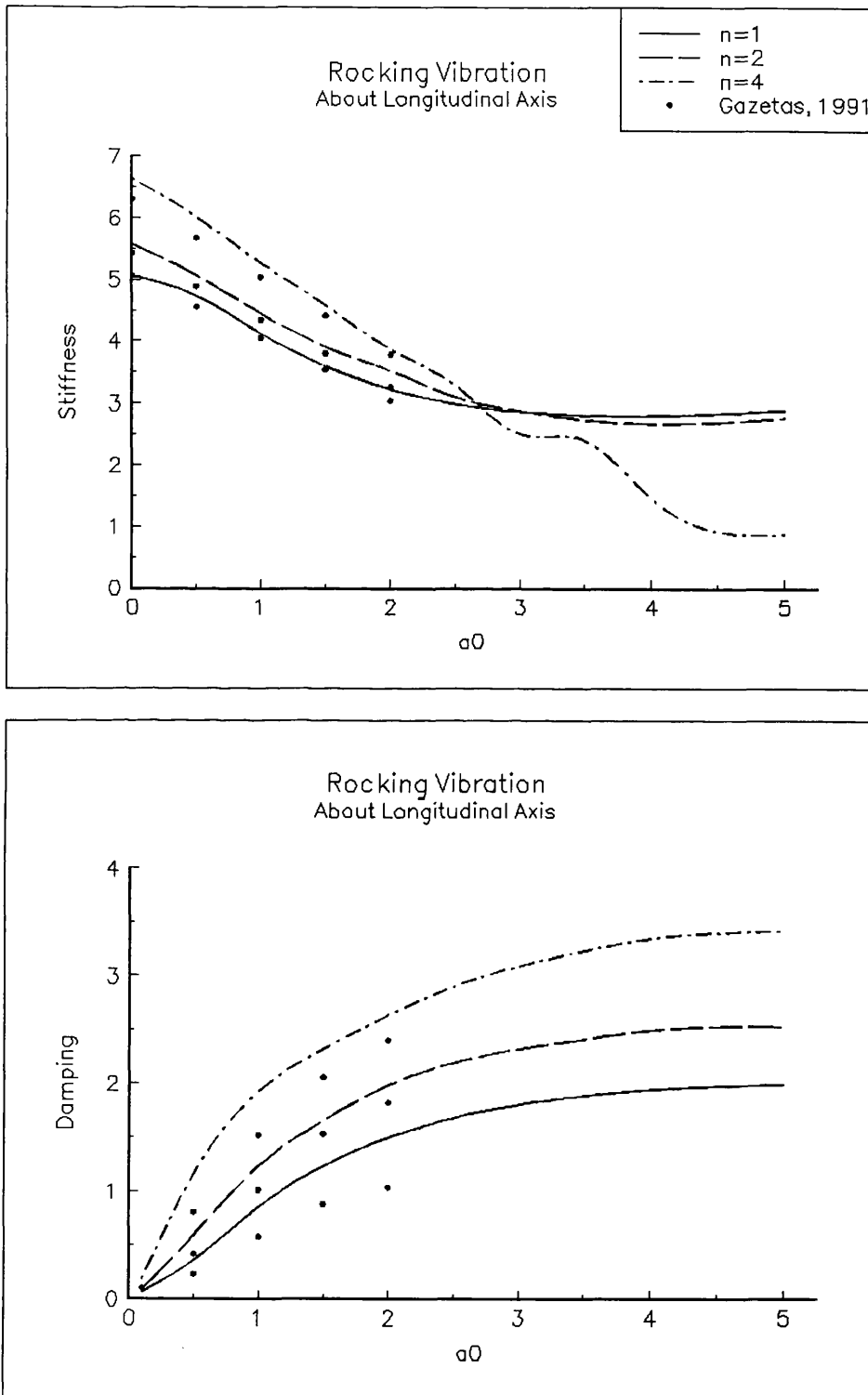


Figure 7.10: Effect of aspect ratio on rocking impedance (about longitudinal axis)

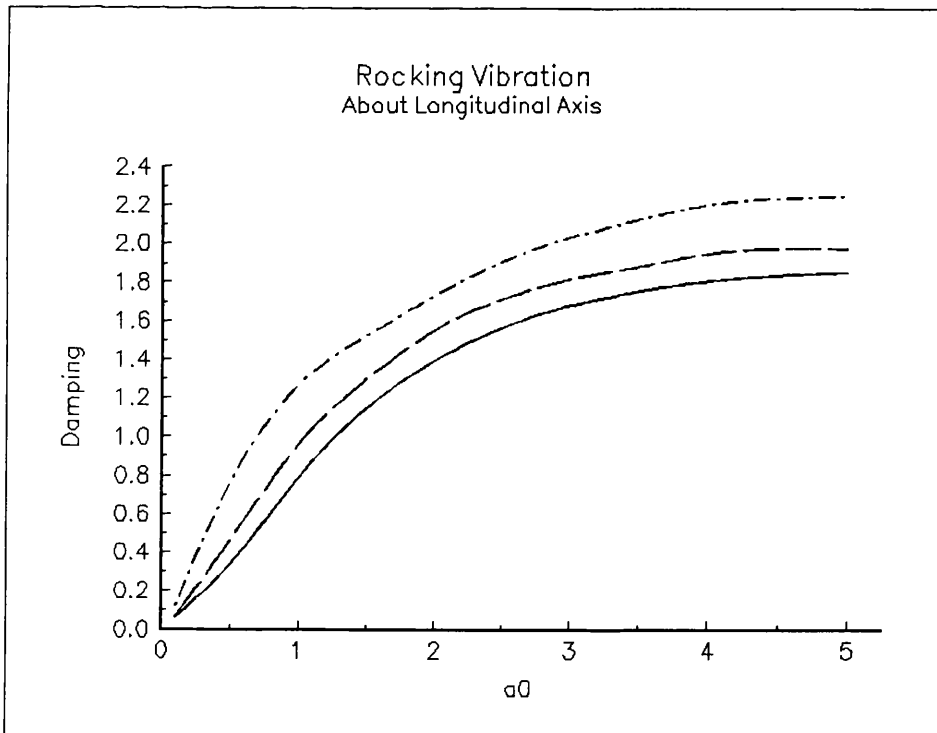
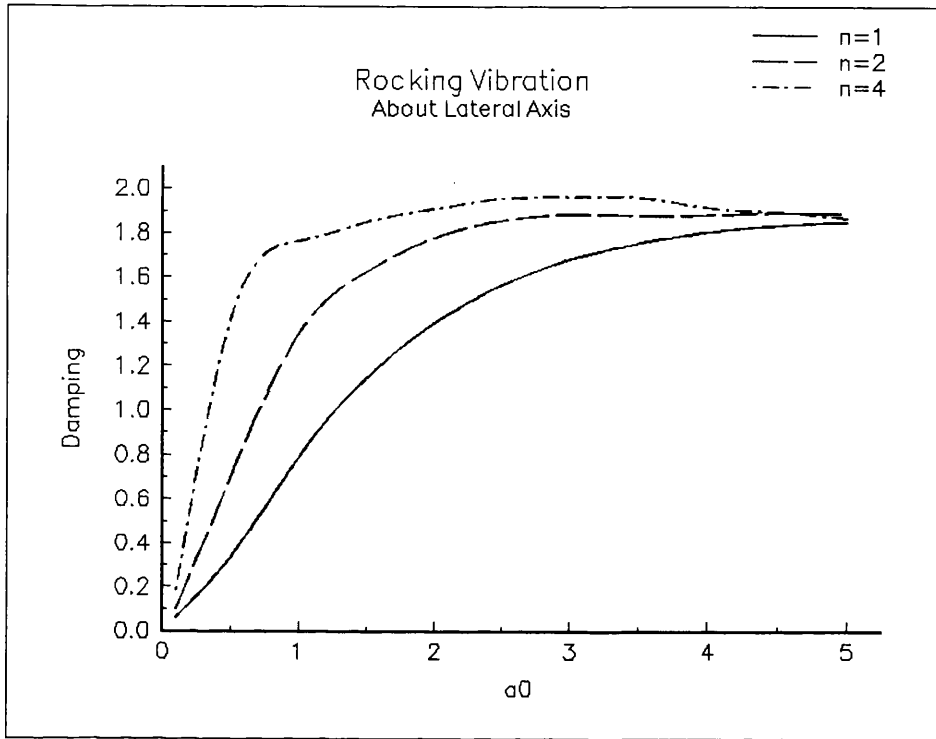
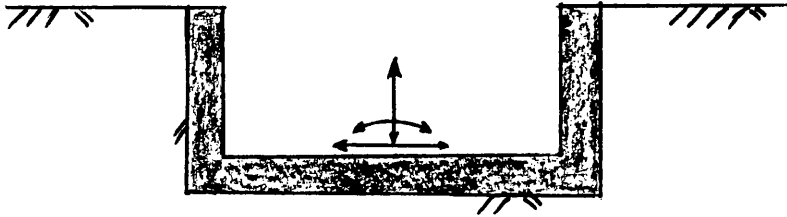
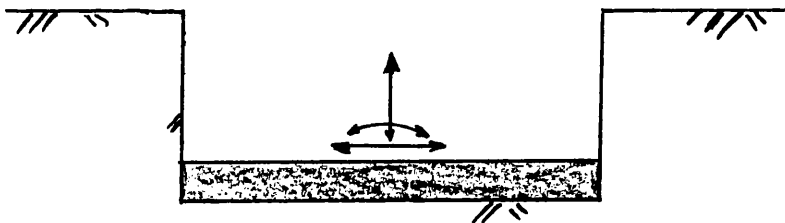


Figure 7.11: Asymptotic damping behaviour in rocking vibration



Cast-In-Place Foundation



Trench Foundation

Figure 7.12: The embedded foundation

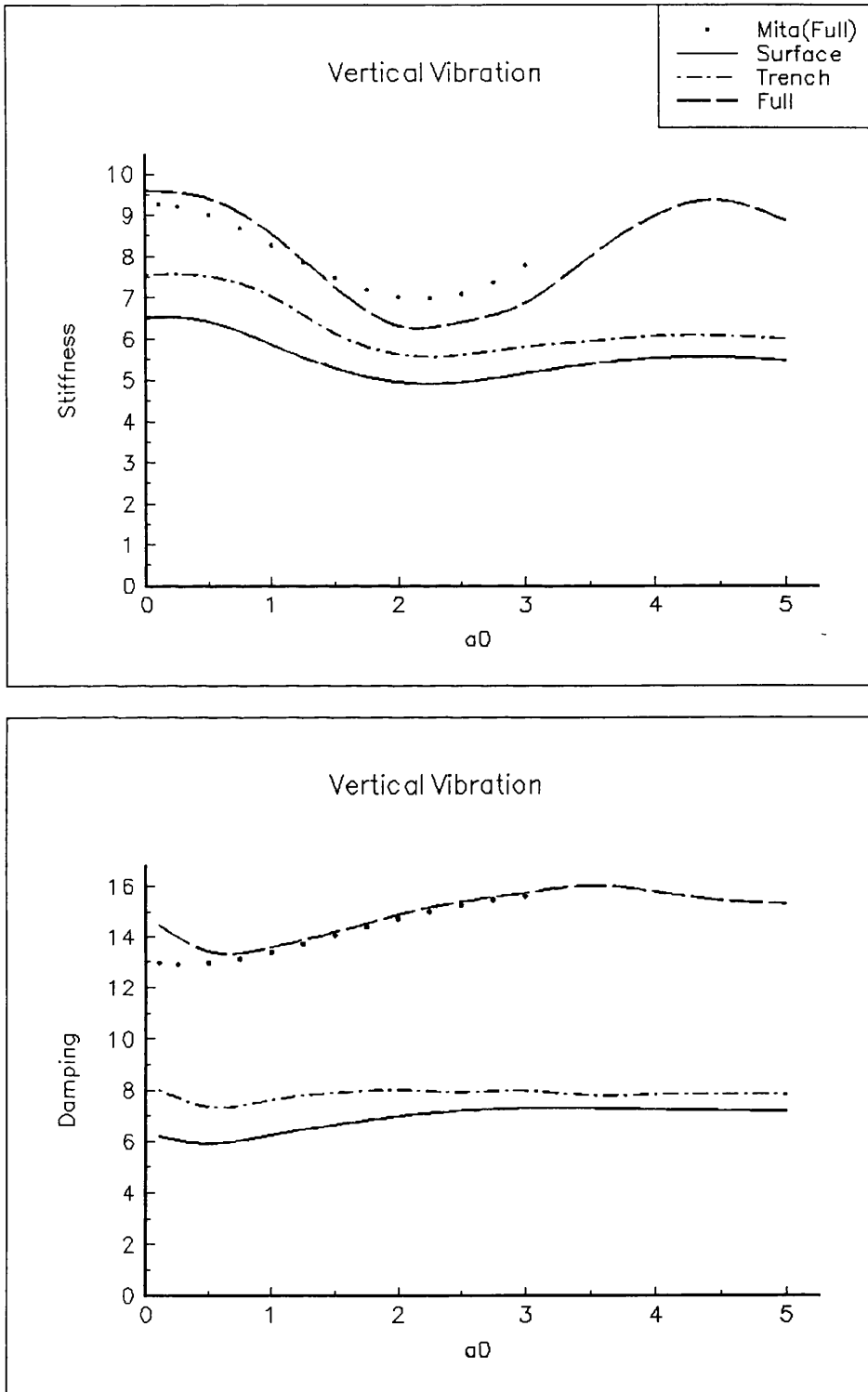


Figure 7.13: Vertical impedance of embedded square foundations

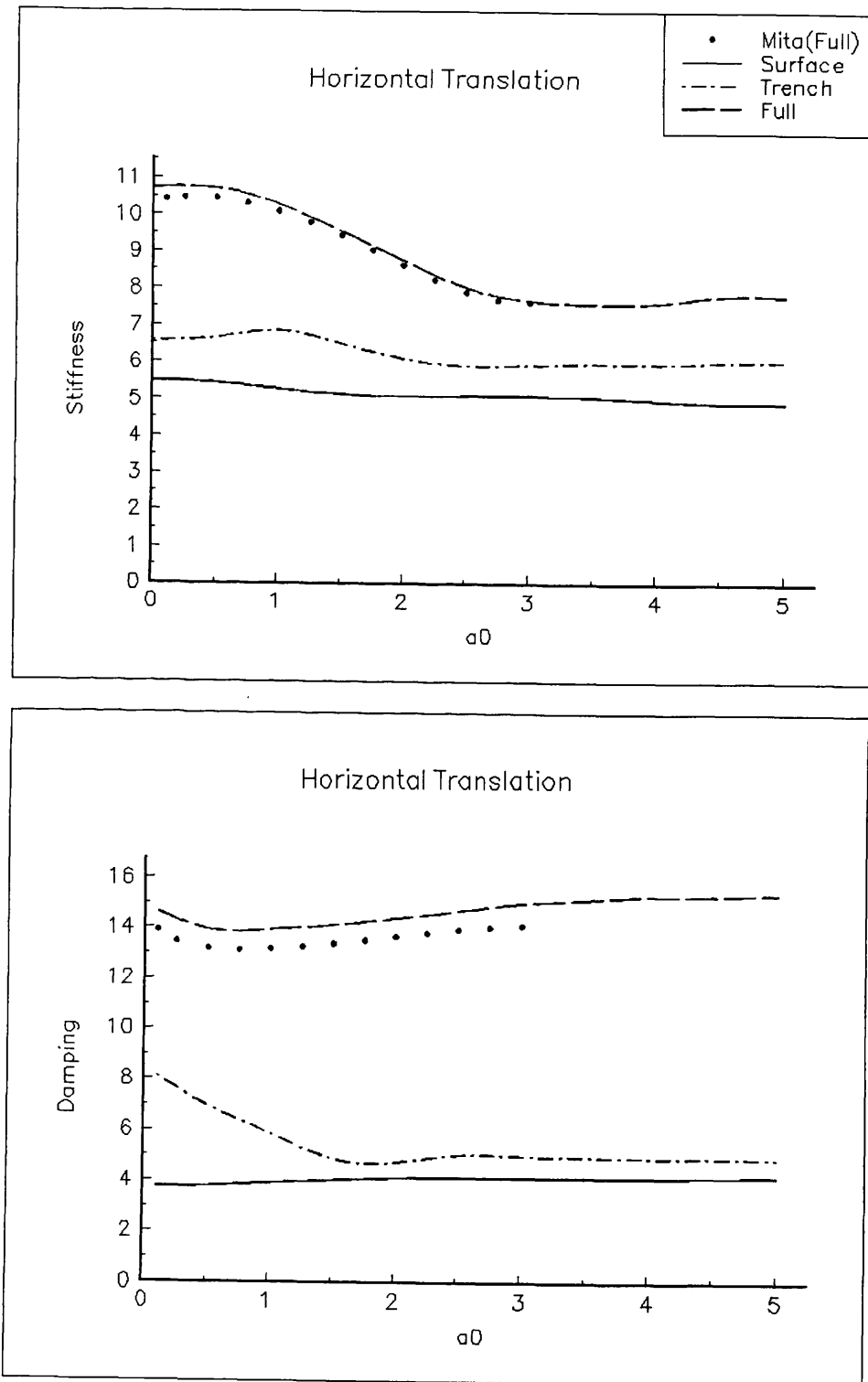


Figure 7.14: Horizontal impedance of embedded square foundations

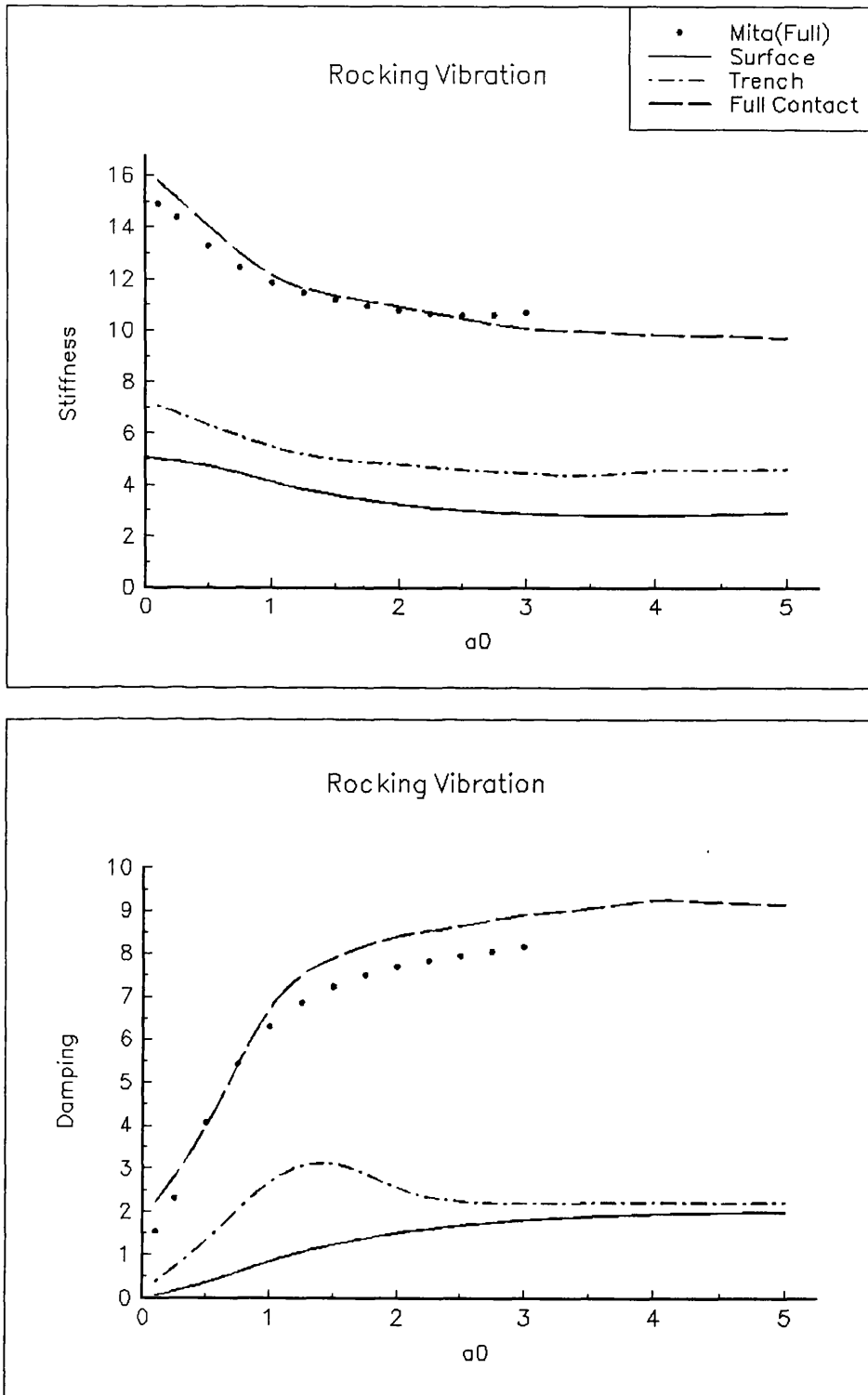


Figure 7.15: Rocking impedance of embedded square foundations

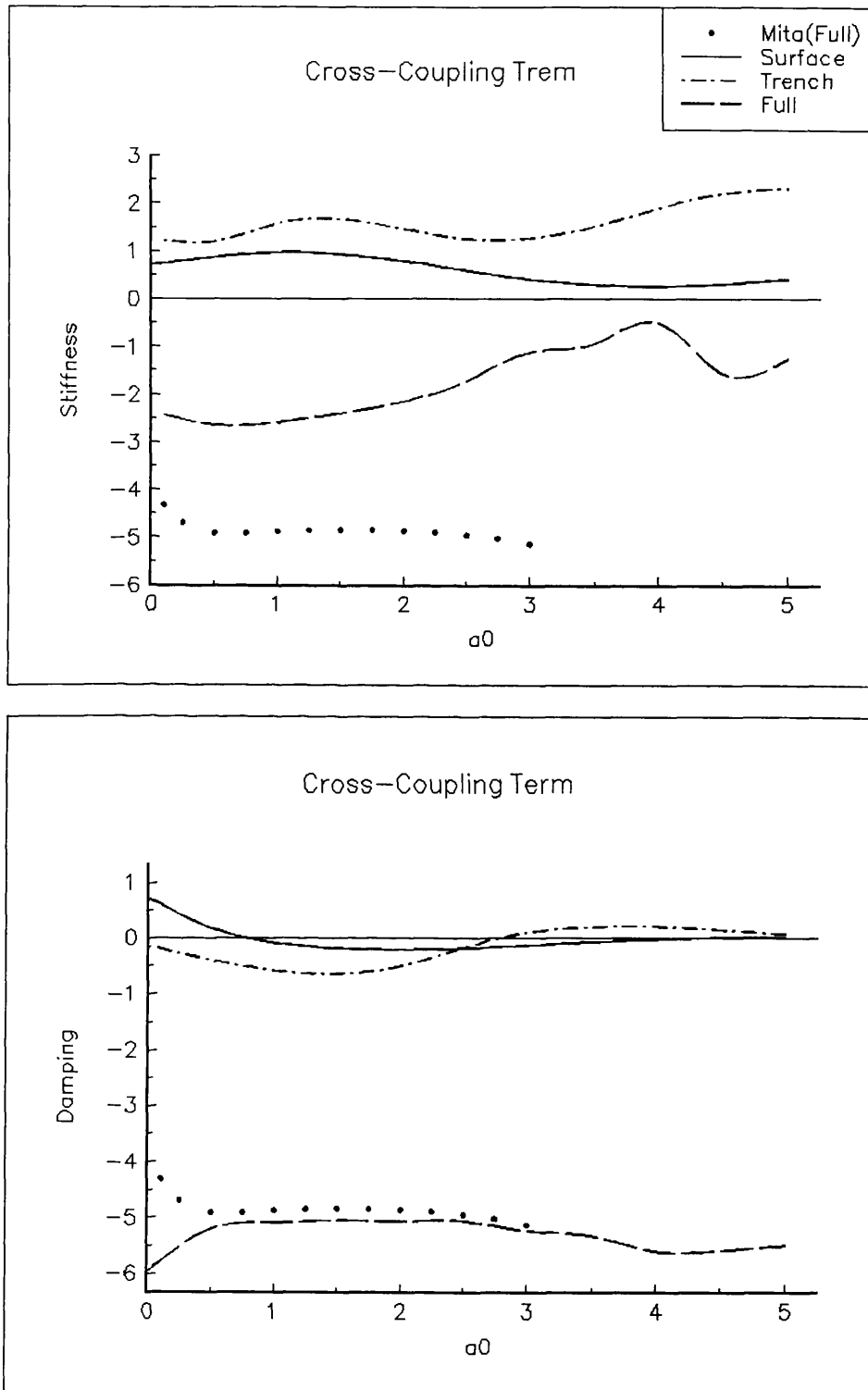


Figure 7.16: Cross-coupled impedance of embedded square foundations

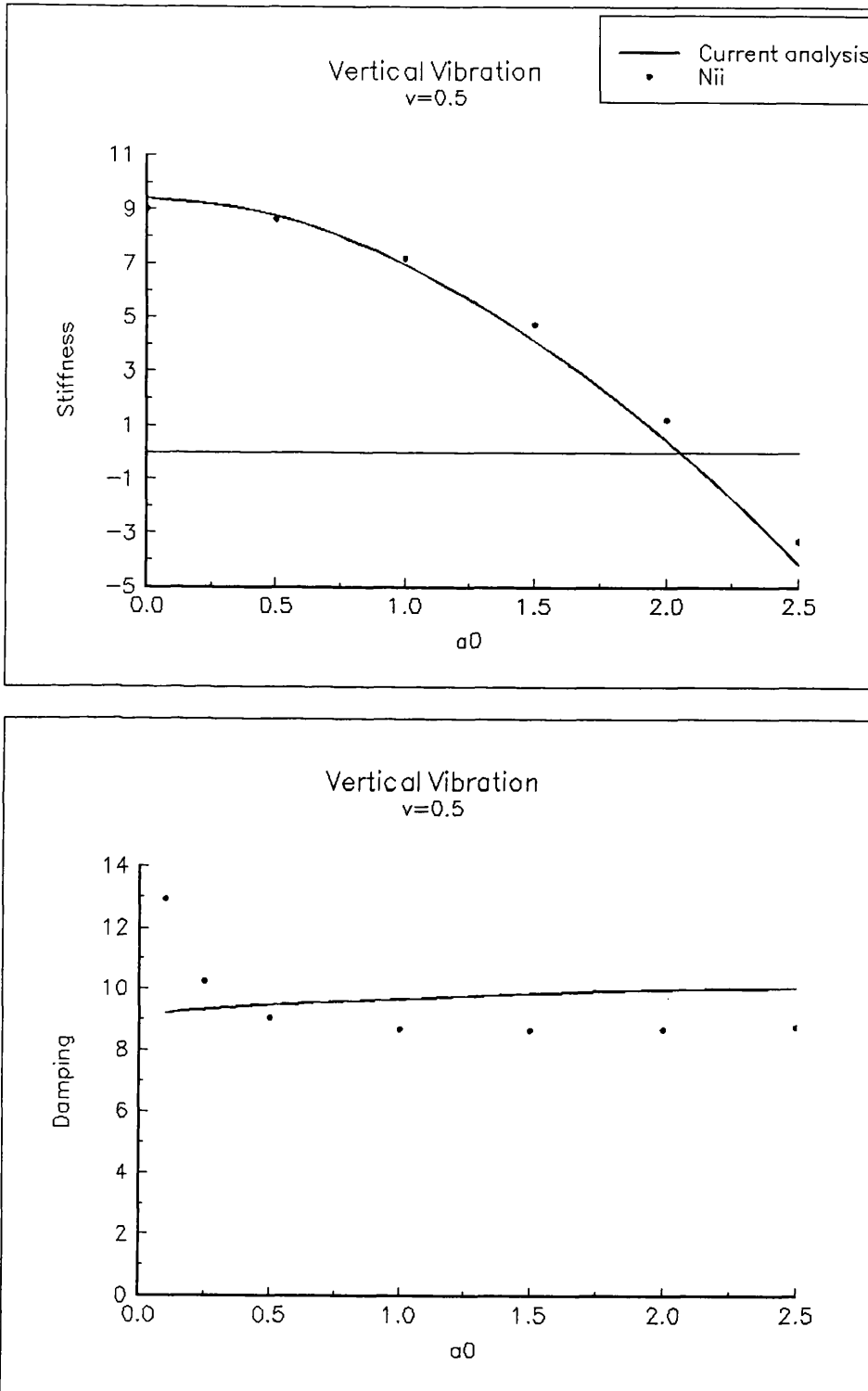


Figure 7.17: Vertical impedances of square foundations on an incompressible halfspace

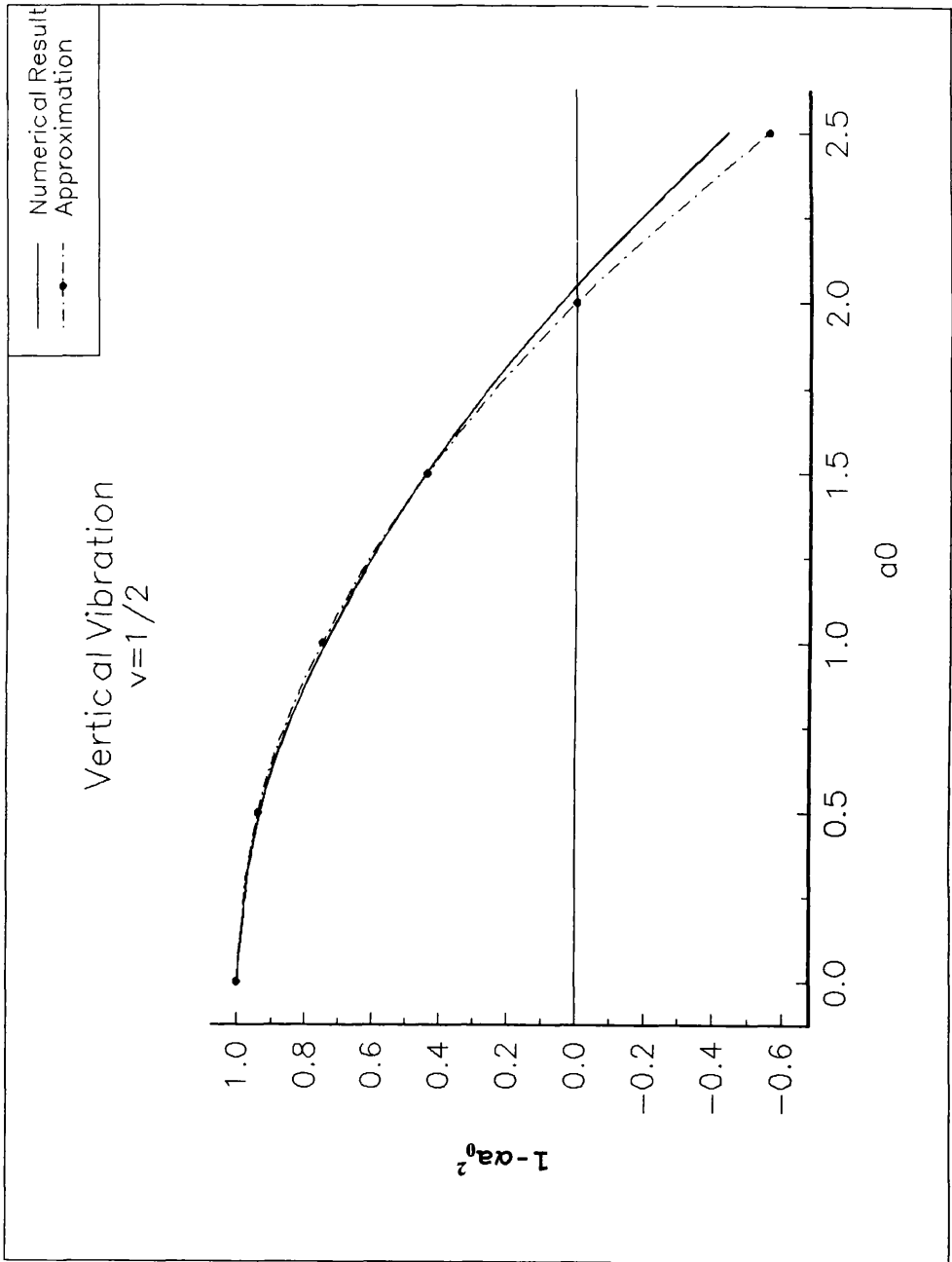


Figure 7.18: The "participating mass" model

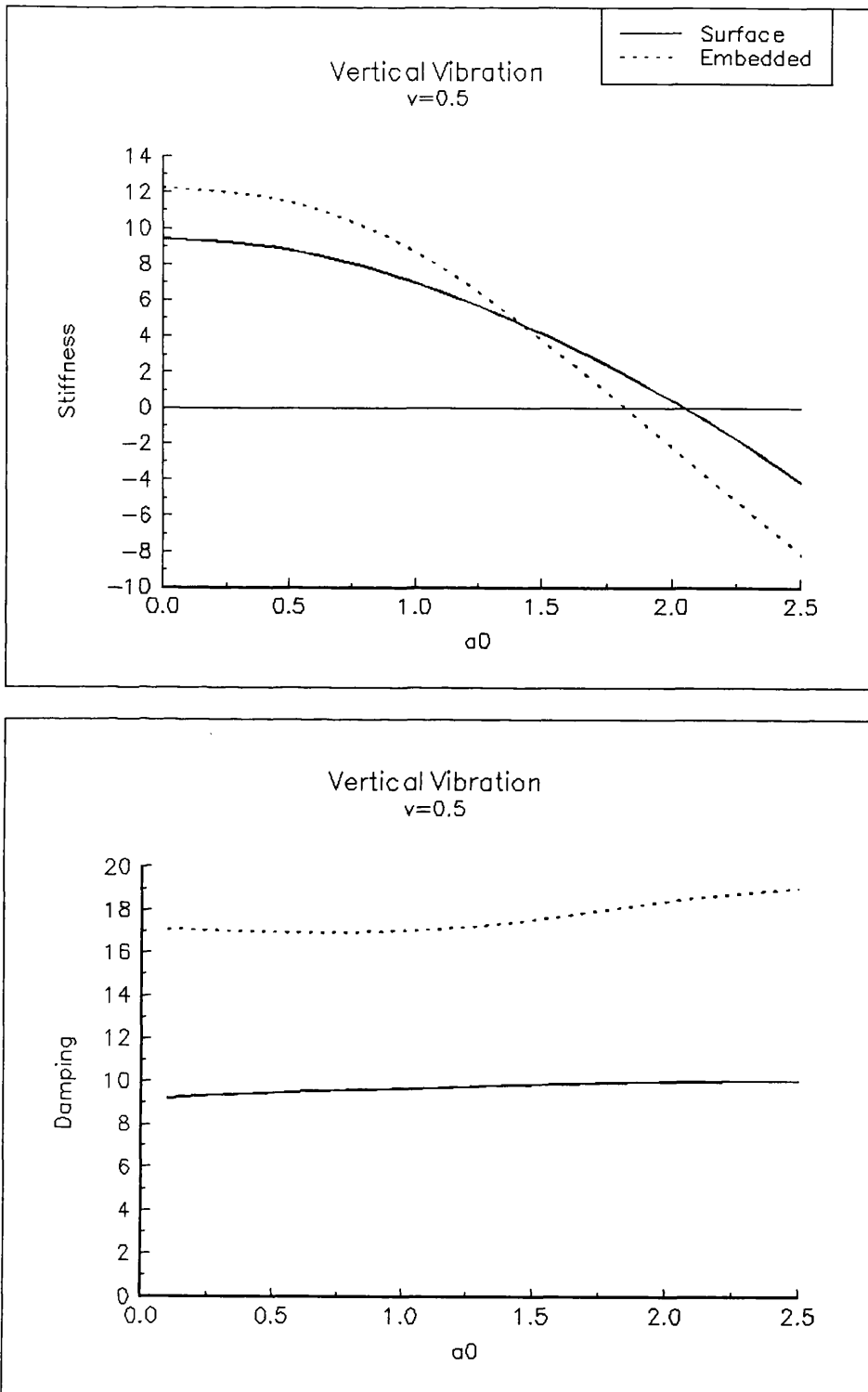


Figure 7.19: Vertical impedances of square foundations embedded in incompressible soils

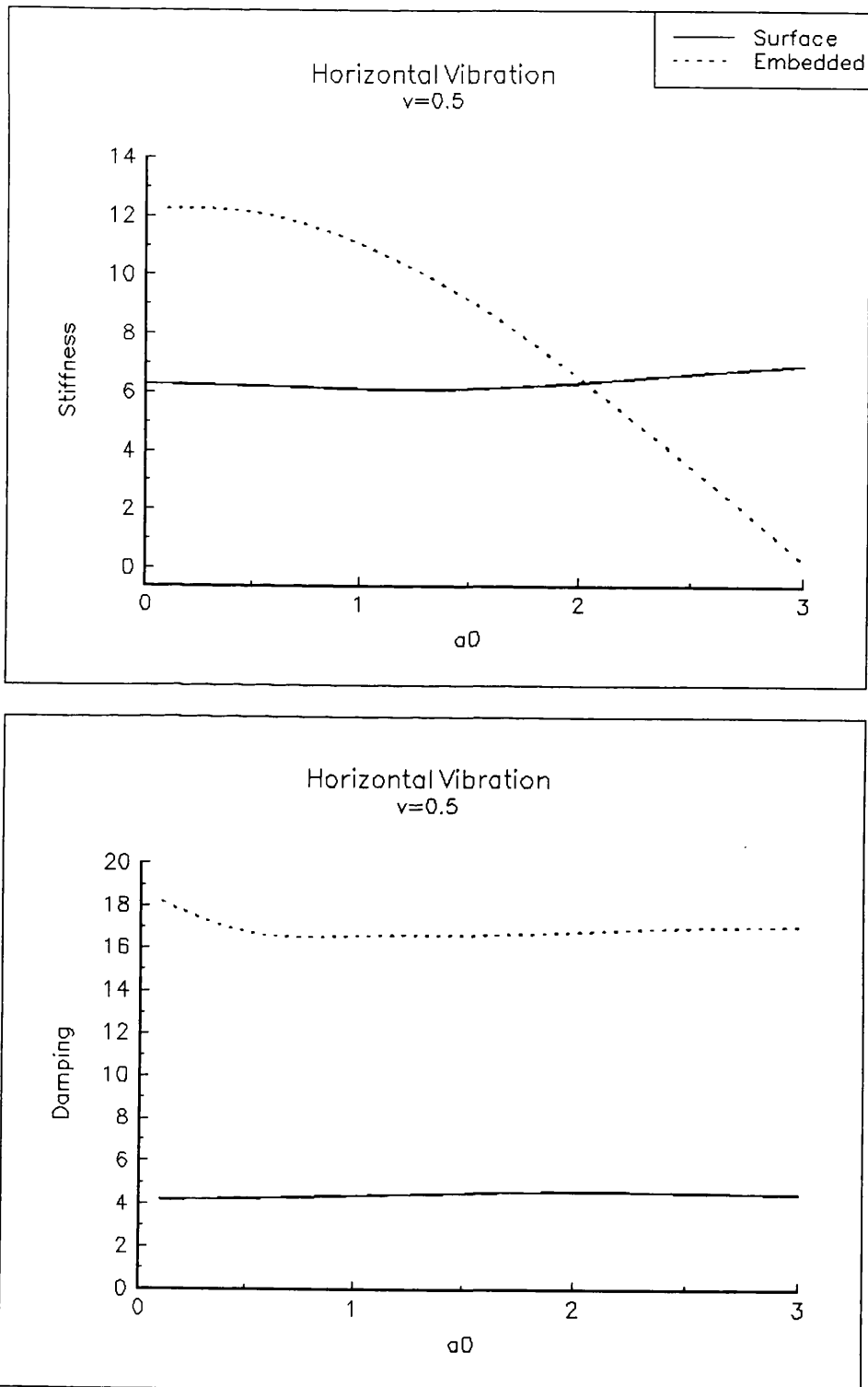


Figure 7.20: Horizontal impedances of square foundations embedded in incompressible soils

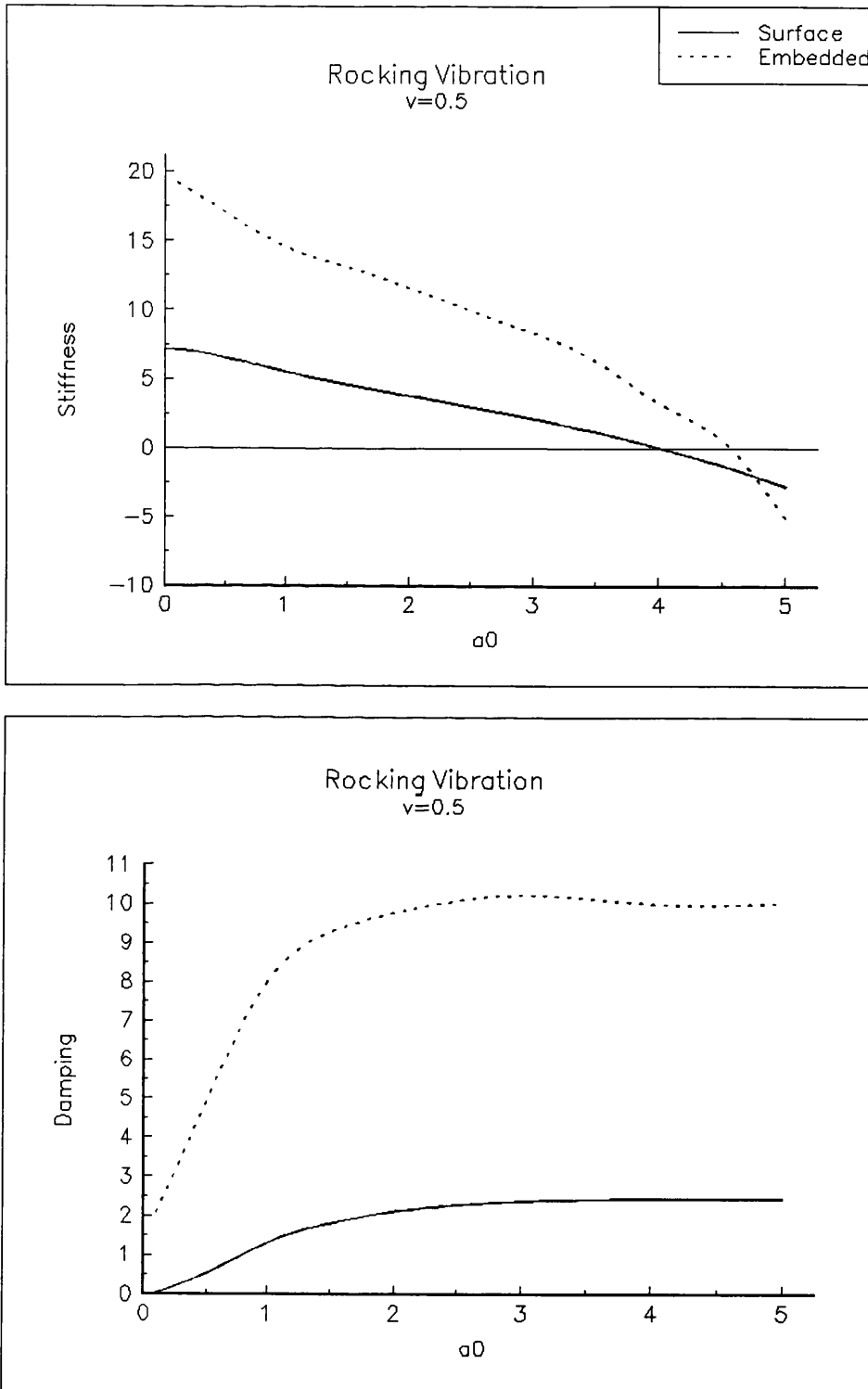


Figure 7.21: Rocking impedances of square foundations embedded in incompressible soils

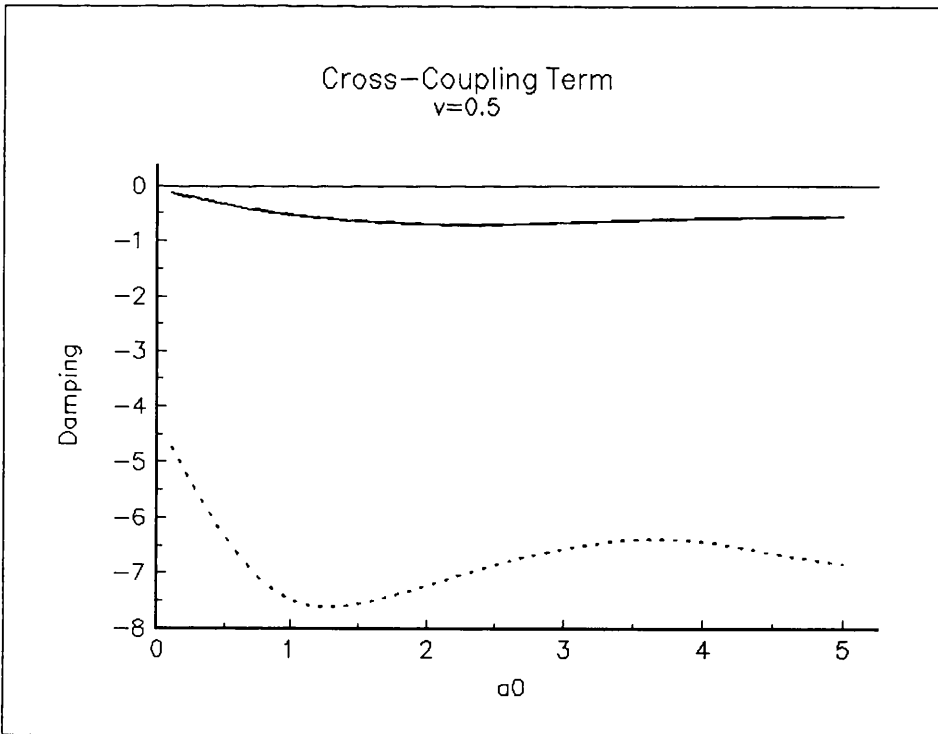
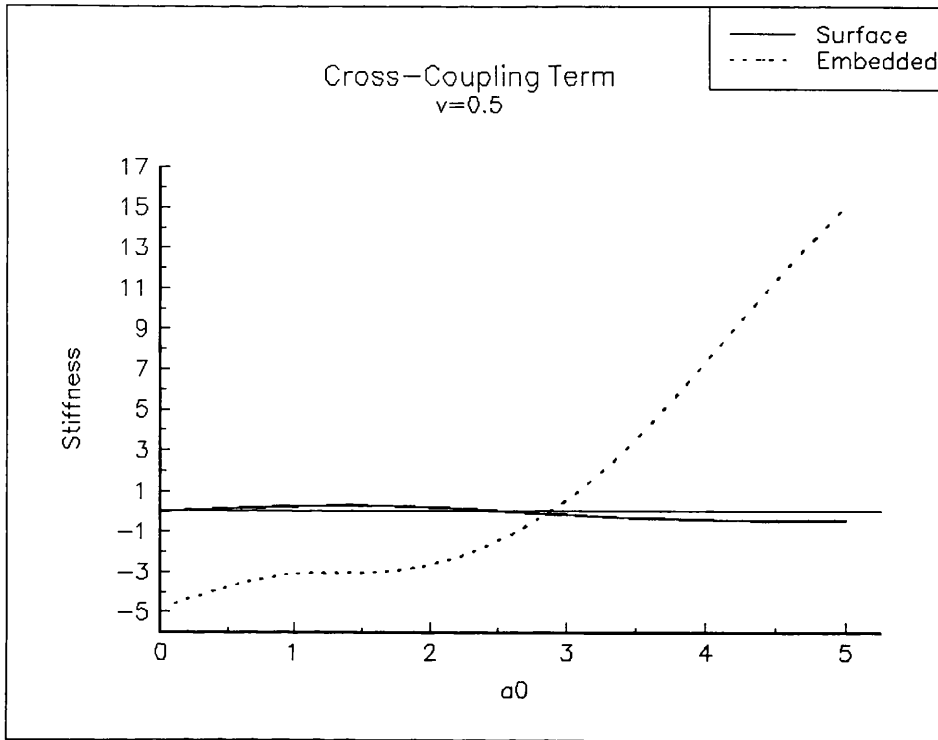


Figure 7.22: Cross-coupled impedances of square foundations embedded in incompressible soils

CHAPTER 8

CONCLUSIONS

8.1 Summary And Conclusions

The central theme of this thesis has been the further extension and refinement of boundary element methods for the analysis of machine foundations, pertaining to various (translational and rotational) modes of vibration, particularly at high frequencies. This work involves both rigorous theoretical studies and effective numerical techniques for the solution of the boundary integral equations.

This thesis includes an exploration of the following topics, relating to the implementation of the boundary element method:

(1) The mathematical properties and physical significance of the fundamental solutions dictate the strategy for the solution of the integral equations. Consequently, the characteristics of the fundamental solutions are studied in Chapter II. The special fundamental solutions developed in this thesis for Poisson's ratio $=1/2$ facilitates application of the boundary element method to problems of incompressible soil (in which the dilatational-wave velocities are, theoretically, infinite).

(2) The evaluation of the integrals over the boundary elements is the most time-consuming part of the boundary element analyses, and the accuracy of these computations largely determines the accuracy of numerical results. Significant effort has been devoted to the problem of how these integrals

may be computed expeditiously. The advanced integration schemes developed in chapter III and IV are based on an improved understanding of the integrals in the boundary element method and are substantiated by the results of extensive, rigorous numerical studies. These effective integration methods could be implemented within other boundary element method codes without much difficulty.

(3) The geometry of machine foundation problems normally suggests use of halfspace models. As the capacity of computers is finite, however, the treatment of semi-infinite surfaces creates serious numerical difficulties. The novel infinite boundary element proposed in chapter V is capable of providing an efficient means for including far-field effects, without the necessity of explicit discrete representation outside the near field.

(4) An effective and rigorous method of dealing with singularities at the boundaries is proposed which involves incorporating the boundary conditions during the assembly of the system equations. This approach can deal with problems of traction discontinuities at corners and edges without increasing the number of degrees of freedom. Consequently, computational costs can be reduced significantly which enables the program to analyze larger problems. Use of this technique could provide significant improvement in computational efficiency for boundary element analyses in general.

(5) The special purpose program (extending to c. 6000 FORTRAN statements) for the analysis of three-dimensional rectangular machine foundations is described in Chapter VI. The application of advanced computer technology (vectorization) in this research accelerates the calculations and, consequently, reduces the computational cost. In general, the "speed-up" due to vectorization reduces computational times by a factor of

about three.

(6) Various results for surface and embedded rectangular machine foundations are presented in chapter VII to illustrate the potential of the infinite boundary element formulation. Several of these results are new and will be published in due course.

In conclusion, significant improvements in the current boundary element techniques, which are by no means limited to the machine foundation problems, have been achieved in the present study. Highly accurate results for three-dimensional machine foundation problems can be obtained by using this advanced boundary element methodology.

8.2 Recommendations For Future Work

The work described in this thesis includes a number of significant advances in dynamic boundary element techniques, in the context of the analysis of machine foundation problems. Further work in this area might include the following:

(1) parametric studies to explore the effects of the following parameters in more detail on the high-frequency response of machine foundations:

- a) the Poisson's ratio of the soil,
- b) the material damping of the soil, and
- c) the depth of embedment.

Note: Some of this work is being undertaken at the time of writing.

(2) Investigation of the intermediate case of frictional slippage at the soil-foundation interface.

(3) Development of simple engineering formulae which can be used for preliminary design purposes and to enhance understanding of the interplay between the key parameters.

(4) The analysis of flexible foundations subjected to dynamic loads.

(5) Analysis of deep rigid (pier) foundations under dynamic loads.

(6) Experimental verification of the design procedures and the predicted dynamic response of machine foundations.

(7) Implementation of "parallel" algorithms.

Some of these issues(1,4,5) can be carried out using the current computer program or with some minor modifications and the results of the parametric studies(1) can be used to develop engineering formulae(3).

The application of boundary element analyses to practical problems requires significant in-core memory capacity and a powerful processor. Because the boundary element method has inherent parallelism and super-computing facilities are becoming more widely available, development of parallel programs should offer substantial benefits in the future.

The extension of the present study to three-dimensional transient problems is currently under way. The focus in this work is the transient response of layered soils and pavements to nondestructive impact loading(Davies et al, 1993).

REFERENCES

- [1] Achenbach, J.D. (1976), *Wave Propagation In Elastic Solids*, North-Holland Publishing Company.
- [2] Achenbach, J.D., Gautesen, A.K., and McMaken, H. (1982), *Ray Methods For Waves In Elastic Solids*, Pitman Publishing Inc., Massachusetts.
- [3] Ahmad, S. and Banerjee, P.K. (1988a), "Multi-domain BEM For Two-dimensional Problems Of Elastodynamics," *Int. J. For Numerical Methods In Engineering*, Vol. 26, pp. 891-911.
- [4] Ahmad, S. and Banerjee, P.K. (1988b), "Time-domain Transient Elastodynamic Analysis Of 3-D Solids By BEM," *Int. J. For Numerical Methods In Engrg.*, Vol. 26, pp. 1709-1728.
- [5] Ahmad, S. and Bharadwaj, A. (1991), "Horizontal Impedance Of Embedded Strip Foundations In Layered Soil," *Journal of Geotechnical Engrg.*, ASCE, Vol. 117, No. 7, pp. 1021-1041.
- [6] Alarcon, E., Cano, J.J. and Dominguez, J. (1989), "Boundary Element Approach To The Dynamic Stiffness Functions Of Circular Foundations," *Int. J. For Numerical Methods In Geomechanics*, Vol. 13, pp. 645-664.
- [7] Aliabadi, M.H. and Hall, W.S. (1987a), "Weighted Gaussian Methods For Three-Dimensional Boundary Element Kernel Integration," *Communications In Applied Numerical Methods*, Vol. 3, pp. 89-96.
- [8] Aliabadi, M.H. and Hall, W.S. (1987b), "Analytical Removal Of Singularities And One-dimensional Integration Of Three-dimensional Boundary Element Method Kernels," *Engrg. Analysis*, Vol 4, No 1, pp 21-24.
- [9] Aliabadi, M.H., Hall, W.S., and Hibbs, T.T. (1987), "Exact Singularity Cancelling For The Potential Kernel In The Boundary Element Method," *Communications in Applied Numerical Methods*, Vol. 3, pp. 123-128.
- [10] Aliabadi, M.H., Hall, W.S., and Phemister, T.G. (1985), "Taylor Expansions For Singular Kernels In The Boundary Element Method," *Int. J. For Num. Meth. In Engrg*, Vol. 21, pp. 2221-2236.
- [11] Aliabadi, M.H. and Rooke, D.P. (1991), *Numerical Fracture Mechanics*, Computational Mechanics Publications, Southampton.
- [12] Anandakrisnan, M. and Krishnaswamy, N.R. (1972), "Response of embedded footings to vertical vibrations," *J. of The Soil Mech. and Foundations*, ASCE, Vol. 99, SM10, pp. 863-883.
- [13] Antes, H. and von Estorff, O. (1989), "Dynamic Response Analysis Of Rigid Foundations And Of Elastic Structures By Boundary Element Procedures," *Soil Dynamics and Earthquake Engineering*, Vol. 8, pp. 68-74.
- [14] Arnold, R.N., Bycroft, G.N., and Warburton, G.B. (1955), "Forced Vibrations of a body on an infinite elastic solid," *Journal of Applied Mechanics*, ASME, pp. 391-400.
- [15] Awojobi, A.O. (1971), "Approximate solution of high-frequency-factor vibrations of rigid bodies on elastic media," *Journal of Applied Mechanics*, ASME, pp. 111-117.
- [16] Awojobi, A.O. and Grootenhuis, P. (1965), "Vibration of rigid bodies on semi-infinite elastic media," *Proc. of The Royal Society*, A287, 27-63.
- [17] Ayala, G. and Gomez, R. (1979), "A General Produce For Solving Three Dimensional Elasticity Problems In Geomechanics," *3rd Int. Conf. on Num. Meth. In Geomechanics*, Achen, pp. 3-13.
- [18] Banerjee, P.K. and Butterfield, R. (1981), *Boundary Element Methods In Engineering Science*, McGraw-Hill, London.
- [19] Banerjee, P.K. and Mamoon, S.M. (1990), "A fundamental solution due to a periodic point force in the interior of an elastic halfspace," *Earthquake Engineering and Structural Dynamics*, Vol. 19, pp.91-105.

- [20] Banerjee, P.K., Wang, H.C. and Ahmad, S.(1992), "Multiregion Periodic Dynamic Analysis By BEM of 2D, 3D and Axisymmetric Problems," *Advanced Dynamic Analysis by Boundary Element Methods, Developments in Boundary Element Methods-7*, Banerjee, P.K. and Kobayashi, S.(eds.), Chapter 2.
- [21] Banerjee, P.K., Wilson, R.B., and Miller, N.(1985), "Development Of A Large BEM System For Three-dimensional Inelastic Analysis," Proc. ASME Conf. on Advanced Boundary Element Analysis.
- [22] Barkan, D.D.(1962), *Dynamics of Bases and Foundations*, McGraw-Hill.
- [23] Barnhill, R.E.(1968a), "An Error Analysis For Numerical Multiple Integration. I," *Mathematics of Computation*, Vol 22, pp. 98-109.
- [24] Barnhill, R.E.(1968b), "An Error Analysis For Numerical Multiple Integration. II," *Mathematics of Computation*, Vol 22, pp 286-292.
- [25] Bathe, K.J.(1982), *Finite Element Procedures In Engineering Analysis*, Prentice-Hall, Inc.
- [26] Becker, A.A.(1992), *The Boundary Element Method in Engineering, A complete Course*, McGraw-Hill Co., London.
- [27] Beer, G. and Watson, J.O.(1989), "Infinite boundary elements, " *Int. J. for Num. Meth. In Engrg.*, Vol 28, pp 1233-1247.
- [28] Beer, G., Watson, J.O. and Swoboda, G.(1987), "Three-dimensional analysis of tunnels using infinite boundary elements," *Computers and Geotechnics*, Vol 3, pp 37-58.
- [29] Beredugo, Y.O. and Novak, M.(1972), "Coupled horizontal and rocking vibration of embedded footings," *Canadian Geotech. J.*, Vol. 9, No. 4, 477-497.
- [30] Berger, B.S. and Bernard, P.S.(1983), "The Numerical Integration Of Green's Functions," *J. of Applied Mechanics*, ASME, Vol. 50, pp. 456-459.
- [31] Beskos, D.E.(1987), "Boundary element methods in dynamic analysis," *Appl. Mech. Reviews*, Vol. 40, No. 1, pp. 1-23.
- [32] Bettess, P.(1992), *Infinite Elements*, Penshaw Press, Sunderland, UK.
- [33] Bettess, P. and Bettess, J.A.(1991), "Infinite elements for dynamic problems: part 1 and 2," *Engineering Computations*, Vol. 8, pp. 99-151.
- [34] *Boundary Elements Abstracts and Newsletters*, Computational Mechanics Publications, UK.
- [35] Brebbia, C.A.(1980), *The Boundary Element Method For Engineers*, Pentech Press, London.
- [36] Brebbia, C.A.(1989), "Fundamental of the boundary element method," in *Supercomputing In Engineering Structures*, eds. Melli, P. and Brebbia, C.A., Springer-Verlag, Berlin.
- [37] Bromwich, T.J.I'A(1908), *An Introduction Of The Theory Of Infinite Series*, Macmillan and Co., Limited, London.
- [38] Chapra, S.C. and Canale, R.P.(1989), *Numerical Methods For Engineers*, McGraw-Hill Co.
- [39] Chen, H.T.J.(1984), "Dynamic Stiffness Of Nonuniformly Embedded Foundations," Dissertation presented to the University of Texas, at Austin, Tex. in partial fulfilment of the requirements for the degree of Doctor of Philos.
- [40] Chuhan, Z., Chongmin, S., and Pekau, O.A.(1991), "Infinite boundary elements for dynamic problems of 3-D half space, " *Int. J. For Num. Meth. In Engrg.*, Vol. 31, pp. 447-462.
- [41] Ciskowski, R.D., Sonnad, V., and Xie, K.(1989), "Parallel Implementation On The ICAP/3090 Of A Boundary Element Method Formulation For Fractional Operator Modeled Viscoelastodynamic Structures," in *Boundary Element Methods In Engineering*, Proceedings of the International Symposium on

- Boundary Element Methods: Advances in Solid and Fluid Mechanics, Annigeri, B.S. and Tseng, K. (eds.), pp. 487-491.
- [42] Crockett, J.H.A. and Hammond, R.E.R. (1948), "The dynamic principles of machine foundations and ground," *Proc. of The Inst. of Mechanical Engrs.*, London, Vol. 160, pp. 512-523.
- [43] Crouse, C.B., Hushmand, B., Luco, J.E., and Wong, H.L. (1990), "Foundation impedance functions: theory versus experiment," *J. of Geotech. Engrg.*, ASCE, Vol. 116, No. 3, pp. 432-449.
- [44] Crotty, J.M. and Wardle, L.J. (1985), "Boundary Integral Analysis Of Piecewise Homogeneous Media With Structural Discontinuities," *Int. J. Rock Mech. Min. Sci. & Geomech. Abstr.*, Vol. 22, No. 6, pp. 419-427.
- [45] Cruse, T.A. (1968), "A Direct Formulation And Numerical Solution Of The General Transient Elastodynamic Problem. II," *Journal of Mathematical Analysis and Applications*, Vol. 22, pp. 341-355.
- [46] Cruse, T.A. and Rizzo, F.J. (1968), "A Direct Formulation And Numerical Solution Of The General Transient Elastodynamic Problem. I," *J. of Mathematical Analysis and Applications*, Vol. 22, pp. 244-259.
- [47] Cruse, T.A. (1969) "Numerical Solutions In Three Dimensional Elastostatics," *Int. J. Solids Structures*, Vol 5, pp. 1259-1274.
- [48] Cruse, T.A. (1974), "An Improved Boundary-Integral Equation Method For Three Dimensional Elastic Stress Analysis," *Computers & Structures*, Vol. 4, pp. 741-754.
- [49] Davies, T.G. (1991), "Machine foundations," Chapter 8 in *Cyclic Loading of Soil-From Theory To Practice*, Brown, S.F. and O'Reilly, M. (eds), Blackie Publ. Co.
- [50] Davies, T.G. (1993), "Numerical Implementation," Chapter 4 in *Boundary Element Techniques in Geomechanics*, Manolis, G.D. and Davies, T.G. (eds), Computational Mechanics Publications, UK.
- [51] Davies, T.G. and Bu, S. (1993), "An infinite element for high-frequency boundary element analyses of machine foundation response," in *Soil Dynamics and Earthquake Engineering VI*, Cakmak, A.S. and Brebbia, C.A. (eds.), Elsevier Applied Science, pp. 619-631.
- [52] Davies, T.G., Chan, A.H.C., and Bu, S. (1993), "Dynamic (boundary element) analysis of nondestructive impact tests on layered soils and pavements," SERC Grant, Glasgow University, Scotland.
- [53] Davis, P.F. and Rabinowitz, P. (1984), *Methods Of Numerical Integration*, Academic Press, Inc.
- [54] de Barros, F.C.P. and Luco, J.E. (1990), "Discrete Models For Vertical Vibrations of surface and embedded foundations," *Earthq. Engrg. and Struct. Dynamics*, Vol. 19, pp. 289-303.
- [55] Delves, L.M. and Walsh, J. (1974), *Numerical Solution of Integral Equations*, Clarendon Press, Oxford.
- [56] Dobry, R. and Gazetas, G. (1985), "Dynamic Stiffness And Damping Of Foundations By Simple Methods," in *Vibration Problems In Geotechnical Engineering*, Gazetas, G. and Selig, E.T. eds, ASCE, pp. 75-107.
- [57] Dobry, R. and Gazetas, G. (1986) "Dynamic Response Of Arbitrarily Shaped Foundations," *J. of Geotech. Engrg.*, ASCE, Vol. 112, No. 2, pp. 109-135.
- [58] Dobry, R., Gazetas, G., and Stokoe, II, K.H. (1986), "Dynamic Response Of Arbitrarily Shaped Foundations: experimental verification," *J. of Geotechnical Engineering*, ASCE, Vol. 112, No. 2, pp. 136-154.
- [59] Dominguez, J. and Gallego, R. (1992), "Time Domain Boundary Element Method For Dynamic Stress Intensity Factor Computations," *Int. J. For Num. Meth. In Engrg.*, Vol 33, pp. 635-647.
- [60] Dominguez, J. and Meise, T. (1991), "On the use of the BEM for wave propagation in infinite domains," *Engineering Analysis with Boundary*

Elements, Vol. 8, No. 3, pp. 132-138.

- [61] Dominguez, J. and Roesset, J.M. (1978), "Dynamic stiffness of rectangular foundations," Research Report R78-20, Department of Civil Engrg., MIT.
- [62] Doyle, J.M. (1966), "Integration Of The Laplace Transformed Equations Of Classical Elastokinetics," J. of Mathematical Analysis and Applications, Vol. 13, pp. 118-131.
- [63] Ellersick, R. (1987), "Vector coding techniques for VS FORTRAN Version 2," IBM SEAS paper, San Jose, California.
- [64] Elsabee, F. and Moray, J.P. (1977), "Dynamic behaviour of embedded foundations", Report No. R77-33, Department of Civil Engrg., MIT.
- [65] Emperador, J.M. and Dominguez, J. (1989), "Dynamic Response Of Axisymmetric Embedded Foundations," Earthq. Engrg. and Struct. Dynamics, Vol. 18, pp. 1105-1117.
- [66] Engels, H. (1980), *Numerical Quadrature And Cubature*, Academic Press, London.
- [67] Eringen, A.C. and Suhubi, E.S. (1975), *Elastodynamics, Volume II, Linear Theory*, Academic Press.
- [68] Fotopoulou, M., Kotsanopoulos, P., Gazetas, G. and Tassoulas, J.L. (1989), "Rocking Damping of Arbitrarily Shaped Embedded Foundations," J. of Geotechnical Engineering, ASCE, Vol. 115, No. 4, pp. 473-489.
- [69] Fox, L. (1964), *An Introduction To Numerical Linear Algebra*, Clarendon Press, Oxford.
- [70] Fukuzawa, R., Chiba, O., and Tohdo, M. (1985), "Seismic Response Analysis Of BWR Buildings With Embedded Foundation," 8th Int. Conf. on Structural Mechanics in Reactor Technology, Brussels, K 6/4, pp. 221-226.
- [71] Gazetas, G. (1983), "Analysis of machine foundation vibrations: state of the art," Soil Dyn. and Earthq. Engrg., Vol. 2, No. 1, pp. 2-42.
- [72] Gazetas, G. (1991), "Formulas and Charts For Impedances of Surface and Embedded Foundations," J. of Geotech. Engrg., ASCE, Vol 117, pp 1363-1381.
- [73] Gazetas, G. and Dobry, R. (1984), "Simple Radiation Damping Model For Piles And Footings," J. of Engrg. Mech., ASCE, Vol 110, No 6, pp. 937-956.
- [74] Gazetas, G., Dobry, R., and Tassoulas, J.L. (1985), "Vertical Response Of Arbitrarily Shaped Embedded Foundations," J. of Geotechnical Engrg., ASCE, Vol. 111, No. 6, pp. 750-771.
- [75] Gazetas, G. and Stokoe, K.H., II (1991), "Vibration of embedded Foundations theory versus experiment," J. of Geotech. Engrg., ASCE, Vol. 117, No. 9, pp. 1382-1401.
- [76] Gazetas, G. and Tassoulas, J.L. (1987a), "Horizontal Stiffness of Arbitrarily Shaped Embedded Foundations," J. of Geotech. Engrg., ASCE, Vol. 113, No. 5, pp. 440-457.
- [77] Gazetas, G. and Tassoulas, J.L. (1987b), "Horizontal Damping of Arbitrarily Shaped Embedded Foundations," J. of Geotech. Engrg., ASCE, Vol. 113, No. 5, pp. 458-475.
- [78] Gazetas, G. and Yegian, M.K. (1979), "Shear and Rayleigh waves in soil dynamics," J. of Geotech. Engrg., ASCE, Vol. 105, pp. 1455-1470.
- [79] Giroud, Jean-Pierre (1968), "Settlement of a linearly loaded rectangular area," J. of Soil Mech. and Fdn, ASCE, Vol. 94, No. SM4, pp. 813-831.
- [80] Gladwell, I. and Wait, R. (1979), *A Survey Of Numerical Methods For Partial Differential Equations*, Clarendon Press, Oxford.
- [81] Goldstine, H.H. (1977), *A History Of Numerical Analysis*, Springer-Verlag, New York.
- [82] Goodier, J.N. and Hodge, P.G. (1958), *Elasticity and Plasticity*, John

Wiley & Sons, Inc., New York.

- [83] Gorbunov-Possadov, M.I. and Serebrjanyi, R.V.(1961), "Design of structures on elastic foundations," *Proc. 5th ICSMFE*, Vol I, pp. 643-648.
- [84] Guiggiani, M.(1991), "The evaluation of Cauchy principal value integrals in the boundary element method-A review," *Mathematical and Computer Modelling*, Vol. 15, No. 3-5, pp. 175-184.
- [85] Guiggiani, M.(1992), "Computing Principal-value Integrals In 3-D BEM For Time-harmonic Elastodynamics - A Direct Approach ," *Communications In Applied Num. Meth.*, Vol. 8, pp. 141-149.
- [86] Guiggiani, M. and Casalini, P.(1987), "Direct Computation Of Cauchy Principal Value Integrals In Advanced Boundary Elements," *Int. J. For Num. Meth. In Engrg*, Vol. 24, pp. 1711-1720.
- [87] Hall, W.S.(1988), "Integration Methods For Singular Boundary Element Integrands," in *Boundary Elements X*, Vol. 1 : Mathematical and Computational Aspects, eds. Brebbia, C.A., Computational Mechanics Publications, pp. 219-236.
- [88] Hartmann, F.(1981), "The Somigliana Identity On Piecewise Smooth Surfaces ," *J. of Elasticity*, Vol. 11, No. 4, pp. 403-423.
- [89] Hartmann, F.(1982), "Elastic Potentials On Piecewise Smooth Surfaces," *J. of Elasticity*, Vol. 12, No. 1, pp. 31-50.
- [90] Hayami, K. and Brebbia, C.A.(1988), "Quadrature Methods For Singular And Nearly Singular Integrals In 3-D Boundary Element Method," in *Boundary Elements X*, Vol. 1 : Mathematical and Computational Aspects, eds. Brebbia, C.A., Computational Mechanics Publications, pp. 237-264.
- [91] Hirose, S.(1991), "Boundary Integral Equation Method For Transient Analysis Of 3-D Cavities And Inclusions," *Engrg. Analysis With Boundary Elements*, Vol 8, No 3, pp. 146-154.
- [92] Hsiao, G.G. and Kleinman, R.E.(1992), "Feasible error estimates in boundary element methods," in *Boundary Element Technology VII*, ed. C.A. Brebbia and M.S. Ingber, Computational Mechanics with Elsevier and Applied Science, pp. 875-886.
- [93] Hsieh, T.K.(1962), "Foundation Vibrations," *Proc. of The Institution of Civil Engineers*, London, Vol. 22, pp. 211-226.
- [94] Hudson, J.A., *The excitation and propagation of elastic waves*, Cambridge University Press, 1980.
- [95] Israil, A.S.M. and Banerjee, P.K.(1992), "Advanced Development Of Boundary Element Method For Two-dimensional Dynamic Elasto-plasticity," *Int. J. Solids Structures*, Vol. 29, No. 11, pp. 1433-1451.
- [96] Israil, A.S.M. and Banerjee, P.K.(1990), "Effects Of Geometrical And Material Properties On The Vertical Vibration Of Three-Dimensional Foundations By BEM," *Int. J. For Num. Meth. In Geomech.*, Vol 14, pp 49-70.
- [97] Jaswon, M.A. and Ponter, A.R.(1963), "An integral equation solution of the torsion problem," *Proc. of the Royal Society*, A273, pp. 237-246.
- [98] Jaswon, M.A. and Symm, G.T.(1977), *Integral Equation Methods In Potential Theory and Elastostatics*, Academic Press, London.
- [99] Jean, W.U., Lin, T.W., and Penzien, J.(1990), "System parameters of soil foundations for time domain dynamic analysis," *Earthq. Engrg. and Struct. Dyn.*, Vol. 19, pp. 541-553.
- [100] Jeng, G. and Wexler, A(1977), "Isoparametric, Finite Element, Variational Solution Of Integral Equations For Three-dimensional Fields," *Int. J. For Num. Meth. In Engrg.*, Vol. 11, pp. 1455-1471.
- [101] Johnson, L.R.(1974), "Green's function for Lamb's problem," *Geophys. J.R. Astr. Soc.*, 37, 99-131.
- [102] Jun, L., Beer, G., and Meek, J.L.(1985), "Efficient Evaluation Of

Integrals Of Order $1/r$, $1/r^2$, $1/r^3$ Using Gauss Quadrature, "Engineering Analysis, Vol. 2, No. 3, pp. 118-123.

- [103] Karabalis, D.L. and Beskos, D.E. (1986), "Dynamic Response Of 3-D Embedded Foundations By The Boundary Element Method," *Computer Meth. In Appl. Mech. and Engrg.*, Vol 56, pp 91-119.
- [104] Karabalis, D.L. and Beskos, D.E. (1987a), "Three-Dimensional Soil-Structure Interaction By Boundary Element Methods," Chapter 1 in *Topics In Boundary Element Research*, Vol. 4, C.A. Brebbia (ed.), Berlin, Springer-Verlag.
- [105] Karabalis, D.L. and Beskos, D.E. (1987b), "Dynamic Soil-structure Interaction," in *Boundary Element Methods In Mechanics*, Beskos, D.E. (eds), Chapter 11, Elsevier Science Publishers, New York.
- [106] Karabalis, D.L. and Rizos, D.C. (1993), "Dynamic analysis of 3D foundations," Chapter 6 in *Boundary Element Techniques in Geomechanics*, Manolis, G.D. and Davies, T.G. (eds), Computational Mechanics Publications, UK.
- [107] Karamanoglu, K. and Beswick, G.E. (1991), "Improving the accuracy of BEM in the use of non-equidistant elements," in *Boundary Element Technology 6*, Brebbia, C.A., Elsevier Applied Science, pp. 321-334.
- [108] Karasudhi, P., Keer, L.M., and Lee, S.L. (1968), "Vibratory motion of a body on an elastic half plane," *J. of Appl. Mechanics*, ASME, pp. 697-705.
- [109] Kausel, E. and Roesset, J.M. (1974), "Soil structure interaction problems for nuclear containment structures," in *Electric Power and the Civil Engineer*, ASCE, Proc. of the Power Division Specialty Conference, Boulder, Colorado, pp. 469-498.
- [110] Kausel, E. and Roesset, J.M. (1975), "Dynamic stiffness of circular foundations," *J. of Engrg. Mechanics*, ASCE, Vol. 101, EM6, pp. 771-785.
- [111] Kausel, E., Whitman, R.V., Morray, J.P., and Elsabee, F. (1978), "The spring method for embedded foundations," *Nuclear Engrg. and Design*, Vol. 48, pp. 377-392.
- [112] Kim, J. and Papageorgiou, A.S. (1993), "Discrete wave-number boundary-element method for 3-D scattering problems," *J. of Engrg. Mechanics*, ASCE, Vol. 119, No. 3, pp. 603-624.
- [113] Kobayashi, S. (1987), "Elastodynamics," in *Boundary Element Methods In Mechanics*, Beskos, D.E. (eds), Chapter 4, Elsevier Science Publishers.
- [114] Kobayashi, S. and Nishimura, N. (1980), "Green's tensors for elastic halfspace," *Memoirs-Fac. Engrg.*, Kyoto U., XLIII, 228-241.
- [115] Kobayashi, S., Nishimura, N., and Kamiya, H. (1989), "An Algorithm For Vectorized Computation In Boundary Element Methods," *Boundary Element Methods In Engineering*, Proc. of the Int. Symp. on Boundary Element Methods: Advances in Solid and Fluid Mechanics, Annigeri, B.S. and Tseng, K. (ed), pp. 310-316.
- [116] Krylov, V.I. (1962), *Approximate Calculation Of Integrals*, MacMillan.
- [117] Kumar, K., Kane, J.H., and Srinivasan, A.V. (1989), "The influence of massively parallel processing in boundary element computations," in *Boundary Element Methods In Engineering*, Proc. of the Int. Symp. on Boundary element Methods: Advances In Solid And Fluid Mechanics, Annigeri, B.S. and Tseng, K. (eds.), pp. 500-507.
- [118] Lachat, J.C. and Watson, J.O. (1976), "Effective Numerical Treatment Of Boundary Integral Equations: A Formulation For Three -dimensional Elastostatics," *Int. J. For Num. Meth. In Engrg.*, Vol. 10, pp. 991-1005.
- [119] Lamb, H. (1904), "On the propagation of tremors over the surface of an elastic solid," *Phil. Trans. Roy. Soc., London*, A203, pp. 1-42.
- [120] Lean, M.H. and Wexler, A. (1985), "Accurate Numerical Integration Of Singular Boundary Element Kernels Over Boundaries With Curvature," *Int. Journal For Numerical Methods In Engineering*, Vol. 21, pp. 211-228.

- [121] Lether, F.G. (1970a), "An error representation for product cubature rules," *SIAM J. of Num. Analysis*, Vol 7, pp 363-365.
- [122] Lether, F.G. (1970b), "Cross-product cubature error bounds," *Mathematical Computation*, Vol. 24, pp. 583-592.
- [123] Lether, F.G. (1971), "Cubature error bounds for Gauss-Legendre product rules," *SIAM J. of Num. Analysis*, Vol. 8, pp. 36-42.
- [124] Lether, F.G. (1981), "Some observations on Gauss-Legendre quadrature error estimates for analytic functions," *J. Comput. Appl. Math.*, Vol. 7, pp. 63-66.
- [125] Li, H.B. and Han, G.M. (1985), "A New Method For Evaluation Singular Integrals In Stress Analysis Of Solids By The Direct Boundary Element Method," *Int. J. For Num. Meth. In Engineering*, Vol. 21, pp. 2071-2098.
- [126] Love, A.E.H. (1944), *A Treatise On The Mathematical Theory Of Elasticity*, 4th ed., New York, Dover Publications, Inc.
- [127] Luchi, M.L. and Rizzuti, S. (1987), "Boundary Elements For Three-dimensional Elastic Crack Analysis," *Int. J. For Numerical Methods In Engineering*, Vol. 24, pp. 2253-2271.
- [128] Luco, J.E. and Westmann, R.A., (1971), "Dynamic response of circular footings," *J. of the Engrg. Mechanics*, ASCE, Vol. 97, EM5, 1381-1395.
- [129] Luco, J.E. and Westmann, R.A., (1972), "Dynamic response of a rigid footing bonded to an elastic half space," *J. of Appl. Mech.*, ASME, pp. 527-534.
- [130] Luco, J.E. and Wong, H.L. (1987), "Seismic Response Of Foundations Embedded In A Layered Half-space," *Earthq. Engrg. and Struct. Dyn.*, Vol. 15, pp. 233-247.
- [131] Lysmer, J. (1980), "Foundation vibrations with soil damping," in *Civil Engineering and Nuclear Power*, Knoxville, TN, pp. 10.4.1-10.4.18.
- [132] Lysmer, J. and Kuhlemeyer, A. (1969), "Finite dynamic model for infinite media," *J. of Engrg. Mechanics*, ASCE, Vol. 95, EM4, pp. 859-877.
- [133] Lysmer, J. and Richart, Jr., F.E. (1966), "Dynamic Response of Footings to Vertical Loading," *J. of Soil Mech. and Fnd.*, ASCE, Vol. 92, No. SM1, pp. 65-91.
- [134] Lysmer, J. and Waas, G. (1972), "Shear waves in plane infinite structures," *J. of Engrg. Mechanics*, ASCE, EM1, pp. 85-105.
- [135] Manolis, G.D. (1983), "A Comparative Study On Three Boundary Element Methods Approaches To Problems In Elastodynamics," *Int. J. For Numerical Methods in Engrg.*, Vol 19, pp 73-91.
- [136] Manolis, G.D. (1989), "Computer Programs," in *Boundary Element Methods in Structural Analysis*, Beskos, D.E. (ed), ASCE, pp. 309-335.
- [137] Manolis, G.D., Ahmad, S., Banerjee, P.K. (1986), "Boundary Element Method Implementation For Three-Dimensional Transient Elastodynamics," in *Developments in Boundary Element Methods-4*, eds., Banerjee, P.K. and Watson, J.O., pp. 29-65.
- [138] Manolis, G.D. and Beskos, D.E. (1988), *Boundary Element Methods in Elastodynamics*, Unwin Hyman, London.
- [139] Manolis, G.D. and Davies, T.G. (1993), *Boundary Element Techniques in Geomechanics*, Computational Mechanics Publications, UK.
- [140] Manolis, G.D., Davies, T.G., Beskos, D.E. (1993), "Overview of boundary element techniques in geomechanics," Chapter 1 in *Boundary Element Techniques in Geomechanics*, Manolis, G.D. and Davies, T.G. (eds), Computational Mechanics Publications.
- [141] McNamee, J. (1964), "Error-Bounds For The Evaluation Of Integrals By The Euler-Maclaurin Formula And By Gauss-Type Formulae," *Mathematics of Computation*, Vol. 18, pp. 368-381.

- [142] Meek, J.W. and Wolf, J.P. (1993), "Cone models for nearly incompressible soil," *Earthq. Engrg. and Struct. Dyn.*, Vol. 22, pp. 649-663.
- [143] Migeot, J.L. (1985), "Numerical Integration In The Vicinity Of A Logarithmic Singularity," *Engineering Analysis*, Vol. 2, No. 2, pp. 92-94.
- [144] Mikhlin, S.G. (1965), *Multidimensional Singular Integrals and Integral Equations*, Pergamon Press.
- [145] Miller, G.F. and Pursey, H. (1954), "The field and radiation impedance of mechanical radiators on the free surface of a semi-infinite isotropic solid," *Proceedings of The Royal Society*, A223, pp. 521-541.
- [146] Min, C.S. and Gupta, A.K. (1991), "Vector Finite-Element Analysis Using IBM 3090-600E VF," *Communications in Appl. Num. Meth.*, Vol 7, pp 155-164.
- [147] Mita, A. and Luco, J.E. (1989a), "Dynamic Response Of A Square Foundation Embedded In An Elastic Half-space," *Soil Dyn. and Earthq. Engrg.*, Vol 8, No 2, pp 54-67.
- [148] Mita, A. and Luco, J.E. (1989b), "Impedance Functions And Input Motions For Embedded Square Foundations," *Journal of Geotechnical Engrg.*, ASCE, Vol. 115, No. 4, pp. 491-503.
- [149] Mitra, A.K. and Ingber, M.S. (1993), "A multiple-node method to resolve the difficulties in the boundary element integral equation method caused by corners and discontinuous boundary conditions," *Int. J. for Num. Meth. in Engrg.*, Vol. 36, pp. 1735-1746.
- [150] Mohammadi, M. and Karabalis, D.L. (1990), "3-D Soil-structure Interaction Analysis By BEM: Comparison Studies And Computational Aspects," *Soil Dynamics and Earthquake Engrg.*, Vol. 9, No. 2, pp. 96-108.
- [151] Mori, M. and Piessens, R. (1987), *Numerical Quadrature*, North-Holland, Amsterdam.
- [152] Muskhelishvili, N.I. (1953), *Some Basic Problems Of The Mathematical Theory Of Elasticity*, P. Noordhoff Ltd, Holland.
- [153] Mustoe, G.G.W. (1984), "Advanced Integration Scheme Over Boundary Elements And Volume Cells For Two And Three Dimensional Non-linear Analysis," in *Developments in Boundary Element Methods-3*, eds. Banerjee, P.K. and Mukherjee, S., Elsevier Applied Science Publishers, London.
- [154] NAG Library, Mark 10, Numerical Analysis Group, NAG Central Office, Oxford, 1983.
- [155] Nii, Y. (1987), "Experimental half-space dynamic stiffness," *J. of Geotech. Engrg.*, ASCE, Vol. 113, No. 11, pp. 1359-1373.
- [156] Novak, M. (1970), "Prediction of footing vibrations," *J. of the Soil Mech. and Foundations*, ASCE, Vol. 96, pp. 837-861.
- [157] Novak, M. (1987), "State-of-the-art in analysis and design of machine foundations," in *Soil-Structure Interaction*, Elsevier, Oxford, England, pp 171-192.
- [158] Pais, A. and Kausel, E. (1988), "Approximate Formulas For Dynamic Stiffnesses Of Rigid Foundations," *Soil Dyn. and Earthquake Engineering*, Vol. 7, No. 4, pp. 213-227.
- [159] Pak, R.Y.S. and Gobert, A.T. (1991), "Forced vertical vibration of rigid discs with arbitrary embedment," *J. of Engrg. Mechanics*, ASCE, Vol. 117, No. 11, pp. 2527-2548.
- [160] Pauw, A. (1953), "A dynamic analogy for foundation-soil system," in "Symposium On Dynamic Testing of Soil", ASTM, Special Technical Publication, 156, pp. 90-112.
- [161] Polychronopoulos, C.D. (1988), *Parallel Programming And Compilers*, Kluwer Academic Publishers, Boston.
- [162] Poulos, H.G. and Davis, E.H. (1974), *Elastic Solutions For Soil And Rock Mechanics*, John Wiley & Sons, INC., New York.

- [163] Ratay, R.T. (1971), "Sliding-rocking vibration of body on elastic medium," *J. of the Soil Mech. and Fnd, ASCE*, Vol. 97, No. SM1, pp. 177-191.
- [164] Rego Silva, J.J., Wrobel, L.C., and Telles, J.C.F. (1993), "A new family of continuous/discontinuous three-dimensional boundary elements with application to acoustic wave propagation," *Int. J. For Num. Meth. In Engrg.*, Vol. 36, pp. 1661-1679.
- [165] Rezayat, M. (1992), "Fast Decomposition Of Matrices Generated By The Boundary Element Method," *Int. J. For Num. Meth. In Engrg.*, Vol. 33, pp. 1109-1118.
- [166] Richart, Jr., F.E. (1960), "Foundation Vibrations," *J. of the Soil Mech. and Foundations, ASCE*, Vol. 86, pp. 1-34.
- [167] Richart, Jr., F.E. (1975), "Some effects of dynamic soil properties on soil-structure interaction," *J. of the Geotechnical Engrg., ASCE*, Vol. 101, GT12, pp. 1197-1240.
- [168] Richart, Jr., F.E., Hall, J.R., and Woods, R.D. (1970), *Vibrations of soils and foundations*, Prentice-Hall, Englewood Cliffs.
- [169] Rizzo, F.J. (1967), "An Integral Equation Approach To Boundary Value Problems Of Classical Elastostatics," *Quarterly of Applied Mathematics*, Vol. 25, pp. 83-95.
- [170] Rizzo, F.J. and Shippy, D.J. (1977), "An Advanced Boundary Integral Equation Method For Three-dimensional Thermoelasticity," *Int. J. for Numerical Methods in Engrg.*, Vol 11, pp 1753-1768.
- [171] Rizzo, F.J., Shippy, D.J., and Rezayat, M. (1985), "A Boundary Integral Equation Method For Radiation And Scattering Of Elastic Waves In Three Dimensions," *Int. J. For Num. Meth. in Engrg.*, Vol. 21, pp. 115-129.
- [172] Roach, G.F. (1982), *Green's Functions*, Cambridge University Press, London.
- [173] Roesset, J.M. (1980a), "The Use Of Simple Models In Soil Structure Interaction," in *Civil Engineering and Nuclear Power, ASCE*, Vol. II, paper no. 10-3, pp. 1-25.
- [174] Roesset, J.M. (1980b), "Stiffness and Damping Coefficients of foundations," in *Dynamic Response of Pile Foundations: Analytical Aspects*, O'Neill, M. and Dobry, R. eds, ASCE, pp. 1-30.
- [175] Rosen, D. and Cormack, D.E. (1993), "Singular and near singular integrals in the BEM: a global approach," *SIAM J. Appl. Math.*, Vol. 53, No.2, pp. 340-357.
- [176] Schiffman, R.L. (1969), "The influence of adhesion on the stresses and displacements in an elastic half-space," *Highway Research Record*, no. 282, pp. 17-24.
- [177] Smith, H.V. (1979), "The evaluation of the error term in some numerical quadrature formulae," *Int. J. For Num. Meth. in Engrg.*, Vol 14, pp 468-472.
- [178] Sofianos, A.I. (1987), "Evaluation of the leading band coefficients of the boundary integral system of equations," *Communications In Appl. Num. Meth.*, Vol. 3, pp. 11-16.
- [179] Spyrakos, C.C., Patel, P.N., and Kokkinos, F.T. (1989), "Assessment of computational practices in dynamic soil-structure interaction," *Journal of Computing in Civil Engineering, ASCE*, Vol. 3, No. 2, pp. 143-157.
- [180] Stenger, F. (1966), "Error bounds for the evaluation of integrals by repeated Gauss-type formulae," *Num. Mathematics*, Vol. 9, pp. 200-213.
- [181] Stokoe, K.H., II and Richart, F.E. (1974), "Dynamic response of embedded machine foundations," *J. of Geotechnical Engrg., ASCE*, pp. 427-447.
- [182] Stroud, A.H. and Secrest, D. (1966), *Gaussian Quadrature Formulas*, Prentice-Hall, Englewood Cliffs, NJ.
- [183] Sung, T.Y. (1953), "Vibration in semi-infinite solids due to periodic

surface loading,"ASTM Special Technical Publication No. 156, Symposium on Soil Dynamics, pp. 35-63.

- [184] Symm, G.T.(1963),"Integral equation methods in potential theory. II," Proc. of the Royal Society, A275, pp. 33-46.
- [185] Tassoulas, J.L. and Kausel, E.(1983),"On the effect of the rigid sidewall on the dynamic stiffness of embedded circular footings,"Earthq. Engrg. and Struct. Dyn., Vol 11, pp 403-414.
- [186] Thomson, W.T. and Kobori, T.(1963),"Dynamical compliance of rectangular foundations on an elastic half-space,"J of Appl Mech, ASME, pp. 579-584.
- [187] Tohdo, M., Chiba, O., and Fukuzawa, R.(1986),"Impedance Functions And Effective Input Motions Of Embedded Rigid Foundations," Proc. 7th Japan Earthq. Engrg. Symp., Tokyo, pp. 1039-1044.
- [188] Touhei, T. and Yoshida, N.(1988),"Dynamic Response Analysis Of Ground Using A Coupled Finite And Boundary Element Method For Time Marching Analysis,"in *Numerical Methods In Geomechanics*, Swoboda(ed.), Rotterdam.
- [189] Valliappan, S., Favaloro, J.J., and White, W.(1977),"Dynamic analysis of embedded footings,"J. of Geotech. Engrg., ASCE, Vol 103, pp. 129-132.
- [190] Veletsos, A.S. and Verbic, B.(1974),"Basic response functions for elastic foundations,"J of Engrg Mech., ASCE, Vol. 100, EM2, pp. 189-202.
- [191] Veletsos, A.S. and Wei, Y.T.(1971),"Lateral and rocking vibration of footings,"J. of Soil Mech. and Fnd., ASCE, Vol. 97, pp. 1227-1248.
- [192] von Estorff, O. and Prabucki, M.J.(1988),"The coupling of boundary and finite elements to solve transient problems in elastodynamics,"*Boundary Elements X*, ed. Brebbia, C.A., Springer-Verlag, pp. 447-459.
- [193] Wang, H.C. and Banerjee, P.K.(1990),"Generalized Axisymmetrical Elastodynamic Analysis By Boundary Element Method,"*Int. J. For Numerical Methods in Engineering*, Vol. 30, pp. 115-131.
- [194] Watson, J.O.(1979),"Advanced Implementation Of The Boundary Element Method For Two- and Three-dimensional Elastostatics,"in *Developments in Boundary Element Methods-1*, Banerjee, P.K. and Butterfield, R.(eds), pp. 31-63.
- [195] Wheeler, L.T. and Sternberg, E.(1968),"Some theorems in classical elastodynamics,"*Archive For Rational Mech. and Anal.*, Vol 31, pp. 51-90.
- [196] Whitman, R.V.(1966),"Analysis of foundation vibrations,"in *Vibration in Civil Engineering*, ed. Skipp, B.O., Butterworths, pp. 159-179.
- [197] Whitman, R.V. and Richart, Jr., F.E.(1967),"Design procedure for dynamically loaded foundations,"*J. of the Soil Mech. and Fnd.*, ASCE, Vol. 93, No. SM6, pp. 169-193.
- [198] Wolf, J.P.(1991),"Consistent lumped-parameter models for unbounded soil: physical representation,"*Earthq. Engrg. and Struct. Dyn.*, Vol. 20, pp. 11-32.
- [199] Wolf, J.P. and Somaini, D.R.(1986),"Approximate dynamic model of embedded foundation in time domain,"*Earthq. Engrg. and Struct. Dyn.*, Vol. 14, pp. 683-703.
- [200] Yokoyama, M. and Zaita, T.(1992),"An Efficient Method For The Two-dimensional Elastostatic Boundary Element Method,"*Int. J. For Numerical Methods in Engrg.*, Vol. 35, pp. 1277-1288.
- [201] Zienkiewicz, O.C. and Taylor, R.L.(1989), *The Finite Element Method*, McGraw-Hill, England.
- [202] Zucchini, A. and Mukherjee, S.(1991),"Vectorial and parallel processing in stress analysis with the boundary element method,"*Int. J. for Num. Meth. in Engrg.*, Vol. 31, pp. 307-317.